Universidade do Minho
Escola de Engenharia

Joana Marina Silva Queirós

Wide range polymeric membranes towards water remediation of contaminants of emerging concern

janeiro de 2026

Wide range polymeric membranes towards water remediation of contaminants of emerging concern

Joana Marina Silva Queirós

UMinho | 2026

Universidade do Minho
Escola de Engenharia

Joana Marina Silva Queirós

Wide range polymeric membranes towards water remediation of contaminants of emerging concern

Tese de Doutoramento
Engenharia de Materiais

Trabalho efetuado sob a orientação de
Professor Doutor Senentxu Lanceros Méndez
Doutor Pedro Manuel Abreu Martins

janeiro de 2026

DIREITOS DE AUTOR E CONDIÇÕES DE UTILIZAÇÃO DO TRABALHO POR TERCEIROS

Este é um trabalho académico que pode ser utilizado por terceiros desde que respeitadas as regras e boas práticas internacionalmente aceites, no que concerne aos direitos de autor e direitos conexos.

Assim, o presente trabalho pode ser utilizado nos termos previstos na licença abaixo indicada.

Caso o utilizador necessite de permissão para poder fazer um uso do trabalho em condições não previstas no licenciamento indicado, deverá contactar o autor, através do RepositóriUM da Universidade do Minho.

Licença concedida aos utilizadores deste trabalho



Atribuição-NãoComercial

CC BY-NC

https://creativecommons.org/licenses/by-nc/4.0/

ACKNOWLEDGEMENTS

Com o culminar deste longo desafio pessoal e profissional ao qual me propus, seria impossível deixar passar em branco sem destacar o suporte e a ajuda imprescindíveis para atingir esta meta.

Primeiro de tudo, gostaria de agradecer à Fundação para a Ciência e Tecnologia (FCT) pela bolsa 2021.08822.BD como suporte financeiro deste projeto.

Aos meus orientadores, ao professor Senentxu, pelos conhecimentos científicos e palavras sábias que me transmitiu e que foram imprescindíveis para a concretização deste trabalho. Por me ter impulsionado a sair da minha zona de conforto através de oportunidades de estadia no estrangeiro a que nunca teria tido acesso sem a sua ajuda. Ao Pedro, não me chegam as palavras para agradecer por tudo. Um verdadeiro mentor, sem o qual esta tese não seria possível, não só pelo conhecimento científico que me transmitiu, base de tudo o que sei nesta área, mas pela forma profundamente humana com que sempre me acompanhou. Acreditou nas minhas capacidades mais do que eu mesma, com incentivos mascarados de elogios que me passavam uma confiança que me sustentava. Nunca me deixou sentir que estava sozinha, mesmo nos piores momentos em que me viu duvidar, cansar e chorar.

À Noélia, à Ana Rita Bragança, à Fang e ao Hugo, de diferentes formas, pela ajuda laboratorial prestada ao longo deste trabalho. Ao Raúl e ao Professor Carlos Tavares por estreitarem colaborações frutíferas que enriqueceram este trabalho e que se estendem a um futuro promissor. Ao Dr. Roberto Fernandez de Luis e Dr. Jorge Saiz pelo acolhimento e suporte durante a estadia no BCMaterials e pelos conhecimentos científicos passados. Aos meus coleguinhas de laboratório, ao André, Diana, Dinis, Joana e Soraia, por terem transformado o laboratório num lugar onde queria estar diariamente. Pelos risos, pelas discussões sem fim e por tornarem tudo mais leve mesmo nos dias mais difíceis. Foram muito mais do que colegas, foram companhia, apoio e amizade verdadeira. Aos meus amigos de sempre, por estarem presentes nos melhores e piores momentos, pelas palavras certas e pelo apoio constante ao longo de todo este percurso.

À minha família, à mãe, ao Berto, à Vó, pelo colo e por todos os ensinamentos e valores, que são na verdade tudo de melhor que posso levar desta vida. Aos meus, que não conto com a sua presença física, mas levo-os comigo para todo o lado, pai e avô, amo-vos eternamente.

Finalmente, ao meu Tiago, por ser o meu pilar emocional e por me guiar para lugares mais leves quando o mundo parece desabar. Pela paciência infinita e pela compreensão nos dias de maior cansaço. Agradeço todos os dias por estares na minha vida, mas aqui agradeço-te, sobretudo, por nunca deixares que eu desista de mim. Sais-me sempre a sorte grande.

Um sincero obrigada a todos vós.

STATEMENT OF INTEGRITY

I hereby declare having conducted this academic work with integrity. I confirm that I have not used plagiarism or any form of undue use of information or falsification of results along the process leading to its elaboration.

I further declare that I have fully acknowledged the Code of Ethical Conduct of the University of Minho.

Resumo: Membranas poliméricas de amplo espetro para a remediação de contaminantes emergentes em água

A poluição aquática por contaminantes emergentes, em particular antibióticos, é uma ameaça devido à sua persistência ambiental e ao papel na disseminação de bactérias resistentes e genes de resistência a antibióticos. Face à ineficácia dos tratamentos convencionais, esta tese desenvolveu membranas fotocatalíticas multifuncionais capazes de atuar simultaneamente sobre antibióticos, bactérias e material genético, superando limitações, como a ativação por radiação solar, a recuperação do catalisador e a difícil reutilização. Numa fase inicial, realizou-se uma triagem de nanopartículas de TiO_2 funcionalizadas com Au e Ag por síntese verde, na degradação de ciprofloxacina (CIP), trimetoprim (TMP) e sulfadiazina (SDZ), sob radiação UV e visível. A funcionalização com Au permitiu a ativação eficiente na região visível por ressonância plasmónica, destacando o Au–TiO_2 na degradação de CIP sob radiação visível (13% com TiO_2 *vs.* 99% com Au-TiO_2 em 90 min). Este nanocompósito foi imobilizado em membranas de poli-fluoreto de vinilideno-co-hexafluoropropileno (PVDF-HFP) produzidas por *thermally induced phase separation* (TIPS), permitindo a reutilização por três ciclos sem perda de eficiência. A identificação de subprodutos de degradação, complementada por ensaios ecotóxicos com *Vibrio fischeri*, revelou compostos tóxicos na degradação de SDZ, reforçando a importância da avaliação ecotóxica em processos fotocatalíticos. Para reforçar a sustentabilidade, TiO_2 funcionalizado com Ag foi imobilizado em membranas de fibroína de seda e PVDF-HFP, também produzidas por TIPS combinado com *salt leaching*, originando estruturas porosas com atividade fotocatalítica e antimicrobiana, com reduções de 1-2 $\log_{10}$ para *E. coli* por *contact killing*. Numa etapa subsequente, a multifuncionalidade foi potenciada pelo aumento da concentração de Ag-TiO_2 em membranas de PVDF-HFP, possibilitando maior atividade antimicrobiana (redução de 8,1 $\log_{10}$) e inibição de biofilme (70%) para *E. coli*, bem como degradação de CIP e TMP e inativação biológica de um plasmídeo resistente à ampicilina. Por fim, para aproximar a tecnologia membranar às condições reais, desenvolveram-se redes flutuantes de TiO_2/PVDF-HFP por impressão 3D, com controlo geométrico, maior exposição solar e de fácil recuperação, alcançando degradação completa de CIP após 120 min de irradiação solar. Esta tese compila materiais fotocatalíticos produzidos por abordagens convencionais e ecológicas, em suspensão e imobilizados, demonstrando eficácia contra antibióticos, bactérias e material genético. A multifuncionalidade dos materiais mais promissores foi validada, quanto à reutilização, avaliação ecotoxicológica, potencial escalabilidade e aplicação em matrizes de água reais, estabelecendo uma plataforma personalizável face aos desafios diversos e complexos da contaminação aquática atual.

Palavras-Chave: antibióticos; fotocatálise; membranas multifuncionais; remediação aquática; resistência antimicrobiana

Abstract: Wide range polymeric membranes towards water remediation of contaminants of emerging concern

Water pollution by contaminants of emerging concern, in particular antibiotics, poses a significant threat due to their environmental persistence and their role in the dissemination of antibiotic-resistant bacteria and resistance genes. Given the inefficiency of conventional treatment methods, this thesis developed multifunctional photocatalytic membranes capable of simultaneously targeting antibiotics, bacteria, and genetic material, overcoming limitations such as activation by solar radiation, catalyst recovery, and complex reusability. Initially, a screening of Au and Ag- functionalised TiO_2 nanoparticles using a green synthesis approach was conducted for the degradation of ciprofloxacin (CIP), trimethoprim (TMP), and sulfadiazine (SDZ) under UV and visible light. Au functionalisation enabled efficient activation in the visible region through plasmonic resonance, underscoring Au–TiO_2 for CIP degradation under visible radiation (13% with TiO_2 *vs*. 99% with Au-TiO_2 within 90 min). This nanocomposite was further immobilised in polyvinylidene fluoride-co-hexafluoropropylene (PVDF-HFP) membranes produced by thermally induced phase separation (TIPS), allowing reuse over three cycles without loss of efficiency. The identification of degradation by-products, complemented by ecotoxicity assays with *Vibrio fischeri*, revealed toxic compounds formed during SDZ degradation, reinforcing the importance of ecotoxicological assessment in photocatalytic processes. To enhance sustainability, Ag-functionalised TiO_2 was immobilised on silk fibroin and PVDF-HFP membranes, also produced by TIPS combined with the *salt leaching* technique, yielding porous structures with photocatalytic and antimicrobial activity, achieving 1–2 $\log_{10}$ reductions for *E. coli* by *contact killing*. In a subsequent step, increasing the Ag-TiO_2 concentration in PVDF-HFP membranes enhanced multifunctionality, enabling higher antimicrobial activity (8.1 $\log_{10}$ reduction), and biofilm inhibition (70%) against *E. coli*, as well as CIP and TMP degradation and biological inactivation of an ampicillin-resistance plasmid. Finally, to bring membrane technology closer to real-world conditions, floating TiO_2/PVDF-HFP grids were developed using 3D printing, providing geometry control, greater solar exposure, and easy recovery, achieving complete CIP degradation after 120 min of solar irradiation. This thesis compiles photocatalytic materials produced via conventional and green approaches, in suspension and immobilised, demonstrating effectiveness against antibiotics, bacteria, and genetic material. The multifunctionality of the most promising materials was validated in terms of reusability, ecotoxicological assessment, potential scalability and application in real-world water matrices, establishing a customisable platform to address the diverse and complex challenges of aquatic contamination today.

Keywords: antibiotics; antimicrobial resistance; multifunctional membranes; photocatalysis; water remediation

Table of contents

Resumo ..... **v**

Abstract ..... **vi**

List of abbreviations ..... **xi**

List of symbols ..... **xvi**

List of Figures ..... **xvii**

List of Tables ..... **xxii**

1 Introduction **1**

1.1 Motivation 2

1.2 Water Remediation 4

1.2.1 Contaminants of Emerging Concern 5

1.3 Conventional Wastewater Treatment Strategies 12

1.3.1 Advanced Oxidation Processes for antibiotics, ARB, and ARG removal 15

1.4 Photocatalysis 15

1.4.1 Photocatalysts 19

1.4.2 Strategies to Enhance Visible-Light Absorption in Photocatalysts 21

1.5 Advanced Membrane Technology 23

1.5.1 Poly(vinilydene fluoride) and its copolymers 26

1.5.2 Silk Fibroin 27

1.5.3 Polymer Membrane Processing Techniques 29

1.6 Ecotoxicity 31

1.7 Objectives and Methodology 33

1.8 Structure of the Thesis 33

1.9 References 36

2 Immobilisation of Nanoparticles on PVDF-HFP Membranes for Photocatalytic Antibiotic Degradation **54**

2.1 Introduction 55
2.2 Materials and methods 58
2.2.1 Materials 58
2.2.2 Synthesis and functionalisation of Au-TiO_2 and Ag-TiO_2 nanoparticles 58
2.2.3 Nanoparticles characterisation 59
2.2.4 Composite Membrane Production 62
2.2.5 Nanocomposites characterisation 62
2.2.6 Photocatalytic Activity of the Composite Membranes 64
2.2.7 Ecotoxicity Assessment 65
2.3 Results and discussion 66
2.3.1 Characterization of Au-TiO_2 and Ag-TiO_2 nanocomposites 66
2.3.2 Composite Membranes characterization 74
2.3.3 Photocatalytic Activity of Composites Membranes 78
2.3.4 Au-TiO_2/PVDF-HFP membrane reusability 80
2.3.5 Photocatalytic degradation Mechanism 83
2.3.6 Ecotoxicity Assessment 89
2.4 Conclusions 93
2.5 References 94
3 Natural and Synthetic Polymer-Based Composite Membranes for Photocatalytic Degradation of Antibiotics and Antimicrobial Properties 102
3.1 Introduction 103
3.2 Materials and methods 105
3.2.1 Materials 105
3.2.2 Synthesis and characterisation of nanoparticles 105
3.2.3 Extraction of SF 106
3.2.4 Development of polymer-based porous membranes 107

3.2.5 Polymer-based membranes' physical-chemical characterisation 108
3.2.6 Polymer-based membranes' functional performance 109
3.3 Results and discussion 110
3.3.1 Synthesis and characterisation of nanoparticles 110
3.3.2 Polymer-based membranes characterisation 112
3.3.3 Photocatalytic performance of nanocomposite membranes 116
3.3.4 Reusability of the SF : TiO_2/5-ASA/Ag membranes 119
3.3.5 Antimicrobial properties of nanocomposite membranes 121
3.4 Conclusions 123
3.5 References 123
4 Multifunctional PVDF-HFP Membranes for Simultaneous Removal of Antibiotics, ARB, and ARGs 132
4.1 Introduction 133
4.2 Materials and methods 136
4.2.1 Reagents 136
4.2.2 Synthesis of AgNPs with Quercetin 136
4.2.3 Synthesis of Ag-TiO_2 136
4.2.4 Nanoparticles characterisation 137
4.2.5 Nanoparticles Photocatalytic Performance 137
4.2.6 Nanocomposite Membrane Production 138
4.2.7 Composite Membrane Characterisation 138
4.2.8 Evaluation of the Antibacterial Activity 139
4.2.9 Photocatalytic Degradation of ARG 140
4.2.10 Photocatalytic Degradation of Antibiotic 142
4.3 Results and Discussion 142
4.3.1 Synthesis of AgNPs using the flavonoid Quercetin 142

4.3.2 Synthesis and characterisation of Ag-TiO_2 144
4.3.3 Screening of photocatalytic nanoparticles 148
4.3.4 Nanocomposite Membrane Characterisation 151
4.3.5 Evaluation of the Antibacterial Activity 153
4.3.6 Photocatalytic Degradation of ARG 156
4.3.7 Photocatalytic Performance 159
4.4 Conclusions 166
4.5 References 167
5 Scalable Floating Photocatalytic Membranes: 3D-Printed PVDF-HFP/TiO_2 Grids for Water Remediation 175
5.1 Introduction 176
5.2 Materials and Methods 178
5.2.1 Reagents 178
5.2.2 Floating grid production and optimisation 179
5.2.3 Floating grid characterisation 180
5.2.4 Photocatalytic Degradation Assays 181
5.3 Results and Discussion 182
5.3.1 Floating grids characterisation 182
5.3.2 Photocatalytic Tests 187
5.4 Conclusions 196
5.5 References 197
6 Conclusions and Future Work 203
6.1 Conclusions 204
6.2 Future work 206

List of abbreviations

#	
2D	Two-dimensional
2-HTA	2-hydroxyterephthalic acid
3D	Three-dimensional
5-ASA	5-aminosalicylic acid
A	
AC	Acetone
AGs	Aminoglycosides
AMX	Amoxicillin
AOP	Advanced Oxidation Processes
AmpR	Ampicillin Resistance Gene
AR	Antibiotic Resistance
ARB	Antibiotic-Resistant bactéria
ARG	Antibiotic-Resistance Genes
B	
BLs	β-Lactams
BQL	Below Quantification Limit
C	
CA	Contact Angle
CB	Conduction Band
CBZ	Carbamazepine
CECs	Contaminants of Emerging Concern
CFU	Colony-forming unit
CIP	Ciprofloxacin
CWWTP	Conventional Wastewater Treatment Plant
D	
DDA	Data-Dependent Acquisition
DDD	Defined Daily Dose

DIW	Direct Ink Writing
DMF	N,N-dimethylformamide
DLS	Dynamic Light Scattering
DNA	Deoxyribonucleic Acid
DRS	Diffuse Reflectance Spectroscopy
DSC	Differential Scanning Calorimetry
	E
EDX	Energy-Dispersive X-ray
EIPS	Evaporation-Induced Phase Separation
EPS	Extracellular Polymeric Substances
Eq.	Equation
ESBL	Extended-spectrum beta-lactamase
EU	European Union
	F
FA	Formic Acid
FE-SEM	Field-Emission Scanning Electron Microscope
FDM	Fused Deposition Modelling
FQs	Fluoro-Quinolones
FTIR	Fourier-Transform Infrared
	G
GDY	Graphdiyne
	H
HGT	Horizontal Gene Transfer
HRTEM	High-Resolution Transmission Electron Microscopy
HWWTP	Hospital Wastewater Treatment Plant
	I
ICP-OES	Inductively Coupled Plasma Optical Emission Spectroscopy
ICT	Interfacial Charge Transfer
	L

LB	Luria Broth
LC-MS	Liquid Chromatography-Mass Spectrometry
LDPE	Low-Density Polyethylene
LED	Light-Emitting Diode
LPS	Lipopolysaccharides
	M
MGE	Mobile Genetic Element
MIP	Mercury Intrusion Porosimetry
MLs	Macrolides
MO	Methyl Orange
MOF	Metal-Organic Framework
MRSA	Methicillin-Resistant *S. aureus*
	N
NB	Nutrient Broth
NCTC	National Collection of Type Cultures
NIPS	Non-solvent-Induced Phase Separation
NPs	Nanoparticles
	O
OD	Optical Density
OFX	Ofloxacin
	P
PABA	Para-Aminobenzoic Acid
PAHs	Polycyclic Aromatic Hydrocarbons
PAN	Polyacrylonitrile
PBPs	Penicillin-binding proteins
PDI	Polydispersity Index
PDMS	Poly(dimethylsiloxane)
PET	Polyethylene Terephthalate
PLA	Polylactic Acid

PTFE	Polytetrafluoroethylene
PVA	Polyvinyl Alcohol
PVDF	Polyvinylidene Fluoride
PVDF-CTFE	Polyvinylidene Fluoride-co-chlorotrifluoroethylene
PVDF-HFP	Polyvinylidene Fluoride-co-trifluoroethylene
PVDF-TrFE	Polyvinylidene Fluoride-co-trifluoroethylene
R	
RB	Rose Bengal
RhB	Rhodamine B
ROS	Reactive Oxygen Species
RT	Room Temperature
S	
SDGs	Sustainable Development Goals
SDZ	Sulfadiazine
SEM	Scanning Electron Microscope
SF	Silk Fibroin
SFs	Sulfonamides
SLA	Stereolithography
SLM	Sun-mimicking light
SLS	Selective Laser Sintering
SMX	Sulfamethoxazole
SPR	Surface Plasmon Resonance
STEM	Scanning Transmission Electron Microscopy
T	
TA	Terephthalic Acid
TAE	Tris-acetate-EDTA
TBBPA	Tetrabromobisphenol A
TBS	Tryptic Soy Broth
TCs	Tetracyclines

TEM	Transmission Electron Microscopy
THF	Tetrahydrofolic Acid
TIPS	Thermally Induced Phase Separation
TMP	Trimethoprim
TSTP	Tertiary Sewage Treatment Plant
	U
UN	United Nations
USEPA	United States Environmental Protection Agency
UTIs	Urinary Tract Infections
UV	Ultraviolet
UV-Vis	Ultraviolet-visible
	V
VB	Valence Band
VGT	Vertical Gene Transfer
VIPS	Vapour-Induced Separation
	W
WHO	World Health Organisation
WW	Wastewater
WWTP	Wastewater Treatment Plants
	X
XRD	X-ray Diffraction

List of symbols

$\boldsymbol{A}$	Absorbance
$\boldsymbol{X}$	Mechanical Stress
$\boldsymbol{x}$	Mechanical Strain
wt.%	Weight Percentage
$\boldsymbol{\Delta H}$	Melting Enthalpy
$\boldsymbol{\Delta X_c}$	Degree of Crystallinity
F ($\boldsymbol{\beta}$)	β-phase Content
ζ	Zeta Potential

List of Figures

Figure 1.1. Schematic representation of the main routes of antibiotic dissemination, inefficiency of wastewater treatment plants in removing them, promoting the proliferation of antibiotic-resistant bacteria and antibiotic-resistance genes, and routes of human exposure after discharges into aquatic effluents. Adapted from [7]. 2

Figure 1.2. Percentage of household wastewater safely treated in 2020 (%). Adapted from [32]. 4

Figure 1.3. Schematic representation of the different classes of antibiotics. 7

Figure 1.4. Main pathways for the origin of ARB and transmission of ARGs. 11

Figure 1.5. Schematic representation of the photocatalyst reaction mechanism over a semiconductor material in the presence of light radiation in water contaminated with organic pollutants. Adapted from [128]..... 16

Figure 1.6. Mechanism of ROS action in bacterial cells and in genomic DNA. Adapted from [92]..... 18

Figure 1.7. Schematic representation of the chain conformation of (a) PVDF and (b) PVDF-HFP. 27

Figure 1.8. Schematic representation of the chain conformation of silk fibroin..... 28

Figure 1.9. Schematic representation of the methods used for the processing of polymer composite membranes..... 30

Figure 1.10. Illustrative overview and logical sequence of the different chapters that constitute this thesis. 35

Figure 2.1. Schematic representation of the processing of PVDF-HFP membranes incorporating Au-functionalised TiO_2 nanoparticles..... 62

Figure 2.2. TEM images of a) TiO_2 b) Au-TiO_2, and c) Ag-TiO_2; d) XRD diffraction pattern of pristine TiO_2, Au-TiO_2, and Ag-TiO_2 nanocomposites. * and # represents the position where the peaks of Au and Ag should appear; e) FTIR spectra of the synthesised nanocomposites compared with pristine TiO_2 and Quercetin; f) Diffuse reflectance spectra; g) Kubelka–Munk plotsh) ζ potential and i) hydrodynamic size distribution of TiO_2, Au-TiO_2 and Ag-TiO_2..... 69

Figure 2.3. Quantification of a) photogenerated hydroxyl radicals (·OH) and b) singlet oxygen ($^1O_2$) by TiO_2, Au-TiO_2 and Ag-TiO_2 nanoparticles under 60 min of UV radiation. 70

Figure 2.4. Photocatalytic degradation of CIP (5 mg/L), SDZ (15 mg/L), and TMP (10 mg/L) under (a) UV and (b) visible light. Each graph compares the photocatalytic performance of TiO_2, Au-TiO_2, and Ag-TiO_2 over 90 min..... 71

Figure 2.5. SEM images and pore size distribution of PVDF-HFP-based membranes: pristine PVDF-HFP, TiO_2/PVDF-HFP and Au-TiO_2/PVDF-HFP. Surface morphology (500×) and cross-sectional views (250×,

2000×, and 5000×) reveal membrane porosity, pore interconnectivity, and internal membrane structure. 75
Figure 2.6. a) FTIR spectra of PVDF-HFP-based membranes (pristine PVDF-HFP, TiO_2/PVDF-HFP and Au-TiO_2/PVDF-HFP), b) DSC thermograms, c) Young's modulus d) and contact angle..... 77
Figure 2.7. Photocatalytic degradation of CIP, SDZ and TMP using Au-TiO_2/PVDF-HFP membranes under a) UV and b) visible light irradiation over a 600 min period. 79
Figure 2.8. Reusability of Au–TiO_2/PVDF-HFP membranes under a) UV radiation and b) visible irradiation for the degradation of CIP, SDZ and TMP. Each test was performed over three consecutive cycles (1800 min). 81
Figure 2.9. Physicochemical characterisation of the Au-TiO_2/PVDF-HFP membrane before and after three photocatalytic reuse cycles for CIP degradation under UV radiation: SEM images of the cross-section of Au-TiO_2/PVDF-HFP membrane a) before use and b) after use, c) EDX mapping of Ti after reuse (magnification: 250×), showing relative atomic percentages of the key elements; d) contact angle and d) FTIR spectra. 82
Figure 2.10. Proposed degradation pathway for CIP. 84
Figure 2.11. Degradation processes of CIP 1 over time: a). The parent CIP is rapidly eliminated from the solution by the photocatalytic activity of the Au-TiO_2/PVDF-HFP and TiO_2/PVDF-HFP; b) Naturally occurring CIP degradation products are accumulated in samples that are not subjected to photocatalysis. 85
Figure 2.12. Proposed degradation pathway for TMP. 86
Figure 2.13. a) Degradation processes of TMP 1 over time and b) its degradation by-products over the time of the experiments in the samples subjected to photocatalysis. 87
Figure 2.14. Proposed degradation pathway for SDZ. 88
Figure 2.15. Concentrations of SDZ and its degradation by-products over the time of the experiments in the samples subjected to photocatalysis 89
Figure 2.16. Luminescence inhibition (%) of *V. fischeri* after exposure to a) PVDF-HFP, TiO_2/PVDF-HFP and Au-TiO_2/PVDF-HFP membranes; b) photocatalytic degradation of by-products of CIP, SDZ and TMP generated after 600 min using TiO_2/PVDF-HFP and Au-TiO_2/PVDF-HFP composite membranes; c) aqueous solutions of antibiotics at different concentrations: CIP (5, 2.5, 1, 0.5 and 0.25 mg/L), TMP (10, 5, 2.5, 1, 0.5 and 0.25 mg/L), and SDZ (15, 7.5, 5, 2.5, 1, 0.5 and 0.25 mg/L). Measurements were conducted over a 240 min according to ISO 11348. 91

Figure 3.1. Schematic representation of the methodology to develop the PVDF-HFP- and SF-based pristine and nanocomposite membranes. 108
Figure 3.2. a) Low and b) high-magnification TEM images of TiO_2/5-ASA/Ag nanocomposites. c) XRD of TiO_2/5-ASA/Ag nanocomposites. d) Kubelka-Munk transformation of reflection spectra of commercial TiO_2 and synthesised TiO_2/5-ASA and TiO_2/5-ASA/Ag nanocomposites. 111
Figure 3.3. a) Cross-sectional and tilted SEM images of porous membranes composed of PVDF-HFP and SF with TiO_2/5-ASA and TiO_2/5-ASA/Ag fillers. SEM images of controls are at 250x magnification, while fillers are at 1000x magnification. b) Contact angle of the different membranes. 113
Figure 3.4. FTIR spectra of the a) PVDF-HFP-based and b) SF-based membranes; DSC thermograms of the c) PVDF-HFP-based and d) SF-based membranes; e) β-phase quantification and degree of crystallinity of PVDF-HFP-based membranes and f) secondary structures of SF-based membranes disclosed by deconvolution of the amide I bands. 115
Figure 3.5. Photocatalytic degradation of CIP (C_0=5 mg/L) with a) PVDF-HFP and b) SF-based membranes over 600 min of UV irradiation; with c) PVDF-HFP and d) SF-based membranes over 600 min of VIS irradiation. 117
Figure 3.6. Photocatalytic degradation of CIP (C_0=5 mg/L) in three consecutive uses of SF: TiO_2/5-ASA/Ag membranes irradiated for 600 min with a) UV, b) VIS and their respective degradation efficiency (%) in c) and d). 120
Figure 3.7. Antibacterial activity of a) PVDF-HFP-based membranes and b) SF-based membranes in terms of *E. coli* and *S. epidermidis* $\log_{10}$ reduction, and dichlorofluorescein fluorescence intensity in *E. coli* in contact with c) PVDF-HFP-based membranes and d) SF-based membranes, in "normal" conditions and after application of the sun-mimicking light. 122
Figure 4.1. Protocol of the synthesis of Ag-TiO_2. 137
Figure 4.2. Schematic illustration of antimicrobial activity assessment. Sterilised PVDF-HFP-based membranes (pristine and nanocomposites) were 1) placed in contact with *E. coli and* S. aureus suspensions under controlled conditions, followed by serial dilution, plating, and 2) quantification of viable bacteria by CFU counting. 139
Figure 4.3. TEM images of AgNPs synthesised using the flavonoid quercetin and their size distribution histogram. 143
Figure 4.4. Proposed mechanism of the reaction for the synthesis of AgNPs using quercetin. 144
Figure 4.5. Synthesised Ag-TiO_2 nanocomposite. 144

Figure 4.6. Representative TEM images of TiO_2 and Ag-TiO_2 samples prepared with varying Ag concentrations. 145
Figure 4.7. a) XRD patterns of pristine TiO_2 and Ag-TiO_2 nanocomposites with different Ag loadings; b) FTIR spectra of Ag-TiO_2 compared with the spectra of TiO_2 and quercetin; c) UV-Vis reflectance spectra and of Ag-TiO_2 compare with pristine TiO_2; d) Kubelka–Munk plots of Ag-TiO_2 compare with pristine TiO_2 employed to estimate the band-gap energy; e) ζ-potential values of TiO_2 and Ag-TiO_2 samples as a function of pH and f) hydrodynamic size (ζ-average) and polydispersity index (PDI) of pristine TiO_2 and Ag-TiO_2 nanocomposites. 146
Figure 4.8. Photocatalytic degradation of a) CIP and b) TMP using TiO_2 and Ag-TiO_2 samples with different Ag loadings under simulated sunlight irradiation (VIS). 149
Figure 4.9. a) SEM images of PVDF-HFP-based membranes: pristine PVDF-HFP, 20%TiO_2/PVDF-HFP, and 20%Ag-TiO_2/PVDF-HFP. Cross-sectional views (250×, 2000×) revealing membrane porosity, pore interconnectivity, and internal membrane structure. b) DSC thermograms of PVDF-HFP-based membranes (pristine PVDF-HFP, 20%TiO_2/PVDF-HFP, and 20%Ag-TiO_2/PVDF-HFP, c) contact angle, d) FTIR spectra and e) pore size distribution. 152
Figure 4.10. a) Antibacterial activity after 2h in suspension by direct contact with PVDF-HFP membrane (control), and PVDF-HFP loaded with 10% of Ag-TiO_2, 20% of TiO_2, and 20% of Ag-TiO_2 NPs against *E. coli* and *S. aureus*; b) biomass inhibition growth after 24h in contact with the same composite membranes. ns: non-significant; $p < 0.05$ (*), $p < 0.01$ (**), $p < 0.001$ (***), $p < 0.0001$ (****) when compared with each other, and c) representative membranes stained with crystal violet, illustrating the biofilm formation for each sample and visually supporting the quantitative results of biomass inhibition. 155
Figure 4.11. Evaluation of plasmid DNA degradation and loss of functionality under UVA irradiation: a) The percentage of plasmid degradation over time (1.5 h, 3 h, 6 h and 10 h) for the different systems: UVA (photolysis), PVDF-HFP, 20% TiO_2/PVDF-HFP and 20% Ag–TiO_2/PVDF-HFP, $p < 0.05$ (*), $p < 0.01$ (**), $p < 0.001$ (***), $p < 0.0001$ (****) when compared with each other; b) Agarose gel electrophoresis of plasmid DNA samples collected at each irradiation time point; c) LB agar plates containing ampicillin (a selective antibiotic) were used to evaluate plasmid functionality after 6 and 10 hours of irradiation. 157
Figure 4.12. Photocatalytic degradation of a) CIP (5 mg/L) and b) TMP (10 mg/L) under UV irradiation, and c) CIP and d) TMP under visible (VIS) irradiation, for 600 min. Experiments were performed using pristine PVDF-HFP, 20%TiO_2/PVDF-HFP and 20% Ag-TiO_2/PVDF-HFP membranes. Photolysis was included as a control in all tests. 162

Figure 4.13. Reusability of 20%Ag–TiO_2/PVDF-HFP membranes under UV radiation and visible irradiation for the degradation of a) CIP, and b) TMP. Each test was performed over three consecutive cycles (1800 min). 164
Figure 5.1. Geometry of the grids in the slicer for grids with different infills. From left to right, infill densities of 8%, 10%, and 12%. 179
Figure 5.2. Scheme representing the printing process of floating grids of PVDF-HFP and PVDF-HFP/TiO_2 and the salt leaching processes. 180
Figure 5.3. Set up of the UV photocatalytic tests. 181
Figure 5.4. a) Tank containing 300 mL of a 5 mg/L CIP aqueous solution containing the floating grid; b) PVDF-HFP/TiO_2 shown folded, illustrating flexibility; c) Setup of the sunlight irradiation assay, orbital shaker, and tank with the TiO_2 floating grid inside; d) Map and coordinates of the spot where the assay was performed. 182
Figure 5.5. Final printed grids with different infill densities: a) 8%, b) 10%, c) 12%. d1) 10% grid and respective SEM ampliations with 100x magnification (d2) and 250x magnification (d3). 183
Figure 5.6. SEM images of the produced samples: Pristine bottom surface, top surface and cross-section; 3% TiO_2 bottom surface, top surface and cross-section; 10% TiO_2 bottom surface, top surface and cross-section. 184
Figure 5.7. For the different grid samples: a) Contact angle measurements on both surfaces; b) FTIR spectra; c) DSC thermograms; d) Stress-strain graphs. 185
Figure 5.8. Photocatalytic degradation of CIP (5 mg/L) in ultrapure water using TiO_2-immobilised grids under 540 min of UV radiation: a) different grid configuration (8, 10, and 12Inf) with the same TiO_2 loading (10%); b) 10Inf grid configuration with different TiO_2 loading (3,5, and 10%). 188
Figure 5.9. Photocatalytic degradation of CIP (5 mg/L) in three consecutive uses in ultrapure water with 10inf/10%TiO_2 grid under 540 min of UV radiation. 191
Figure 5.10. Photocatalytic degradation of CIP (5 mg/L) with pristine grid, 10Inf, and TiO_2-immobilised grid,10Inf/10%TiO_2 under 360 min of natural sunlight radiation: a) degradation efficiency; b) corresponding kinetic rate. 193

List of Tables

Table 1.1. Presence of antibiotics and their concentrations in wastewater before and after treatment processes and in natural water. N.D. – not detectable, A- Average, BQL – Below quantification limit, CWWTP - conventional wastewater treatment plant, HWWTP - hospital wastewater treatment plant, TSTP - tertiary sewage treatment plant, WW – Wasterwater. 9

Table 1.2. Overview of reported studies on the occurrence and removal efficiencies of antibiotics, ARB, and ARGs in different wastewater treatment processes. 14

Table 1.3. Summary of representative photocatalysts used for the degradation of emerging pollutants. 20

Table 1.4. Catalysts and modified catalysts used for antibiotic, ARB, and ARGs removal; ND- No Data. 24

Table 2.1. Photolysis (600 min) and photocatalytic degradation efficiencies and kinetics degradation of CIP (5 mg/L), SDZ (15 mg/L), and TMP (10 mg/L) under UV and visible light irradiation (VIS), comparing the performance of TiO_2, Au-TiO_2, and Ag-TiO_2 over 90 min..... 72

Table 2.2. Photocatalytic degradation efficiencies and kinetics degradation of CIP (5 mg/L), SDZ (15 mg/L), and TMP (10 mg/L) under UV and visible light, comparing the performance of PVDF-HFP, and Au-TiO_2/PVDF-HFP membranes over 600 min. 78

Table 2.3. Photocatalytic degradation efficiencies and kinetics degradation of CIP (5 mg/L), SDZ (15 mg/L), and TMP (10 mg/L) under UV and visible light, comparing the performance of PVDF-HFP, and Au-TiO2/PVDF-HFP membranes over 600 min. 81

Table 3.1. ICP-OES measuring of Ti and Ag content. 112

Table 3.2. CIP degradation efficiencies (%), apparent reaction rates (kapp) and adsorption (%) under UV and VIS radiation for the different pristine and nanocomposite membranes..... 112

Table 4.1. Band gap energy estimated for the synthesised Ag-TiO_2 nanocomposites compared with TiO_2 nanoparticles..... 148

Table 4.2. Degradation efficiencies (%DE), adsorption capacity (%Ads) and degradation kinetics (k) of TiO_2 and Ag-TiO_2 nanocomposites on CIP and TMP degradation under simulated sunlight radiation. . 149

Table 4.3. Adsorption capacity, photocatalytic degradation efficiencies, and kinetics degradation of CIP (5 mg/L), and TMP (10 mg/L) under UV, comparing the performance of photolysis, PVDF-HFP, 20%TiO_2/PVDF-HFP, and 20%Ag-TiO_2/PVDF-HFP membranes over 600 min. 160

Table 4.4. Adsorption capacity, photocatalytic degradation efficiencies, and kinetics degradation of CIP (5 mg/L), and TMP (10 mg/L) under VIS (simulated sunlight radiation), comparing the performance of photolysis, PVDF-HFP, 20%TiO_2/PVDF-HFP, and 20%Ag-TiO_2/PVDF-HFP membranes over 600 min.. 160

Table 4.5. Reuse of 20%Ag-TiO_2/PVDF-HFP membranes under UV and visible radiation during the degradation of CIP and TMP. Each test was performed in three consecutive cycles (1800 min)..... 163

Table 4.6. Summary of the multifunctional performance of the developed composite membranes, comparing photocatalytic degradation efficiencies under UV and visible radiation for both antibiotics, antimicrobial reduction and biomass inhibition against two different strains, and ARG degradation for PVDF-HFP membranes containing 20%TiO_2 and 20%Ag-TiO_2..... 166

Table 5.1. CIP (5 mg/L) degradation efficiency kinetic rate in ultrapure water under 540 min of UV radiation for pristine grid and TiO_2-immobilised grids with different configurations..... 189

Table 5.2. Comparison of the photocatalytic efficiency of 3D-printed grids with gird/mesh configuration. 190

Table 5.3. CIP (5 mg/L) degradation efficiency and kinetic rate in three consecutive uses with 10Inf/10%TiO_2 in ultrapure water under 540 min of UV radiation. 191

Table 5.4. CIP (5 mg/L) degradation efficiency and kinetic rate with 10Inf/10%TiO_2 in ultrapure water under 360 min of natural sunlight radiation..... 193

Table 5.5. Comparison of photocatalytic efficiency for immobilised floating photocatalytic system based on TiO_2. 194

Table 5.6. Comparison of photocatalytic efficiency for CIP degradation under natural solar radiation 196

CHAPTER 1

INTRODUCTION

The contamination of aquatic systems by antibiotics represents an emerging environmental and public health concern, due to their persistence and their role in the dissemination of antimicrobial resistance. Given the limitations of conventional wastewater treatment processes, there is a clear need for sustainable solutions that can simultaneously address antibiotics, bacteria, and genetic contamination. The current chapter aims to provide a thorough overview of the problem, present the state of the art of the main water treatment technologies, with an emphasis on photocatalysis, establish the scientific basis for the materials developed in this thesis, and outline its objectives and overall structure.

1.1 Motivation

Water pollution represents one of the most critical environmental challenges of the 21st century, impacting ecosystems, human health, and socioeconomic development [1]. Water contamination has been increasing steadily each year, driven by population growth, industrial expansion, and rising human activity [2, 3]. Current projections indicate a significant increase in untreated or insufficiently treated wastewater discharges, from approximately 24% in 2030 to more than 50% by 2052 [4]. This growing issue has attracted global attention and has become a priority for international organisations. The United Nations (UN) has recognised the urgency through Sustainable Development Goal 6, which aims to ensure universal access to clean water and the sustainable management of aquatic resources [5, 6].

Among the various contaminants, Contaminants of Emerging Concern (CECs) are of particular relevance due to their lack of monitoring and persistence in aquatic environments, increasing risks to both ecosystems and human health [8, 9]. Within this class of contaminants, antibiotics are a major concern due to their excessive and still-increasing use in human medicine, veterinary practices, and agriculture [10-12]. Following administration, a significant proportion of antibiotics remains unmetabolised and is excreted, entering wastewater systems, where it persists after treatment (Figure 1.1) [13]. Official estimates suggest that global antimicrobial consumption will increase by 67% between 2010 and 2030 [14].

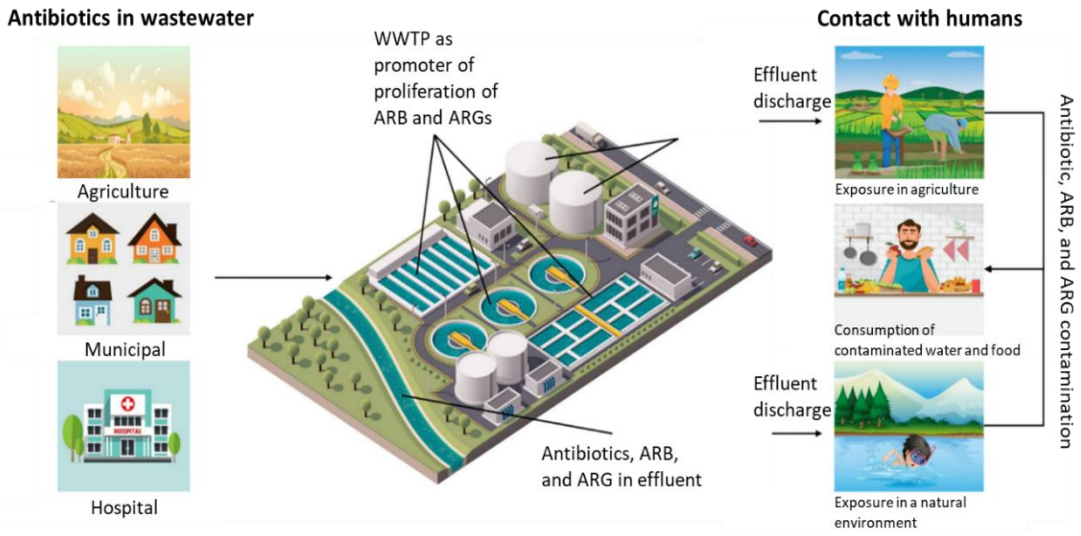


Figure 1.1. Schematic representation of the main routes of antibiotic dissemination, inefficiency of wastewater treatment plants in removing them, promoting the proliferation of antibiotic-resistant bacteria and antibiotic-resistance genes, and routes of human exposure after discharges into aquatic effluents. Adapted from [7].

Along with this increase, the persistence of antibiotics is exacerbated by the limited efficiency of conventional wastewater treatment plants (WWTP), which are not designed to remove such pollutants [15, 16]. As a result, antibiotics are frequently detected in water matrices even after treatment, contributing to their continuous dissemination in the environment, that have been associated with toxic, carcinogenic, and mutagenic effects in aquatic organisms [17].

The presence of antibiotics in all types of water bodies, including drinking water, directly exerts selection pressure on microbial communities, leading to the proliferation of antibiotic-resistant bacteria (ARB) and antibiotic-resistance genes (ARGs) [18, 19]. Given this alarming situation, the World Health Organisation (WHO) has identified ARB and ARG as primary threats to public health in the 21st century [20]. Furthermore, this cycle of contamination leads to human exposure through the consumption of contaminated water and food, as well as contact with the natural environment (Figure 1.1) [21, 22]. If current consumption levels and inadequate water treatment methods persist, antibiotics—one of the foundations of modern medicine—will become ineffective due to the increasing bacterial resistance, resulting in the death of millions worldwide [23]. This highlights the urgent need for effective and sustainable remediation strategies to address these CECs. Despite significant advances in wastewater treatment technologies, conventional methods, such as ultraviolet (UV) radiation, ozonation, biological treatments, or coagulation, remain ineffective at removing these contaminants [24]. Among various strategies, Advanced Oxidation Processes (AOPs), particularly photocatalysis, have emerged as a promising technology with potential to degrade antibiotics and serve as a solution for decontaminating ARB and ARG [25].

One challenge that may limit large-scale implementation of photocatalysis is the use of photocatalytic particles in suspension, which not only complicates recovery and increases operational costs but also raises concerns about particle release and environmental impact [26]. The immobilisation of photocatalysts on polymeric matrices, such as those used in this study, has been demonstrated to prevent the release of nanoparticles into the environment and facilitate the recovery and reuse of the material, thereby enhancing the sustainability and practicality of the process [27].

In this context, the development of advanced composite materials that combine photocatalysts with membrane technology, using natural or synthetic polymers, represents a promising solution for multifunctional water remediation. These systems can simultaneously degrade antibiotics, inactivate bacteria, and eliminate ARGs, addressing several aspects of water pollution. Furthermore, integrating sustainable principles, such as green solvents, renewable energy sources, natural polymers, and three-dimensional (3D) membrane design, creates new opportunities for efficient large-scale applications.

1.2 Water Remediation

The rapid development of technologies during the 20th and 21st centuries has been directly linked to environmental pollution, including contamination of water sources [28]. The combination of the Industrial Revolution, accelerated consumption of fossil fuels, intensive agriculture, exponential growth in chemical development, and natural events has contributed to a frightening increase in toxic pollutants in ecosystems, particularly in drinking water sources [29].

Access to safe drinking water is an essential condition for human health and well-being, as it represents not only an essential element for life but also a critical requirement for sustaining ecosystems. Nowadays, one of the most significant challenges humanity faces is the availability of water and/or its quality [30]. These limitations have caused about 1.5 million deaths related to the consumption of unsafe/contaminated drinking water and unavoidable exposure to pathogens or toxic substances [31].

The inadequate treatment of domestic wastewater has been identified as a contributing factor to water contamination. In many countries, a significant proportion of household wastewater is discharged into the environment without adequate treatment, further increasing the risk of exposure to pathogens and chemical pollutants. As demonstrated in Figure 1.2, in 2020, less than half of the domestic wastewater in 62 of the 128 countries for which data are available was safely treated [32]. Moreover, the contamination of water sources is not confined to inadequately treated domestic effluents.

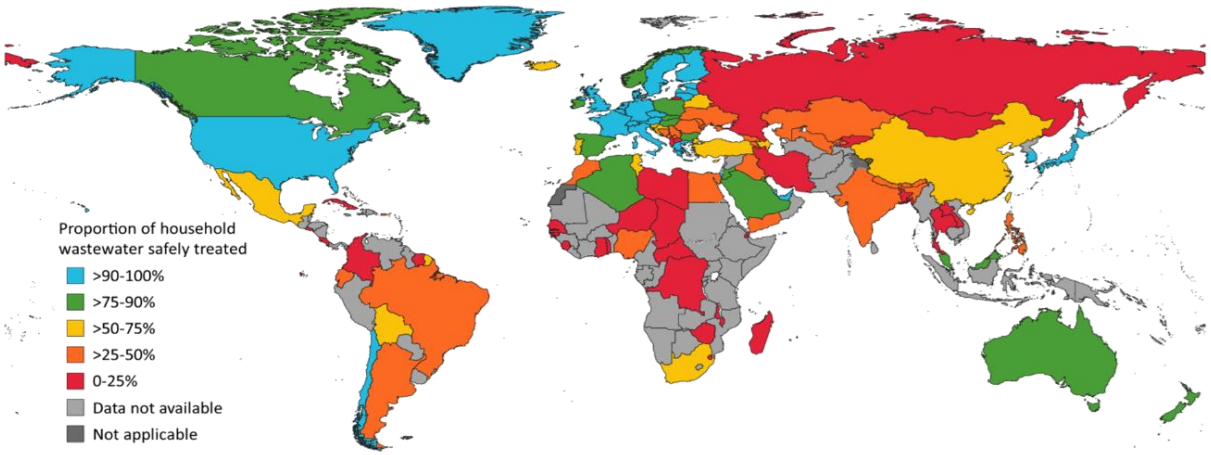


Figure 1.2. Percentage of household wastewater safely treated in 2020 (%). Adapted from [32].

The complexity of water pollutants has increased over time, encompassing both traditional pollutants, including inorganic compounds (e.g., heavy metals and nitrates) and organic compounds (e.g., pesticides

and dyes), as well as a more recent group of substances associated with modern anthropogenic activities [33]. The continuous production and widespread use of pharmaceuticals, personal care products, and other synthetic chemicals have led to the occurrence of "contaminants of emerging concern", which are discharged daily into wastewater and often escape conventional monitoring and treatment processes [9].

Conventional and advanced wastewater treatment plants can effectively address the water disinfection and decontamination of a wide range of inorganic and organic compounds [34]. However, these treatments are not designed to remove this new group of emergent pollutants, as the effectiveness of removal depends on several factors, such as the specificity of the compound and the treatment used, as well as the high complexity and stability of the molecules [35].

1.2.1 Contaminants of Emerging Concern

Considering the current and future pressures on water availability and issues related to its quality, it is urgent to demand sustainable solutions in aquatic remediation, which requires a clear understanding of the CECs, their occurrence, their chemical nature, and their potential impacts on aquatic organisms and human life.

The Network of Reference Laboratories, Research Centres and Related Organisations for Monitoring of Emerging Environmental Substances (NORMAN group) posits that CECs are compounds that are not widely included in standard monitoring programs [36], yet may be regulated in the future, depending on scientific evidence regarding their (eco)toxicity, potential risks to public health, and occurrence data in various environments [34]. These contaminants are characterised by persistence and biotransformation into metabolites or by-products that are equally resistant to degradation [37], largely due to their complex molecular structures, designed to ensure stability under physiological conditions and to confer resistance to environmental degradation [38]. Despite their presence in the environment for decades, the qualitative and quantitative occurrence of these substances has only recently begun to be studied, mainly due to the need for advanced analytical techniques capable of detecting them at very low concentrations (μg/L or ng/L) [39]. The toxicity and ubiquity of these substances are a growing concern, as they accumulate and can cause adverse effects on ecosystems and human health after prolonged exposure.

CECs encompass a wide range of substances, including both natural and synthetic substances, such as pharmaceuticals, cosmetics, personal care products, disinfecting by-products, algal toxins, biocides, and nanomaterials, among others [40]. To date, more than a hundred different compounds have been identified in surface and groundwater, as well as in WWTPs [41]. In recognition of their environmental

relevance, most of the compounds currently included in the European Union's (EU) Watch List are CECs, which are a regulatory and monitoring priority in the EU [42].

Among these, the presence of pharmaceuticals stands out owing to their high consumption volumes, multiple therapeutic applications, and their diverse physicochemical and biological properties [43]. Their occurrence in water bodies has been documented [44]. Diclofenac has been detected in water bodies, with concentrations ranging from 1100 to 1276 ng/L in surface water in Mexico [45], and elevated concentrations of salicylic acid, a skin care product, were detected in influents of wastewater treatment plants in Northwest Ohio (United States) at levels ranging from 433 to 8036 ng/L [46].

One of the primary pathways for pharmaceutical residues to enter the environment is wastewater discharge from hospitals, outpatient clinics, and veterinary facilities [47]. Among these compounds, antibiotics deserve particular attention, not only due to their widespread use and frequent detection, but also because of their critical role in antimicrobial resistance (AR) [48].

Recent global models indicate that approximately 6 million km of rivers worldwide are subject to antibiotic concentrations exceeding the limits for ecosystem protection and resistance promotion, particularly during low-flow conditions. For ciprofloxacin and clarithromycin, for instance, the observed concentrations of these drugs in these rivers were found to be approximately 0.064 µg/L and 0.25 µg/L, respectively, which were frequently exceeded in rivers in Bangladesh, Ghana, Kenya, Nigeria, and Pakistan [49].

This poses a significant public health concern, as recognised by the WHO, which considers AR to be the most pressing current threat to global health, food security, and development. The potential consequences of this resistance include the ineffectiveness of treatments for currently treatable infectious diseases [9], which is classified as the third leading cause of death after cardiovascular disease. It is estimated that in 2019 alone, 1.27 million deaths were attributed to AR infections, with this number predicted to rise to 10 million per year by 2050, far exceeding deaths from cancer [50]. Moreover, the economic consequences are projected to be substantial, with potential losses totalling trillions of dollars and significant financial implications for health systems and agricultural sectors [51].

1.2.1.1 Antibiotics

Antibiotics are a distinct group of CECs that require special attention due to their prevalence, persistence, and direct implications for antimicrobial resistance. A global analysis of antibiotics for human consumption reveals a 16.3% increase between 2016 and 2023 (from 29.5 to 34.3 billion defined daily

doses (DDDs)), with projections indicating a potential growth of up to 52.3% by 2030 if current trends persist [52, 53]. This extensive use significantly increases the likelihood of release into the environment, making them among the most frequently detected drugs in aquatic systems [54].

Antibiotics can be categorised into three distinct classifications: chemical compounds, natural derivatives, and synthetic or semi-synthetic formulations. These compounds can either kill (bactericidal) or inhibit the growth of a microorganism at low concentrations (bacteriostatic). The effectiveness of antibiotics is associated with their capacity to selectively target pathogens, interfering with vital processes of the infectious cell without affecting the host [54, 55].

Antibiotics can be classified into several chemical groups, as shown in Figure 1.3. Distinct structural features and mechanisms of action characterise each group. β-Lactams act by inhibiting bacterial cell wall synthesis by targeting penicillin-binding proteins (PBPs), key components of the bacterial cell wall. Tetracyclines target bacterial protein synthesis, as do the aminoglycosides and macrolides, by interfering at the ribosomal level. In contrast, quinolones and fluoroquinolones interfere with nucleic acid synthesis, indispensable for deoxyribonucleic acid (DNA) replication. Other relevant classes include sulphonamides, which have been demonstrated to alter cellular metabolism [40, 52, 56].

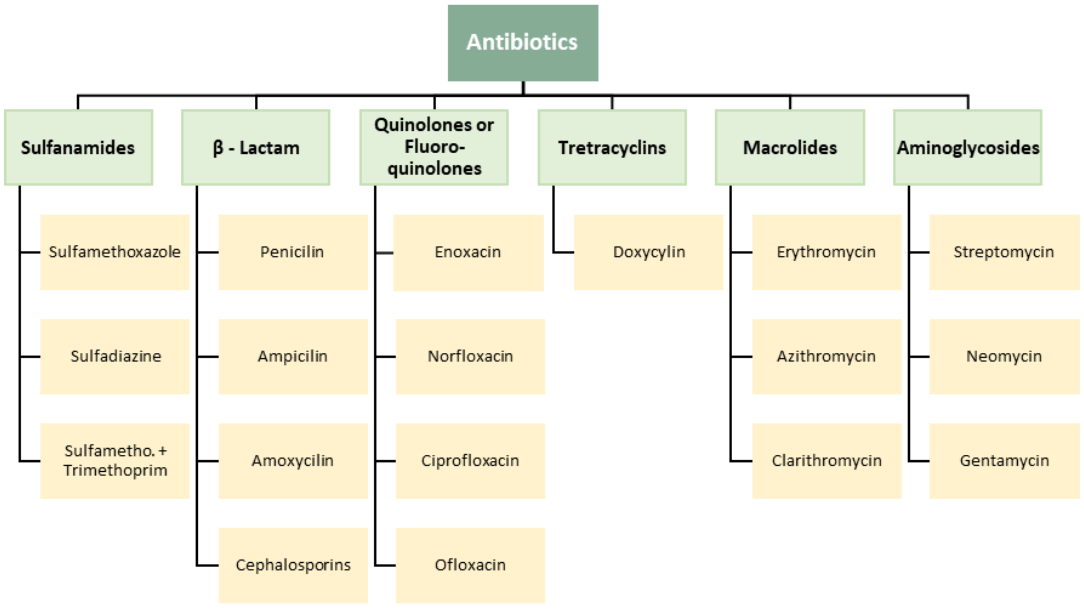


Figure 1.3. Schematic representation of the different classes of antibiotics.

Despite their therapeutic importance, the widespread and often uncontrolled use of these different classes of antibiotics has resulted in their continuous release into the environment. One of the main reasons for this occurrence is incomplete metabolic processing of antibiotics in both humans and

animals, resulting in substantial excretion of the original active principle [57]. A significant proportion of the administered dose (often 30–90%) remains unmetabolised and is excreted, reaching sewage systems and subsequently WWTPs [13]. For instance, up to 60% of ciprofloxacin (CIP) [58] and of amoxicillin (AMX) [59] are excreted unchanged in urine, while sulfamethoxazole (SMX) shows values around 15-30% [60].

Until now, WWTP has mainly focused on removing carbon compounds (such as carbohydrates, proteins, and lipids) and biogenic pollutants [61]. However, conventional treatment methods have been ineffective in eliminating antibiotics, as evidenced by the widespread presence of antibiotics in treated wastewater across many countries (see Table 1.1). The reported concentrations vary depending on the antibiotic class, the type of wastewater treatment plant, and the geographical location. Nevertheless, their persistence in effluents deemed "treated" indicates the limited effectiveness of current processes. Moreover, the ongoing release of antibiotics into the environment continues to exert selective pressure on microbial communities, allowing the development of resistant microorganisms, and highlighting the urgent need for more advanced remediation strategies.

1.2.1.2 Antibiotic-Resistant Bacteria and Antibiotic-Resistance Genes

A direct correlation has been observed between the widespread use of antibiotics and the development of bacterial resistance. The global dissemination of antibiotics has led to the emergence of antibiotic resistance among bacterial populations, thereby selecting and propagating antibiotic-resistant strains [72].

ARB are defined as bacterial strains that can survive and multiply in the presence of antibiotics that would normally inhibit or kill them. The use of these compounds in humans and veterinary medicine, as well as in livestock farming, combined with the current inability of WWTPs to eliminate them, has resulted in microbial communities being continuously exposed to subinhibitory concentrations of antibiotics [73, 74]. This selective pressure promotes survival, allowing bacteria sufficient time and exposure to adapt by altering their cellular mechanisms and genes, thereby developing resistant strains through spontaneous mutations (Figure 1.4) [75].

Table 1.1. Presence of antibiotics and their concentrations in wastewater before and after treatment processes, and in natural water. N.D. – not detectable, A-Average, BQL – Below quantification limit, CWWTP - conventional wastewater treatment plant, HWWTP - hospital wastewater treatment plant, TSTP - tertiary sewage treatment plant, WW – Wastewater.

Class	Antibiotic	Concentration (ng/L)		Treatment	Country, or type of water	References
		Raw Sewage	Treated sewage			
β-Lactams (BLs)	Amoxicillin	6940	50	WWTP	Queensland, Australia	[62]
		-	1670	-	Hong Kong, China –WW	[63]
Aminoglycosides (AGs)	Streptomycin	-	3400	-	Tunisia, sea	[64]
	Neomycin	-	16400	-	Tunisia, WW	[64]
Fluoro-quinolones (FQs)	Ciprofloxacin	107-330 A-221	127- 1396 A-369	HWWTP	Portugal, Coimbra	[65]
		A 320	A 31,5	TSTP	Sweden, Kristianstad City	[66]
	Enrofloxacin	ND-58	ND- 52	CWWTP	Spain, Girona City	[67]
	Ofloxacin	450–2200 (A-1000)	220–520 (A 390)	HWWTP	Italy, North region	[68]
		51.9-4986 A-946	110-366 A-233	HWWTP	Portugal, Coimbra	[65]
Sulfonamides (SFs)	Sulfadiazine	-	ND- 132		Bosnia and Herzegovina, Croatia & Serbia	[69]
	Trimethoprim	2925	876	WWTP	Cilfynydd, Wales	[70]
			350-2550		Bosnia and Herzegovina, Croatia & Serbia	[69]
Tetracyclines (TCs)	Tetracycline	BQL – 32.3	BQL-22.8	HWWTP	Portugal, Coimbra	[65]
Macrolides (MLs)	Clarithromycin	110–780 A-310	260–310 A - 280	HWWTP	Italy, North region	[68]
	Erythromycin	20–300	30–350	CWWTP	Czech Republic, České Budějovice City	[71]
	Azithromycin	79.7 – 295 A-186	93.7-296 A-171	HWWTP	Portugal, Coimbra	[65]

Some pathogenic bacteria have developed resistance, rendering antibiotics ineffective, reducing treatment success, and increasing morbidity and mortality rates. *Klebsiella pneumoniae* (*K. pneumoniae*), commonly found in the mouth, skin, and intestines, includes resistant strains associated with pneumonia, urinary tract infections (UTIs), wound, and respiratory infections [76]. Similarly, resistant *Escherichia coli* (*E. coli*) strains, such as β-lactamase-producing isolates, are major causes of gastroenteritis, UTIs, and neonatal meningitis. A study in India reported that 51.9 % of *E. coli* isolates from hospitalised patients were resistant to cefoxitin, confirming their high prevalence and association with increased mortality rates [77]. Projections estimate that ARB infections will result in 10 million deaths globally by the year 2050 [78].

The existing literature has focused on ARB bacteria such as K. pneumoniae, *Acinetobacter baumannii* (*A. baumannii*) [79], *Staphylococcus aureus* (*S. aureus*) [80], *E. coli* [81], *Enterococcus faecalis* (*E. faecalis*) [82], and *Pseudomonas aeruginosa* (*P. aeruginosa*) [83], which are the most prevalent bacterial species generally found downstream of WWTPs. Several studies have demonstrated that WWTPs act as a dissemination hotspot for ARB into the aquatic environment [84, 85]. For instance, Watkinson *et al.* detected the antibiotic-resistant *E. coli* at concentrations of ≈1,730 colony-forming units (CFU)/100 mL in WWTP discharges near Brisbane, Australia, compared to only ≈22 CFU/100 mL in unaffected sites. In addition to their higher abundance, the ARB from the discharges exhibited higher rates of resistance, especially to tetracycline (51%), cephalothin, and sulfafurazole, compared with less exposed downstream locations [86]. Another study conducted in Germany found significantly higher concentrations of antibiotic-resistant *P. aeruginosa*, *Klebsiella spp.*, *Enterobacter spec.*, and *Citrobacter spec.* in wastewater systems that received different proportions of hospital and municipal effluents. In locations with a strong clinical influence, values for *Enterobacteria spec.* and *P. aeruginosa* exceeded $4\log_{10}$ CFU/mL. The abundance of resistance genes was up to ten times higher in hospital-influenced wastewater than in municipal wastewaters [87].

Consequently, it is demonstrated that WWTP not only release antibiotics and viable microorganisms into the environment, but also contribute to the proliferation of resistant strains, transforming aquatic ecosystems into reservoirs and transmission routes of antibiotic resistance information.

Beyond their existence as resistant organisms, which already pose a public health concern due to their potential to cause infections, ARBs also serve as hosts for antibiotic resistance genes (ARG). A bacterial host cell may acquire antibiotic resistance through three main mechanisms: vertical gene transfer (VGT), spontaneous mutations, and horizontal gene transfer (HGT) (Figure 1.4). VGT occurs when ARGs are passed during bacterial reproduction. Spontaneous mutations arise as single-nucleotide polymorphisms

caused by errors during DNA replication and expand under selective pressure. Conversely, HGT is the process by which ARGs are transferred between different bacterial cells, and it is hypothesised that HGT plays a significant role in the spread of ARGs, particularly in wastewater treatment environments [7].

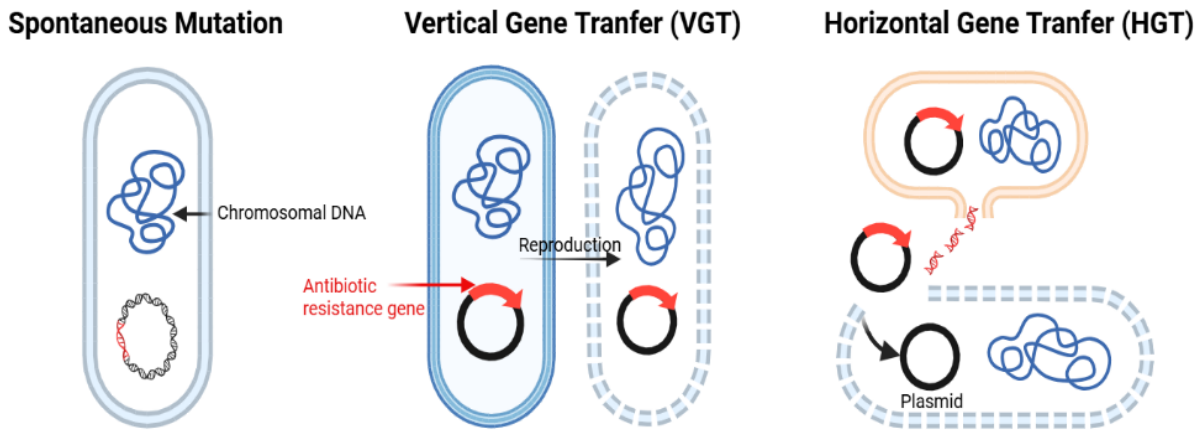


Figure 1.4. Main pathways for the origin of ARB and transmission of ARGs.

ARGs are often found within mobile genetic elements (MGEs), such as plasmids, integrons, and transposons, which aid their transfer across different bacterial species. This mobility allows resistance genes to spread beyond their original host, increasing the risk of reintroduction into human and animal populations via water use, irrigation, aquaculture, and direct contact. As a result, even without selective pressure from antibiotics, ARGs can persist in the environment, representing a long-term, persistent threat to public health.

Numerous studies have documented the presence of ARGs in both raw sewage and treated wastewater, indicating resistance to nearly all the most prescribed and used antibiotics across the healthcare, veterinary, and livestock sectors [7]. For example, β -lactam resistance genes (e.g., *blaCTXM*, *blaTEM*)[88], sulfonamide resistance genes (e.g., *sul1*, *sul2*)[89], tetracycline resistance genes (e.g., *tetO*, *tetQ*, *tetW*)[90], and macrolide resistance genes such as *ermB* are among the most commonly identified in WWTPs [91]. A more detailed review of the available reports highlights the existence of additional ARGs that provide resistance to quinolones, macrolides, and trimethoprim.

Currently, ARB and ARGs are not included in the control parameters for water and wastewater treatment systems, as there are no regulations or recognised standards for antimicrobial resistance. As stated in Section 1.2.1, antibiotics are already included in the "European Union's Watch List", to improve the monitoring of antimicrobial substances in aquatic ecosystems, the European Water Framework

Directive (2000/60/EC) still focuses on hazardous and priority substances, excluding the monitoring of ARB and ARGs [73].

Therefore, it is urgent to assess current treatment methods and develop advanced strategies that can effectively mitigate the persistence and dissemination of these contaminants of emerging concern.

1.3 Conventional Wastewater Treatment Strategies

Wastewater disinfection processes were introduced to eliminate micropollutants and protect public health and the environment. The first documented case of disinfection dates to the 19th century, when chlorine was first used as a wastewater disinfectant in London in 1854 [92]. Despite this long history and evolutionary development, WWTPs still prioritise the removal of organic matter and nutrients, and they are not precisely designed to eliminate this new class of persistent emerging pollutants with high molecular complexity [35]. As shown in Table 1.2, several studies conducted worldwide have demonstrated that, despite advances in disinfection technologies, conventional wastewater treatment processes are unable to guarantee the complete removal of antibiotics, ARBs, and ARGs.

Conventional wastewater treatment includes biological treatments, sedimentation, filtration, and chemical disinfection. The most common methods of disinfection to remove organic pollutants and microorganisms are UV irradiation and chlorination [93]. Many pharmaceuticals can absorb radiation, usually in the UV spectrum, and photodegrade. However, the degradation efficiency of drugs varies among different classes of pharmacologically active compounds (β-blockers < analgesics < antibiotics < pesticides), making the method ineffective against antibiotics [94]. Chlorination, although it effectively inactivates pathogens, can also promote resistance by increasing the abundance of ARGs and facilitating HGT. As reported in Table 1.2, in Las Cruces, Mexico, it has been found the persistence and increase of resistance to antibiotics such as ampicillin, ciprofloxacin, and tetracycline [95].

Biological treatments, such as the activated sludge process, have limited effectiveness due to the reduced ability of microorganisms to metabolise most compounds for use as a carbon source [96]. Consequently, antibiotics such as tetracyclines, macrolides, trimethoprim, and fluoroquinolones have been shown to persist in wastewater [63] (Table 1.2). However, alternative approaches, as the use of enzymes, also face practical obstacles, including high processing costs, operational instability, and intolerance to adverse environmental conditions. The inherently low biodegradability of many antibiotics further exacerbates these limitations [52].

Membrane technologies— including reverse osmosis, nanofiltration, and ultrafiltration—have demonstrated a high contaminant removal efficiency [97]. However, the applicability of these membranes is restricted by critical limitations. Specifically, pollutants are not destroyed; instead, they accumulate in the membranes, leading to fouling and frequent replacements that increase operating costs [98]. Furthermore, the complexity of wastewater requires the implementation of combined or multi-stage systems to achieve adequate treatment performance, restricting the large-scale implementation of membrane-based technologies.

In response to these limitations, innovative strategies have been explored, including adsorption, electrochemical oxidation, and AOPs. Although these approaches offer greater removal efficiency, they also present challenges in terms of cost, energy demand, secondary waste generation, and scalability [103]. The most widely applicable technology is the adsorption of antibiotics with activated carbon-based compounds or other adsorbents [104]. The technology has been demonstrated to be effective against sulphonamides, tetracyclines, beta-lactams, and nitroimidazole antibiotics, with materials such as carbon-based materials [105], silica-based materials [106], and metal oxides [107]. Nevertheless, this method merely transfers pollutants from water to solid waste, with low removal efficiency, slow removal rate, and complex material recovery [108]. Electrochemical oxidation has also shown promising results, such as the degradation of 95% of levofloxacin (500 mg/L) using a lead dioxide (PbO_2) electrode. However, it employs unaffordable materials and presents a slow mass transfer [109].

The contrast between the limited performance of conventional methodologies and the incomplete solutions offered by innovative alternatives reinforces the need to adopt treatment technologies that are both efficacious and sustainable. In most cases, current methods only transfer pollutants to a different phase without degrading them, while still facing challenges such as high cost-benefit, fouling, or even the promotion of antimicrobial resistance [110]. Thus, it is essential to develop strategies capable not only of removing but also of efficiently degrading antibiotics, resistant bacteria, and resistance genes. In this context, AOPs emerge as up-and-coming alternatives, offering the capacity to mineralise persistent contaminants [111] and providing a practical option for the decontamination of ARB and ARG, overcoming many of the limitations associated with traditional strategies [25].

Table 1.2. Overview of studies on the occurrence and removal efficiencies of antibiotics, ARB, and ARGs with different wastewater treatment processes.

Location	Wastewater type	Treatment process	Contaminants	Main findings	References
European countries (UK, France, Turkey, Austria, Norway, Portugal, Germany, Netherlands, Italy)	Municipal domestic sewage and industrial wastewater	Conventional microbial treatment processes	*bla*$_{TEM}$, *bla*$_{OXA-48}$, *bla*$_{OXA-58}$, *bla*$_{CTX-M-15}$, *bla*$_{CTX-M-32}$, *bla*$_{KPC-3}$, *sul*1, *tet*M and *mcr*-1	ARGs abundance ranking after treatment: *sul*1 > *tet*M > *bla*$_{OXA-58}$ > TEM > *bla*$_{OXA-48}$ > *bla*$_{CTX-M-32}$ > *mcr*-1 > *bla*$_{CTX-M-15}$ > *bla*$_{KPC-3}$.	[99]
Hong Kong, China	*Sewage treatment plant*	Activated Sludge and Sedimentation	Erythromycin, trimethoprim, norfloxacin, ofloxacin, and oxytetracycline	Even after primary and secondary treatments, removal efficiency was under 50 %.	[63]
Netherlands	Municipal domestic sewage and industrial wastewater	Conventional microbial treatment processes	*E. coli, ermB, sul1, sul2, tetM, qnrS, bla*$_{CTXM}$	The removal effect of ARGs was not significant and persists after treatment.	[100]
Las cruces, New Mexico, United States of America	Wastewater effluent from WWTP	Primary settling tank, trickling filter, activated sludge, chlorination	qnrA, qnrB, qnrC, qnrS, tetW, tetM, tetO, sul1, sul2, ermB, blaTEM, intI1	Secondary treatment increased ARG abundance, while disinfection reduced their levels but broadened host range, and chlorination increased ARB in the effluent.	[95]
Italy	WWTP	Chlorination, peracetic acid (PAA), and UV radiation	tetA, ermB, blaTEM, qnrS	PAA removed bacterial cells but promoted a microbial community even more resistant to antibiotics	[101]
Wenchan Harbin, China	Effluent of WWTP	Activated sludge process (ASP), modified trickling filter (MTF), and anaerobic reactors (anaerobic flow-through reactor	total coliform, faecal coliform, extended-spectrum beta-lactamase, and carbapenem-resistant bacteria	Aerobic reactors were more effective at removing ARB (~1.5–2 log reduction) than the anaerobic reactors (~0.5 log reduction) at all tested HRT values.	[102]

1.3.1 Advanced Oxidation Processes for antibiotics, ARB, and ARG removal

In recent years, AOPs have gained significant attention in the treatment of organic pollutants due to their high reactivity, efficient removal capabilities, and environmental friendliness [112]. These processes involve the production of reactive oxygen species (ROS) with potent oxidising properties, such as $O_2^{\bullet-}$ and $OH^{\bullet}$, which are non-selective. ROS can attack a broad spectrum of organic contaminants, breaking down complex molecules and mineralising into carbon dioxide (CO_2) and water (H_2O) [113]. This ability makes AOPs particularly attractive for the degradation of recalcitrant pollutants such as antibiotics, the inactivation of ARB, and the removal of ARG, making it a suitable process for wastewater treatment and disinfection [114, 115]. Selecting an appropriate method is crucial to improving the remediation effects of AOPs. Different AOP processes include ozonation, Fenton/Fenton-like, ultrasonic irradiation, and photocatalysis [116].

Despite their promising potential, the large-scale applications remain restricted. The challenges associated with this process include high operating costs, the need for chemical reagents (e.g., H_2O_2 or Fe^{2+}), energy-intensive requirements, and the generation of secondary waste streams that require additional treatment [117]. These limitations hinder their implementation in wastewater treatment facilities, where cost-effectiveness and operational simplicity are paramount [118].

Among the various AOPs, heterogeneous photocatalysis, also known as photocatalysis, stands out as an attractive option. It combines photochemical stability with sustainable cost-effectiveness, while maintaining high degradation efficiency even under variable environmental conditions [119, 120]. This process is a promising candidate for future wastewater remediation technologies, given that it has the potential to remove emerging contaminants from effluents [94].

1.4 Photocatalysis

The term "photocatalysis" was first introduced by Plotnikow in 1910 to describe radiation-induced catalytic processes using a photocatalyst [121]. Since then, its efficiency has been proven in the treatment of effluents and the decomposition of organic pollutants [122]. Among the various AOPs, photocatalysis is the most used in degrading organic pollutants and is a process about which the scientific community's interest has intensified in recent years [123, 124]. The simplicity and efficiency of this technique can be attributed to its requirement for only radiation light and a photocatalyst, making it a simpler approach than related techniques. Moreover, its energy demand can be met by renewable solar radiation [125].

The photocatalytic process, illustrated schematically in Figure 1.5, consists of three stages: *1) Excitation*: under radiation with equal or higher energy than its bandgap, the semiconductor absorbs the energy that will allow the transition of an electron ($\boldsymbol{e^-}$) from the valence band (VB) to the conduction band (CB), creating a hole ($\boldsymbol{h^+}$) in the VB. *2) Charge Migration:* the photogenerated charges ($\boldsymbol{e^-/h^+}$) migrate to the surface of the semiconductor. *3) Oxidation*: at the surface, these charges induce redox reactions, where they can react with adsorbed molecules [126-128].

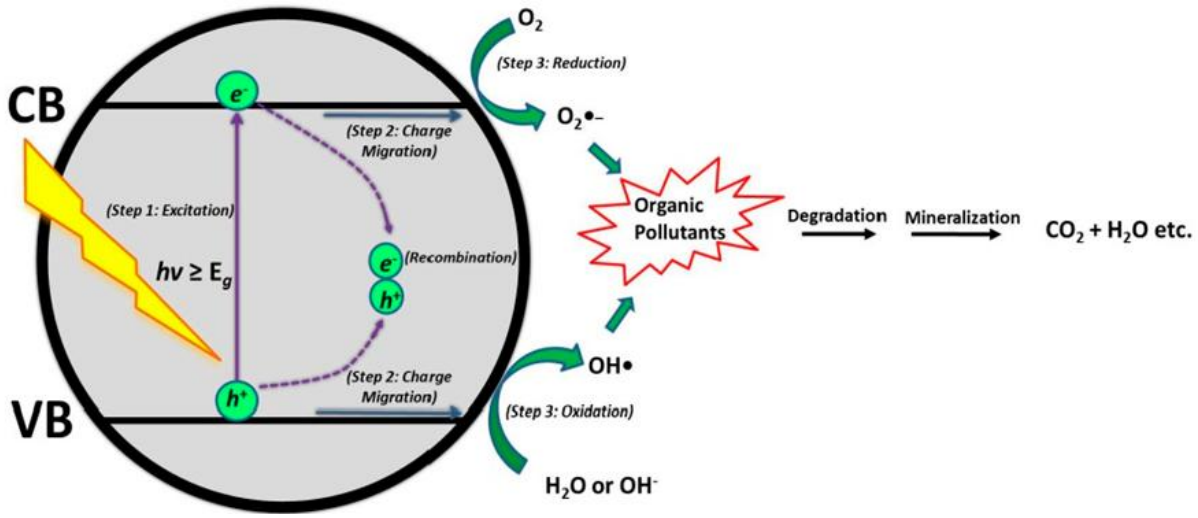


Figure 1.5. Schematic representation of the photocatalyst reaction mechanism over a semiconductor material in the presence of light radiation in water contaminated with organic pollutants. Adapted from [128].

The holes possess positive charges, which react with water to produce hydroxyl radicals (OH•) and hydrogen ions ($\boldsymbol{H^+}$.) On the other hand, under aerobic conditions, electrons react with the dissolved oxygen in the water, forming superoxide anions ($\boldsymbol{O_2^-}$•). These react with water molecules to produce hydroxide ions ($\boldsymbol{OH^-}$and peroxide radicals (•OOH) [125, 129, 130]. The produced peroxide radicals combine with $\boldsymbol{H^+}$ions to form OH• and $\boldsymbol{OH^-}$. The holes can oxidise $\boldsymbol{OH^-}$ to OH• and oxidise organic pollutants. Subsequently, all species contribute to the production of OH•, the main responsible species in the degradation of contaminant molecules present in an aqueous solution [131, 132].

In general, these pathways highlight two parallel oxidation routes: (1) oxidation by $\boldsymbol{OH}$• radicals in solution, relevant for weakly adsorbed pollutants, and (2) direct oxidation of strongly adsorbed species at the surface of photocatalysts by photo-induced holes. Both processes ultimately mineralise organic pollutants into CO_2, water, and inorganic by-products [133-135].

Another critical aspect in photocatalyst degradation studies is reaction kinetics [136]. Most investigations report that heterogeneous photocatalysis follows the Langmuir-Hinshelwood (L-H) model, which can be simplified to pseudo-first-order or zero-order kinetics, depending on the experimental conditions [129, 131, 137]. The initial concentration of the pollutant is found to be a key factor in this process, with elevated levels saturating the catalyst surface and leading to zero-order kinetics, in which the rate is independent of mass transfer limitations. At lower concentrations, the kinetics are frequently described as pseudo-first-order, in which the reaction rate depends solely on mass transfer, regardless of the initial concentration [138].

The classic L-H model is typically used to estimate the kinetics of photocatalytic materials if the catalyst has attained adsorption/desorption equilibrium with the reactants. The general L–H rate expression is given by Eq. 1.1 [139, 140]:

$$\boldsymbol{r = -\frac{dC}{dt} = \frac{k_r K_L C}{1+K_L C}} \qquad \text{Eq. 1.1}$$

Where $\boldsymbol{r}$ is the degradation rate, $\boldsymbol{k_r}$ is the reaction rate constant, $\boldsymbol{K_L}$ is the Langmuir adsorption constant, and $\boldsymbol{C}$ is the contaminant concentration.

For dilute systems, where $\boldsymbol{K_L C}$ 1, the equation reduces to the pseudo-first-order expression (Eq. 1.2), which upon integration yields Eq. 1.2 [140] and Eq.1.3 [141]:

$$\boldsymbol{r = -\frac{dC}{dt} = kC} \qquad \text{Eq. 1.2}$$

$$\boldsymbol{C = C_0 e^{-kt}} \qquad \text{Eq. 1.3}$$

Here, $\boldsymbol{k}$ represents the apparent first-order rate constant ($\boldsymbol{k = k_r K_L}$). It should be emphasised that this model assumes adsorption–desorption equilibrium between pollutants and the catalyst surface and therefore cannot accurately describe systems where the contaminant does not adsorb efficiently. Nevertheless, the L–H model remains widely applied due to its simplicity and suitability under low contaminant concentrations, where catalyst saturation is avoided [129, 142].

Although it provides valuable insights, the L–H model disregards several mechanistic steps that may influence photocatalysis, such as: (i) electron–hole generation in the semiconductor, (ii) charge carrier recombination, (iii) trapping of photogenerated holes at surface states, and (iv) reduction of oxygen by

conduction band electrons. Despite these limitations, it remains a valuable reference framework for evaluating photocatalytic degradation kinetics [131, 143].

Although kinetic models, such as the L-H model, help describe the photocatalytic degradation rate, they do not capture the full mechanisms and events that constitute the process. The core of these mechanisms lies in the generation of ROS, which acts as the predominant factor of the photocatalytic activity [128].

The ROS generated in the photocatalyst process are potent oxidants, allowing the cleavage of stable bonds in organic molecules and, therefore, the degradation of antibiotics and other persistent contaminants [144]. At the biological level, these species have also been proven to inactivate bacteria without the need for additional chemical oxidants [72, 145]. The mechanisms involved in this process, illustrated in Figure 1.6, include (1) damage of the cell membrane, (2) protein denaturation or changes in protein structure and function, (3) inhibition of enzymatic activity, (4) fragmentation of peptidoglycan, causing more cell permeability, (5) mutation and interference with replication and transcription processes, and ultimately leading to (7) cell death [92].

Nevertheless, bacterial lysis can result in the release of intracellular material, including resistance genes, into the surrounding environment. In this context, ROS can also play a crucial role, as they can oxidise and fragment DNA (8), promoting chain breaks and degrading genetic material before it becomes available for HGT [146]. Both photocatalytic degradation mechanisms are illustrated in Figure 1.6.

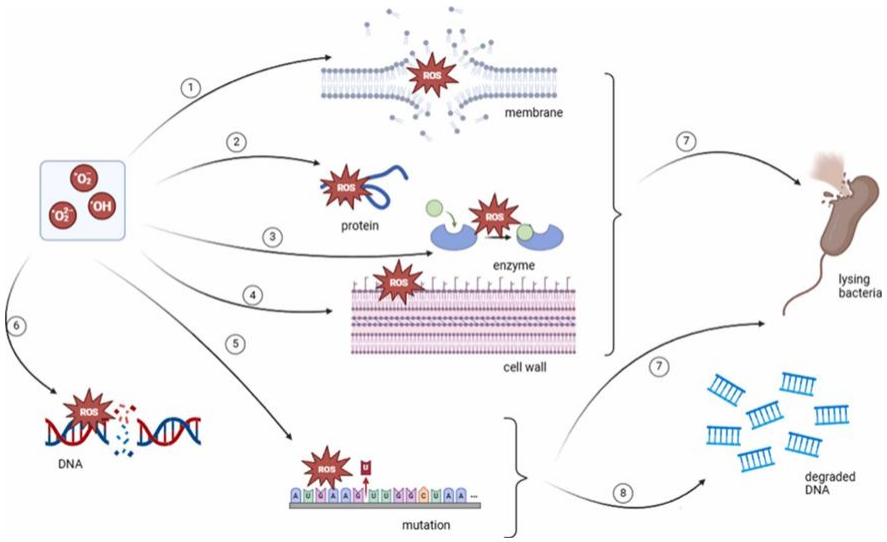


Figure 1.6. Mechanism of ROS action in bacterial cells and in genomic DNA. Adapted from [92].

Thus, photocatalysis is a versatile process that operates on three distinct contaminants: degradation of antibiotics, inactivation of ARB, and elimination of ARG, positioning this approach as an effective strategy against different types of CECs and opening the possibility of newly developed materials acting in a multifunctional removal mode.

1.4.1 Photocatalysts

Conventional photocatalysts have been studied for the remediation of emerging pollutants. Metal oxides have been the most frequently reported materials within this class, including titanium dioxide (TiO_2) [147], zinc oxide (ZnO) [148], hematite (Fe_2O_3) [149], and zirconium oxide (ZrO_2), among others [150]. These materials have attracted attention for their numerous advantages, including stability, cost-effectiveness, and eco-friendliness [151].

Among the materials most frequently used in photocatalysis, TiO_2 and ZnO are the most widely studied concerning photocatalytic applications for aquatic remediation [116]. TiO_2 is a transition metal oxide that exists in three primary forms: anatase, rutile, and brookite. Anatase is known to exhibit superior photocatalytic activity. The band gaps of these forms are 3.2 eV (anatase) and 3.0 eV (rutile), which restricts absorption to the UV region [152]. ZnO has a similar band gap of 3.4 eV, which is notable for its optoelectronic and photocatalytic properties. In fact, ZnO has been observed to outperform TiO_2 in degrading certain contaminants. However, TiO_2 stands out due to its stability, low cost, and non-toxicity [153]. These properties set it apart from other photocatalysts, such as cadmium sulfide (CdS) and ZnO, which are susceptible to photo-corrosion [154]. Despite its robustness and reusability without loss of efficiency, TiO_2 has limitations, including its low utilisation of visible radiation and a high electron/hole recombination rate. These limitations have driven extensive research into modification strategies, including metal/non-metal doping and heterojunction engineering, to enhance its efficiency under solar irradiation [152].

In recent years, new types of photocatalysts have been developed based on advanced structural designs and architectures, gaining prominence. The evolution of this technology has progressed from the use of pure semiconductors to complex systems for combining complementary functionalities. Two-dimensional (2D) materials, including graphene oxides and carbon-based materials such as g-C_3N_4 and derivatives, have attracted considerable attention due to their high surface area and short electron transport paths, which facilitate charge separation [155]. Similarly, metal-organic frameworks (MOFs) offer a unique degree of tunability through their porous structure, adjustable bandgaps, and ease of functionalisation [156]. Furthermore, hybrid heterostructures combining 2D materials, MOFs, metal

sulphides [157], bismuth-based materials [158], and conductive polymers have been reported to enhance visible light absorption and pollutant mineralisation [151]. To summarise the main characteristics and comparative advantages of the photocatalysts discussed, Table 1.3 provides an overview of the main classes of materials reported for the degradation of organic pollutants. These are divided into two categories: classical metal oxides and emerging photocatalysts.

Table 1.3. Summary of representative photocatalysts used for the degradation of emerging pollutants.

	Photocatalyst	Bandgap (eV)	Main advantages	Main limitations	Reference
Metal Oxides	TiO_2 (anatase)	3.2	Chemically stable; Low cost; Non-toxic; Reusable	Poor visible light absorption; Fast e^-/h^+ recombination	[159]
	ZnO	3.4	High activity; Easy synthesis; Strong oxidation power	Photo corrosion; Low visible-light response	[148]
	Fe_2O_3	2.7	Narrow bandgap; abundance; Non-toxic	Low conductivity; High recombination	[149]
	ZrO_2	5.0-5.5	High chemical and thermal stability; Non-toxic; Corrosion resistance	Wide bandgap; Low isolated photocatalytic activity; High e^-/h^+ recombination	[160]
	WO_3	2.6-2.8	Good visible light absorption; Stable in acidic environments; High oxidative potential	Low conductivity; Unstable in alkaline environments; Rapid recombination	[161]
	CuO	1.2-1.9	Visible light absorption; Low cost; Good conductivity; Antibacterial effect	Photo corrosion; Aqueous instability; Release of toxic Cu^{2+} ions	[162]
Emerging Photocatalysts	Carbon-Based (g-C_3N_4, carbon nanotubes (CNTs), graphene oxide	2.7-	Excellent electron transport properties; Tunable electronic properties; Good stability under visible light	Agglomeration; Inactive alone (needs coupling), complex synthesis	[155, 163]
	MOFs (MIL 125, ZIF-67, UiO-66, PCN-244)	2.5-3.5	Tunable structure; Large surface area; Excellent light absorption capacity (UV-Visible)	Poor water stability; High synthesis cost	[164-167]
	Metal Sulfides (CdS, PbS, MoS_2 and ZnS)	1.5-2-5	Good visible light absorption; High quantum efficiency; Lower bandgap energy	Photo corrosion; Potential toxicity; Low photoelectrochemical stability	[157]
	Bismuth-based ($BiVO_4$, BiO_2WO_6, Bi_2S_3)	2.4-2.6	Effective photon irradiation (visible and UV); High and rapid photocatalytic performance; Narrow bandgap energy	Limited surface area; Possible photo corrosion	[158, 168]

Although several emerging photocatalysts exhibit enhanced activity under visible light and offer structural versatility, many of these materials are characterised by instability in aqueous environments, intricate or expensive synthesis procedures, and issues related to scalability or secondary environmental risks, such as the leaching of toxic components. Conversely, metal oxides, most notably TiO_2, remain the standard due to their optimal balance of efficiency, cost-effectiveness, robustness, and reduced ecotoxicity.

These characteristics justify the continued interest in optimising TiO_2 rather than replacing it, especially through modifications that overcome its limitations, such as its activation under visible light.

1.4.2 Strategies to Enhance Visible-Light Absorption in Photocatalysts

Conventional semiconductors, such as TiO_2, are limited in their capacity to absorb visible radiation, restricting their photocatalytic efficiency. Given that only 2-5% of solar energy falls within the UV spectrum, it has become essential to extend the activity of the photocatalyst to the visible light spectrum for solar-powered energy applications [169].

Different strategies have been developed to expand light absorption and enhance charge-carrier dynamics and surface reactivity [170, 171].

Doping is one of the most widely used approaches. The incorporation of non-metallic elements (e.g., nitrogen [172] and carbon [173]) creates states located above the valence band, narrowing the band gap and allowing the absorption of visible photons [174]. Metallic dopants (e.g., Ag [175], Au [176], Pt [177], Fe [178], Cu [179], Cr [180], Mg [181], Sn [182]) can also promote visible light activation by reducing the band gap and, more importantly, capturing electrons, which delays recombination and prolongs the lifetime of charge carriers [183].

Nanocomposites represent another significant category. In these systems, photocatalytic domains are combined with metals or carbon-based materials [184, 185]. For instance, the deposition of noble metals (e.g., Ag [186] and Au [187]) on TiO_2 has been shown to form Schottky junctions, thereby facilitating the separation of electrons and holes [188]. In addition to charge separation, noble metals are associated with surface plasmon resonance (SPR), in which visible light excites conduction electrons on the metal surface, generating hot electrons that can be transferred across Schottky junction barriers into the semiconductor conduction band. This dual effect increases the lifetime of the charge carrier, broadens the photo response to the visible spectrum, and enhances photocatalytic efficiency. Similarly, the combination of semiconductors with carbon-based materials, such as graphene [189] or carbon

nanotubes [190], has been shown to provide efficient electron pathways, thereby enhancing charge mobility.

Heterojunctions, or coupling with other semiconductors (e.g., SnO_2 [191], WO_3 [192], ZnO, and CdS [193]) have also proven to be effective. In these systems, band alignment enables directional electron and hole transfer between semiconductors, thereby reducing recombination and extending photocatalytic activity.

Finally, surface modification strategies [194], including sol-gel synthesis [195] and deposition of porous or nanostructured architectures [196], aim to optimise surface properties. Increased roughness and porosity improve adsorption capacity, while adapting hydrophilicity, surface charge, or oxygen affinity (e.g., through the incorporation of polytetrafluoroethylene (PTFE)) can further enhance interaction with pollutants and redox efficiency [197].

The diversity of modification strategies described above has been extensively evaluated in experimental studies targeting antibiotics, ARB, and ARG. In summary, Table 1.4 has been compiled to facilitate comparison of the practical results obtained with modified photocatalysts for CEC degradation under defined conditions. For instance, MOF-based MIL-88A completely degraded tetracycline under visible light [198], while Mn–WO_3 nanoparticles achieved full removal of SMX in 60 min under light-emitting diode (LED) irradiation [199]. Beyond antibiotics, metal-doped semiconductors have demonstrated remarkable antibacterial performance: Ag–TiO_2 composites completely inactivated *E. coli* [200, 201], whereas Ag-doped TiO_2 prepared by sol–gel showed moderate activity against *K. pneumoniae* [202]. More recently, hybrid systems have simultaneously targeted antibiotics, ARB, and ARGs. For instance, Ag/AgBr/g-C_3N_4 achieved a 7-log reduction of tetracycline-resistant *E. coli* while also degrading multiple resistance genes under visible light [203]. Overall, these studies emphasise the importance of catalyst modification (metal doping, MOFs, heterojunctions) but also reveal limitations related to dosage, irradiation time, and reusability.

Besides the limited photocatalyst activation under visible light, another challenge is the recovery of particles after water treatment. Although these catalysts demonstrate potential for degrading pollutants, as evidenced in Table 1.4, their practical application is constrained by material recovery, potential for leaching into the environment, and the costs associated with recovery processes [204]. Immobilising photocatalysts in solid matrices offers several advantages, including eliminating post-use separation processes, reducing secondary contamination, and improving cost-effectiveness [205]. Several materials can be employed as immobilisation supports, such as polymeric membranes (e.g., polyacrylonitrile (PAN)

[206], polyvinylidene fluoride (PVDF) [207], or chitosan [208]) and inorganic substrates (e.g., glass [209], silica [210], or alumina [211]).

As previously stated in Chapter 1.3, conventional membranes, when used exclusively as physical barriers, exhibit limitations in water treatment. However, their combination with photocatalysis creates a hybrid system that simultaneously retains the active material and degrades pollutants. This synergy enhances the sustainability and reuse of the active material, unlocking the development of advanced membrane technologies for aquatic remediation.

1.5 Advanced Membrane Technology

The immobilisation of the photocatalyst is a suitable option for enhancing the degradation system, preventing the release of particles into the environment, and enabling the material to be reused without the necessity for complex separation or recovery processes [221].

For effective immobilisation of the photocatalyst material, it is crucial to consider key conditions for selecting and processing the matrix. In pursuit of an ideal support system, it is essential to have 1) a strong adhesion between the catalyst and the matrix; 2) high specific surface area, facilitating the interaction with the pollutant; 3) maintenance of catalyst activity after the immobilisation process; 4) strong adsorption affinity for pollutants; 5) stability of the physical-chemical properties of the catalyst even after immobilisation [222].

Despite the operational and environmental advantages of immobilisation, it can lead to significant reductions in photocatalytic efficiency, mainly due to the decrease in available surface area, limitations in mass transfer, and reduced exposure of active catalytic sites to light radiation [116, 120, 223]. However, several studies have demonstrated the continued potential of immobilising photocatalysts, particularly in the context of water remediation [224-227].

A range of materials has been investigated as supports for photocatalyst immobilisation [205, 222]. These include inorganic matrices such as ceramics, glass [209], silica [210], and metal oxides [211], which offer excellent thermal and chemical stability. However, processing these materials often requires complex methodologies, offering limited flexibility for surface property modification [228].

.

Table 1.4. Catalysts and modified catalysts used for antibiotic, ARB, and ARGs removal; ND- No Data.

	Target Pollutant	Catalyst	Specifications/ synthesis technique	Dosage	Degradation efficiency (%)	Catalyst dosage	Illumination type/time (min)	Reference
Antibiotics	Tetracycline (TC)	MOF MIL 88A	hydrothermal method	200 mg/L	100	1.0 g/L	Vis; 80 min	[198]
		TiO_2	Commercial	40 mg/L	50	0.5 g/L	UV-A lamp; 120 min	[212]
	Sulfamethoxazole	Nitrogen-doped ZnO	Nanoparticles	30 mg/L	97	300 mg/l	Xenon lamp; 120 min	[213]
		Manganese-Tungsten trioxide (Mn-WO3)	microwave radiation - nanoparticles	3.25 mg/L	100	1.0 g/L	Light Emitting Diodes (LED); 60 min	[199]
	Ciprofloxacin	ZnO	Nanoparticles	5 mg/L	48	20 mg/L	Xenon lamp; 60 min	[214]
		Zn-doped Cu_2O	solvothermal method - particles	20 mg/L	94.6	600 mg/L	Metal halide lamp; 240 min	[215]
	Amoxicillin	Ag-TiO_2	nanoparticles	20 mg/L	60.23	4 mg/L	Tungsten-halogen lamp; 300 min	[216]
	Sulfadiazine	TiO_2/Zeolite	sol-gel method – nanoparticles 50 nm size	10 mg/L	93.4	1.0 g/L	U.V. lamp; 120 min	[217]
ARB	*E. coli*	Ag-TiO_2-FeO_x	hydrothermal synthesis	1×10^6 CF U/mL	100	100mg/L	8h incubation at 37 °C	[200, 201]
		Ag/TiO_2	Facile polyol synthesis	1×10^7 CF U/mL	99.9	ND	8h incubation at 37 °C	[201]

	K. pneumoniae	Ag-doped-TiO_2	sol–gel method	10^6 CFU/mL	30.5	ND	24h incubation at 37 °C	[202]
	P. aeruginosa	TiO_2–SiO_2	Sonochemistry method -Composite	ND	98.69	ND	12h incubation	[218]
Antibiotics, ARB and ARG	SMX/TMP-*Sul1, sul2, sul3, dfr 2, dfr5 and dfr13*	TiO_2	Commercial non-porous titanium dioxide	100 ppb	90 SMX/TMP removal No promoting of corresponding genes	0.1 g/L	UVA/LED lamps;	[219]
	E. coli + *ampC sul1 ermB*, *mecA*	TiO_2, TiO_2-rGO composite	1- hydrothermal treatment 2- photocatalytic treatment	10^7 CFU/mL	100 to ARB 2 log ampC (TiO_2-rGO); 0.5 log ermB (TiO_2)	100 mg/L	ARB elimination in 120 min and no regrowth (24h) with 180 min treatment under solar radiation	[220]
	TC-resistant E.colitetA, tetM, tet Q and intl1	*Ag/AgBr/g-C_3N_4*	thermal condensation polymerisation and adsorption–deposition	10^7 CFU/mL	7 logs - TC- *E. coli* 49, 86, 69 and 86, respectively - ARGs	211.0 mg/L	Visible light-driven radiation; 90 min	[203]

In this context, polymers emerge as attractive supports for the immobilisation of photocatalysts due to their excellent processability. The potential to control the polymer microstructure, from macroporous to nanoporous, enables effective integration of photocatalysts within the matrix, thereby facilitating the formation of homogeneous functional composites [229]. Furthermore, polymers are distinguished by their economic advantages, commercial availability, mechanical resistance, and structural versatility, making them suitable for scalable photocatalytic systems [230].

In recent years, there has been a significant increase in the use of polymeric composites, both synthetic and natural, in water remediation. This interest is reflected in the development and functionalisation of materials such as polyethylene terephthalate (PET) [231], chitosan (CS) [232], polyvinylidene fluoride (PVDF) [233], and silk fibroin (SF) [234]. In fact, most commercial water filtration and purification technologies are currently based on polymeric membranes, which reinforces the relevance of these materials in the development of immobilised photocatalytic systems [235].

In this thesis, PVDF co-polymer polyvinylidene fluoride-co-trifluoroethylene (PVDF-HFP) and a natural-based silk fibroin were selected as substrates to immobilise photocatalyst materials. For this reason, both will be introduced and described in more detail.

1.5.1 Poly(vinilydene fluoride) and its copolymers

PVDF is a thermoplastic fluoropolymer produced from the polymerisation of vinylidene fluoride, with the chemical formula -CH2–CF2- (Figure 1.7-a). It has been known since the 1960s for its outstanding mechanical properties, which have extended its use to many research areas and industrial uses [236].

PVDF and its copolymers have received considerable attention as a membrane material for water remediation applications, thanks to their chemical, thermal, and mechanical stability, wide processing temperature range, and resistance to aging. Furthermore, these polymers exhibit tuneable porosity and pore size that depend on their processing conditions, allowing the production of materials with different morphologies [224, 225, 237].

However, PVDF is a hydrophobic material; thus, selecting an appropriate membrane preparation methodology for PVDF membranes is paramount so they can be employed for water remediation applications [238].

In the last few decades, various PVDF copolymers have been developed to improve certain properties and make this material more suitable for specific applications. Among others, polyvinylidene fluoride-co-chlorotrifluoroethylene) (PVDF-CTFE), polyvinylidene fluoride-co-trifluoroethylene (PVDF-TrFE), and

polyvinylidene fluoride-co-hexafluoropropylene (PVDF-HFP) have gained considerable attention due to their improved properties. PVDF-HFP (Figure 1.7-b) is especially interesting because of its higher mechanical strength, increased free volume, and lower crystallinity. Conventionally, PVDF has been dissolved using highly toxic solvents such as dimethylformamide (DMF) [239-241]. Conversely, PVDF-HFP can be processed with more environmentally friendly alternatives, such as acetone (AC), which offers the dual benefits of reducing environmental impact and enabling faster, safer processing. Membranes obtained with acetone dry quickly, a particularly advantageous feature for incorporating multiple layers when multifunctionality is required. These features have made PVDF-HFP an attractive and versatile substrate for nanoparticle incorporation. Thanks to the structuration of PVDF-HFP composites, they can immobilise various nanoparticulate materials without compromising their efficiency in capturing and separating both inorganic and organic pollutants.

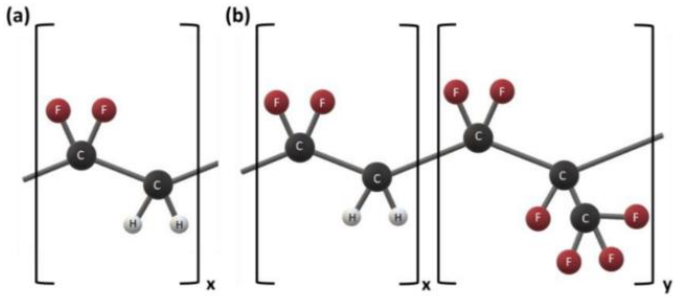


Figure 1.7. Schematic representation of the chain conformation of (a) PVDF and (b) PVDF-HFP.

Among others, Martins *et al.* developed nanocomposite membranes using PVDF-HFP as a matrix with Au-functionalised TiO_2 nanoparticles, which showed photocatalytic efficiency tested in norfloxacin and arsenic removal [240]. Titanium dioxide nanocomposites have also been introduced into PVDF-HFP matrices for antibiotic degradation [242]. As a given Aoudjit *et al.*, introduced Ag@TiO_2 into PVDF-HFP polymeric matrix to develop a composite system able to remove of metronidazole under solar radiation after 5 hours fully. The membranes obtained exhibited well-defined, interconnected micrometric porous structures and demonstrated consistent degradation efficiency across multiple reuse cycles [243].

1.5.2 Silk Fibroin

Natural polymers are increasingly gaining attention for advanced applications as a material substrate due to their capacity to offer a more sustainable and environmentally friendly alternative to synthetic polymers [244, 245]. The appeal of these materials lies in their renewable sources, potential non-toxicity

and biodegradability, and alignment with the principles of the circular economy. They offer viable alternatives to traditional applications based on fossil-based polymers [246].

Among the most studied natural polymers for the production of remediation membranes are chitosan, alginate, cellulose and its derivatives, and silk fibroin. Chitosan stands out for its hydrophilicity, functional groups that increase adsorption capacity, and good biocompatibility, although its mechanical stability remains a limitation [247]. Alginate, on the other hand, is abundant, inexpensive, and easy to process; however, it is unstable in aqueous media [248]. Cellulose and its derivatives are widely available, renewable, and biodegradable, with good mechanical strength; however, their chemical functionalization can sometimes be challenging [249]. In addition, silk fibroin has emerged as a desirable option [250].

The silk cocoon of the silkworm, *Bombyx mori* (*B. mori*), is a remarkable example of a natural biomaterial with unique structural and biochemical properties [251]. Composed mainly of fibroin and sericin proteins, silk fibroin (SF), which acts as the main structural protein, is composed of long polypeptide chains rich in amino acids such as glycine, alanine, and serine (Figure 1.8) [252]. These chains form beta-sheet structures, giving silk its renowned mechanical strength and flexibility. Acting as a binding protein, sericin surrounds the fibroin fibres, acting as a glue and contributing to the integrity and protection of the silk fibres [253]. The remarkable biocompatibility, biodegradability, and robust mechanical properties of fibroin make it a versatile material for a myriad of applications, making it an ideal material for using it as a polymeric matrix in water remediation membranes. Its ability to incorporate nanoparticles and maintain stability in aqueous environments further enhances its suitability for advanced membrane systems [245, 254].

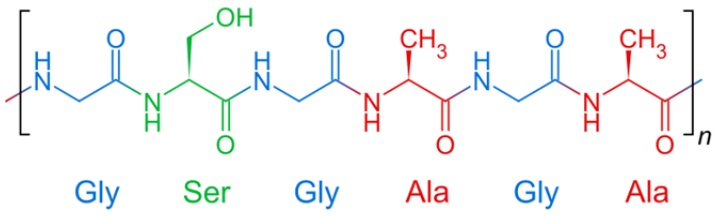


Figure 1.8. Schematic representation of the chain conformation of silk fibroin.

Natural polymers thus provide a versatile platform for developing sustainable membranes, offering distinct advantages but also notable limitations. Challenges such as limited large-scale production, higher costs, and variability in functional properties often hinder their wider application when compared to their synthetic counterparts [255]. However, their environmental benefits and functional versatility justify their continued exploration [256]. To unlock their full potential, however, it is essential to select appropriate

processing techniques that optimise their performance and adapt their specific features towards water treatment applications.

1.5.3 Polymer Membrane Processing Techniques

Polymeric membranes can be processed using a variety of different techniques to immobilise nanoparticles for CECs removal. The performance of the immobilised active material is directly related to the type of material processing, which controls the final morphology, porosity, and homogeneous distribution of the photocatalyst within the polymer matrix [257, 258].

A wide variety of approaches have been used to achieve immobilisation, including solvent casting [259], spin coating [260], electrospinning [261], additive manufacturing (e.g., direct ink writing and spray printing) [227, 262], and chemical and physical vapour deposition [263]. Figure 1.9 schematically illustrates the main processing techniques used for the fabrication of polymer composites.

Solvent casting methods are considered among the simplest and most efficient ways to immobilise nanoparticles in membrane processing. The polymer is dissolved or dispersed in a solvent, and the liquid solution is then deposited onto a substrate. Large-area membranes with a predetermined thickness can be obtained by blade casting (doctor blade method), in which a blade, whose pressure is controlled by micrometric screws, ensures surface uniformity. This method also enables the polymer solution to be applied to various substrates, particularly relevant for practical applications [224, 264]. In the context of solvent casting, three predominant forms of phase separation (solvent/polymer) have been identified, namely: (i) non-solvent-induced phase separation (NIPS), (ii) thermally induced phase separation (TIPS), and (iii) vapour-induced separation (VIPS) [259].

Complementary to phase-separation techniques, salt leaching can be used to control membrane porosity and surface topology. The method involves the incorporation of a removable porogen (e.g., NaCl, sugar) into the polymer matrix, which is subsequently dissolved to generate a network of interconnected pores (Figure 1.9 b). The combination of the two methods, solvent casting, for instance, is an efficient means of adjusting permeability and active surface area.

Conventional processing methods, including moulding (injection and blow moulding) and polymer extrusion, have already been extensively implemented in industry, demonstrating feasibility and scalability for large-scale applications. However, these processes are associated with difficulties in precisely controlling the porosity and morphology of the membrane, as well as consuming high volumes of material and energy [244].

However, more versatile methods have emerged as alternatives, such as the production of electrospun nanofibres and additive manufacturing. Electrospinning is a relatively straightforward technique for producing fibres from a wide variety of materials, allowing control over morphology, high specific surface area, and porosity [265]. However, the membranes obtained have limitations in terms of mechanical properties and practical applicability [266].

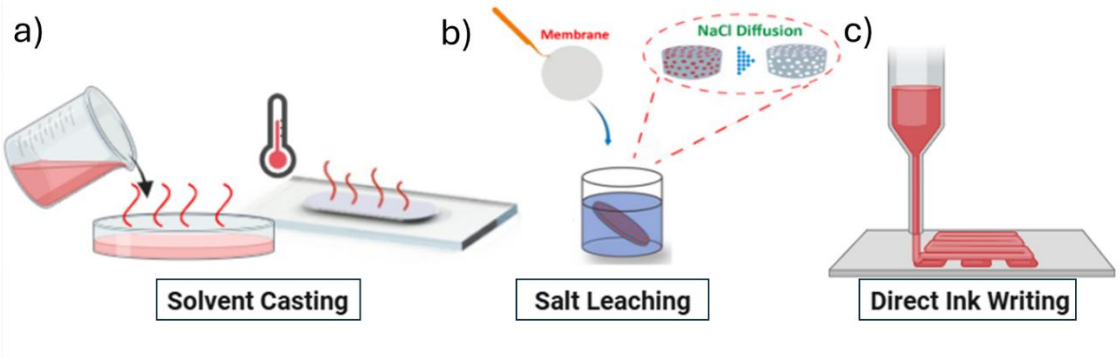


Figure 1.9. Schematic representation of the methods used for the processing of polymer composite membranes.

Additive manufacturing, frequently associated with printing technologies, is a promising strategy for membrane production. By enabling the construction of structures layer by layer, it provides high flexibility in design, precise control of pore distribution, and the possibility of tailoring permeability and robustness to specific applications in water treatment

Within this method, direct ink writing (DIW) has gained scientific relevance [267]. This technique controls the extrusion of viscoelastic inks through a needle or nozzle, allowing the direct printing of predefined patterns with high precision. DIW offers significant advantages, including compatibility with various polymer formulations, the homogeneous incorporation of photocatalytic nanoparticles, and the ability to produce membranes with complex geometries tailored to specific applications [263]. Moreover, the process can be scaled up, is less expensive, and generates less material waste, positioning it as one of the most versatile and sustainable approaches to developing advanced membranes [268].

In this work, attention will primarily focus on the conventional solvent-casting/solvent-evaporation (TIPS) technique, widely used to produce porous polymer membranes. This method enables the production of materials with a controlled degree of porosity and pore distribution. This is achieved by adjusting the polymer microstructure to allow water percolation, thereby increasing the contact area with the photocatalyst and enabling the efficient recovery and reuse of the immobilised material.

When contemplating scale-up methodologies, DIW will also be considered, as it offers structural flexibility, precise control over morphology, and has the potential for adaptation to large-scale production processes. Thus, this study integrates the reliability of the conventional methods with the innovation and future potential of additive manufacturing, seeking to maximise the efficiency and sustainability of photocatalytic processes.

1.6 Ecotoxicity

Despite advances in developing more efficient photocatalysts and membranes for contaminant removal, the transformation does not guarantee the process's non-toxicity. The ecotoxicological assessment is, therefore, a vital step to understanding the effects of both the materials produced (membrane immobilisation and possible leaching) and the photocatalytic process itself. This assessment provides a comprehensive understanding of the potential environmental impacts associated with the materials and possible by-products generated during the photocatalytic degradation of organic compounds.

Numerous studies have shown that the degradation of antibiotics and other organic compounds can yield intermediates that exhibit greater toxicity or persistence than the original compounds [269]. At the same time, the materials themselves, including modified semiconductors and composite membranes, may pose additional risks if they lack sufficient stability or release constituents into the environment (such as nanoparticles, polymers, or solvents). Therefore, incorporating ecotoxicological evaluation is crucial not only to assess the direct effects of by-products on aquatic organisms but also to guarantee the environmental safety and sustainability of the developed materials.

Ecotoxicological tests can be designed to assess either acute toxicity or chronic toxicity, depending on the duration of exposure and the biological parameters being measured. Acute toxicity refers to the short-term effects observed after brief exposure (ranging from 15 minutes to 96 hours), which are often expressed as mortality, growth inhibition, or luminescence inhibition. These tests are used as a preliminary evaluation of the environmental safety of new materials, as they provide rapid, sensitive, and cost-effective information on potential toxic effects when applied in real-world environments. In contrast, chronic toxicity assessments evaluate the effects of prolonged or repeated exposure to lower concentrations, providing information on sublethal responses such as growth inhibition, reproductive impairment, or enzymatic and genetic alterations. Although more time-consuming, chronic tests provide

complementary information on long-term ecological risks and the potential for bioaccumulation or genetic effects [270].

A wide range of aquatic test organisms has been used in ecotoxicity studies to represent different trophic levels and ecological systems. These include luminous bacteria [271], algae [272], water fleas [273], fish [274], benthic animals [275], invertebrates [276], and plants [277]. Among them, the marine bacterium *Vibrio fischeri* is one of the most widely used indicators of acute toxicity, due to its sensitivity, reproducibility, and rapid response measured through bioluminescence inhibition [278]. Other frequently used model organisms include microalgae (e.g., *Pseudokirchneriella subcapitata* [279*], Chlorella vulgaris* [280]), water flea (e.g., *Daphnia magna*) [281], and fish embryos (e.g., *Danio rerio*) [282], which together provide a broad spectrum of ecological responses to pollutants and their degradation products.

Several studies have demonstrated the relevance of associating the efficiency of AOP processes with their ecotoxicological assessment [283]. Tests with aquatic microorganisms, including *Artemia salina* and *Daphnia magna*, have revealed that, even when oxidation processes effectively remove the parent contaminant, the resulting degradation products may still exhibit measurable toxicity. For instance, the chlorination of norfloxacin produced several by-products, four of which were identified, that, despite losing their antibacterial activity against *E. coli*, exhibited higher acute toxicity towards *Artemia salina* than the original compound, posing a further threat to aquatic biota [284]. Similarly, *Danio rerio* (zebrafish) is widely recommended by the United States Environmental Protection Agency (USEPA) for aquatic acute toxicity testing due to its ecological relevance and sensitivity. Chen *et al.* observed behavioural alterations in zebrafish larvae exposed to carbamazepine (CBZ) and its degradation products, reporting decreased frequency of movement relative to the control group, suggesting that transformation products may retain or even enhance toxic effects [285].

In addition to acute testing, several studies have explored the chronic toxicity of nanomaterials, revealing potential long-term ecological implications. The effect of $CdCl_2$ and TiO_2 nanoparticles on *Aquarana catesbeiana* tadpoles over 30 days. The results demonstrated that prolonged exposure resulted in oxidative stress, changes in antioxidant enzyme activity, and morphological abnormalities, particularly under combined Cd/TiO_2 exposure [286]. These demonstrate that TiO_2, often considered an inert photocatalyst, can induce sublethal effects under chronic exposure conditions [287].

The immobilisation of the photocatalyst can play a crucial role in mitigating the release of nanoparticles into the environment, significantly reducing secondary contamination and toxicity to organisms. However, even when immobilised, composite materials must be systematically evaluated for their ecotoxicity, as

leaching of active components or degradation of the polymer matrix may still pose risks to aquatic organisms.

Consequently, incorporating ecotoxicological assessments of the developed materials, along with potential by-products generated during the photocatalytic process, provides a better understanding of the entire process. This demonstrates that efficiency alone is insufficient, and it is essential to ensure that treatments do not yield products that are equally or more hazardous than the original contaminants, thereby promoting environmental safety.

1.7 Objectives and Methodology

The main objective of the thesis is to develop a hybrid polymeric platform to produce robust membranes that combat three types of water contaminants of emerging concern: antibiotics, ARB, and ARGs. The combination of membranes and photocatalytic technologies will yield multifaceted membranes capable of removing multiple CECs. Also, this project addresses the sustainability of the membranes by using natural polymers (silk) and performs an ecotoxicity assessment of materials and by-products. To achieve the proposed objective, the following scientific methodology was applied:

1. Synthesis, characterisation, and application of photocatalytic (e.g., Au/TiO_2 and Ag/TiO_2) materials against antibiotics (ciprofloxacin, trimethoprim, and sulfadiazine);
2. Production of porous polymeric membranes (synthetic and natural polymers) with the best photocatalysts;
3. Perform physical-chemical characterisation of all the produced membranes to allow optimisation.
4. Degradation of ciprofloxacin, trimethoprim and sulfadiazine with the produced membranes;
5. Identification of photocatalytic degradation by-products, assessment of their ecotoxicity, as well as the materials used in the removal of contaminants;
6. Assessment of the photocatalytic efficiency of the membranes against antibiotics, ARB, and ARGs;
7. Design and validation of photocatalytic systems immobilised on DIW-printed polymeric supports, enabling scalable, reusable, and efficient solar-driven aquatic remediation.

1.8 Structure of the Thesis

This thesis is structured into six chapters, of which four are based on published or submitted scientific manuscripts. The chapters were organised to facilitate a logical and comprehensive progression through

the study, from an overview of environmental problems and the state of the art of the current aquatic remediation situation, to the development of strategies and materials that enable solutions to the present problems.

The following provides a summary of the work covered in each chapter.

Chapter 1 provides a general introduction to the problem of aquatic contamination, including a review of the literature and an explanation of the motivation for the subject. The thesis also delineates the main objectives, methodology, and structure. It should be noted that the state of the art for the various problems addressed in the present work is provided in the respective chapters.

Chapter 2 presents the screening of commercial TiO_2 nanoparticles functionalised with Au (Au-TiO_2) and Ag (Ag-TiO_2) for the photocatalyst degradation of three model antibiotics (ciprofloxacin, sulfadiazine, and trimethoprim), under both UV and simulated solar radiation. The most efficient photocatalysts (Au-TiO_2) were subsequently immobilised into a PVDF-HFP membrane, enabling their reuse and preventing nanoparticle release into the aqueous medium. The resulting composite materials were characterised and evaluated for their performance in antibiotic degradation. The generated by-products were detected and identified, and as with the developed materials, both were subjected to ecotoxicological assays, providing a comprehensive assessment of photocatalytic efficiency and environmental safety.

Chapter 3 describes the development of a green functionalisation strategy for TiO_2 nanoparticles with Ag (Ag-TiO_2), aiming to achieve photocatalytic degradation of ciprofloxacin and attain antibacterial activity towards *S. epidermidis* and *E. coli*. This chapter also explores a sustainable transition by immobilising the nanocomposite in PVDF-HFP membranes and, as a sustainable alternative, in a silk fibroin substrate. Both polymeric matrices were tested against CIP and reused for several cycles. The antibacterial capacity of the composite membranes was also tested, thus evaluating their multifunctional potential for water remediation.

Chapter 4 focuses on the development of a nanocomposite (Ag-TiO_2) synthesised via an environmentally friendly method, with the silver concentration optimised to maximise photocatalytic efficiency under UV and visible light. The nanocomposite immobilised on a PVDF-HFP substrate was conceived to simultaneously address three critical types of aquatic contaminants: antibiotics, bacteria, and ARG Its photocatalytic performance was assessed through the degradation of ciprofloxacin and

trimethoprim, while its antibacterial activity was evaluated against *E. coli* and *S. aureus*. Additionally, its capacity to degrade resistant genetic material was investigated using a plasmid DNA carrying ampicillin resistance gene, thus addressing the main routes of antimicrobial resistance spread. The biofilm formation inhibition was also investigated to maximise the material's lifetime and efficiency.

Chapter 5 addresses the transition from membranes to scalability and practical implementation by developing photocatalytic systems through the manufacture of floating PVDF-HFP/TiO_2 grids by 3D printing via DIW. The technique, combined with salt leaching, allows for precise control of geometry, porosity, and mechanical stability. The grids were tested against CIP, reused for three consecutive cycles, and applied under natural solar radiation. Their buoyancy, ease of retrieval, and reusability make them a practical and flexible approach that can be deployed across diverse water matrices, from natural water to wastewater effluents.

The last chapter of this thesis, **Chapter 6**, presents the conclusions derived from this work and outlines open perspectives for future development.

Figure 1.10 presents a schematic representation of the structure and logical sequence of the different chapters of the thesis.

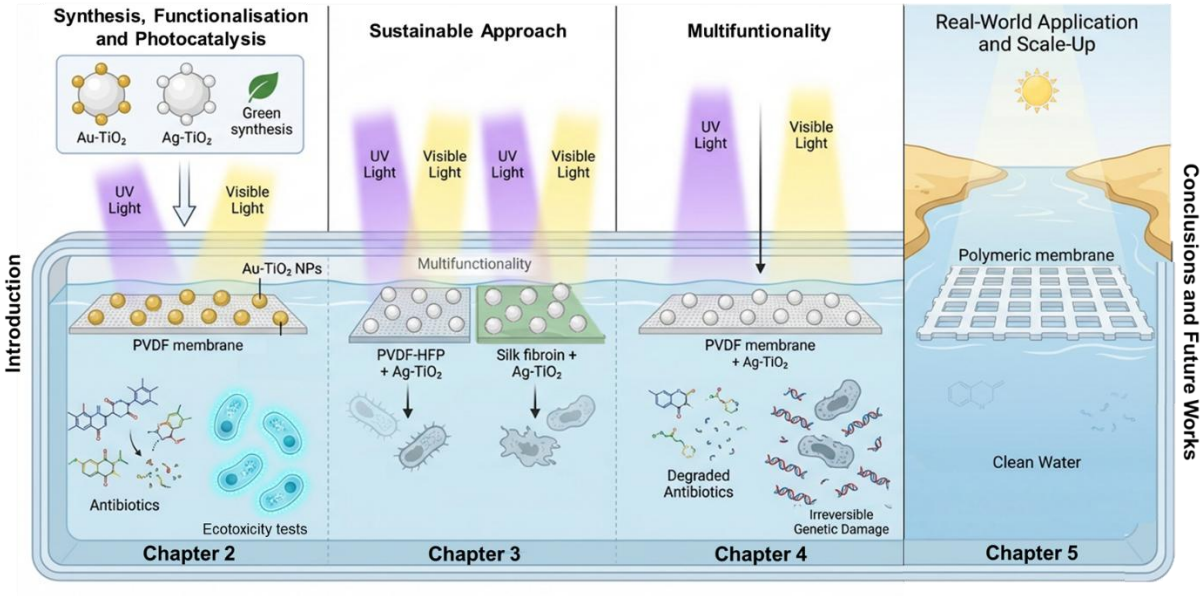


Figure 1.10. Illustrative overview and logical sequence of the different chapters that constitute this thesis.

1.9 References

[1] R.K. Mishra, S.S. Mentha, Y. Misra, N. Dwivedi, Emerging pollutants of severe environmental concern in water and wastewater: A comprehensive review on current developments and future research, Water-Energy Nexus, 6 (2023) 74-95.

[2] W. Rosińska, J. Jurasz, K. Przestrzelska, K. Wartalska, B. Kaźmierczak, Climate change's ripple effect on water supply systems and the water-energy nexus – A review, Water Resources and Industry, 32 (2024) 100266.

[3] M. Bhadarka, D. Vaghela, P.K. Bamaniya, H. Sikotariya, N. Kharadi, M. Bamaniya, P. Verma, Water pollution: Impacts on environment, 2019.

[4] Y.G. Wibowo, D. Anwar, H. Safitri, A. Rohman, A. Rinovian, B.S. Ramadan, I. Surya, Sudibyo, A.T. Yuliansyah, H.T. Bayu Murti Petrus, Biochar-Layered Double Hydroxide vs Biochar-Layered Double Oxide: A Critical Review on Their Applications in Water Pollution Control, Water-Energy Nexus, (2025).

[5] N.K. Arora, I. Mishra, Sustainable development goal 6: global water security, Environmental Sustainability, 5 (2022) 271-275.

[6] G. Mujtaba, M.U.H. Shah, A. Hai, M. Daud, M. Hayat, A holistic approach to embracing the United Nation's Sustainable Development Goal (SDG-6) towards water security in Pakistan, Journal of Water Process Engineering, 57 (2024) 104691.

[7] A.Q. Nguyen, H.P. Vu, L.N. Nguyen, Q. Wang, S.P. Djordjevic, E. Donner, H. Yin, L.D. Nghiem, Monitoring antibiotic resistance genes in wastewater treatment: Current strategies and future challenges, Science of The Total Environment, 783 (2021) 146964.

[8] F. Impellitteri, C.R. Multisanti, P. Rusanova, G. Piccione, F. Falco, C. Faggio, Exploring the Impact of Contaminants of Emerging Concern on Fish and Invertebrates Physiology in the Mediterranean Sea, Biology, 12 (2023) 767.

[9] I.C. Vasilachi, D.M. Asiminicesei, D.I. Fertu, M. Gavrilescu, Occurrence and fate of emerging pollutants in water environment and options for their removal, Water, 13 (2021) 181.

[10] L.O. Omuferen, B. Maseko, J. Olowoyo, Occurrence of antibiotics in wastewater from hospital and convectional wastewater treatment plants and their impact on the effluent receiving rivers: current knowledge between 2010 and 2019, Environmental Monitoring and Assessment, 194 (2022) 306.

[11] J. Wu, J. Wang, Z. Li, S. Guo, K. Li, P. Xu, Y.S. Ok, D.L. Jones, J. Zou, Antibiotics and antibiotic resistance genes in agricultural soils: A systematic analysis, Critical Reviews in Environmental Science and Technology, 53 (2023) 847-864.

[12] L.E. Robles-Jimenez, E. Aranda-Aguirre, O.A. Castelan-Ortega, B.S. Shettino-Bermudez, R. Ortiz-Salinas, M. Miranda, X. Li, J.C. Angeles-Hernandez, E. Vargas-Bello-Pérez, M. Gonzalez-Ronquillo, Worldwide Traceability of Antibiotic Residues from Livestock in Wastewater and Soil: A Systematic Review, Animals, 12 (2022) 60.

[13] T. Gangar, S. Patra, Antibiotic persistence and its impact on the environment, 3 Biotech, 13 (2023) 401.

[14] K. Tiseo, L. Huber, M. Gilbert, T.P. Robinson, T.P. Van Boeckel, Global trends in antimicrobial use in food animals from 2017 to 2030, Antibiotics, 9 (2020) 918.

[15] K.D. Burch, B. Han, J. Pichtel, T. Zubkov, Removal efficiency of commonly prescribed antibiotics via tertiary wastewater treatment, Environmental Science and Pollution Research, 26 (2019) 6301-6310.

[16] P. Kulkarni, N.D. Olson, G.A. Raspanti, R.E. Rosenberg Goldstein, S.G. Gibbs, A. Sapkota, A.R. Sapkota, Antibiotic concentrations decrease during wastewater treatment but persist at low levels in reclaimed water, International journal of environmental research and public health, 14 (2017) 668.

[17] M. Bilal, S. Mehmood, T. Rasheed, H.M.N. Iqbal, Antibiotics traces in the aquatic environment: persistence and adverse environmental impact, Current Opinion in Environmental Science & Health, 13 (2020) 68-74.

[18] Y. Ben, C. Fu, M. Hu, L. Liu, M.H. Wong, C. Zheng, Human health risk assessment of antibiotic resistance associated with antibiotic residues in the environment: A review, Environmental research, 169 (2019) 483-493.

[19] E. Sanganyado, W. Gwenzi, Antibiotic resistance in drinking water systems: Occurrence, removal, and human health risks, Science of the Total Environment, 669 (2019) 785-797.

[20] P. Giri, A. Aikat, The Impending Global Challenge of Antimicrobial Resistance: A Call for Urgent Action, Indian Journal of Community Health, 36 (2024) 624-628.

[21] L.L. Founou, R.C. Founou, S.Y. Essack, Antibiotic resistance in the food chain: a developing country-perspective, Frontiers in microbiology, 7 (2016) 1881.

[22] P. Kovalakova, L. Cizmas, T.J. McDonald, B. Marsalek, M. Feng, V.K. Sharma, Occurrence and toxicity of antibiotics in the aquatic environment: A review, Chemosphere, 251 (2020) 126351.

[23] C. Manyi-Loh, S. Mamphweli, E. Meyer, A. Okoh, Antibiotic Use in Agriculture and Its Consequential Resistance in Environmental Sources: Potential Public Health Implications, Molecules, 23 (2018) 795.

[24] E.M. Bayan, L.E. Pustovaya, M.G. Volkova, Recent advances in TiO2-based materials for photocatalytic degradation of antibiotics in aqueous systems, Environmental Technology & Innovation, 24 (2021) 101822.

[25] M. Umar, F. Roddick, L. Fan, Moving from the traditional paradigm of pathogen inactivation to controlling antibiotic resistance in water-Role of ultraviolet irradiation, Science of the Total Environment, 662 (2019) 923-939.

[26] P. Martins, S. Kappert, H. Nga Le, V. Sebastian, K. Kühn, M. Alves, L. Pereira, G. Cuniberti, M. Melle-Franco, S. Lanceros-Méndez, Enhanced photocatalytic activity of Au/TiO2 nanoparticles against ciprofloxacin, Catalysts, 10 (2020) 234.

[27] M.J. Silva, J. Gomes, P. Ferreira, R.C. Martins, An Overview of Polymer-Supported Catalysts for Wastewater Treatment through Light-Driven Processes, Water, 14 (2022) 825.

[28] M.A. Salam, N. Sultana, Chapter 18 - Pollution of water resources, in: A.K. Tiwari, A. Kumar, A.K. Singh, T.N. Singh, E. Suozzi, G. Matta, S. Lo Russo (Eds.) Current Directions in Water Scarcity Research, Elsevier2022, pp. 355-378.

[29] K. Jayaswal, V. Sahu, B. Gurjar, Water pollution, human health and remediation, Water remediation, Springer2017, pp. 11-27.

[30] A. du Plessis, Persistent degradation: Global water quality challenges and required actions, One Earth, 5 (2022) 129-131.

[31] W.H. Organization, Progress on household drinking water, sanitation and hygiene 2000-2017: special focus on inequalities, Progress on household drinking water, sanitation and hygiene 2000-2017: special focus on inequalities2019.

[32] UN-Water, Summary progress update 2021: SDG 6 – water and sanitation for all, (2021) Version: July 2021. Geneva, Switzerland.

[33] F. Kordbacheh, G. Heidari, Water Pollutants and Approaches for Their Removal, Materials Chemistry Horizons, 2 (2023) 139-153.

[34] J.C.G. Sousa, A.R. Ribeiro, M.O. Barbosa, C. Ribeiro, M.E. Tiritan, M.F.R. Pereira, A.M.T. Silva, Monitoring of the 17 EU Watch List contaminants of emerging concern in the Ave and the Sousa Rivers, Science of The Total Environment, 649 (2019) 1083-1095.

[35] N.I. Rousis, R. Bade, P. Dewapriya, J. Li, H. Duan, N.S. Thomaidis, Removal of emerging contaminants from wastewater by various treatment technologies in wastewater treatment plants,

Sustainable Remediation Technologies for Emerging Pollutants in Aqueous Environment, Elsevier2024, pp. 389-409.

[36] V. Dulio, B. van Bavel, E. Brorström-Lundén, J. Harmsen, J. Hollender, M. Schlabach, J. Slobodnik, K. Thomas, J. Koschorreck, Emerging pollutants in the EU: 10 years of NORMAN in support of environmental policies and regulations, Environmental Sciences Europe, 30 (2018) 5.

[37] D. Yadav, S. Rangabhashiyam, P. Verma, P. Singh, P. Devi, P. Kumar, C.M. Hussain, G.K. Gaurav, K.S. Kumar, Environmental and health impacts of contaminants of emerging concerns: Recent treatment challenges and approaches, Chemosphere, 272 (2021) 129492.

[38] F. Ahmad, D. Zhu, J. Sun, Environmental fate of tetracycline antibiotics: degradation pathway mechanisms, challenges, and perspectives, Environmental Sciences Europe, 33 (2021) 64.

[39] Y. Luo, W. Guo, H.H. Ngo, L.D. Nghiem, F.I. Hai, J. Zhang, S. Liang, X.C. Wang, A review on the occurrence of micropollutants in the aquatic environment and their fate and removal during wastewater treatment, Science of the total environment, 473 (2014) 619-641.

[40] A. Nuro, Emerging contaminants, BoD–Books on Demand2021.

[41] Y. Tang, Y. Zhong, H. Li, Y. Huang, X. Guo, F. Yang, Y. Wu, Contaminants of emerging concern in aquatic environment: Occurrence, monitoring, fate, and risk assessment, Water Environment Research, 92 (2020) 1811-1817.

[42] E. Commission, Commission Implementing Decision (EU) 2022/1307 establishing a watch list of substances for Union-wide monitoring in the field of water policy pursuant to Directive 2000/60/EC, Official Journal of the European Union, 2025.

[43] O.I. González Peña, M.Á. López Zavala, H. Cabral Ruelas, Pharmaceuticals Market, Consumption Trends and Disease Incidence Are Not Driving the Pharmaceutical Research on Water and Wastewater, International Journal of Environmental Research and Public Health, 18 (2021) 2532.

[44] S. Ahmadi, J.M. Quimbayo, V.B.K. Yaah, S.B. de Oliveira, S. Ojala, A critical review on combining adsorption and photocatalysis in composite materials for pharmaceutical removal: Pros and cons, scalability, TRL, and sustainability, Energy Nexus, 17 (2025) 100396.

[45] J.A. Rivera-Jaimes, C. Postigo, R.M. Melgoza-Alemán, J. Aceña, D. Barceló, M. López de Alda, Study of pharmaceuticals in surface and wastewater from Cuernavaca, Morelos, Mexico: Occurrence and environmental risk assessment, Science of The Total Environment, 613-614 (2018) 1263-1274.

[46] A.L. Spongberg, J.D. Witter, Pharmaceutical compounds in the wastewater process stream in Northwest Ohio, Science of The Total Environment, 397 (2008) 148-157.

[47] U. Szymańska, M. Wiergowski, I. Sołtyszewski, J. Kuzemko, G. Wiergowska, M.K. Woźniak, Presence of antibiotics in the aquatic environment in Europe and their analytical monitoring: Recent trends and perspectives, Microchemical Journal, 147 (2019) 729-740.

[48] N. Yadav, A. Mandpe, S. Shukla, A brief account of the antibiotics and antibiotic resistance genes in an aquatic environment, Detection and treatment of emerging contaminants in wastewater, (2024) 73.

[49] H. Ehalt Macedo, B. Lehner, J.A. Nicell, U. Khan, E.Y. Klein, Antibiotics in the global river system arising from human consumption, PNAS Nexus, 4 (2025).

[50] M.A. Salam, M.Y. Al-Amin, M.T. Salam, J.S. Pawar, N. Akhter, A.A. Rabaan, M.A.A. Alqumber, Antimicrobial Resistance: A Growing Serious Threat for Global Public Health, Healthcare, 11 (2023) 1946.

[51] S.K. Ahmed, S. Hussein, K. Qurbani, R.H. Ibrahim, A. Fareeq, K.A. Mahmood, M.G. Mohamed, Antimicrobial resistance: Impacts, challenges, and future prospects, Journal of Medicine, Surgery, and Public Health, 2 (2024) 100081.

[52] H. Fatima, A. Bhattacharya, S. Gupta, S.K. Khare, Combating antibiotic pollution and its impacts on the environment through sustainable remediation options: Current developments and challenges, International Biodeterioration & Biodegradation, 205 (2025) 106166.

[53] E.Y. Klein, I. Impalli, S. Poleon, P. Denoel, M. Cipriano, T.P. Van Boeckel, S. Pecetta, D.E. Bloom, A. Nandi, Global trends in antibiotic consumption during 2016–2023 and future projections through 2030, Proceedings of the National Academy of Sciences, 121 (2024) e2411919121.

[54] Q. Yang, Y. Gao, J. Ke, P.L. Show, Y. Ge, Y. Liu, R. Guo, J. Chen, Antibiotics: An overview on the environmental occurrence, toxicity, degradation, and removal methods, Bioengineered, 12 (2021) 7376-7416.

[55] A. Sceglovs, I. Skadins, M. Chitto, J. Kroica, K. Salma-Ancane, Failure or future? Exploring alternative antibacterials: a comparative analysis of antibiotics and naturally derived biopolymers, Frontiers in microbiology, 16 (2025) 1526250.

[56] H. Fomnya, S. Ngulde, K. Amshi, G. Bilbonga, Antibiotics: Classifications and mechanism of resistance, International Journal of Applied Microbiology and Biotechnology Research, 9 (2021) 38-50.

[57] C. Muoghalu, H.C. Kaboggoza, S. Semiyaga, S. Lebu, C. Liu, C. Niwagaba, F. Nansubuga, M. Manga, Antibiotic resistant bacteria (ARB) and genes (ARGs) in urban wastewater treatment plants: influencing factors, mechanisms, and removal efficiency, Environmental Pollution, 383 (2025) 126851.

[58] M. Šíma, D. Bobek, P. Cihlářová, P. Ryšánek, J. Roušarová, J. Beroušek, M. Kuchař, T. Vymazal, O. Slanař, Factors Affecting the Metabolic Conversion of Ciprofloxacin and Exposure to Its Main Active Metabolites in Critically Ill Patients: Population Pharmacokinetic Analysis of Desethylene Ciprofloxacin, Pharmaceutics, 14 (2022).

[59] F. Zhao, X. Sun, J. Li, J. Du, Z. Wu, S. Liu, L. Chen, B. Fang, A Comprehensive Study to Determine the Residual Elimination Pattern of Major Metabolites of Amoxicillin–Sulbactam Hybrid Molecules in Rats by UPLC–MS/MS, Molecules, 29 (2024) 2169.

[60] P.A. Masters, T.A. O'Bryan, J. Zurlo, D.Q. Miller, N. Joshi, Trimethoprim-Sulfamethoxazole Revisited, Archives of Internal Medicine, 163 (2003) 402-410.

[61] O. Solcova, M. Dlaskova, F. Kastanek, Challenges and Advances in Tertiary Waste Water Treatment for Municipal Treatment Plants, Processes, 12 (2024) 2084.

[62] A.J. Watkinson, E.J. Murby, D.W. Kolpin, S.D. Costanzo, The occurrence of antibiotics in an urban watershed: From wastewater to drinking water, Science of The Total Environment, 407 (2009) 2711-2723.

[63] H.W. Leung, T.B. Minh, M.B. Murphy, J.C.W. Lam, M.K. So, M. Martin, P.K.S. Lam, B.J. Richardson, Distribution, fate and risk assessment of antibiotics in sewage treatment plants in Hong Kong, South China, Environment International, 42 (2012) 1-9.

[64] L. Tahrani, J. Van Loco, H. Ben Mansour, T. Reyns, Occurrence of antibiotics in pharmaceutical industrial wastewater, wastewater treatment plant and sea waters in Tunisia, Journal of water and health, 14 (2016) 208-213.

[65] L.H. Santos, M. Gros, S. Rodriguez-Mozaz, C. Delerue-Matos, A. Pena, D. Barceló, M.C.B. Montenegro, Contribution of hospital effluents to the load of pharmaceuticals in urban wastewaters: identification of ecologically relevant pharmaceuticals, Science of the Total Environment, 461 (2013) 302-316.

[66] M. Gros, S. Rodríguez-Mozaz, D. Barceló, Rapid analysis of multiclass antibiotic residues and some of their metabolites in hospital, urban wastewater and river water by ultra-high-performance liquid chromatography coupled to quadrupole-linear ion trap tandem mass spectrometry, Journal of Chromatography A, 1292 (2013) 173-188.

[67] S. Zorita, L. Mårtensson, L. Mathiasson, Occurrence and removal of pharmaceuticals in a municipal sewage treatment system in the south of Sweden, Science of the total environment, 407 (2009) 2760-2770.

[68] P. Verlicchi, M. Al Aukidy, A. Galletti, M. Petrovic, D. Barceló, Hospital effluent: investigation of the concentrations and distribution of pharmaceuticals and environmental risk assessment, Science of the total environment, 430 (2012) 109-118.

[69] S. Terzić, I. Senta, M. Ahel, M. Gros, M. Petrović, D. Barcelo, J. Müller, T. Knepper, I. Martí, F. Ventura, Occurrence and fate of emerging wastewater contaminants in Western Balkan Region, Science of the total environment, 399 (2008) 66-77.

[70] B. Kasprzyk-Hordern, R.M. Dinsdale, A.J. Guwy, The removal of pharmaceuticals, personal care products, endocrine disruptors and illicit drugs during wastewater treatment and its impact on the quality of receiving waters, Water research, 43 (2009) 363-380.

[71] O. Golovko, V. Kumar, G. Fedorova, T. Randak, R. Grabic, Seasonal changes in antibiotics, antidepressants/psychiatric drugs, antihistamines and lipid regulators in a wastewater treatment plant, Chemosphere, 111 (2014) 418-426.

[72] O. Baaloudj, I. Assadi, N. Nasrallah, A. El Jery, L. Khezami, A.A. Assadi, Simultaneous removal of antibiotics and inactivation of antibiotic-resistant bacteria by photocatalysis: A review, Journal of Water Process Engineering, 42 (2021) 102089.

[73] M. Foroughi, M. Khiadani, S. Kakhki, V. Kholghi, K. Naderi, S. Yektay, Effect of ozonation-based disinfection methods on the removal of antibiotic resistant bacteria and resistance genes (ARB/ARGs) in water and wastewater treatment: a systematic review, Science of The Total Environment, 811 (2022) 151404.

[74] M. McKenna, The antibiotic paradox: why companies can't afford to create life-saving drugs, Nature, 584 (2020) 338-342.

[75] S. Li, B.S. Ondon, S.-H. Ho, Q. Zhou, F. Li, Drinking water sources as hotspots of antibiotic-resistant bacteria (ARB) and antibiotic resistance genes (ARGs): Occurrence, spread, and mitigation strategies, Journal of Water Process Engineering, 53 (2023) 103907.

[76] L.S. Munoz-Price, L. Poirel, R.A. Bonomo, M.J. Schwaber, G.L. Daikos, M. Cormican, G. Cornaglia, J. Garau, M. Gniadkowski, M.K. Hayden, Clinical epidemiology of the global expansion of Klebsiella pneumoniae carbapenemases, The Lancet infectious diseases, 13 (2013) 785-796.

[77] R. Bala, V.A. Singh, N. Gupta, P. Rakshit, Prevalence, multidrug-resistance and risk factors for AmpC β-lactamases producing Escherichia coli from hospitalized patients, The Journal of Infection in Developing Countries, 14 (2020) 1466-1469.

[78] Y. Ahmed, J. Lu, Z. Yuan, P.L. Bond, J. Guo, Efficient inactivation of antibiotic resistant bacteria and antibiotic resistance genes by photo-Fenton process under visible LED light and neutral pH, Water Research, 179 (2020) 115878.

[79] F. Gordillo Altamirano, J.H. Forsyth, R. Patwa, X. Kostoulias, M. Trim, D. Subedi, S.K. Archer, F.C. Morris, C. Oliveira, L. Kielty, Bacteriophage-resistant Acinetobacter baumannii are resensitized to antimicrobials, Nature microbiology, 6 (2021) 157-161.

[80] T. Azuma, K. Otomo, M. Kunitou, M. Shimizu, K. Hosomaru, S. Mikata, M. Ishida, K. Hisamatsu, A. Yunoki, Y. Mino, T. Hayashi, Environmental fate of pharmaceutical compounds and antimicrobial-resistant bacteria in hospital effluents, and contributions to pollutant loads in the surface waters in Japan, Science of The Total Environment, 657 (2019) 476-484.

[81] S. Chen, J. Chen, X. Wang, J. Li, B. Dong, Z. Xu, Footprints of total coliforms, faecal coliforms and E. coli in a wastewater treatment plant and the probabilistic assessment and reduction of E. coli infection risks, Science of The Total Environment, 900 (2023) 165845.

[82] D.O. Fatoba, D.G. Amoako, A.L.K. Akebe, A. Ismail, S.Y. Essack, Genomic analysis of antibiotic-resistant Enterococcus spp. reveals novel enterococci strains and the spread of plasmid-borne Tet (M),

Tet (L) and Erm (B) genes from chicken litter to agricultural soil in South Africa, Journal of environmental management, 302 (2022) 114101.

[83] F. Baghal Asghari, M.H. Dehghani, R. Dehghanzadeh, D. Farajzadeh, D. Shanehbandi, A.H. Mahvi, K. Yaghmaeian, A. Rajabi, Performance evaluation of ozonation for removal of antibiotic-resistant Escherichia coli and Pseudomonas aeruginosa and genes from hospital wastewater, Scientific Reports, 11 (2021) 24519.

[84] Z.Z. Noor, Z. Rabiu, M.H.M. Sani, A.F.A. Samad, M.F.A. Kamaroddin, M.F. Perez, J.R. Dib, H. Fatima, R. Sinha, S.K. Khare, A review of bacterial antibiotic resistance genes and their removal strategies from wastewater, Current Pollution Reports, 7 (2021) 494-509.

[85] M. Herraiz-Carboné, S. Cotillas, E. Lacasa, C. Sainz de Baranda, E. Riquelme, P. Cañizares, M.A. Rodrigo, C. Sáez, Are we correctly targeting the research on disinfection of antibiotic-resistant bacteria (ARB)?, Journal of Cleaner Production, 320 (2021) 128865.

[86] A.J. Watkinson, G.B. Micalizzi, G.M. Graham, J.B. Bates, S.D. Costanzo, Antibiotic-Resistant Escherichia coli in Wastewaters, Surface Waters, and Oysters from an Urban Riverine System, Applied and Environmental Microbiology, 73 (2007) 5667-5670.

[87] A.M. Voigt, N. Zacharias, C. Timm, F. Wasser, E. Sib, D. Skutlarek, M. Parcina, R.M. Schmithausen, T. Schwartz, N. Hembach, A. Tiehm, C. Stange, S. Engelhart, G. Bierbaum, T. Kistemann, M. Exner, H.A. Faerber, C. Schreiber, Association between antibiotic residues, antibiotic resistant bacteria and antibiotic resistance genes in anthropogenic wastewater – An evaluation of clinical influences, Chemosphere, 241 (2020) 125032.

[88] S.S. Seyedjavadi, M. Goudarzi, F. Sabzehali, Relation between blaTEM, blaSHV and blaCTX-M genes and acute urinary tract infections, Journal of Acute Disease, 5 (2016) 71-76.

[89] Y. Hu, T. Zhang, L. Jiang, Y. Luo, S. Yao, D. Zhang, K. Lin, C. Cui, Occurrence and reduction of antibiotic resistance genes in conventional and advanced drinking water treatment processes, Science of The Total Environment, 669 (2019) 777-784.

[90] C.X. Hiller, U. Hübner, S. Fajnorova, T. Schwartz, J.E. Drewes, Antibiotic microbial resistance (AMR) removal efficiencies by conventional and advanced wastewater treatment processes: A review, Science of The Total Environment, 685 (2019) 596-608.

[91] M. Pazda, J. Kumirska, P. Stepnowski, E. Mulkiewicz, Antibiotic resistance genes identified in wastewater treatment plant systems – A review, Science of The Total Environment, 697 (2019) 134023.

[92] K. Stefaniak, M. Harnisz, M. Męcik, E. Korzeniewska, ARB inactivation, ARGs and antibiotics degradation in hospital wastewater, Journal of Hazardous Materials, 495 (2025) 138833.

[93] M. Kalli, C. Noutsopoulos, D. Mamais, The Fate and Occurrence of Antibiotic-Resistant Bacteria and Antibiotic Resistance Genes during Advanced Wastewater Treatment and Disinfection: A Review, Water, 15 (2023) 2084.

[94] E. Bayan, L. Pustovaya, M. Volkova, Recent advances in TiO2-based materials for photocatalytic degradation of antibiotics in aqueous systems, Environmental Technology & Innovation, 24 (2021) 101822.

[95] X. Cheng, J. Xu, G. Smith, Y. Zhang, Metagenomic insights into dissemination of antibiotic resistance across bacterial genera in wastewater treatment, Chemosphere, 271 (2021) 129563.

[96] D. Dionisi, Potential and limits of biodegradation processes for the removal of organic xenobiotics from wastewaters, ChemBioEng reviews, 1 (2014) 67-82.

[97] H. Chen, M. Huang, Y. Liu, L. Meng, M. Ma, Functionalized electrospun nanofiber membranes for water treatment: A review, Science of The Total Environment, 739 (2020) 139944.

[98] S. Foorginezhad, M.M. Zerafat, A.F. Ismail, P.S. Goh, Emerging membrane technologies for sustainable water treatment: a review on recent advances, Environmental Science: Advances, 4 (2025) 530-570.

[99] D. Cacace, D. Fatta-Kassinos, C.M. Manaia, E. Cytryn, N. Kreuzinger, L. Rizzo, P. Karaolia, T. Schwartz, J. Alexander, C. Merlin, H. Garelick, H. Schmitt, D. de Vries, C.U. Schwermer, S. Meric, C.B. Ozkal, M.-N. Pons, D. Kneis, T.U. Berendonk, Antibiotic resistance genes in treated wastewater and in the receiving water bodies: A pan-European survey of urban settings, Water Research, 162 (2019) 320-330.

[100] R. Pallares-Vega, H. Blaak, R. van der Plaats, A.M. de Roda Husman, L. Hernandez Leal, M.C.M. van Loosdrecht, D.G. Weissbrodt, H. Schmitt, Determinants of presence and removal of antibiotic resistance genes during WWTP treatment: A cross-sectional study, Water Research, 161 (2019) 319-328.

[101] A. Di Cesare, D. Fontaneto, J. Doppelbauer, G. Corno, Fitness and Recovery of Bacterial Communities and Antibiotic Resistance Genes in Urban Wastewaters Exposed to Classical Disinfection Treatments, Environmental Science & Technology, 50 (2016) 10153-10161.

[102] C.-s. Zhou, J.-w. Wu, L.-l. Dong, B.-f. Liu, D.-f. Xing, S.-s. Yang, X.-k. Wu, Q. Wang, J.-n. Fan, L.-p. Feng, G.-l. Cao, Removal of antibiotic resistant bacteria and antibiotic resistance genes in wastewater effluent by UV-activated persulfate, Journal of Hazardous Materials, 388 (2020) 122070.

[103] S. Satyam, S. Patra, Innovations and challenges in adsorption-based wastewater remediation: A comprehensive review, Heliyon, 10 (2024).

[104] Z.-Y. Lu, Y.-L. Ma, J.-T. Zhang, N.-S. Fan, B.-C. Huang, R.-C. Jin, A critical review of antibiotic removal strategies: Performance and mechanisms, Journal of Water Process Engineering, 38 (2020) 101681.

[105] X. Zhu, Z. Wan, D.C. Tsang, M. He, D. Hou, Z. Su, J. Shang, Machine learning for the selection of carbon-based materials for tetracycline and sulfamethoxazole adsorption, Chemical Engineering Journal, 406 (2021) 126782.

[106] C. Hu, J. Jiang, Y. An, X. Jiang, Q. Sun, H. Zheng, H. Li, A novel self-floating silica adsorbent for antibiotic ciprofloxacin and nickel (II) ion, Chemical Engineering Journal, 429 (2022) 132227.

[107] T.J. Al-Musawi, A.H. Mahvi, A.D. Khatibi, D. Balarak, Effective adsorption of ciprofloxacin antibiotic using powdered activated carbon magnetized by iron (III) oxide magnetic nanoparticles, Journal of porous materials, 28 (2021) 835-852.

[108] C. Du, Z. Zhang, G. Yu, H. Wu, H. Chen, L. Zhou, Y. Zhang, Y. Su, S. Tan, L. Yang, A review of metal organic framework (MOFs)-based materials for antibiotics removal via adsorption and photocatalysis, Chemosphere, 272 (2021) 129501.

[109] Y. Xia, Q. Dai, Electrochemical degradation of antibiotic levofloxacin by PbO2 electrode: Kinetics, energy demands and reaction pathways, Chemosphere, 205 (2018) 215-222.

[110] M.B. Ahmed, J.L. Zhou, H.H. Ngo, W. Guo, Adsorptive removal of antibiotics from water and wastewater: Progress and challenges, Science of The Total Environment, 532 (2015) 112-126.

[111] L. Aoudjit, H. Salazar, D. Zioui, A. Sebti, P.M. Martins, S. Lanceros-Méndez, Solar Photocatalytic Membranes: An Experimental and Artificial Neural Network Modeling Approach for Niflumic Acid Degradation, Membranes, 12 (2022) 849.

[112] T. An, H. Yang, G. Li, W. Song, W.J. Cooper, X. Nie, Kinetics and mechanism of advanced oxidation processes (AOPs) in degradation of ciprofloxacin in water, Applied Catalysis B: Environmental, 94 (2010) 288-294.

[113] S. Navalon, M. Alvaro, H. Garcia, Reaction of chlorine dioxide with emergent water pollutants: product study of the reaction of three β-lactam antibiotics with ClO2, Water Research, 42 (2008) 1935-1942.

[114] S. Ghosh, G. Zhang, Y. Chen, J. Hu, The efficacies of degrading antibiotic resistance genes (ARGs) by applying UV light emitting diodes (UV-LEDs) based advanced oxidation processes (AOPs), Water Research, 276 (2025) 123197.

[115] X. Wang, Y. Lu, X. Zhang, Y. Wang, G. Che, H. Guo, C. Liu, PMS activation over carbon nitride to effectively eliminate ARBs and ARGs from lake water under natural light, Chemical Engineering Journal, 523 (2025) 168510.

[116] M. Klavarioti, D. Mantzavinos, D. Kassinos, Removal of residual pharmaceuticals from aqueous systems by advanced oxidation processes, Environment international, 35 (2009) 402-417.

[117] T.-H. Zheng, Z.-Z. Zhang, Y. Liu, L.-H. Zou, Recent Progress in Catalytically Driven Advanced Oxidation Processes for Wastewater Treatment, Catalysts, 15 (2025) 761.

[118] J. Mukherjee, B.K. Lodh, R. Sharma, N. Mahata, M.P. Shah, S. Mandal, S. Ghanta, B. Bhunia, Advanced oxidation process for the treatment of industrial wastewater: A review on strategies, mechanisms, bottlenecks and prospects, Chemosphere, 345 (2023) 140473.

[119] R.V. Prihod′ ko, N.M. Soboleva, Photocatalysis: Oxidative processes in water treatment, Journal of Chemistry, 2013 (2013) 168701.

[120] V. Homem, L. Santos, Degradation and removal methods of antibiotics from aqueous matrices–a review, Journal of environmental management, 92 (2011) 2304-2347.

[121] S.L. Suib, New and future developments in catalysis: Catalysis for remediation and environmental concerns, Newnes2013.

[122] S.N. Frank, A.J. Bard, Heterogeneous photocatalytic oxidation of cyanide ion in aqueous solutions at titanium dioxide powder, Journal of the American Chemical Society, 99 (1977) 303-304.

[123] L. El Gaini, Enhancing solar-driven photocatalysis: Synergistic integration of biochar, semiconductors, and magnetic materials for degrading organic pollutants, Desalination and Water Treatment, 320 (2024) 100798.

[124] F.K. Sadiq, A.A. Sadiq, T.A. Matsika, B.A. Momoh, Sustainable remediation of persistent organic Pollutants: A review on Recent innovative technologies, Current Research in Biotechnology, 9 (2025) 100293.

[125] K. Hashimoto, H. Irie, A. Fujishima, TiO2 photocatalysis: a historical overview and future prospects, Japanese journal of applied physics, 44 (2005) 8269.

[126] H. Tong, S. Ouyang, Y. Bi, N. Umezawa, M. Oshikiri, J. Ye, Nano-photocatalytic materials: possibilities and challenges, Advanced materials, 24 (2012) 229-251.

[127] S. Pasternak, Y. Paz, On the similarity and dissimilarity between photocatalytic water splitting and photocatalytic degradation of pollutants, ChemPhysChem, 14 (2013) 2059-2070.

[128] K. Perović, F.M. dela Rosa, M. Kovačić, H. Kušić, U.L. Štangar, F. Fresno, D.D. Dionysiou, A. Loncaric Bozic, Recent achievements in development of TiO2-based composite photocatalytic materials for solar driven water purification and water splitting, Materials, 13 (2020) 1338.

[129] C. Minero, Kinetic analysis of photoinduced reactions at the water semiconductor interface, Catalysis Today, 54 (1999) 205-216.

[130] D. Bahnemann, Photocatalytic water treatment: solar energy applications, Solar energy, 77 (2004) 445-459.

[131] M.A. Lazar, S. Varghese, S.S. Nair, Photocatalytic water treatment by titanium dioxide: recent updates, Catalysts, 2 (2012) 572-601.

[132] V. Augugliaro, L. Palmisano, A. Sclafani, C. Minero, E. Pelizzetti, Photocatalytic degradation of phenol in aqueous titanium dioxide dispersions, Toxicological & Environmental Chemistry, 16 (1988) 89-109.

[133] M.R. Hoffmann, S.T. Martin, W. Choi, D.W. Bahnemann, Environmental applications of semiconductor photocatalysis, Chemical reviews, 95 (1995) 69-96.

[134] J.-M. Herrmann, Heterogeneous photocatalysis: fundamentals and applications to the removal of various types of aqueous pollutants, Catalysis today, 53 (1999) 115-129.

[135] A. Fujishima, X. Zhang, D.A. Tryk, TiO2 photocatalysis and related surface phenomena, Surface science reports, 63 (2008) 515-582.

[136] J. Montoya, J. Velasquez, P. Salvador, The direct–indirect kinetic model in photocatalysis: A reanalysis of phenol and formic acid degradation rate dependence on photon flow and concentration in TiO2 aqueous dispersions, Applied Catalysis B: Environmental, 88 (2009) 50-58.

[137] M. Faramarzpour, M. Vossoughi, M. Borghei, Photocatalytic degradation of furfural by titania nanoparticles in a floating-bed photoreactor, Chemical Engineering Journal, 146 (2009) 79-85.

[138] H. Lin, K.T. Valsaraj, Development of an optical fiber monolith reactor for photocatalytic wastewater treatment, Journal of Applied Electrochemistry, 35 (2005) 699-708.

[139] E. Hapeshi, A. Achilleos, M.I. Vasquez, C. Michael, N.P. Xekoukoulotakis, D. Mantzavinos, D. Kassinos, Drugs degrading photocatalytically: kinetics and mechanisms of ofloxacin and atenolol removal on titania suspensions, Water research, 44 (2010) 1737-1746.

[140] H. Yang, G. Li, T. An, Y. Gao, J. Fu, Photocatalytic degradation kinetics and mechanism of environmental pharmaceuticals in aqueous suspension of TiO2: A case of sulfa drugs, Catalysis Today, 153 (2010) 200-207.

[141] M.N. Chong, B. Jin, C.W. Chow, C. Saint, Recent developments in photocatalytic water treatment technology: a review, Water research, 44 (2010) 2997-3027.

[142] H.D. Tran, D.Q. Nguyen, P.T. Do, U.N. Tran, Kinetics of photocatalytic degradation of organic compounds: a mini-review and new approach, RSC advances, 13 (2023) 16915-16925.

[143] S. Valencia, F. Catano, L. Rios, G. Restrepo, J. Marín, A new kinetic model for heterogeneous photocatalysis with titanium dioxide: Case of non-specific adsorption considering back reaction, Applied Catalysis B: Environmental, 104 (2011) 300-304.

[144] L. Pretali, E. Fasani, M. Sturini, Current advances on the photocatalytic degradation of fluoroquinolones: photoreaction mechanism and environmental application, Photochemical & Photobiological Sciences, 21 (2022) 899-912.

[145] R.K. Singh, L. Philip, S. Ramanujam, Disinfection of water by pulsed power technique: a mechanistic perspective, RSC Advances, 6 (2016) 11980-11990.

[146] T.-H. Lee, T.-H. Kang, DNA Oxidation and Excision Repair Pathways, International Journal of Molecular Sciences, 20 (2019) 6092.

[147] T.P. Savchuk, L.S. Volkova, A.A. Dronov, D.D. Butmanov, O.V. Pinchuk, E.V. Kytina, S.A. Gavrilov, E.A. Konstantinova, Synthesis and investigation of multifunctional TiO2 photocatalysts modified by metal nanoparticles, Catalysis Communications, 187 (2024) 106907.

[148] D.P. Jaihindh, Y.-F. Lin, L.-H. Tseng, P.A. Krisbiantoro, K.C.W. Wu, K. Shukla, M. Sone, T.-F.M. Chang, C.-Y. Chen, Heterogeneous Z-scheme CuO/ZnO aerogel photocatalyst for photocatalytic degradation of organic dye, Journal of the Taiwan Institute of Chemical Engineers, 175 (2025) 106281.

[149] L. Yang, Y. Liu, Z. Shen, B. Shi, R. Chen, Fabrication of H2PO4-–α-Fe2O3/BiOBr heterostructure photocatalyst to active peroxymonosulfate for efficient degradation of tetracycline, Journal of Environmental Chemical Engineering, 13 (2025) 119777.

[150] P. Pascariu, C. Gherasim, A. Airinei, Metal Oxide Nanostructures (MONs) as Photocatalysts for Ciprofloxacin Degradation, International Journal of Molecular Sciences, 24 (2023) 9564.

[151] J.A. Oyetade, K. Oluwafemi, V.N.K. Hammond, A. Boateng, R.L. Machunda, A. Hilonga, Photocatalytic remediation of selected emerging organic pollutants in industrial effluent using conducting

polymeric-based nanocomposites photocatalysts -A review, Materials Science in Semiconductor Processing, 199 (2025) 109832.

[152] H. Khan, M.U.H. Shah, Modification strategies of TiO2 based photocatalysts for enhanced visible light activity and energy storage ability: A review, Journal of Environmental Chemical Engineering, 11 (2023) 111532.

[153] F. Zheng, J.M. Queirós, P.M. Martins, R.F. de Luis, A. Fidalgo-Marijuan, J.L. Vilas-Vilela, S. Lanceros-Méndez, J. Reguera, Au-sensitised TiO2 and ZnO nanoparticles for broadband pharmaceuticals photocatalytic degradation in water remediation, Colloids and Surfaces A: Physicochemical and Engineering Aspects, 671 (2023) 131594.

[154] T. Tüken, G. Sığırcık, M. Erbil, Deterioration of semiconducting materials: Photocorrosion, Photoelectrocatalysis, Elsevier2023, pp. 421-440.

[155] M.M. Kandy, Carbon-based photocatalysts for enhanced photocatalytic reduction of CO 2 to solar fuels, Sustainable Energy & Fuels, 4 (2020) 469-484.

[156] B. Yao, J. Yuan, T. Yue, S. Yu, S. Xiao, Mechanism optimization and research progress of MOFs-based photocatalysts in antibiotic degradation, Journal of Alloys and Compounds, 1039 (2025) 182955.

[157] S. Zhang, X. Ou, Q. Xiang, S.A. Carabineiro, J. Fan, K. Lv, Research progress in metal sulfides for photocatalysis: From activity to stability, Chemosphere, 303 (2022) 135085.

[158] V. Thakur, S. Singh, P. Kumar, S. Rawat, V.C. Srivastava, S.-L. Lo, U.L. Štangar, Photocatalytic behaviors of bismuth-based mixed oxides: Types, fabrication techniques and mineralization mechanism of antibiotics, Chemical engineering journal, 475 (2023) 146100.

[159] M. Shareef, H. Batool, A. Shehzadi, F. Aftab, A. Munir, S. Manzoor, R.S. Gohar, Z. Rehman, M.N. Ashiq, M.F. Nazar, Structural Functionalized TiO2-Mediated Photocatalysts as Dye Degradation Agents: A Systematic Review, Materials Research Bulletin, (2025) 113852.

[160] J. Liu, J. Liu, B. Xue, R. Yu, ZrO2-based improved visible-driven composite photocatalysts for removal of oxytetracycline in mariculture wastewater, Optical Materials, 157 (2024) 116378.

[161] S. Bhowmik, M.S. Uddin, T. Sarker, P. Paul, S.C. Dey, A. Sarkar, F. Khalil, M.T. Islam, M.A.I. Molla, M. Sarker, A review on WO3-based photocatalysts: Functionalization, properties and applications for the removal of organic pollutants from wastewater, Inorganic Chemistry Communications, 182 (2025) 115577.

[162] J. Cai, Z. Hao, L. Xia, J. Wang, Z. Sun, A new p-n heterojunction CuO–Ag2WO4 supported on Ni foam as an efficient photocatalyst in the synthesis of some 2-substituted benzimidazoles, as effective antibacterial drugs, Journal of Physics and Chemistry of Solids, 205 (2025) 112806.

[163] J.A. Oyetade, S.W. Van Hulle, V.N. Hammond, A. Boateng, R.L. Machunda, A. Hilonga, Process modeling and optimization of photocatalytic treatment of dye-polluted effluent using novel polyaniline/graphene oxide-Fe3O4-Ag nanocomposites, Journal of Water Process Engineering, 68 (2024) 106548.

[164] N.T. Tran, M.K. Nguyen, The degradation of organic dye contaminants in wastewater and solution from highly visible light responsive ZIF-67 monodisperse photocatalyst, Journal of Solid State Chemistry, 300 (2021) 122287.

[165] J.K.E. Erum, Y. Yu, J. Gao, Recent progress in Zr-MOFs for antibiotic adsorption and photocatalysis, Separation and Purification Technology, (2025) 132138.

[166] P. Jin, L. Wang, X. Ma, R. Lian, J. Huang, H. She, M. Zhang, Q. Wang, Construction of hierarchical ZnIn2S4@ PCN-224 heterojunction for boosting photocatalytic performance in hydrogen production and degradation of tetracycline hydrochloride, Applied Catalysis B: Environmental, 284 (2021) 119762.

[167] L. Liu, Y. Chen, J. Zhang, F. Zeng, J. Bao, W. Li, G. Tian, Engineering defect-rich H-W18O49 nanowire/MIL-125 (Ti) nanosheet S-scheme heterostructure for remarkable CO2 photoconversion, Chemical Engineering Journal, 501 (2024) 157310.

[168] A.A. Oladipo, F.S. Mustafa, Bismuth-based nanostructured photocatalysts for the remediation of antibiotics and organic dyes, Beilstein Journal of Nanotechnology, 14 (2023) 291-321.

[169] T. Ochiai, A. Fujishima, Photoelectrochemical properties of TiO2 photocatalyst and its applications for environmental purification, Journal of Photochemistry and photobiology C: Photochemistry reviews, 13 (2012) 247-262.

[170] X.-T. Yin, H. Huang, J.-L. Xie, D. Dastan, J. Li, Y. Liu, X.-M. Tan, X.-C. Gao, W.A. Shah, X.-G. Ma, High-performance visible-light active Sr-doped porous LaFeO3 semiconductor prepared via sol–gel method, Green Chemistry Letters and Reviews, 15 (2022) 546-556.

[171] I. Arora, H. Chawla, A. Chandra, S. Sagadevan, S. Garg, Advances in the strategies for enhancing the photocatalytic activity of TiO2: Conversion from UV-light active to visible-light active photocatalyst, Inorganic Chemistry Communications, 143 (2022) 109700.

[172] J. Zhang, Y. Wu, M. Xing, S.A.K. Leghari, S. Sajjad, Development of modified N doped TiO 2 photocatalyst with metals, nonmetals and metal oxides, Energy & Environmental Science, 3 (2010) 715-726.

[173] M. Shen, Z. Wu, H. Huang, Y. Du, Z. Zou, P. Yang, Carbon-doped anatase TiO2 obtained from TiC for photocatalysis under visible light irradiation, Materials Letters, 60 (2006) 693-697.

[174] R. Daghrir, P. Drogui, D. Robert, Modified TiO2 for environmental photocatalytic applications: a review, Industrial & Engineering Chemistry Research, 52 (2013) 3581-3599.

[175] D. Kanakaraju, F.D. anak Kutiang, Y.C. Lim, P.S. Goh, Recent progress of Ag/TiO2 photocatalyst for wastewater treatment: Doping, co-doping, and green materials functionalization, Applied Materials Today, 27 (2022) 101500.

[176] M.B. Kanoun, F. Ahmed, C. Awada, C. Jonin, P.-F. Brevet, Band gap engineering of Au doping and Au–N codoping into anatase TiO2 for enhancing the visible light photocatalytic performance, International Journal of Hydrogen Energy, 51 (2024) 907-913.

[177] Y. Da, Z. Tian, R. Jiang, G. Chen, Y. Liu, Y. Xiao, J. Zhang, S. Xi, W. Chen, X. Han, Single-atom Pt doping induced p-type to n-type transition in NiO nanosheets toward self-gating modulated electrocatalytic hydrogen evolution reaction, ACS nano, 17 (2023) 18539-18547.

[178] P. Jithin, K. Sudheendran, K. Sankaran, J. Kurian, Influence of Fe-doping on the structural and photoluminescence properties and on the band-gap narrowing of SnO2 nanoparticles, Optical Materials, 120 (2021) 111367.

[179] G.A. Ali, M. Emam-Ismail, M. El-Hagary, E.R. Shaaban, S.H. Moustafa, M.I. Amer, H. Shaban, Optical and microstructural characterization of nanocrystalline Cu doped ZnO diluted magnetic semiconductor thin film for optoelectronic applications, Optical Materials, 119 (2021) 111312.

[180] M. Fang, E.-H. Yang, Advances in two-dimensional magnetic semiconductors via substitutional doping of transition metal dichalcogenides, Materials, 16 (2023) 3701.

[181] A.G. Oliveira, J. de Lara Andrade, M.C. Montanha, C.Y.L. Ogawa, T.K.F. de Souza Freitas, J.C.G. Moraes, F. Sato, S.M. Lima, L.H. da Cunha Andrade, A.A.W. Hechenleitner, Wastewater treatment using Mg-doped ZnO nano-semiconductors: A study of their potential use in environmental remediation, Journal of Photochemistry and Photobiology A: Chemistry, 407 (2021) 113078.

[182] Y. Liu, P.-A. Chen, X. Qiu, J. Guo, J. Xia, H. Wei, H. Xie, S. Hou, M. He, X. Wang, Doping of Sn-based two-dimensional perovskite semiconductor for high-performance field-effect transistors and thermoelectric devices, Iscience, 25 (2022).

[183] H. Guo, C.-Y. Yang, X. Zhang, A. Motta, K. Feng, Y. Xia, Y. Shi, Z. Wu, K. Yang, J. Chen, Transition metal-catalysed molecular n-doping of organic semiconductors, Nature, 599 (2021) 67-73.

[184] H. Arora, C. Doty, Y. Yuan, J. Boyle, K. Petras, B. Rabatic, T. Paunesku, G. Woloschak, Titanium dioxide nanocomposites, Nanomaterials for Life Sciences; Kumar, CSSR, Ed.; Wiley-VCH Verlag GmbH & Co. KGaA: Weinheim, German, 8 (2010).

[185] A. Tayel, A.R. Ramadan, O.A. El Seoud, Titanium dioxide/graphene and titanium dioxide/graphene oxide nanocomposites: Synthesis, characterization and photocatalytic applications for water decontamination, Catalysts, 8 (2018) 491.

[186] G. Sanzone, M. Zimbone, G. Cacciato, F. Ruffino, R. Carles, V. Privitera, M. Grimaldi, Ag/TiO2 nanocomposite for visible light-driven photocatalysis, Superlattices and Microstructures, 123 (2018) 394-402.

[187] N. Gonzalez-Ballesteros, P.M. Martins, C.J. Tavares, S. Lanceros-Mendez, Quercetin-mediated green synthesis of Au/TiO2 nanocomposites for the photocatalytic degradation of antibiotic ciprofloxacin, Journal of Industrial and Engineering Chemistry, 143 (2025) 526-537.

[188] S.G. Kumar, L.G. Devi, Review on modified TiO2 photocatalysis under UV/visible light: selected results and related mechanisms on interfacial charge carrier transfer dynamics, The Journal of physical chemistry A, 115 (2011) 13211-13241.

[189] D. Zhao, G. Sheng, C. Chen, X. Wang, Enhanced photocatalytic degradation of methylene blue under visible irradiation on graphene@ TiO2 dyade structure, Applied Catalysis B: Environmental, 111 (2012) 303-308.

[190] S. Scalese, V. Scuderi, D. D'angelo, M. Buscema, S. Libertino, R. Puglisi, M. Miritello, V. Privitera, Photocatalytic properties of carbon nanotubes/titania nanoparticles composite layers deposited by electrophoresis, Materials Science in Semiconductor Processing, 42 (2016) 45-49.

[191] K. Vinodgopal, P.V. Kamat, Enhanced rates of photocatalytic degradation of an azo dye using SnO2/TiO2 coupled semiconductor thin films, Environmental science & technology, 29 (1995) 841-845.

[192] S. Higashimoto, M. Sakiyama, M. Azuma, Photoelectrochemical properties of hybrid WO3/TiO2 electrode. Effect of structures of WO3 on charge separation behavior, Thin Solid Films, 503 (2006) 201-206.

[193] N. Serpone, P. Maruthamuthu, P. Pichat, E. Pelizzetti, H. Hidaka, Exploiting the interparticle electron transfer process in the photocatalysed oxidation of phenol, 2-chlorophenol and pentachlorophenol: chemical evidence for electron and hole transfer between coupled semiconductors, Journal of Photochemistry and Photobiology A: Chemistry, 85 (1995) 247-255.

[194] R. Amadelli, L. Samiolo, P. Pichat, Photoelectrocatalysis for water purification, in photocatalysis and water purification: From Fundamentals to Recent Applications, Weinheim: Wiley-VCH Verlag GmbH & Co. KGaA, 2013.

[195] X. Fu, L.A. Clark, Q. Yang, M.A. Anderson, Enhanced photocatalytic performance of titania-based binary metal oxides: TiO2/SiO2 and TiO2/ZrO2, Environmental science & technology, 30 (1996) 647-653.

[196] A. Goossens, E.L. Maloney, J. Schoonman, Gas-Phase Synthesis of Nanostructured Anatase TiO2, Chemical Vapor Deposition, 4 (1998) 109-114.

[197] H. Uchida, S. Katoh, M. Watanabe, Photocatalytic degradation of trichlorobenzene using immobilized TiO2 films containing poly (tetrafluoroethylene) and platinum metal catalyst, Electrochimica acta, 43 (1998) 2111-2116.

[198] Y. Zhang, J. Zhou, X. Chen, L. Wang, W. Cai, Coupling of heterogeneous advanced oxidation processes and photocatalysis in efficient degradation of tetracycline hydrochloride by Fe-based MOFs: synergistic effect and degradation pathway, Chemical Engineering Journal, 369 (2019) 745-757.

[199] A. Yazdanbakhsh, A. Eslami, M. Massoudinejad, M. Avazpour, Enhanced degradation of sulfamethoxazole antibiotic from aqueous solution using Mn-WO3/LED photocatalytic process: Kinetic, mechanism, degradation pathway and toxicity reduction, Chemical Engineering Journal, 380 (2020) 122497.

[200] M. Mangayayam, J. Kiwi, S. Giannakis, C. Pulgarin, I. Zivkovic, A. Magrez, S. Rtimi, FeOx magnetization enhancing E. coli inactivation by orders of magnitude on Ag-TiO2 nanotubes under sunlight, Applied Catalysis B: Environmental, 202 (2017) 438-445.

[201] Y. Shi, J. Ma, Y. Chen, Y. Qian, B. Xu, W. Chu, D. An, Recent progress of silver-containing photocatalysts for water disinfection under visible light irradiation: A review, Science of The Total Environment, 804 (2022) 150024.

[202] T. Ali, A. Ahmed, U. Alam, I. Uddin, P. Tripathi, M. Muneer, Enhanced photocatalytic and antibacterial activities of Ag-doped TiO2 nanoparticles under visible light, Materials Chemistry and Physics, 212 (2018) 325-335.

[203] P. Yu, X. Zhou, Z. Li, Y. Yan, Inactivation and change of tetracycline-resistant Escherichia coli in secondary effluent by visible light-driven photocatalytic process using Ag/AgBr/g-C3N4, Science of The Total Environment, 705 (2020) 135639.

[204] A. Kumar, S.K. Kansal, Magnetically Recyclable Photocatalysts for Degradation of Organic Pollutants in Aquatic Environment, Nanostructured Materials for Environmental Applications, Springer2021, pp. 365-382.

[205] S. Kumar, R. Sharma, A. Gupta, K.K. Dubey, A. Khan, R. Singhal, R. Kumar, A. Bharti, P. Singh, R. Kant, TiO2 based Photocatalysis membranes: An efficient strategy for pharmaceutical mineralization, Science of The Total Environment, 845 (2022) 157221.

[206] B. Xu, X. Wang, Y. Huang, J. Liu, D. Wang, S. Feng, X. Huang, H. Wang, Electrospinning preparation of PAN/TiO2/PANI hybrid fiber membrane with highly selective adsorption and photocatalytic regeneration properties, Chemical Engineering Journal, 399 (2020) 125749.

[207] M. Wang, F. Qu, R. Jia, S. Sun, G. Li, H. Liang, Preliminary Study on the Removal of Steroidal Estrogens Using TiO2-Doped PVDF Ultrafiltration Membranes, Water, 8 (2016) 134.

[208] D. Wang, J. Lin, J. Huang, H. Zhang, S. Lin, L. Chen, Y. Ni, L. Huang, A chitosan/dopamine-TiO2 composite nanofiltration membrane for antifouling in water purification, Cellulose, 28 (2021) 4959-4973.

[209] Y. Zhang, H. Tan, C. Wang, B. Li, H. Yang, H. Hou, C. Xiao, TiO2-coated glass hollow fiber membranes: preparation and application for photocatalytic methylene blue removal, Journal of the European Ceramic Society, 42 (2022) 2496-2504.

[210] T. Ribeiro, C. Baleizão, J.P.S. Farinha, Functional films from silica/polymer nanoparticles, Materials, 7 (2014) 3881-3900.

[211] Y. Wang, B. Ma, M. Ulbricht, Y. Dong, X. Zhao, Progress in alumina ceramic membranes for water purification: Status and prospects, Water Research, 226 (2022) 119173.

[212] C. Reyes, J. Fernandez, J. Freer, M. Mondaca, C. Zaror, S. Malato, H. Mansilla, Degradation and inactivation of tetracycline by TiO2 photocatalysis, Journal of Photochemistry and Photobiology A: Chemistry, 184 (2006) 141-146.

[213] X. Chen, X. Xu, J. Cui, C. Chen, X. Zhu, D. Sun, J. Qian, Visible-light driven degradation of tetracycline hydrochloride and 2, 4-dichlorophenol by film-like N-carbon@ N-ZnO catalyst with three-dimensional interconnected nanofibrous structure, Journal of hazardous materials, 392 (2020) 122331.

[214] M. El-Kemary, H. El-Shamy, I. El-Mehasseb, Photocatalytic degradation of ciprofloxacin drug in water using ZnO nanoparticles, Journal of Luminescence, 130 (2010) 2327-2331.

[215] X. Yu, J. Zhang, J. Zhang, J. Niu, J. Zhao, Y. Wei, B. Yao, Photocatalytic degradation of ciprofloxacin using Zn-doped Cu2O particles: analysis of degradation pathways and intermediates, Chemical Engineering Journal, 374 (2019) 316-327.

[216] K.H. Leong, B.L. Gan, S. Ibrahim, P. Saravanan, Synthesis of surface plasmon resonance (SPR) triggered Ag/TiO2 photocatalyst for degradation of endocrine disturbing compounds, Applied Surface Science, 319 (2014) 128-135.

[217] X. Liu, Y. Liu, S. Lu, W. Guo, B. Xi, Performance and mechanism into TiO2/Zeolite composites for sulfadiazine adsorption and photodegradation, Chemical Engineering Journal, 350 (2018) 131-147.

[218] A. Luthfiah, M.D. Permana, Y. Deawati, M.L. Firdaus, I. Rahayu, D.R. Eddy, Photocatalysis of nanocomposite titania–natural silica as antibacterial against Staphylococcus aureus and Pseudomonas aeruginosa, RSC Advances, 11 (2021) 38528-38536.

[219] Q. Cai, J. Hu, Effect of UVA/LED/TiO2 photocatalysis treated sulfamethoxazole and trimethoprim containing wastewater on antibiotic resistance development in sequencing batch reactors, Water Research, 140 (2018) 251-260.

[220] P. Karaolia, I. Michael-Kordatou, E. Hapeshi, C. Drosou, Y. Bertakis, D. Christofilos, G.S. Armatas, L. Sygellou, T. Schwartz, N.P. Xekoukoulotakis, Removal of antibiotics, antibiotic-resistant bacteria and their associated genes by graphene-based TiO2 composite photocatalysts under solar radiation in urban wastewaters, Applied Catalysis B: Environmental, 224 (2018) 810-824.

[221] K. Wang, Y. Luo, C. Gu, T. Zhi, L. Wang, D. Yan, Recent Developments In Immobilized Photocatalyst For Hydrogen Production, ChemCatChem, 16 (2024) e202400930.

[222] A.Y. Shan, T.I.M. Ghazi, S.A. Rashid, Immobilisation of titanium dioxide onto supporting materials in heterogeneous photocatalysis: A review, Applied Catalysis A: General, 389 (2010) 1-8.

[223] C. Yu, W. Zhou, H. Liu, Y. Liu, D.D. Dionysiou, Design and fabrication of microsphere photocatalysts for environmental purification and energy conversion, Chemical Engineering Journal, 287 (2016) 117-129.

[224] C.M. Costa, V.F. Cardoso, P. Martins, D.M. Correia, R. Goncalves, P. Costa, V. Correia, C. Ribeiro, M.M. Fernandes, P.M. Martins, Smart and multifunctional materials based on electroactive poly (vinylidene fluoride): recent advances and opportunities in sensors, actuators, energy, environmental, and biomedical applications, Chemical reviews, 123 (2023) 11392-11487.

[225] C. Ribeiro, C.M. Costa, D.M. Correia, J. Nunes-Pereira, J. Oliveira, P. Martins, R. Gonçalves, V.F. Cardoso, S. Lanceros-Méndez, Electroactive poly (vinylidene fluoride)-based structures for advanced applications, Nature protocols, 13 (2018) 681-704.

[226] J.M. Queirós, F. Zheng, R. Brito-Pereira, M.M. Fernandes, E.O. Carvalho, P.M. Martins, V. Lazić, J.M. Nedeljković, S. Lanceros-Mendez, Photocatalytic and antimicrobial polymer-based hybrid membranes with surface-modified TiO2 nanoparticles with 5-aminosalicylic acid and silver nanoparticles, RSC Sustainability, 3 (2025) 4568-4582.

[227] D.C. Alves, P.M. Martins, R. Pinto, P. Costa, B. Bazán, R.F. de Luis, D.M. Correia, S. Lanceros-Méndez, 3D-printed multilayer membranes for photocatalytic degradation of ciprofloxacin, Applied Materials Today, 44 (2025) 102728.

[228] A. Joseph, A. Vijayanandan, Review on support materials used for immobilization of nano-photocatalysts for water treatment applications, Inorganica Chimica Acta, 545 (2023) 121284.

[229] S. Sikiru, Y.O. Busari, J.O. Olutoki, M.M. Mahat, S.Y. Kolawole, Recent Advances in Polymer-Based Photocatalysts for Environmental Remediation and Energy Conversion: A Review, Journal of Polymer Materials, 42 (2025).

[230] S. Shukla, Polymer-Based Catalysts for Water Purification: Fundamentals to Applications, Polymeric Materials for Clean Water, Springer2018, pp. 121-148.

[231] B.T.I. Ali, Y. Kusumawati, J. Jaafar, D.O. Sulistiono, N. Widiastuti, Low-cost membrane from polyethylene terephthalate bottle waste for water purification and chromium removal: modification and application, RSC advances, 13 (2023) 8985-8995.

[232] A.A. Alshahrani, M. Alsuhybani, M.S. Algamdi, D. Alquppani, I. Mashhour, M.S. Alshammari, I.H. Alsohaimi, T.S. Alraddadi, Evaluating the performance of chitosan and chitosan-palm membrane for water treatment: preparation, characterization and purification study, Journal of Taibah University for Science, 15 (2021) 77-86.

[233] K. Li, W. Xu, G. Wen, Z. Zhou, M. Han, S. Zhang, T. Huang, Aging of polyvinylidene fluoride (PVDF) ultrafiltration membrane due to ozone exposure in water treatment: Evolution of membrane properties and performance, Chemosphere, 308 (2022) 136520.

[234] M. Shilpa, K. Harisha, S. Thripthi, M. Arpitha, Y. Sangappa, Eco-friendly magnetic silk fibroin films for heavy metal adsorption in water purification, Next Materials, 9 (2025) 101062.

[235] A. Ashley, B. Thrope, M.R. Choudhury, A.H. Pinto, Emerging investigator series: photocatalytic membrane reactors: fundamentals and advances in preparation and application in wastewater treatment, Environmental Science: Water Research & Technology, 8 (2022) 22-46.

[236] D. Seiler, J. Scheirs, PVDF in the chemical process industry, Modern fluoropolymers, (1997) 487-506.

[237] P. Saxena, P. Shukla, A comprehensive review on fundamental properties and applications of poly (vinylidene fluoride)(PVDF), Advanced Composites and Hybrid Materials, 4 (2021) 8-26.

[238] P.M. Martins, J.M. Queirós, H. Salazar, C. Costa, S. Lanceros-Mendez, Poly (Vinylidene Fluoride)-Based Membranes for Water Remediation, Piezoelectric Polymers and Polymer Composites for Advanced Applications, Springer2025, pp. 371-387.

[239] J.M. Queirós, H. Salazar, A. Valverde, G. Botelho, R.F. de Luis, J. Teixeira, P. Martins, S. Lanceros-Mendez, Reusable composite membranes for highly efficient chromium removal from real water matrixes, Chemosphere, 307 (2022) 135922.

[240] P. Martins, B. Santos, H. Salazar, S.A. Carabineiro, G. Botelho, C.J. Tavares, S. Lanceros-Mendez, Multifunctional hybrid membranes for photocatalytic and adsorptive removal of water contaminants of emerging concern, Chemosphere, 293 (2022) 133548.

[241] F. Zheng, P.M. Martins, J.M. Queirós, C.J. Tavares, J.L. Vilas-Vilela, S. Lanceros-Méndez, J. Reguera, Size effect in hybrid TiO2: Au nanostars for photocatalytic water remediation applications, International Journal of Molecular Sciences, 23 (2022) 13741.

[242] G.S. Padovani, A.O. Sanches, M.R. Moura Aouada, L.F. Malmonge, F.R. de Paula, Photocatalytic and antimicrobial efficacy of PVDF/TiO2 membranes fabricated by solution blow spinning, Journal of Applied Polymer Science, 141 (2024) e54761.

[243] L. Aoudjit, H. Salazar, D. Zioui, A. Sebti, P.M. Martins, S. Lanceros-Mendez, Reusable Ag@TiO2-Based Photocatalytic Nanocomposite Membranes for Solar Degradation of Contaminants of Emerging Concern, Polymers, 13 (2021) 3718.

[244] R. Gonçalves, J. Serra, A. Reizabal, D.M. Correia, L.C. Fernandes, R. Brito-Pereira, E. Lizundia, C.M. Costa, S. Lanceros-Méndez, Biobased polymers for advanced applications: Towards a sustainable future, Progress in Polymer Science, 162 (2025) 101934.

[245] R. Policia, R. Brito-Pereira, C.M. Costa, S. Lanceros-Méndez, F.N. Crespilho, Sustainable Power Generation with an All-Silk Electronics-Based Yeast Wearable Biobattery, ACS Omega, 10 (2025) 12522-12529.

[246] H.S. Samuel, F.-D.M. Ekpan, M.O. Ori, Biodegradable, recyclable, and renewable polymers as alternatives to traditional petroleum-based plastics, Asian Journal of Environmental Research, 1 (2024) 152-165.

[247] A.S. Castro, B.D.D. Cruz, D.M. Correia, S. Lanceros-Méndez, P.M. Martins, Sustainable Lignin-Reinforced Chitosan Membranes for Efficient Cr(VI) Water Remediation, Polymers, 16 (2024) 1766.

[248] R. Dubovenko, A. Kuzminova, M. Dmitrenko, A. Stepanova, A. Selyutin, R. Su, A. Penkova, Enhanced Sodium Alginate Membranes Modified with Metal–Organic Frameworks Based on Zirconium for Energy-Efficient Isopropanol Dehydration by Pervaporation, ACS Applied Polymer Materials, 6 (2024) 12675-12690.

[249] A. Etale, A.J. Onyianta, S.R. Turner, S.J. Eichhorn, Cellulose: a review of water interactions, applications in composites, and water treatment, Chemical reviews, 123 (2023) 2016-2048.

[250] S. Gupta, A. Nighojkar, N. Mayilswamy, B. Kandasubramanian, Recent trends in the application of silk-based composites for remediation of toxic contaminants from wastewater, Journal of Polymers and the Environment, 31 (2023) 2243-2272.

[251] T. Schiller, T. Scheibel, Bioinspired and biomimetic protein-based fibers and their applications, Communications Materials, 5 (2024) 56.

[252] J. Yang, Z. Wang, X. Liang, W. Wang, S. Wang, Multifunctional polypeptide-based hydrogel bio-adhesives with pro-healing activities and their working principles, Advances in Colloid and Interface Science, 327 (2024) 103155.

[253] A. Reizabal, C.M. Costa, L. Pérez-Álvarez, J.L. Vilas-Vilela, S. Lanceros-Méndez, Silk fibroin as sustainable advanced material: material properties and characteristics, processing, and applications, Advanced Functional Materials, 33 (2023) 2210764.

[254] Y. Zhang, S. Peng, X. Li, X. Wang, J. Jiang, X. Liu, L. Wang, Design and function of lignin/silk fibroin-based multilayer water purification membranes for dye adsorption, International Journal of Biological Macromolecules, 253 (2023) 126863.

[255] A. Naeem, B. Saeed, H. AlMohamadi, M. Lee, M.A. Gilani, R. Nawaz, A.L. Khan, M. Yasin, Sustainable and green membranes for chemical separations: A review, Separation and Purification Technology, 336 (2024) 126271.

[256] M.M.H. Mizan, F.R. Omi, H. Sultana, M. Sadrzadeh, Bio-sourced and biodegradable materials for membrane fabrication, Green Membrane Technologies towards Environmental Sustainability, Elsevier2023, pp. 169-208.

[257] P.M. Martins, J.M. Queirós, H. Salazar, C.M. Costa, S. Lanceros-Mendez, Poly(Vinylidene Fluoride)-Based Membranes for Water Remediation, in: S. Lanceros-Méndez, C.M. Costa (Eds.) Piezoelectric Polymers and Polymer Composites for Advanced Applications, Springer Nature Switzerland, Cham, 2025, pp. 371-387.

[258] C. Ursino, R. Castro-Muñoz, E. Drioli, L. Gzara, M.H. Albeirutty, A. Figoli, Progress of nanocomposite membranes for water treatment, Membranes, 8 (2018) 18.

[259] X. Dong, D. Lu, T.A.L. Harris, I.C. Escobar, Polymers and Solvents Used in Membrane Fabrication: A Review Focusing on Sustainable Membrane Development, Membranes, 11 (2021) 309.

[260] T. Xie, H. Wang, K. Chen, F. Li, S. Zhao, H. Sun, X. Yang, Y. Hou, P. Li, Q.J. Niu, High-performance polyethyleneimine based reverse osmosis membrane fabricated via spin-coating technology, Journal of Membrane Science, 668 (2023) 121248.

[261] A. Abedi, M. Hasanzadeh, L. Tayebi, Conductive nanofibrous Chitosan/PEDOT: PSS tissue engineering scaffolds, Materials Chemistry and Physics, 237 (2019) 121882.

[262] Y. Majooni, S.O. Abioye, K. Fayazbakhsh, N. Yousefi, Nano-enabled 3D-printed structures for water treatment, ACS ES&T Water, 4 (2024) 1952-1965.

[263] F. Guo, A. Servi, A. Liu, K.K. Gleason, G.C. Rutledge, Desalination by membrane distillation using electrospun polyamide fiber membranes with surface fluorination by chemical vapor deposition, ACS applied materials & interfaces, 7 (2015) 8225-8232.

[264] V.F. Cardoso, A.C. Lopes, G. Botelho, S. Lanceros-Mendez, Poly (vinylidene fluoride-trifluoroethylene) porous films: Tailoring microstructure and physical properties by solvent casting strategies, Soft Materials, 13 (2015) 243-253.

[265] L.A. Mercante, L.E. Iwaki, V.P. Scagion, O.N. Oliveira Jr, L.H. Mattoso, D.S. Correa, Electrochemical detection of bisphenol a by tyrosinase immobilized on electrospun nanofibers decorated with gold nanoparticles, Electrochem, 2 (2021) 41-49.

[266] A.M. Nasir, N. Awang, J. Jaafar, A.F. Ismail, M.H.D. Othman, M.A. Rahman, F. Aziz, M.A.M. Yajid, Recent progress on fabrication and application of electrospun nanofibrous photocatalytic membranes for wastewater treatment: A review, Journal of Water Process Engineering, 40 (2021) 101878.

[267] N. Yanar, P. Kallem, M. Son, H. Park, S. Kang, H. Choi, A New era of water treatment technologies: 3D printing for membranes, Journal of Industrial and Engineering Chemistry, 91 (2020) 1-14.

[268] S. Roy Barman, P. Gavit, S. Chowdhury, K. Chatterjee, A. Nain, 3D-printed materials for wastewater treatment, JACS Au, 3 (2023) 2930-2947.

[269] P. Calza, C. Medana, F. Carbone, V. Giancotti, C. Baiocchi, Characterization of intermediate compounds formed upon photoinduced degradation of quinolones by high-performance liquid chromatography/high-resolution multiple-stage mass spectrometry, Rapid Communications in Mass Spectrometry: An International Journal Devoted to the Rapid Dissemination of Up-to-the-Minute Research in Mass Spectrometry, 22 (2008) 1533-1552.

[270] Y. Pei, K. Luo, J. Zeng, J. Gao, H. Zhang, Review of the zebrafish (Danio rerio) model in disinfection by-products (DBPs) toxicity research: Opportunities and challenges, Journal of Hazardous Materials, 495 (2025) 138976.

[271] Q. Zhong, Z. Zhang, Q. Fu, J. Yu, X. Liao, J. Zhao, D. He, Molecular level insights into HO• and Cl2 • −-mediated transformation of dissolved organic matter in landfill leachate concentrates during the Fenton process, Chemical Engineering Journal, 446 (2022) 137062.

[272] A. Harada, K. Komori, N. Nakada, K. Kitamura, Y. Suzuki, Biological effects of PPCPs on aquatic lives and evaluation of river waters affected by different wastewater treatment levels, Water Science and Technology, 58 (2008) 1541-1546.

[273] K.A. Bawa-Allah, A.O. Ehimiyein, Ecotoxicological effects of human and veterinary antibiotics on water flea (Daphnia magna), Environmental Toxicology and Pharmacology, 94 (2022) 103932.

[274] Y. Shao, Z. Chen, H. Hollert, S. Zhou, B. Deutschmann, T.-B. Seiler, Toxicity of 10 organic micropollutants and their mixture: Implications for aquatic risk assessment, Science of The Total Environment, 666 (2019) 1273-1282.

[275] E. Costa, V. Piazza, C. Gambardella, R. Moresco, E. Prato, F. Biandolino, D. Cassin, M. Botter, D. Maurizio, R. D'Adamo, Ecotoxicological effects of sediments from Mar Piccolo, South Italy: toxicity testing with organisms from different trophic levels, Environmental Science and Pollution Research, 23 (2016) 12755-12769.

[276] J. Bellas, L. Saco-Álvarez, Ó. Nieto, R. Beiras, Ecotoxicological evaluation of polycyclic aromatic hydrocarbons using marine invertebrate embryo–larval bioassays, Marine Pollution Bulletin, 57 (2008) 493-502.

[277] S. Ceschin, A. Bellini, M. Scalici, Aquatic plants and ecotoxicological assessment in freshwater ecosystems: a review, Environmental Science and Pollution Research, 28 (2021) 4975-4988.

[278] E. Gripa, S.D.A. Daflon, R. de Almeida, F.V. da Fonseca, J.C. Campos, Landfill leachate treatment by high-pressure membranes and advanced oxidation techniques with a focus on ecotoxicity and by-products management: A review, Process Safety and Environmental Protection, 173 (2023) 747-764.

[279] V. Aruoja, H.-C. Dubourguier, K. Kasemets, A. Kahru, Toxicity of nanoparticles of CuO, ZnO and TiO2 to microalgae Pseudokirchneriella subcapitata, Science of the total environment, 407 (2009) 1461-1468.

[280] C. Adochite, L. Andronic, Aquatic toxicity of photocatalyst nanoparticles to green microalgae Chlorella vulgaris, Water, 13 (2020) 77.

[281] L.L. Oliveira, S.C. Antunes, F. Gonçalves, O. Rocha, B. Nunes, Evaluation of ecotoxicological effects of drugs on Daphnia magna using different enzymatic biomarkers, Ecotoxicology and environmental safety, 119 (2015) 123-131.

[282] R.S. Brito, A. Canedo, D. Farias, T.L. Rocha, Transgenic zebrafish (Danio rerio) as an emerging model system in ecotoxicology and toxicology: Historical review, recent advances, and trends, Science of the total environment, 848 (2022) 157665.

[283] X. Zhao, N. Wang, X. Sun, Transformation mechanisms and ecological risks of polybrominated benzene compounds in natural waters and AOPs, Process Safety and Environmental Protection, 200 (2025) 107450.

[284] R.V. Médice, R.J.d.C.F. Afonso, M.L.B. Almeida, S.F. de Aquino, M. Libânio, Preliminary assessment of antimicrobial activity and acute toxicity of norfloxacin chlorination by-product mixture, Environmental Science and Pollution Research, 28 (2021) 3828-3836.

[285] H. Chen, T. Lin, P. Wang, X. Zhang, F. Jiang, Y. Wang, Novel solar/sulfite advanced oxidation process for carbamazepine degradation: Radical chemistry, transformation pathways, influence on disinfection byproducts and toxic changes, Chemical Engineering Journal, 451 (2023) 138634.

[286] C.A. de Moraes, F.N. Oliveira, G. Qualhato, P.V.d.A. Brito, K. Simões, T.L. Rocha, R.F. Salla, L.G. Vieira, Single and combined chronic toxicity of cadmium and titanium dioxide nanoparticles in Aquarana catesbeiana (Anura: Ranidae) tadpoles, Aquatic Toxicology, 279 (2025) 107246.

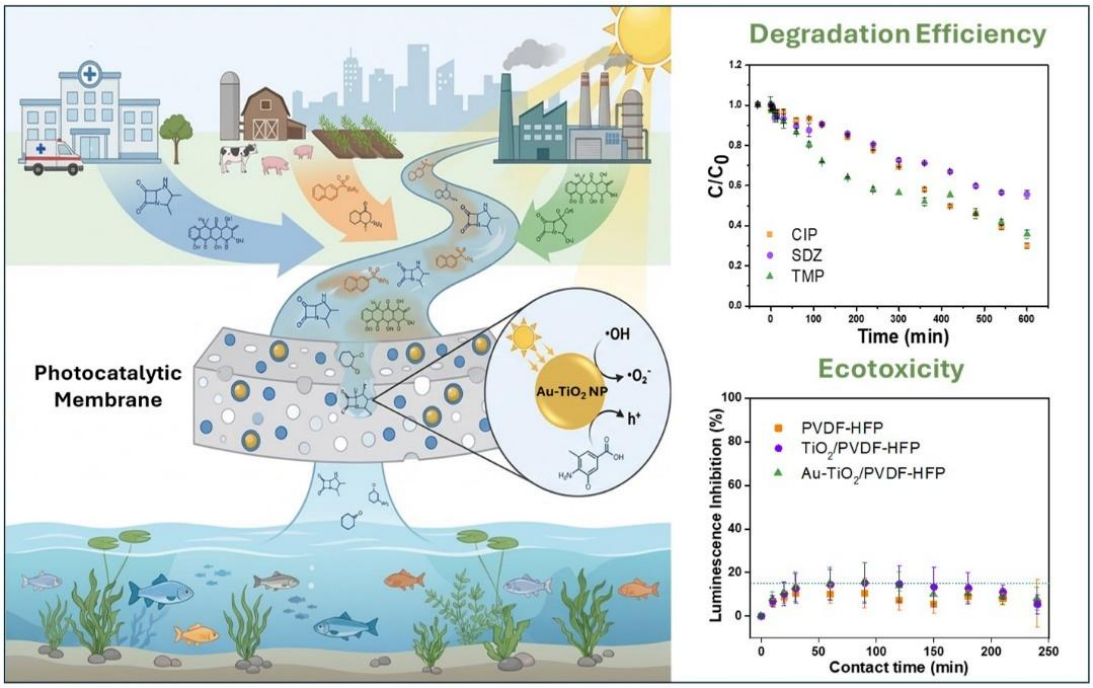
[287] A.R. Silva, P.M. Martins, S. Teixeira, S.A.C. Carabineiro, K. Kuehn, G. Cuniberti, M.M. Alves, S. Lanceros-Mendez, L. Pereira, Ciprofloxacin wastewater treated by UVA photocatalysis: contribution of irradiated TiO2 and ZnO nanoparticles on the final toxicity as assessed by Vibrio fischeri, RSC Advances, 6 (2016) 95494-95503.

CHAPTER 2

IMMOBILISATION OF NANOPARTICLES ON PVDF-HFP MEMBRANES FOR PHOTOCATALYTIC ANTIBIOTIC DEGRADATION

This chapter focuses on an eco-friendly synthesis of Au- and Ag-functionalised TiO_2 nanoparticles for the visible-light-driven photocatalytic degradation of antibiotics in water. The immobilisation of the selected nanomaterials on PVDF-HFP membranes is discussed as a strategy to enable catalyst reuse and minimise secondary release of nanoparticles. The chapter also includes the identification of degradation products and an ecotoxicological assessment of the by-products and the developed membranes.

This chapter is based on the following publication: **Joana M. Queirós**, Noelia González-Ballesteros, Jorge Sáiz, H. Salazar, Fangyuan Zheng, Soraia C. V. Rodrigues, Sónia A.C. Carabineiro, Carlos J. Tavares, S. Lanceros-Mendez, P.M. Martins, From Nanoparticles to Functional Membranes: Green-Synthesised Hybrid Photocatalysts for the Degradation of Antibiotics. *Submitted*



2.1 Introduction

Water is essential for all forms of life, and its pollution represents one of the most pressing challenges facing humanity in the 21st century. Poor water quality is estimated to be associated with more than 50 diseases, contributing to approximately 80% of illness cases and nearly half of all child deaths worldwide [1]. The consequences of water contamination include diarrheal and skin diseases, malnutrition, and even cancer [2].

Water contamination arises from the presence of various pollutants, traditionally classified as inorganic compounds, such as heavy metals [3], and organic compounds, such as pesticides [4, 5]. However, with the increasing production and consumption of chemicals, a new group of contaminants has emerged, known as contaminants of emerging concern (CECs). These contaminants are primarily associated with anthropogenic activities, including industry, agriculture, and healthcare [6, 7]. They are continuously released into the environment and persist in water bodies due to the inefficiency of conventional treatment processes [8]. Among CECs, antibiotics represent a major concern due to their incomplete metabolic transformation in humans and animals, leading to the excretion of active metabolites into sewage systems [9, 10]. The widespread use of antibiotics results in their accumulation in aquatic environments, posing significant risks to both human health and ecosystems. Such contamination contributes to the development of antibiotic-resistant bacteria, thereby complicating medical treatments and compromising the effectiveness of essential therapies for bacterial infections [11]. These concerns are reflected in the

inclusion of several antibiotics on the European Union (EU) Watch List of emerging pollutants, signifying growing regulatory pressures to control their presence in aquatic environments [12].

Wastewater treatment plants (WWTPs) have traditionally been the primary technology for removing antibiotics from wastewater [13]. However, conventional treatment processes are often ineffective, leading to the persistence of these contaminants in treated effluents. For example, ciprofloxacin (CIP) has been detected at concentrations ranging from 127 to 1396 ng/L in hospital effluents [14], sulfadiazine (SDZ) at up to 108 ng/L in surface waters [15], and trimethoprim (TMP) at 876 ng/L in river water [16]. Although these concentrations are in the ng/L range, they are considered environmentally significant, as they have been linked to ecotoxicological effects, such as the inhibition of algae growth [17], changes in microbial communities [18], and sublethal toxicity in aquatic organisms [19], all of which contribute to long-term ecological risks [20].

To overcome the limitations of conventional treatments, novel materials and technologies, such as advanced oxidation processes (AOPs), have been explored as promising alternatives capable of effectively degrading antibiotics while ensuring environmental safety [21]. Among these, photocatalysis has emerged as a suitable mechanism due to its simplicity, ease of implementation, and ability to mineralise complex organic molecules through the interaction of radiation by a photocatalyst [22].

Semiconductors, such as titanium dioxide (TiO_2) or zinc oxide (ZnO) are extensively utilised in photocatalysis due to their favourable optical properties, low cost, availability, high activity, chemical and thermal stability, chemical resistance to breakdown, and mechanical robustness. However, their photocatalytic activity is primarily confined to the UV-A region (315-400 nm), which limits the efficient use of solar radiation as an energy source [23].

To enhance the visible-light responsiveness of these photocatalysts [24, 25], functionalisation with noble metals such as gold (Au) [26] silver (Ag) [27] or copper (Cu) [28] has been explored, as they promote the presence of the surface plasmon resonance (SPR) and facilitate electron transfer and suppresses electron-hole recombination [29]. Despite these advantages, conventional synthesis routes for such nanomaterials often rely on toxic and expensive chemical reagents, emphasising the necessity for more environmentally friendly and sustainable synthesis approaches.

In response, green synthesis approaches using natural compounds derived from plants [30], bacteria [31], fungi [32], and algae [33] have gained increasing attention [34]. In this context, quercetin, a flavonoid commonly found in apples, onions, and berries, has emerged as a promising sustainable reducing agent for the synthesis of gold (Au NPs) [35] and silver (Ag NPs) nanoparticles [36]. Its well-

documented antioxidant and antimicrobial properties further underline the potential of plant-derived compounds as eco-friendly reducing and stabilising agents in nanoparticles synthesis [37].

In addition to the limited visible activation of the photocatalysts, another major challenge lies in the recovery of the particles in water treatment. The immobilisation of photocatalysts onto solid substrates offers several benefits, including the elimination of post-treatment filtration steps, simplification of the process, and overall cost reduction [38, 39]. Moreover, immobilisation promotes reusability and mitigates the risk of secondary particulate pollution [40].

Polymeric materials are particularly attractive for nanoparticle immobilisation due to their low cost and ease of processing through various techniques [41, 42]. Among them, polyvinylidene fluoride (PVDF) and its copolymers are extensively studied as polymeric matrices for nanoparticle incorporation. These materials are especially suitable for environmental remediation applications due to their excellent thermal and mechanical stability, chemical and UV resistance, and versatility in being processed into different morphologies [43].

Although immobilisation addresses the practical challenges associated with the application and recovery of photocatalysts, it does not eliminate all environmental concerns. Water treatments, such as AOPs, can generate transformation products that are more toxic than the original contaminants [44]. In addition, the presence of nanocomposites in treated water may result in incompatibilities or degradation that introduce further ecotoxicological risks [45].

Beyond efficiency and reusability, toxicity bioassays are essential tools for evaluating the environmental impact of photocatalytically treated wastewater [46]. The luminescent bacterium Vibrio fischeri, known for its high sensitivity to toxic substances, provides a rapid and reliable method for evaluating both treated samples and generated by-products [47, 48]. These assays measure bacterial luminescence, which correlates with metabolic activity — a reduction in light emission indicates increased toxicity in the tested sample [49]. The application of these bioassays ensures that the proposed treatment systems are not only effective in contaminant removal but also safe for aquatic ecosystems, aligning with the principles of sustainability and environmental protection.

In this study, Au-TiO_2 and Ag-TiO_2 nanoparticles are synthesised through a green method and immobilised on a porous polyvinylidene fluoride-co-trifluoroethylene (PVDF-HFP) substrate, enabling material reuse and efficient degradation of CIP, SDZ, and TMP. The evaluation of these antibiotics as model pollutants is crucial due to their structural and chemical diversity in real aquatic systems, allowing the validation of the photocatalysts' applicability and efficiency.

Emphasis was placed on identifying materials that exhibit enhanced photocatalytic activity under visible light, representing a sustainable approach for the remediation of antibiotic-contaminated water. Furthermore, by correlating photocatalytic degradation behaviour with the specific chemical characteristics of each compound, this work aims to gain broader insights into how molecular structure influences degradation pathways and efficiency, thereby establishing general guidelines for selecting photocatalysts according to pollutant type. Finally, detailed degradation pathway analyses and ecotoxicological assessments are conducted, including by-product analysis identification and toxicity evaluation using the luminescent bacterium *Vibrio fischeri*, to determine potential adverse environmental effects.

2.2 Materials and methods

2.2.1 Materials

Titanium dioxide nanoparticles (P25 TiO_2) were supplied by Evonik (Evonik Corporation, USA). Quercetin hydrate (95 %), gold (III) chloride solution (99.99 %) and silver nitrate (99 %) were purchased from Sigma Aldrich. Sodium hydroxide (NaOH, 98.0-100.5 %) was obtained from PanReac. Terephthalic acid (TA, >99 %) and 2-hydroxyterephthalic acid (2-HTA, ≥98 %) were acquired from Thermo Fisher Scientific (Kandel) GmbH, while L-histidine (98 %) was also purchased from Sigma-Aldrich. N,N-dimethyl-N-dimethyl-4-nitrosoaniline, 98 %) was supplied by Alfa Aesar. PVDF-HFP was obtained by Solvay, and N,N-dimethylformamide (DMF) from Merck. Ciprofloxacin (CIP, $C_{17}H_{18}FN_3O_3$), sulfadiazine (SDZ, $C_{10}H_{10}N_4O_2S$), and trimethoprim (TMP, $C_{14}H_{18}N_4O_3$) were purchased from Thermo Fisher Scientific (Kandel, Germany). Ultrapure water (UP) was produced using a Millipore Milli-Q purification system. The luminescent bacterium *Vibrio fischeri* was obtained from Macherey-Nagel GmbH & Co. KG (Düren, Germany).

2.2.2 Synthesis and functionalisation of Au-TiO_2 and Ag-TiO_2 nanoparticles

Quercetin was used for the green synthesis of Au- and Ag-modified TiO_2 nanoparticles (Au-TiO_2 and Ag-TiO_2, respectively), following a previously reported protocol [37]. For the synthesis of Au-TiO_2, 200 mg of TiO_2 (P25) were dispersed in 40 mL of ultrapure water under sonication (ULTRASONS-HD, JP Selecta, Spain) at room temperature for 30 min. Subsequently, an aqueous solution of $HAuCl_4$ (0.05 wt. %) was added dropwise and stirred for 15 min to ensure a homogeneous distribution of gold ions (final gold concentration: 0.1 wt.%). A freshly prepared quercetin solution (0.05%, in basic medium) was then added,

and the mixture was allowed to react until a visible colour change from pale yellow to pink occurred, indicating nanoparticle formation (final quercetin concentration: 20 μg/mL). The resulting suspension was centrifuged (Sigma 4-16KS, Sigma, Germany) twice at 14,000 rpm for 30 min and redispersed in ultrapure water using ultrasound and subsequently dried overnight at 80 °C in an oven (Digitronic, JP Selecta, Spain).

The synthesis of Ag-TiO_2 followed the same protocol, but using silver nitrate ($AgNO_3$, 0.05 wt. %), to achieve a final silver concentration of 0.2 wt. %.

2.2.3 Nanoparticles characterisation

Transmission electron microscopy (TEM) was employed to investigate the morphology of the Au-TiO_2 and Ag-TiO_2 nanoparticles using a JEOL JEM-1010 microscope (JEOL, Tokyo, Japan) operating at an accelerating voltage of 100 kV. For sample preparation, nanoparticles were ultrasonically dispersed in ultrapure water for 30 min, a drop of the suspension was deposited onto 400-mesh copper grids coated with formvar/carbon, and then it was allowed to dry at room temperature

X-ray diffraction (XRD) patterns were recorded using a D8 Discover diffractometer (Bruker AXS, Billerica, MA, USA) equipped with a Cu K α radiation source (λ = 1.5406 Å), operated at 40 kV and 30 mA. Scans were performed over a 2 θ range of 20°-80° with a step size of 0.02°.

Fourier-transform infrared (FTIR) spectra were obtained using a Jasco FT/IR-6100 spectrophotometer (JASCO, Tokyo, Japan) and the potassium bromide (KBr) pellet method within the range of 4000-400 cm^{-1} at a resolution of 4 cm^{-1}. Ultraviolet-visible (UV-Vis) diffuse reflectance spectroscopy (DRS) measurements were carried out using a Shimadzu UV-2501-PC spectrophotometer (Shimadzu Corporation, Kyoto, Japan) equipped with an integrating sphere. $BaSO_4$ was used as a standard for 100% reflectance. Reflectance spectra were recorded between 240 and 800 nm and converted to absorbance using the Kubelka-Munk function, according to Eq. 2.1:

$$F(R) = (1 - R_\infty)^2/(2R_\infty) \qquad \text{Eq. 2.1}$$

where R∞ represents the ratio of the sample reflectance to that of $BaSO_4$.

The optical band gap energy (E_g) values were estimated using Tauc plots, according to Eq. 2.2:

$$[F(R)h\upsilon]^{1/n} \text{ versus } h\upsilon \qquad \text{Eq. 2.2}$$

where h is Planck's constant (6.626 × 10-34 J·s), υ is the photon frequency, and n=2 corresponds to indirect electronic transitions.

The hydrodynamic diameter and zeta potential (ζ -potential) of the nanoparticles were determined by dynamic light scattering (DLS) using a Zetasizer Nano S system (Malvern Instruments, Malvern, UK) equipped with a 633 nm He-Ne laser and a backscattering detection angle of 173°. Prior to analysis, samples were dispersed in ultrapure water at a concentration of 0.5 mg/mL and sonicated in an ultrasonic bath for 30 min to prevent aggregation. For ζ -potential analysis, the pH of the dispersions was adjusted to 3, 5, 7, 9, and 11 using HCl and NaOH solutions. Each measurement was repeated five times to ensure reproducibility. Data were processed using Zetasizer software (version 7.13) to obtain the particle size distribution, the polydispersity index (PDI), and ζ -potential values.

2.2.3.1 Photogenerated Reactive Oxygen Species (·OH and $^1O_2$) measurements

2.2.3.1.1 Detection of hydroxyl radicals (•OH)

Based on the previously reported method [26], hydroxyl radicals (•OH) generated upon illumination were detected and quantified through the hydroxylation of terephthalic acid (TA) to 2-hydroxyterephthalic acid (2-HTA) in a heterogeneous system.

In brief, a 0.5 mM TA solution was prepared by dissolving TA in a 2 mM NaOH solution. Subsequently, 50 mg nanoparticles were dispersed in 50 mL of TA solution (0.5 mM) and stirred in the dark for 30 min to achieve adsorption-desorption equilibrium. The suspension was then irradiated under UV radiation for 60 min with continuous stirring. At selected irradiation intervals, aliquots were withdrawn, centrifuged to remove the nanoparticles, and 200 μL of the resulting supernatant was collected and analysed using a microplate reader (Infinite 200 Pro, Tecan Group Ltd). The fluorescence intensity of 2-HTA was measured at an emission wavelength of 425 nm, with excitation at 315 nm [50]. A standard calibration curve of 2-HTA was established to correlate fluorescence intensity with the concentration of generated hydroxyl radicals.

2.2.3.1.2 Detection of singlet oxygen ($^1O_2$)

As described in a previous work [26], the histidine test was employed to detect and quantify singlet oxygen ($^1O_2$), which indirectly reflects the formation of superoxide radicals ($\cdot O_2^-$). Briefly, a reaction mixture was prepared by mixing 40 mL of L-histidine solution (0.2 mM) with 10 mL of N,N-dimethyl-4-nitrosoaniline solution (0.2 mM). Afterwards, 50 mg of nanoparticles were added to the mixture and

stirred in the dark for 30 min to reach adsorption equilibrium. Subsequently, the suspension was irradiated under UV light for 60 min with continuous stirring. At predetermined irradiation intervals, aliquots were withdrawn, centrifuged to remove the nanoparticles, and the resulting supernatant was analysed using a microplate reader (Infinite 200 Pro, Tecan Group Ltd). The absorbance decrease of N,N-dimethyl-4-nitrosoaniline at 440 nm in the UV-vis spectrum was monitored to quantify $^1O_2$ generation.

The reaction between L-histidine and $^1O_2$ yields a trans-annular peroxide, which oxidises N,N-dimethyl-4-nitrosoaniline, resulting in decolorization at 440 nm. A standard calibration curve was established to correlate between the absorbance decrease with the concentration of N,N-dimethyl-4- nitrosoaniline.

2.2.3.2 Photocatalysts Performance

The photocatalytic activity of the synthesized nanoparticles was evaluated through the degradation of three model antibiotics: CIP, TMP and SDZ. These were selected as representative contaminants due to their environmental relevance and distinct chemical structures. Initial concentrations of 5, 10 and 15 mg/L for CIP, SDZ and TMP, respectively, were chosen to achieve comparable initial absorbance values (≈0.5) at their respective maximum absorption wavelengths, ensuring consistent sensitivity and linearity in UV-Vis spectroscopy monitoring across all experiments. Photocatalytic suspensions were prepared by dispersing the nanoparticles at a concentration of 1 g/L in aqueous solutions within a batch reactor, under continuous stirring, to ensure homogenisation. As a control, antibiotic solutions were first exposed to UV radiation in the absence of catalysts to evaluate the degree of direct photolysis of each antibiotic. Additionally, prior to light irradiation, all suspensions were kept in the dark for 30 min to establish adsorption-desorption equilibrium between the antibiotics and the nanoparticle surface.

The reaction mixtures were then irradiated for 90 min under both UV and visible light sources. UV-induced degradation was carried out in a photoreactor equipped with eight 8 W UV lamps (λ = 365 nm) positioned 13.5 cm from the solution, providing an irradiance of 3.3 W/m^2. For visible light degradation, a xenon lamp (350-1400 nm, λ = 550 nm, 1400 W/m^2) was used at 21 cm from the solution.

Antibiotic degradation was monitored at defined times by withdrawing aliquots and determining concentrations via UV-Vis spectroscopy using the Infinite 200 Pro microplate reader (Tecan Group Ltd), in the range of 230-350 nm.

The degradation kinetics were analysed according to a pseudo-first-order reaction, described by the Langmuir-Hinshelwood model in Eq. 1.3 in Chapter 1 [51].

2.2.4 Composite Membrane Production

The Au-TiO_2/PVDF-HFP and TiO_2/PVDF-HFP composite membranes were prepared following established procedures in the literature [27], as schematically illustrated in Figure 2.1. The concentration of immobilised nanoparticles (10 wt.%) was selected based on previous reports, indicating that this composition provides an optimal compromise between photocatalytic efficiency and mechanical stability of the polymeric matrix [41]. Initially, the required amount of photocatalyst was first dispersed in DMF using an ultrasonic bath for 3 h to achieve complete homogenization. Subsequently, 1 g of PVDF-HFP was added to the dispersion and magnetically stirred until fully dissolved, yielding a polymer-to-solvent ratio of 10:90 (v/v). The resulting solution was then cast onto a clean glass substrate, spread using a doctor blade, and left to dry at room temperature for approximately 7 days.

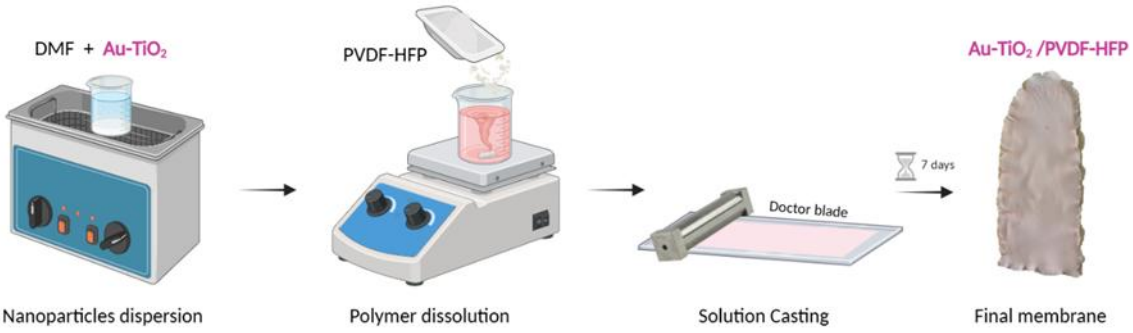


Figure 2.1. Schematic representation of the processing of PVDF-HFP membranes incorporating Au-functionalised TiO_2 nanoparticles.

2.2.5 Nanocomposites characterisation

The morphology of the nanocomposite membranes was examined using a field-emission scanning electron microscope (FE-SEM, Hitachi S-4800N, Tokyo, Japan). Prior to imaging, the membrane surfaces were sputter-coated with a thin Au layer by using a Polaron SC502 sputter coater to enhance conductivity and prevent charging effects.

The porous structure of the membranes was characterized by mercury intrusion porosimetry (MIP) with a Micromeritics Autopore IV at the Requimte Analysis Laboratory, operating in a vacuum pressure range up to 207 MPa.

The vibrational spectra of PVDF-HFP, TiO_2/PVF-HFP and Au-TiO_2/PVDF-HFP membranes were recorded by FTIR spectroscopy within the range of 4000-600 cm^{-1}. From these spectra, the relative fraction of the polar β-phase in the polymer was calculated with Eq. 2.3 [52]:

$$F(\beta) = \frac{A_\beta}{\left(\frac{K_\beta}{K_\alpha}\right)A_\alpha + A_\beta} \qquad \text{Eq. 2.3}$$

where A_α and A_β are the absorbance of the characteristic absorption bands of the α- and β-phases of PVDF-HFP, located at 763 and 838 cm^{-1}, respectively; K_α and K_β are the corresponding absorption coefficients, with values of 6.1×10^4 and 7.7×10^4 cm^2/mol, respectively.

Differential Scanning Calorimetry (DSC) was performed to evaluate the thermal properties of pristine PVDF-HFP and the composite membranes. The analysis was carried out using a Mettler Toledo DSC822e instrument over a temperature range of 30 to 220 °C, at a heating rate of 10 °C/min, under a N_2 atmosphere. The crystallinity of the membranes (X_c) was evaluated by Eq. 2.4 [52]:

$$X_c(\%) = \frac{\Delta H_f}{x\Delta H_\alpha + y\Delta H_\beta} \times 100 \qquad \text{Eq. 2.4}$$

where ΔH_f is the melting enthalpy of the membrane (J/g), x and y represent the α and β phase contents of the sample, respectively, ΔH_α and ΔH_β correspond to the enthalpies of fusion of perfect crystals of α-PVDF (93.04 J/g) and β-PVDF (104.4 J/g), respectively [53].

The mechanical properties of the membranes were evaluated in tensile testing using a Shimadzu Universal testing device (AD-IS) equipped with a 500 N load cell. Membrane samples with dimensions of 20 × 10 mm^2 were subjected to tensile loading at a rate of 1 mm per min. The thickness of each membrane, obtained using a Fischer Dualscope MPOR, was approximately 200 µm. Measurements were performed on both dry and wet states of Au-TiO_2/PVDF-HFP membranes, the wet samples being prepared by immersion in deionised water for 2 min. The stress-strain measurements were conducted in triplicate and the data provided is the average of the three measurements

The surface wettability was evaluated by contact angle (CA) measurements using an Ossila contact angle goniometer. For each sample, three droplets (5 µL each) of ultrapure water were deposited on different areas of the membrane surface. The contact angle values were recorded immediately after droplet deposition, and the mean CA value was calculated as the average of the three measurements, with the corresponding standard deviation reported.

2.2.6 Photocatalytic Activity of the Composite Membranes

Following the screening process, the NPs that exhibited the highest photocatalytic efficiency across all the antibiotics were immobilised onto PVDF-HFP membranes to enhance reusability and prevent secondary pollution. Prior to the degradation experiments, the functionalised membranes (surface area = 15 cm^2) were secured in a beaker reactor, ensuring uniform irradiation across all samples.

Photocatalytic tests were performed under the same lighting conditions described in Section 2.2.3.2 for the nanoparticle suspension experiments, but with an extended exposure time of 600 min to account for the immobilized configuration. The stability and reusability of the membranes were evaluated over three consecutive degradation cycles, with intermediate washing steps using ultrapure water to remove residual contaminants.

The degradation of antibiotics was monitored following the methodology outlined in Section 2.2.3.2, and the corresponding kinetic data were fitted to the pseudo-first-order model.

2.2.6.1 Photocatalytic degradation Mechanism

The samples were analysed by Liquid Chromatography-Mass Spectrometry (LC-MS) in an Agilent 1290 Infinity II coupled to a Revident G6575A LC-Q-TOF MS system. The mobile phase consisted of (A) 0.1 % (v/v) formic acid in ultrapure water, and the mobile phase (B) 0.1 % (v/v) of formic acid in acetonitrile. The injection volume was set to 2 µL, using a multi-wash cycle of the injection needle and port under the initial chromatographic conditions. The temperature in the column oven was maintained at 30°C, and the flow rate was set to 0.500 mL/min throughout the analysis. The chromatographic gradient was programmed as follows: 0.00-2.00 min: 0 % B (isocratic); linear increase to 100 % B; 10.00-12.00 min: 100 % B (isocratic hold); and 12.01-15 min: return to initial conditions (0 % B) for re-equilibration. Mass spectrometric detection was performed using a dual AJS ESI ion source operated in positive ionisation mode under the following conditions: gas temperature 325 °C, drying gas flow 8 L/min, nebuliser pressure 2.07×10^5 Pa, sheath gas temperature 250 °C, and sheath gas flow 11 L/min. The capillary voltage was 3500 V, the nozzle voltage 1000 V, and fragmentor voltage 175 V, the Oct 1 RF Vpp 750 V, and the skimmer voltage 45 V. The system was operated in auto MS/MS acquisition mode, with data recorded in centroid format. For MS-only acquisition, the m/z range was 20-1000, at a scan rate of 9 spectra/s. For MS/MS acquisition, the m/z range was 20-450, also at 9 spectra/s. A maximum of three precursor ions per cycle were selected using a narrow isolation window and an absolute threshold of 1000 counts. Reference masses used of m/z 121.050873 and m/z 922.009798 were used for mass calibration during analysis.

Raw data acquired in data-dependent acquisition (DDA) were processed using MS-DIAL version 5.3.240719 for deconvolution, peak detection and alignment. The mass tolerances for MS1 and MS2 were set at 0.0010 and 0.0025 Da, respectively. The retention time range for data collection was from 0.0 min to 12.5 min. The mass range for MS1 and MS2 were 50-400 Da and 20-400 Da, respectively. A minimum peak height of 3000 and a mass slice width of 0.1 Da were applied for peak detection. Smoothing was performed using a linear weighted moving average with a level of 3 and a minimum peak width of 5 scans. For deconvolution, a sigma window value of 0.5 was used, and the MS/MS abundance cut-off was set to 0 in amplitude. Masses above the precursor ions were excluded, while isotopic ions up to 5 Da above the precursor were retained. Only the $[M+H]^+$ adduct was considered during processing. Peak alignment was performed with a retention time tolerance of 0.1 min and a MS1 tolerance of 0.0015 Da. Both the retention time factor and MS1 alignment factors were set to 0.5. No peaks were excluded based on count, and blank subtraction was carried out in a later stage.

Using these parameters, a total of 129 features were detected. After applying a blank subtraction with a fold change threshold of 5, removing features that appeared in only one sample and excluding ion source-generated fragments, 45 features remained in the final dataset.

The resulting list of compounds was compiled through manual examination, supported by information obtained from Biotransformer 3.0, which included parent compounds with up to three iterations of abiotic reactions, and from the EAWAG-BBD database for pathway prediction.

Quantification of TMP, CIP and SDZ was performed using calibration curves. The degradation products were semi-quantified based on these calibration curves to provide relative concentration estimates.

2.2.7 Ecotoxicity Assessment

Ecotoxicity testing was performed using the bioluminescent bacterium *Vibrio fischeri*, obtained from Macherey-Nagel GmbH & Co. KG (Düren, Germany). The bacterial cultivation and testing procedures followed the ISO 11348-1 standard "Water quality – Determination of the inhibitory effect of water samples on the light emission of *Vibrio fischeri* (Luminescent bacteria test)", using the freeze-dried bacteria method [54].

The freeze-dried *V. fischeri* was reactivated with 1 mL of reconstitution solution, manually shaken, and subsequently incubated on Petri dishes with solid growth medium for 3 days at 20°C. The luminescent colonies were then transferred to Erlenmeyer flasks containing 50 mL of liquid growth medium and incubated at 20 ± 1°C, with continuous shaking at 180 rpm.

For ecotoxicity testing, *V. fischeri* cell cultures were centrifuged at 6000 rpm for 5 min and washed twice with a 2.0 % (w/v) NaCl solution at pH 6.5. The optical density (OD) of the bacterial suspension was adjusted to 0.6 ± 0.01 at 578 nm using sterile saline solution, corresponding to a final bacterial concentration of 1.5×10^6 cells/mL. Potassium dichromate ($K_2Cr_2O_7$) was used as a positive control in accordance with ISO 11348-3.

Luminescence assays were conducted using a Biotek® Cytation3 microplate reader and 96-well black optical plates (Nalge Nunc™ International). Sterilised membrane films (5.0 mm in diameter) were placed in contact with 250 µL of the bacterial suspension and incubated at 20 ± 1°C under shaking at 180 rpm. Luminescence intensity was measured at multiple time intervals (0, 10, 20, 30, 40, 60, 90, 120, 150, 180, 210 and 240 min) using an Infinite M Plex spectrophotometer (TECAN). The initial measurement (I_0) corresponded to the emission intensity recorded immediately after sample exposure to the bacterial suspension.

Toxicity was expressed as the percentage of luminescence inhibition (INH %), calculated according to Eq. 2.5 [55]:

$$\text{INH } \% = 100 - \left(\frac{IT_T}{KF \times IT_0}\right) \times 100, \quad with \quad KF = \frac{IC_T}{IC_0} \qquad \text{Eq. 2.5}$$

Where KF is the correction factor accounting for natural luminescence decay observed in the control. IC_0 represents the initial luminescence of the control, IT_0 is the initial luminescence of the test sample, IC_T corresponds to the control luminescence after the contact time, and IT_T is the luminescence of the test sample after the contact time. All assays were performed in triplicate to ensure reproducibility and statistical reliability.

2.3 Results and discussion

2.3.1 Characterization of Au-TiO_2 and Ag-TiO_2 nanocomposites

Quercetin was employed as a green reducing agent for the functionalisation of TiO_2 surfaces with gold and silver nanoparticles. The Ag and Au loaded used to functionalise the TiO_2 nanoparticles were previously optimised in another works [29, 37]. Both Au-TiO_2 and Ag-TiO_2 nanocomposites were successfully produced, demonstrating the versatility of quercetin-mediated processes for the environmentally friendly synthesis of metallic nanostructures on semiconductor surfaces. [37].

The morphology of TiO_2, Au-TiO_2, and Ag-TiO_2 was examined by TEM analysis, as shown in Figures 2.2a, b, and c, respectively. The TEM images show that the deposition of gold and silver nanoparticles does not result in significant morphological changes in the nanocomposites. Due to the low metal loading and the limited contrast between TiO_2 and the metallic nanoparticles, distinguishing the Au and Ag particles from the TiO_2 background is challenging. Nevertheless, the overall size and shape of the TiO_2 nanoparticles remain consistent with those of the pristine material, confirming that the functionalisation process preserves the structural integrity of the semiconductor.

The crystalline structure of the nanocomposites was analysed by XRD and compared with that of pristine TiO_2 (Figure 2.2d). The results show that the synthesis procedure does not alter the crystalline structure of TiO_2. All samples exhibit the characteristic diffraction peaks of the anatase (25.3°, 36.9°, 37.9°, 48.0°, 54.0°, 55.1°, 62.8° and 69.0°) and the rutile (27.4°, 36.1° and 41.3°) crystalline phases, consistent with the reference TiO_2 patterns (JCPDS card no. 00-021-1272 for anatase and 01-070-7347 for rutile) [39]. No distinct diffraction peaks corresponding to metallic gold or silver are observed in the Au-TiO_2 and Ag-TiO_2 samples, which is attributed to the low loading of metal nanoparticles relative to the TiO_2 content, resulting in diffraction signals below the instrument's detection limit. The expected diffraction positions for metallic Au (JCPDS card no. 04-0784) and Ag (JCPDS card no. 04-0783) are indicated in Figure 2.2d by * and #, respectively. It is worth noting that the most intense diffraction peak for both Au and Ag (≈38°) overlap with an anatase TiO_2 reflection, further contributing to the absence of distinguishable metallic peaks.

Figure 2.2e presents the FTIR spectra of the Au-TiO_2 and Ag-TiO_2 composites, compared to pristine TiO_2 and pure quercetin. In both nanocomposite spectra, only the characteristic bands of TiO_2 are observed: a broad absorption band around ≈3400 cm^{-1}, associated with O–H stretching vibrations of adsorbed water molecules and hydroxyl groups; a band near ≈1600 cm^{-1}, corresponding to the bending vibrations of molecular water; and a strong, broad absorption below 1000 cm^{-1} attributed to Ti-O-Ti lattice vibrations [56, 57]. No significant new bands or spectral shifts are detected upon the incorporation of gold or silver, suggesting that their presence does not alter the TiO_2 lattice structure. This observation supports the conclusion that the noble metal nanoparticles are deposited on the TiO_2 surface rather than incorporated into its crystalline framework (as confirmed later by the similar XRD patterns of pristine TiO_2 and Ag/Au-doped TiO_2). Moreover, the absence of vibrational bands characteristic of quercetin in the Au-TiO_2 and Ag-TiO_2 spectra confirms the effective removal of organic residues during the synthesis and purification steps. This is a crucial aspect, as the presence of residual organic compounds on the TiO_2

surface can hinder the photocatalytic performance by reducing light-harvesting and reactive oxygen species (ROS) generation [58, 59].

The formation of Au-TiO_2 and Ag-TiO_2 nanocomposites was confirmed by DRS measurements (Figure 2.2f). In both cases, a pronounced decrease in the diffuse reflectance is observed in the characteristic SPR regions of the respective metals, confirming the effective functionalisation of TiO_2. In the case of the Au-containing nanocomposite, the diffuse reflectance decreases from approximately 90% for pristine TiO_2 to approximately 50% within the range of 500–600 nm, which is consistent with the typical SPR band of gold nanoparticles. Similarly, for the Ag-TiO_2 nanocomposites, a substantial decrease in diffuse reflectance to approximately 30% is detected between 400 and 500 nm, corresponding to the SPR band of silver nanoparticles.

To further investigate the optical properties, the optical band gap (Eg) values were estimated using Tauc plots derived from the Kubelka–Munk function (Figure 2.2g). Pristine TiO_2 exhibits a band gap of 3.05±0.02 eV, which is consistent with values previously reported in the literature [60, 61]. Upon functionalisation, a reduction in the band gap is observed, decreasing to 2.96±0.01 eV for Au-TiO_2 and to 2.90±0.06 eV for Ag-TiO_2. This band gap narrowing is attributed to the localised surface plasmonic effects induced by the metallic nanoparticles, which introduce additional electronic states near the conduction band of TiO_2, thereby enhancing visible light absorption and facilitating more efficient photocatalytic activity [62].

The colloidal stability of the synthesised Au-TiO_2 and Ag-TiO_2 nanocomposites in aqueous media was evaluated by measuring their ζ-potential at five different pH values (3, 5, 7, 9, and 11), as shown in Figure 2.2h. Both composites exhibit good colloidal stability under acidic and basic conditions, with absolute ζ-potential values ranging between 20 and 50 mV, indicating a low tendency for particle aggregation. All the samples exhibit positive ζ-potential values under acidic conditions and negative values under alkaline conditions, with isoelectric points located between pH 7 and 8.

DLS measurements were performed to evaluate the hydrodynamic size of TiO_2, Au-TiO_2, and Ag-TiO_2 (Figure 2.2i). The results revealed that the surface functionalisation of TiO_2 with gold and silver nanoparticles leads to a significant reduction in the average aggregate size. Specifically, the hydrodynamic diameter decreases from 251 ± 4 nm for pristine TiO_2 to 147 ± 2 nm for Au-TiO_2 and 162 ± 1 nm for Ag-TiO_2. In addition to the decrease in particle size, the polydispersity index (PDI) values also markedly improve, decreasing from 0.29 ± 0.02 for unmodified TiO_2 to 0.14 ± 0.02 and 0.15 ± 0.01 for Au-TiO_2 and Ag-TiO_2, respectively. These results suggest that the decoration of TiO2 with metallic nanoparticles not only prevents particle aggregation but also promotes a uniform particle dispersion in aqueous media.

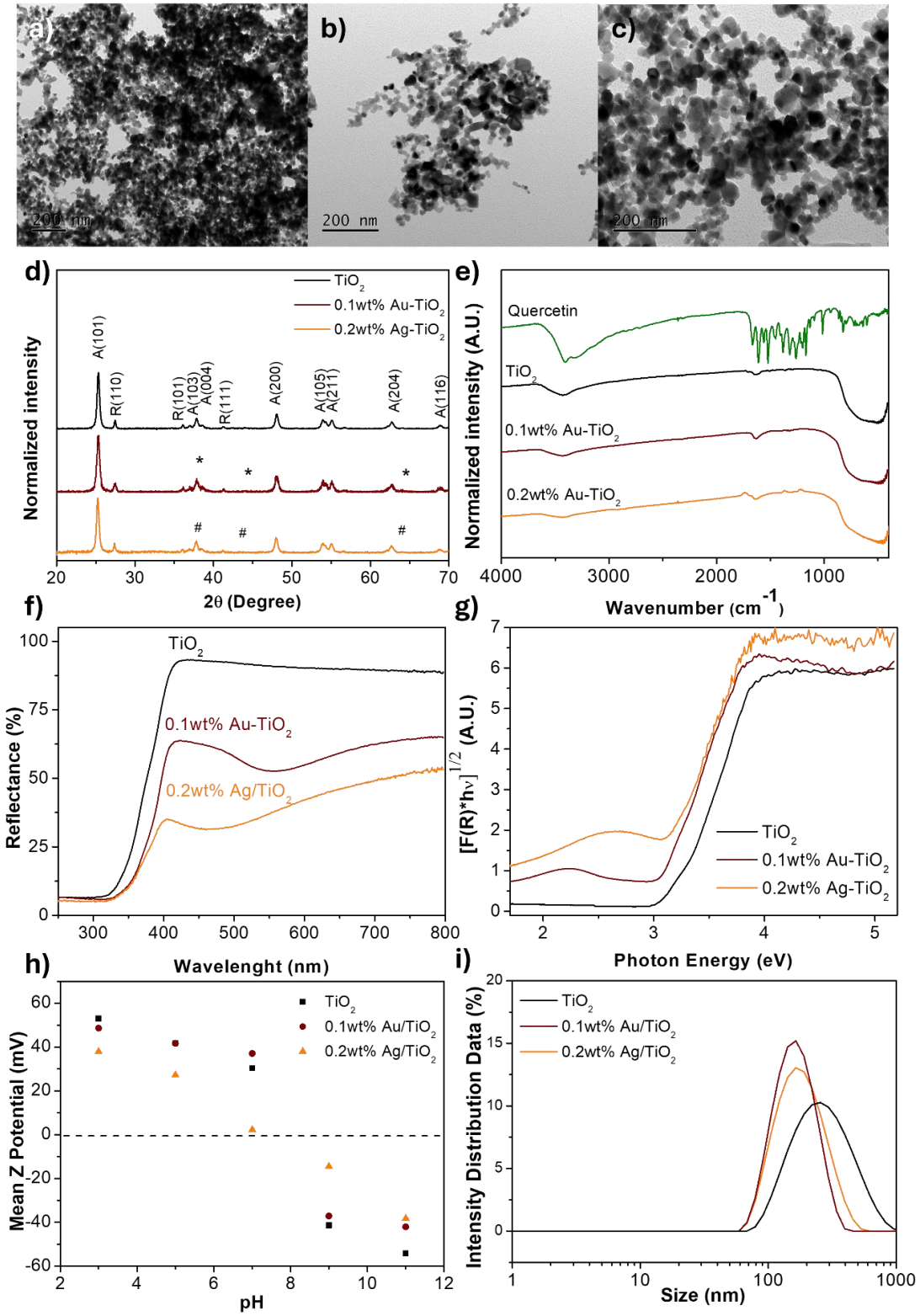


Figure 2.2. TEM images of a) TiO_2 b) Au-TiO_2, and c) Ag-TiO_2; d) XRD diffraction pattern of pristine TiO_2, Au-TiO_2, and Ag-TiO_2 nanocomposites. * and # represent the position where the peaks of Au and Ag should appear; e) FTIR spectra of the synthesised nanocomposites compared with pristine TiO_2 and Quercetin; f) Diffuse reflectance spectra; g) Kubelka–Munk plotsh) ζ potential and i) hydrodynamic size distribution of TiO_2, Au-TiO_2 and Ag-TiO_2.

2.3.1.1 Photogenerated reactive oxygen species (·OH and $^1O_2$) measurements

According to previous studies [26, 63-65], ROS generated on the photocatalyst surface play an essential role in the photocatalytic degradation of contaminants. Hence, quantifying ROS formation is essential for understanding the photocatalytic efficiency of nanoparticles. In this study, tests to measure ROS generation were performed under UV light, as TiO_2-based materials mainly absorb in this region of the spectrum, as shown in reflectance graphs (Figure 2.2f).

Figure 2.3a shows the concentration of hydroxyl radicals (·OH) generated by TiO_2, Au-TiO_2 and Ag-TiO_2 nanoparticles under UV irradiation. A gradual increase in ·OH generation with irradiation time is observed for all samples. Pristine TiO_2 nanoparticles exhibit the highest concentration of ·OH radicals, whereas the functionalised samples, Au-TiO_2 and Ag-TiO_2, show slightly lower levels. Compared to pristine TiO_2, the total generation of ·OH decreases by 18 % and 16 % after functionalization of pristine TiO_2 with Au and Ag, respectively. This reduction may be attributed to the partial occupation or modification of surface-active sites on TiO_2 after metal nanoparticle deposition [60, 63, 66].

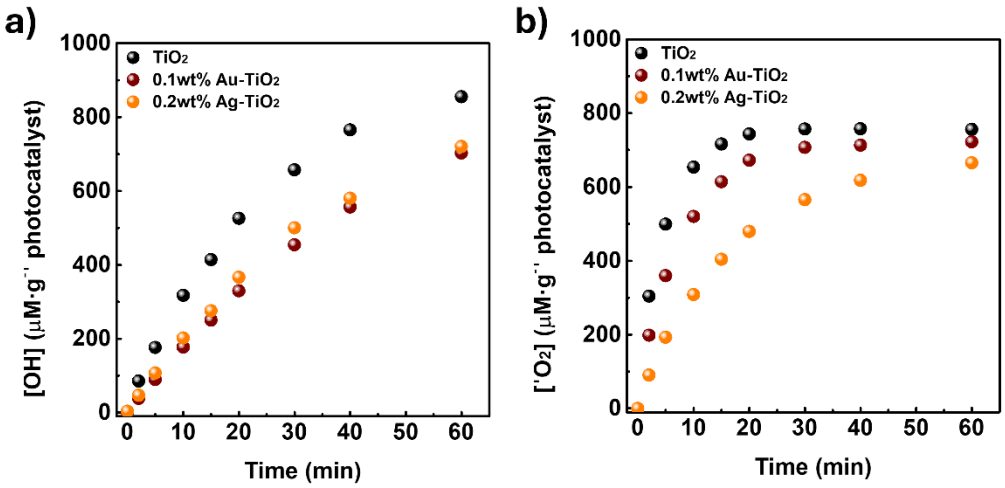


Figure 2.3. Quantification of a) photogenerated hydroxyl radicals (·OH) and b) singlet oxygen ($^1O_2$) by TiO_2, Au-TiO_2 and Ag-TiO_2 nanoparticles under 60 min of UV radiation.

The time evolution of the singlet oxygen ($^1O_2$) generation by TiO_2, Au-TiO_2, and Ag-TiO_2 nanoparticles under UV radiation is presented in Figure 2.3b. Again, pristine TiO_2 produces the highest amount of $^1O_2$ throughout the irradiation period, reaching a steady production rate after an initial rapid increase within the first 30 min. In contrast, the Au-TiO_2 and Ag-TiO_2 nanocomposites exhibit reduced $^1O_2$ generation by approximately 4% and 12%, respectively, after 60 min irradiation. As observed for ·OH radicals, this decrease is attributed to the partial loss of or blockage of surface-active sites on TiO_2 after the

incorporation of Au or Ag nanoclusters [29, 63, 66]. Furthermore, the concentration of $^1O_2$ for both Au-TiO_2 and Ag-TiO_2 nanocomposites reaches a maximum concentration after 40 min of irradiation, and then becomes constant, indicating the attainment of a steady-state generation rate.

2.3.1.2 Nanoparticle photocatalytic performance

The photocatalytic efficiency of the nanoparticles was evaluated through the degradation of three model antibiotics: CIP (5 mg/L), SDZ (15 mg/L), and TMP (10 mg/L), in aqueous solution, under both UV and visible light irradiation. The initial screening aimed to identify the most efficient nanoparticles by comparing their degradation activity across different classes of antibiotics and their response to different light sources.

This aspect is particularly relevant for potential environmental applications, where materials must operate effectively in sustainable conditions, such as natural environments under natural sunlight. As shown in Figure 2.4, all samples demonstrate progressive antibiotic degradation during the 90 min irradiation period, with distinct differences in activity depending on the light source and nanoparticle composition.

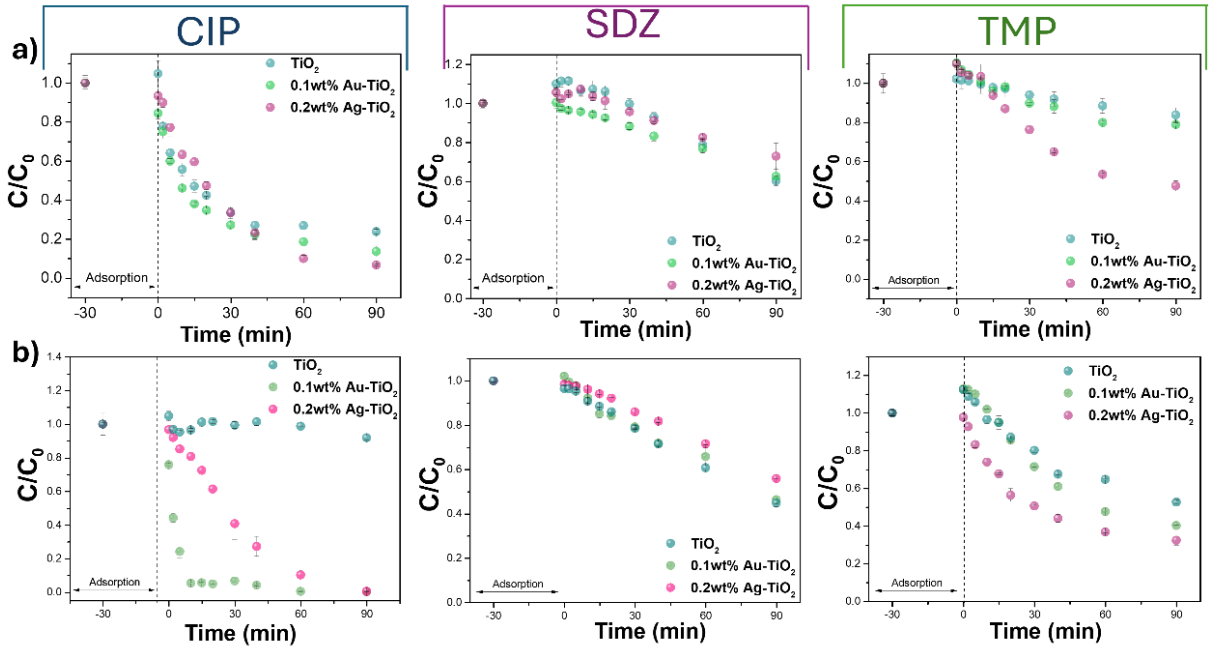


Figure 2.4. Photocatalytic degradation of CIP (5 mg/L), SDZ (15 mg/L), and TMP (10 mg/L) under (a) UV and (b) visible light. Each graph compares the photocatalytic performance of TiO_2, Au-TiO_2, and Ag-TiO_2 over 90 min.

Control experiments were conducted to evaluate the individual contributions of photolysis and adsorption processes (see Table 2.1). The dark adsorption tests confirm that no significant antibiotic removal occurred in the absence of light, indicating that photocatalysis, rather than adsorption, was the dominant removal mechanism during catalytic tests. Photolysis experiments further revealed that antibiotic degradation under both UV and visible light was minimal (Table 2.1). Among the tested compounds, only CIP exhibits partial photodegradation, with removal efficiencies of 6% under UV and 16% under visible light. In contrast, TMP and SDZ remained stable under UV and exhibited only minimal degradation (6 – 8%) under visible light.

Table 2.1. Photolysis (600 min) and photocatalytic degradation efficiencies and kinetics degradation of CIP (5 mg/L), SDZ (15 mg/L), and TMP (10 mg/L) under UV and visible light irradiation (VIS), comparing the performance of TiO_2, Au-TiO_2, and Ag-TiO_2 over 90 min.

		UV		VIS	
	Material/conditions	***Degradation efficiency (%)***	***K_{app} (min^{-1})***	***Degradation efficiency (%)***	***K_{app} (min^{-1})***
CIP	photolysis	7		16	
	TiO_2	77.3	1.5×10^{-2}	13.0	6.0×10^{-4}
	0.1wt%Au-TiO_2	83.9	2.7×10^{-2}	99.6	5.4×10^{-2}
	0.2wt%Ag-TiO_2	92.9	3.1×10^{-2}	99.4	5.3×10^{-2}
SDZ	photolysis	0	-	8	
	TiO_2	45.2	7.0×10^{-3}	51.7	9.0×10^{-3}
	0.1wt%Au-TiO_2	37.7	5.0×10^{-3}	54.6	8.0×10^{-3}
	0.2wt%Ag-TiO_2	31.0	4.0×10^{-3}	43.2	6.0×10^{-3}
TMP	photolysis	0		0	
	TiO_2	18.0	2.0×10^{-3}	59.7	9.0×10^{-3}
	0.1wt%Au-TiO_2	28.5	4.0×10^{-3}	64.3	1.3×10^{-2}
	0.2wt%Ag-TiO_2	56.7	1.0×10^{-2}	66.3	1.3×10^{-2}

These results confirm that direct photodegradation alone is insufficient to achieve significant antibiotic removal, thereby highlighting the necessity of an active photocatalyst. The photocatalytic activities of the TiO_2-P25, Au-TiO_2, and Ag-TiO_2 were subsequently evaluated under UV and visible light irradiation (Figure 2.4), with the corresponding efficiencies and kinetics summarised in Table 2.1.

- ***UV irradiation***

Under UV irradiation, all catalysts exhibit photocatalytic activity, with varying efficiencies depending on the antibiotic tested. Pristine TiO_2 shows high degradation efficiency for CIP (80 %), whereas its

performance decreases considerably for TMP and SDZ. In contrast, the functionalized TiO_2 catalysts (Au-TiO_2 and Ag-TiO_2) demonstrate superior photocatalytic efficiency across all antibiotics, particularly for CIP, where Ag-TiO_2 achieves the highest degradation of 93%. The pseudo-first-order rate constants (k) follow the order: Ag-TiO_2 > Au-TiO_2 > TiO_2 for CIP, suggesting that functionalization promotes more efficient charge separation and improves photocatalytic activity. For SDZ and TMP, pristine TiO_2 exhibits lower degradation effectiveness, achieving only 45% and 18%, respectively. In contrast, the incorporation of metallic nanoparticles enhances these results, with Au-TiO_2 demonstrating moderate activity (37.7 % for SDZ and 28.5 % for TMP), while Ag-TiO_2 achieves the highest TMP degradation (56.7%) and 32.2% for SDZ, following the trend: Ag-TiO_2 > Au-TiO_2 > TiO_2 for TMP and TiO_2>Au-TiO_2 > Ag-TiO_2 for SDZ.

- ***VIS radiation***

The present study focuses on evaluating the functionalised photocatalysts (Ag-TiO_2 and Au-TiO_2), which exhibit enhanced light absorption in the visible range (Figure 2a). Both catalysts demonstrate superior efficiencies in UV-driven degradation, making them promising candidates for further evaluation under simulated solar irradiation. Under these conditions, both materials achieve nearly complete degradation of CIP (99% for both). For SDZ and TMP, Au-TiO_2 show higher activity towards SDZ (54.6%) compared to Ag-TiO_2 (43.2%), while for TMP both catalysts exhibit similar degradation efficiencies (64.3% and 66.3%, respectively).

In contrast to the results obtained under UV radiation, a significant enhancement in photocatalytic activity is observed when TiO_2 is functionalized. Under visible light, the degradation rates reach 13.0% for CIP, 51.7% for SDZ, and 59.7% for TMP. Notably, the efficiency for CIP degradation is approximately eight times higher than that achieved by Au-TiO_2 under UV radiation.

The degradation kinetics follow a logarithmic decay, and the process can be accurately described by a pseudo-first-order reaction model, which is a particular case of the Langmuir-Hinshelwood mechanism applicable to low pollutant concentrations. The highest rate constants (*k*) are obtained for the noble metal-functionalised TiO_2 catalysts, consistent with the expected plasmonic enhancement that promotes visible light absorption and charge separation. In particular, Au-TiO_2 exhibits a k value of 5.4×10^{-2} min^{-1} for CIP degradation, which is approximately 90 times larger than that of pristine TiO_2 (6.0×10^{-4} min^{-1}).

The superior photocatalytic performance of Au-TiO_2 and Ag-TiO_2 compared to pristine TiO_2 is attributed to the plasmonic effect of noble metal nanoparticles. This phenomenon enhances light absorption and facilitates charge separation through the formation of Schottky junctions at the metal-semiconductor interface [67]. Upon irradiation, these photogenerated charges subsequently react with O_2 and H_2O to

produce ROS, as illustrated in Figure 2.3, including superoxide anions and hydroxyl radicals, that are responsible for initiating and sustaining the degradation of organic pollutants [68].

TiO_2 is excited under UV radiation, generating electron-hole pairs that drive ROS formation. However, the high energy of these photons can also increase charge recombination, limiting the degradation process, particularly for complex structures such as SDZ and TMP [69]. Conversely, under visible light, TiO_2 has limited activity due to its wide bandgap (3.05 eV), while the incorporation of Au and Ag enhances visible light absorption through SPR excitation. This process generates energetic ("hot") electrons within the nanoparticles that overcome the Schottky barrier, being transferred to the conduction band of TiO_2, promoting efficient charge separation and reducing recombination [70]. A similar behaviour was reported by Zheng *et al.* [26] for Au-TiO_2 systems, reinforcing that noble metal deposition increases charge separation through SPR and extends photocatalytic activity to the visible spectrum.

The degradation efficiencies are also indicative of the chemical structure of each antibiotic, where CIP, which contains carboxyl and piperazinyl groups, is more prone to oxidative degradation, while SDZ and TMP exhibited greater aromatic stability, resulting in lower degradation rates.

Although Ag-TiO_2 and Au-TiO_2 showed comparable photocatalytic performance, Au-TiO_2 is selected in this work for further investigation due to its superior long-term stability under photocatalytic conditions. It has been reported that silver nanoparticles are known to undergo oxidation and partial dissolution during irradiation, which may reduce their effectiveness over time [71]. Additionally, the leaching of silver ions into aqueous media poses potential environmental risks, including toxicity to aquatic organisms [72]. Thus, only and evident superior performance of Ag functionalized nanocomposites, which is not the case, would justify actual applications in specific scenarios. In contrast, gold nanoparticles exhibit remarkable chemical stability and a significantly lower tendency to leach [73]. Hence, Au-TiO_2 nanoparticles were immobilised within a PVDF-HFP polymer matrix, representing an optimal balance between photocatalytic efficiency, stability, and environmental safety.

2.3.2 Composite Membranes characterization

SEM analysis of the pristine and composite membranes reveals a homogeneous spherulitic porous structure characteristic of PVDF-HFP, resulting from liquid-liquid phase separation (Figure 2.5) [74]. The incorporation of TiO_2 and Au-TiO_2 slightly modifies the morphology of the composite membrane's internal structure, which remains uniform and highly porous (Figure 2.5).

Mercury Intrusion Porosimetry (MIP) analysis reveals an average pore diameter of 6.7 μm and a porosity of 81 % for the pristine PVDF-HFP membrane, values consistent with those typically reported for TIPS-processed membranes [75] (see Figure 2.5). Upon incorporation of TiO_2 and Au-TiO_2 nanoparticles, a slight decrease in average pore size is observed, 4.2 and 4.7 μm, respectively, accompanied by marginal reductions in porosity (80% and 79%, respectively) [64]. These results indicate that, although the presence of nanoparticles may slightly influence the phase separation process, the membranes retain a highly porous morphology, as further supported by the SEM observations.

In the PVDF-HFP pristine membrane, characteristic FTIR absorption bands are observed at 878 and 1401 cm^{-1}, corresponding to C–F_2 bonds; 1072 and 1171 cm^{-1}, associated with C–C bending and C–H_2 stretching vibrations, respectively; and at 1231 cm^{-1}, attributed to the PVDF γ-phase of PVDF (Figure 2.6a). Additionally, characteristic bands of the α and β-phases of PVDF are detected at 767 and 834 cm^{-1}, respectively [43]. Notably, the pristine PVDF-HFP membrane exhibits a highly polar β-phase content of 93 %.

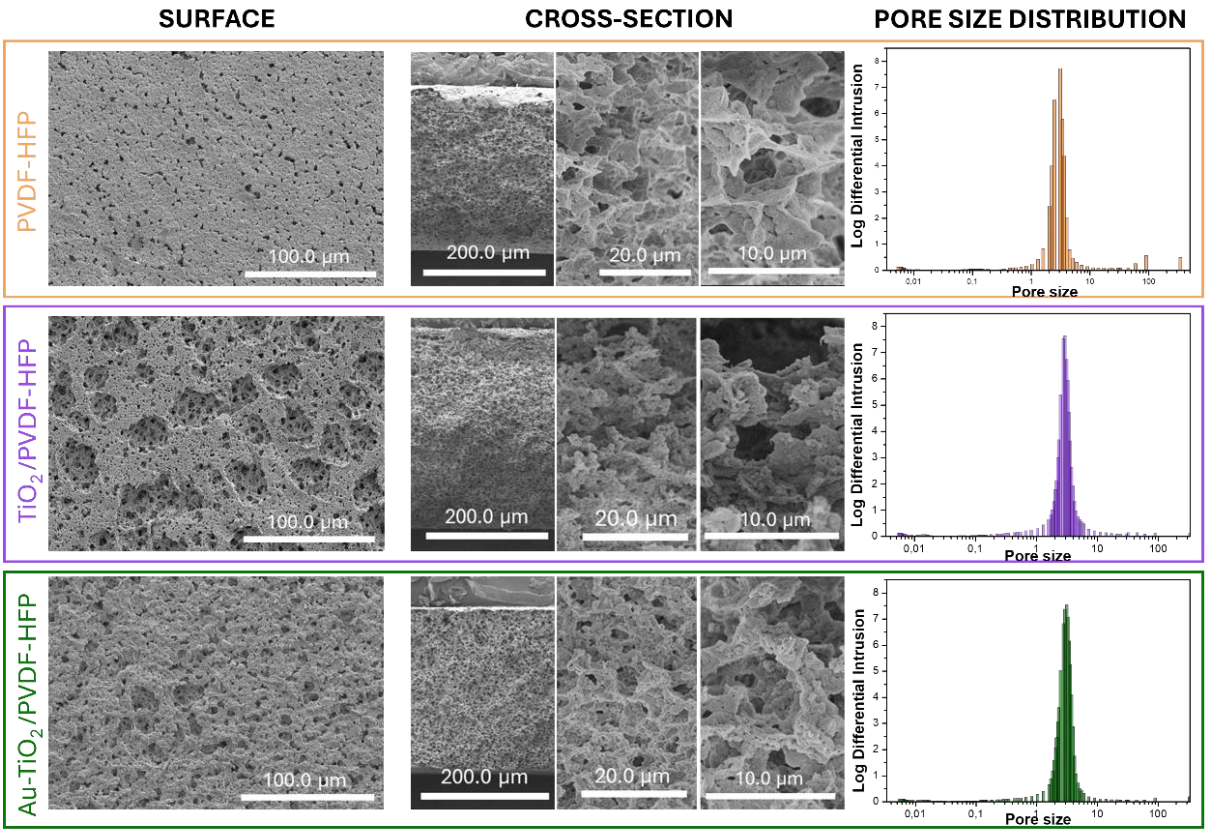


Figure 2.5. SEM images and pore size distribution of PVDF-HFP-based membranes: pristine PVDF-HFP, TiO_2/PVDF-HFP and Au-TiO_2/PVDF-HFP. Surface morphology (500×) and cross-sectional views (250×, 2000×, and 5000×) reveal membrane porosity, pore interconnectivity, and internal membrane structure.

The incorporation of TiO_2 and Au-TiO_2 nanoparticles into the polymer matrix does not significantly influence membrane vibrational spectra and phase, as no additional absorption bands are detected. The β-phase fraction remains nearly unchanged at 94% and 95% after the addition of TiO_2 and Au-TiO_2, respectively, indicating that the polymer phase crystallization behavior is not influenced by the catalysts. The high β-phase content can be attributed to the processing conditions, particularly solvent evaporation at room temperature, which promotes β-phase formation. Consequently, the resulting composite membranes are expected to exhibit enhanced electrical properties, including piezo-, pyro-, and ferroelectric properties, associated with this crystalline phase [52].

Figure 2.6b displays the DSC thermograms of PVDF-HFP, TiO_2/PVDF-HFP, and Au-TiO_2/PVDF-HFP membranes. The pristine PVDF-HFP exhibits a characteristic endothermic melting peak at 142 °C and a minor endothermic event at 56 °C, which may be attributed to the evaporation of residual solvent evaporation, as previously observed [76]. The degree of crystallinity for PVDF-HFP is determined after Eq. 2.4 to be 31%, decreasing slightly to 29% after the incorporation of TiO_2 and Au/TiO_2. This reduction suggests that the catalysts act as crystallization defects within the polymer matrix [77]. The presence of both catalysts does not significantly influence the endothermic peak associated with polymer melting, which exhibits only a negligible shift to 140 °C. These results indicate that TiO_2 and Au-TiO_2 do not influence much the stability of the crystalline phase of the PVDF-HFP matrix.

The mechanical properties of the produced membranes were evaluated mainly through the determination of the Young's modulus, which provides information on their resistance to permanent deformation. Mechanical stress-strain tests were performed on dry membranes, while additional measurements under wet conditions were conducted for the Au-TiO_2/PVDF-HFP membrane to simulate its performance in a realistic operational environment. As illustrated in Figure 2.6c, the pristine PVDF-HFP membrane leads to a Young's modulus of 40.77 MPa, consistent with values reported in the literature for electrospun or solution-casted porous PVDF-HFP membranes [75]. The incorporation of TiO_2 and Au-TiO_2 nanoparticles does not produce significant variations in the mechanical properties of the membranes, indicating that the addition of these photocatalysts preserves the intrinsic flexibility and mechanical integrity of the polymer matrix.

The Young's modulus values of the TiO_2/PVDF-HFP and Au-TiO_2/PVDF-HFP composites are 37.4 ± 0.7 MPa and 43.7 ± 9 MPa, respectively, remaining comparable to the pristine membrane, with variations falling within the experimental error. Incorporating these nanoparticles into the polymeric matrix did not compromise the mechanical integrity of the membranes, confirming that the composites maintain their structural robustness [42]. Furthermore, the TiO_2/PVDF-HFP membrane demonstrates mechanical

stability after 2 min in contact with water, with a Young's modulus of 50 ± 10 MPa, consistent with the values obtained for the dry samples.

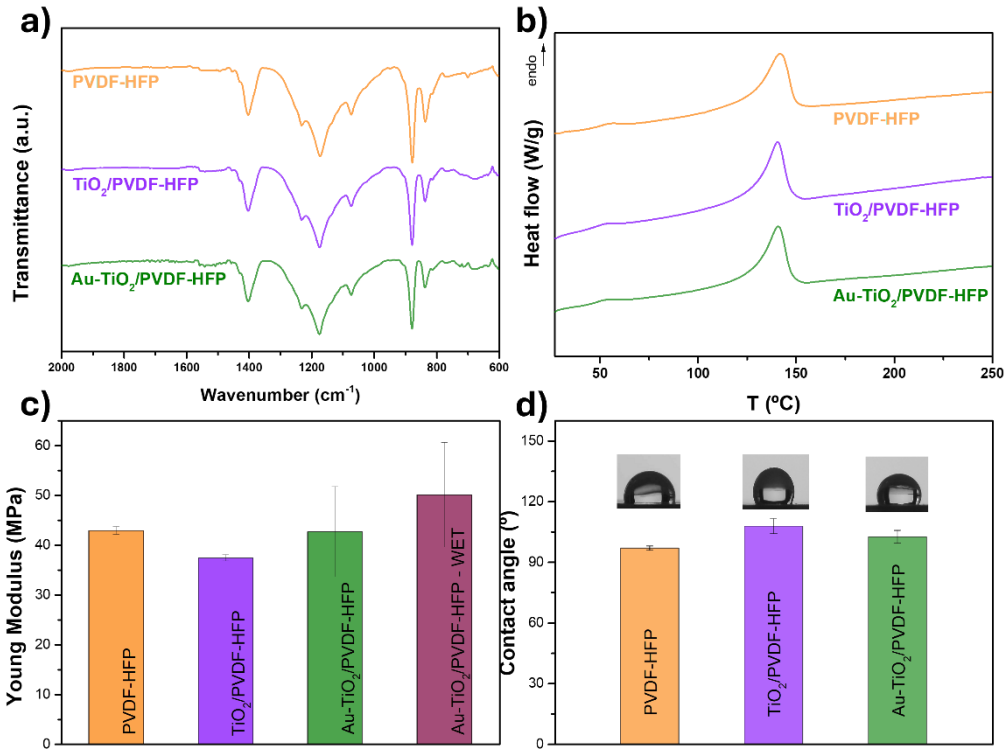


Figure 2.6. a) FTIR spectra of PVDF-HFP-based membranes (pristine PVDF-HFP, TiO_2/PVDF-HFP and Au-TiO_2/PVDF-HFP), b) DSC thermograms, c) Young's modulus d) and contact angle.

Water contact angle measurements were performed to evaluate the wettability of the membranes without and with nanoparticle incorporation (Figure 2.6d). All membranes exhibit contact angles above 90°, confirming their hydrophobic nature, which is typical of PVDF-HFP [78]. The incorporation of TiO_2 and Au-TiO_2 nanoparticles leads to a slight increase in contact angle values (108° and 102°, respectively), indicating an increase in hydrophobicity compared to the pristine membrane (97°). This increase is commonly attributed to greater surface roughness, resulting from the presence of nanoparticles incorporated in the porous polymer matrix, as well as from the surface chemical variations due to the presence of the nanoparticles [27, 79]. The morphological differences observed in Figure 2.5 further corroborate this effect, showing a rougher surface for the composite membranes compared to the pristine PVDF-HFP.

2.3.3 Photocatalytic Activity of Composites Membranes

2.3.3.1 Au-TiO_2/PVDF membrane photocatalytic performance

Following the screening of the suspended photocatalysts, the immobilisation strategy was directed towards the most promising photocatalyst: Au-TiO_2. All experiments were conducted under conditions identical to those utilised in the suspension tests, except for the extended exposure time, which was increased to 600 min, applied to compensate for the reduced contact area between the immobilized photocatalyst and the solution.

The photocatalytic activity of the Au-TiO_2/PVDF-HFP membranes was evaluated against two control conditions: photolysis (under UV and visible light) and adsorption in the dark using pristine PVDF-HFP membranes. Both control tests exhibited negligible antibiotic removal, confirming that photocatalysis was the dominant degradation mechanism. The detailed results of these control experiments are provided in Tables 2.1 and 2.2.

Table 2.2. Photocatalytic degradation efficiencies and kinetics degradation of CIP (5 mg/L), SDZ (15 mg/L), and TMP (10 mg/L) under UV and visible light, comparing the performance of PVDF-HFP, and Au-TiO_2/PVDF-HFP membranes over 600 min.

		UV		VIS	
	Material	***Degradation efficiency (%)***	***K_{app} (min^{-1})***	***Degradation efficiency (%)***	***K_{app} (min^{-1})***
CIP	PVDF/HFP	6.2	-	13.9	-
	Au-TiO_2/PVDF-HFP	95.9	7.0×10^{-3}	69.6	2.0×10^{-3}
SDZ	PVDF	0	-	0	-
	Au-TiO_2/PVDF-HFP	33.6	6×10^{-4}	44.6	1.0×10^{-3}
TMP	PVDF	3.3	-	14.1	-
	Au-TiO_2/PVDF-HFP	48.1	0.001	64.7	0.002

As shown in Figure 2.7a, under UV irradiation, the immobilized membranes exhibit photocatalytic activity against all tested antibiotics, with CIP showing the highest removal efficiency, followed by TMP and SDZ. The same performance trend is maintained under visible light irradiation (Figure 2.7b), confirming the dual-light activation capability of the Au-TiO_2/PVDF membrane system, consistent with the behaviour previously observed for the nanoparticles in suspension (Section 2.3.2.1).

Under UV light, degradation efficiencies of 95.9%, 33.6% and 48.1% are achieved for CIP, SDZ, and TMP, respectively. These correspond to k values of 0.0070, 0.0006, and 0.0010 min^{-1} for CIP, SDZ, and TMP, respectively.

Although the *k* values are slightly smaller than those obtained for the photocatalyst nanoparticles in suspension (0.0090 min^{-1} for CIP), the results demonstrate that the immobilisation process effectively preserves the photocatalyst performance of the composite.

Under visible radiation, the Au-TiO_2/PVDF-HFP membrane maintains relevant photocatalytic activity, achieving degradation efficiencies of 44.6%, 69.6% and 64.7% for SDZ, CIP, and TMP, respectively, with corresponding *k* values of 0.001, 0.002, and 0.002 min^{-1}.

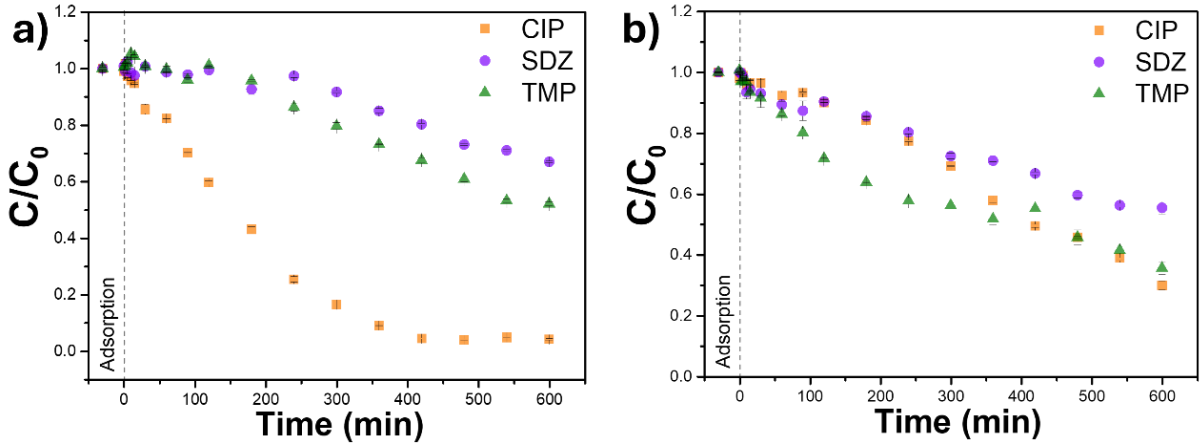


Figure 2.7. Photocatalytic degradation of CIP, SDZ and TMP using Au-TiO_2/PVDF-HFP membranes under a) UV and b) visible light irradiation over a 600 min period.

As observed under UV irradiation, a reduction in reaction kinetics is evident when comparing the immobilised system with its suspended counterpart. This attenuation aligns with previous reports, where immobilisation commonly leads to a partial decrease in diffusion photocatalytic efficiency due to mass transfer limitations and restricted surface accessibility of the photocatalyst [80].

The Au-TiO_2/PVDF-HFP membranes achieve degradation efficiencies exceeding 40% for all antibiotics tested under visible light irradiation, highlighting the crucial role of Au nanoparticles in extending photocatalytic activity beyond the UV region. This behaviour aligns with previous studies related to immobilised TiO_2-based photocatalysts, where the incorporation of noble metals significantly enhances visible light performance. For example, Liu *et al.* [81] reported that an Ag-modified flexible TiO_2 nanofiber film achieved approximately 73% removal of the less persistent and stable contaminant, rhodamine B (RhB) dye, under visible light, compared to <40 % for the unmodified TiO_2 film [81]. Similarly, in another study, Ag-doped TiO_2 and ZnO films required over 4 h to reach 80% dye degradation under visible light

irradiation, while undoped semiconductors, such as TiO_2, failed to exceed 20% efficiency [82]. The enhanced visible-light response observed in this study can be primarily attributed to the SPR effect of Au nanoparticles, which promotes visible light absorption and efficient charge separation, thereby improving photocatalytic performance.

Overall, although the kinetic constants obtained for the immobilised systems are lower than those observed in suspension, the Au-TiO_2/PVDF-HFP membranes provide a more sustainable and practical alternative. The immobilisation strategy enables membrane reuse, prevents NP leaching, and allows the use of sunlight as a clean energy source. These findings confirm the photocatalytic effectiveness of the system under visible radiation, demonstrating its potential for environmentally friendly and sustainable water treatment applications driven by solar energy.

2.3.4 Au-TiO_2/PVDF-HFP membrane reusability

The reusability of the Au-TiO_2/PVDF-HFP membrane was evaluated to assess its practical implementation, long-term viability, and cost-effectiveness. This parameter is critical for real-world applications, as it reflects the durability of the photocatalyst and the efficiency of the immobilisation strategy [83]. The membrane was subjected to three consecutive photocatalytic cycles under both UV and visible light irradiation for the degradation of CIP, SDZ, and TMP as model pollutants (Figure 2.8 and Table 2.3).

Concerning CIP degradation, the membrane maintains high photocatalytic activity, achieving approximately 96% removal under UV radiation throughout the three cycles. Assuming complete CIP degradation, this consistent performance indicates excellent stability and reusability of the immobilized photocatalyst. Under visible light, the membrane exhibits an initial efficiency of 69.6%, which progressively increases to 77.3 % in the last cycle, suggesting a possible photoactivation or surface conditioning effect upon repeated use.

For SDZ, the degradation efficiency increases by 34% under UV (Figure 2.8a) and 21 % under visible light (Figure 2.8b), from the first to the third cycle.

Regarding TMP reusability, a slight variation in photocatalytic efficiency is observed under UV irradiation, with values ranging from 43% to 49% across three consecutive cycles. In contrast, under visible light, the membrane exhibits larger and progressively increasing efficiencies, from 65% in the first cycle to 70% in the third.

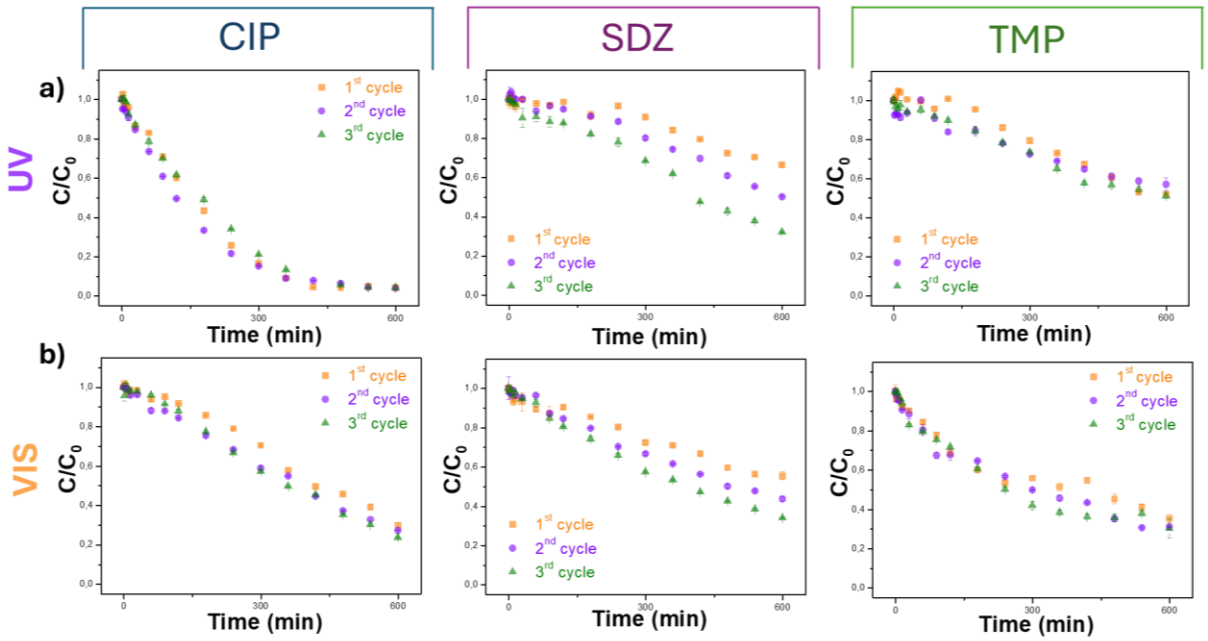


Figure 2.8. Reusability of Au–TiO_2/PVDF-HFP membranes under a) UV radiation and b) visible irradiation for the degradation of CIP, SDZ and TMP. Each test was performed over three consecutive cycles (1800 min).

Interestingly, the degradation efficiencies for all tested antibiotics increase with reuse, diverging from the typical trend reported in the literature [84, 85], where a gradual decline in activity is usually observed due to factors such as nanoparticle leaching, membrane fouling, or photocatalyst deactivation [86, 87].

Table 2.3. Photocatalytic degradation efficiencies and kinetics degradation of CIP (5 mg/L), SDZ (15 mg/L), and TMP (10 mg/L) under UV and visible light, comparing the performance of PVDF-HFP, and Au-TiO2/PVDF-HFP membranes over 600 min.

		UV	VIS
CIP	1st Au-TiO_2/PVDF-HFP	95.9 %	69.6 %
	2nd Au-TiO_2/PVDF-HFP	96.0 %	72.8 %
	3rd Au-TiO_2/PVDF-HFP	95.8 %	77.3 %
SDZ	1st Au-TiO_2/PVDF-HFP	33.6 %	44.6 %
	2nd Au-TiO_2/PVDF-HFP	49.8 %	56.3 %
	3rd Au-TiO_2/PVDF-HFP	67.9 %	66.0 %
TMP	1st Au-TiO_2/PVDF-HFP	48.1 %	64.7 %
	2nd Au-TiO_2/PVDF-HFP	43.1 %	68.9 %
	3rd Au-TiO_2/PVDF-HFP	49.0 %	69.9 %

To elucidate the mechanisms underlying the observed performance trends, a physical-chemical characterisation of the membrane was performed after three consecutive photocatalytic cycles. SEM analysis (Figure 2.9) reveals that the porous spherulitic structure of PVDF-HFP matrix remains intact, with no detectable morphological degradation or structural collapse or after repeated use. This confirms that the immobilisation strategy provides sufficient mechanical and structural robustness, even under prolonged exposure to high-energy irradiation.

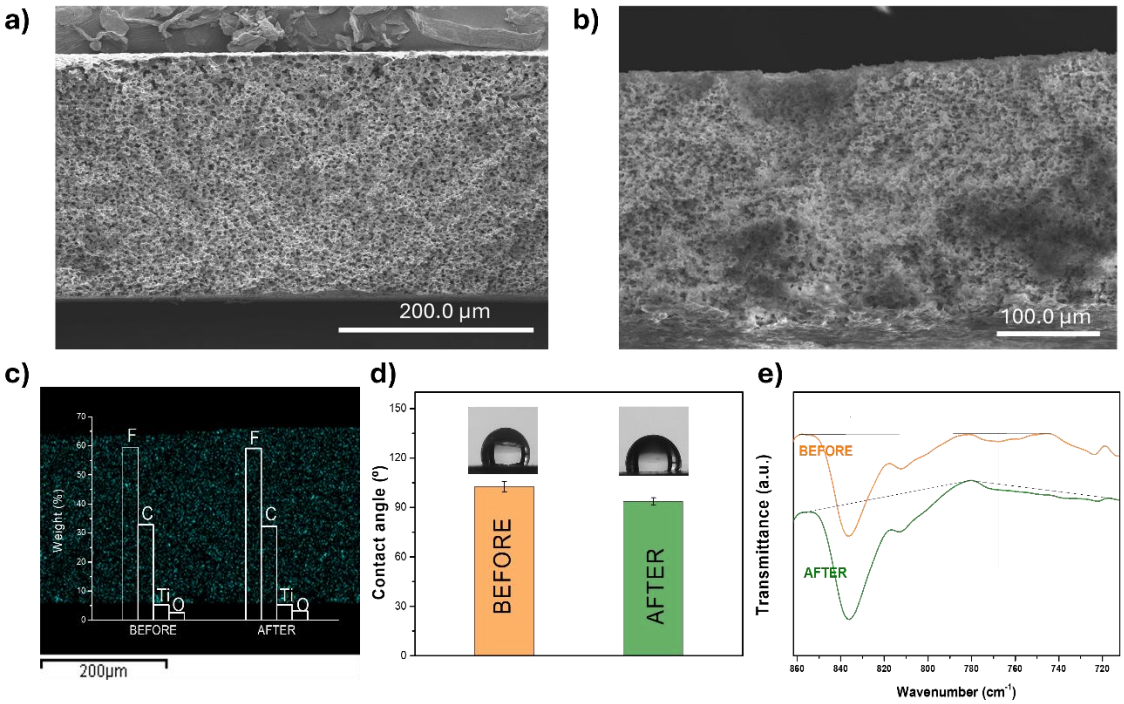


Figure 2.9. Physicochemical characterisation of the Au-TiO_2/PVDF-HFP membrane before and after three photocatalytic reuse cycles for CIP degradation under UV radiation: SEM images of the cross-section of Au-TiO_2/PVDF-HFP membrane a) before use and b) after use, c) EDX mapping of Ti after reuse (magnification: 250×), showing relative atomic percentages of the key elements; d) contact angle and d) FTIR spectra.

Scanning electron microscopy - energy dispersive X-ray spectroscopy (SEM-EDX) mapping further confirms the morphological stability and uniform dispersion of TiO_2 across both the surface membrane cross-section of the membrane before and after use. The TiO_2 weight percentage remains constant throughout the cycles (Figure 2.9c), indicating negligible catalyst loss. Although Au is not detected by EDX, ascribed to its low loading and dispersion, the maintained and even enhanced photocatalytic performance under visible light confirms the stability of the Au-TiO_2 component. Additionally, a decrease

in the water contact angle from 102° to 93° (Figure 2.9d) is registered, reflecting a gradual increase in the membrane's hydrophilicity. This enhanced wettability likely facilitates improved water infiltration and percolation, enabling the interaction between the photocatalyst and the aqueous medium, thereby promoting greater accessibility of antibiotic molecules to the active sites and contributing to the observed improvement in degradation efficiency.

The FTIR spectra present in Figure 2.9e reveal the disappearance of the band associated with the α-phase of PVDF-HFP, accompanied by an increase in the β-phase content from 95% to 97%. This subtle phase transition does not induce significant chemical modifications, confirming the structural robustness of the membrane after reuse. Notably, the enrichment in the β phase, combined with the decrease in the contact angle, points to greater surface wettability, which may promote better interaction between the photocatalyst, water, and target pollutants, thus contributing to greater photocatalytic activity.

2.3.5 Photocatalytic degradation Mechanism

2.3.5.1 Pathways

While immobilisation effectively overcomes the practical challenges associated with photocatalyst nanoparticle recovery and reuse, it is equally important to elucidate and optimise the degradation pathways of the target contaminants to ensure a comprehensive process.

Under energetic UV irradiation, the composite membranes become photoactivated, leading to the generation of electron-hole (e^-/h^+) pairs. The photoexcited electrons migrate to the conduction band (CB), while the holes remain in the valence band (VB). These charge carriers initiate a cascade of redox reactions: photogenerated electrons react with dissolved oxygen molecules (O_2) to produce superoxide radicals ($\cdot O_2^-$), whereas holes oxidise water molecules or hydroxide ions, yielding highly reactive hydroxyl radicals (·OH). These ROS have strong oxidative potential and non-selectivity, attacking a broad range of organic molecules and leading to the formation of transient intermediate compounds during the degradation process.

In this context, it is essential to evaluate whether photocatalysis leads to complete mineralisation of contaminants or, instead, generates intermediate by-products, which can be more persistent or toxic than the parent pollutants [88]. These potential risks highlight the importance of conducting a detailed mechanistic analysis, not only to optimise the efficiency of immobilised photocatalysts but also to ensure the environmental safety of the treatment process [89].

The proposed degradation mechanism of CIP is illustrated in Figure 2.10, revealing three primary transformation pathways, based on MS fragmentation data and the identified intermediates: i) hydroxylation of the piperazine ring, ii) progressive oxidation and ring opening leading to the formation of di-carbonyl compounds, and iii) defluorination and decarboxylation.

The initial oxidation of the parent compound (CIP 1) yields the intermediate CIP 2, primarily through hydroxylation on the piperazine ring. Subsequent oxidative fragmentation of this intermediate leads to the formation of CIP 3, which results from the cleavage of the piperazine ring, generating terminal amine groups, a transformation commonly observed under oxidative photocatalytic conditions.

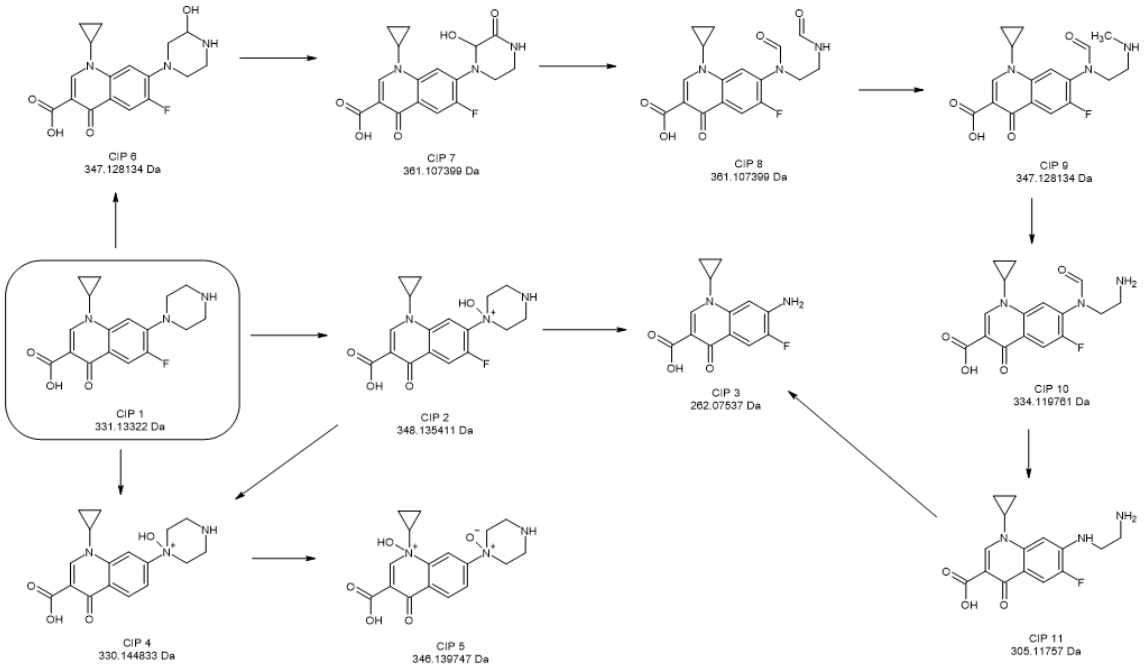


Figure 2.10. Proposed degradation pathway for CIP.

Similarly, the conversion of intermediates, such as CIP 9 to CIP 10 and to CIP 11, involves progressive oxidative cleavage of the piperazine moiety, resulting in open-ring structures and the formation of partially mineralised terminal amine-containing species. Additional intermediates, CIP 4 and CIP 5, indicate the occurrence of minor hydroxylation, partial oxidation and defluorination reactions, suggesting multiple parallel degradation pathways contributing to the overall breakdown of CIP.

Monitoring of CIP 1 reveals its complete disappearance after 420 min of irradiation. Although a minor contribution from direct photolysis is detected, the results demonstrate that the photocatalytic activity of Au-TiO_2/PVDF-HFP and TiO_2/PVDF-HFP membranes is the predominant degradation mechanism, as depicted in Figure 2.11.

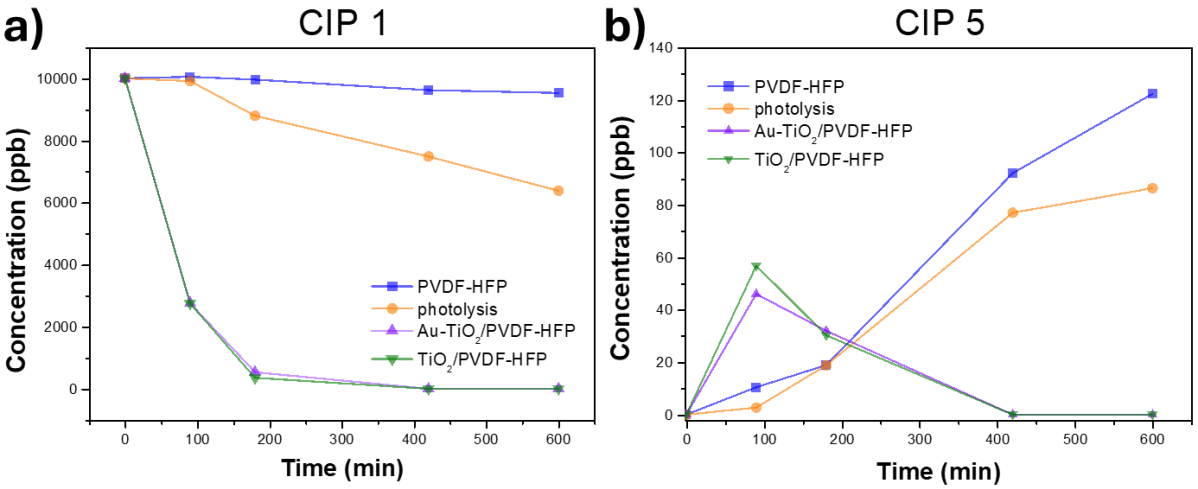


Figure 2.11. Degradation processes of CIP 1 over time: a). The parent CIP is rapidly eliminated from the solution by the photocatalytic activity of the Au-TiO_2/PVDF-HFP and TiO_2/PVDF-HFP; b) Naturally occurring CIP degradation products are accumulated in samples that are not subjected to photocatalysis.

Following the disappearance of the parent compound CIP 1, an increase in the concentration of its degradation products is observed. Remarkably, these intermediates are also eliminated from the solution through the photocatalytic activity of the membranes. This behavior, exemplified by CIP 5 in Figure 2.11, represents a general trend that is observed for all identified degradation products. Interestingly, similar degradation products are also detected in control experiments using PVDF-HFP membranes and irradiated CIP solutions without photocatalytic materials. In these cases, natural photolytic degradation leads to the accumulation of intermediates rather than their removal. These findings demonstrate the superior remediation capability of the Au-TiO_2/PVDF-HFP and TiO_2/PVDF-HFP composite membranes, which effectively degrade both the parent antibiotic and its naturally occurring degradation products.

The photocatalytic degradation of TMP proceeded through a complex multi-step oxidative pathway, as depicted in Figure 2.12. The mechanism involves: i) oxidative hydroxylation of aromatic rings via radical attack, ii) cleavage of the ether bond linkage connecting the methoxyphenyl and pyrimidine moieties, and iii) deamination and ring opening, leading to the progressive fragmentation and mineralization of TMP.

One of the predominant transformation pathways involves the hydroxylation of the aromatic rings, observed in the early-stage intermediates (TMP 2a, TMP 3 and TMP 4a), leading to the formation of more polar and less bioactive derivatives.

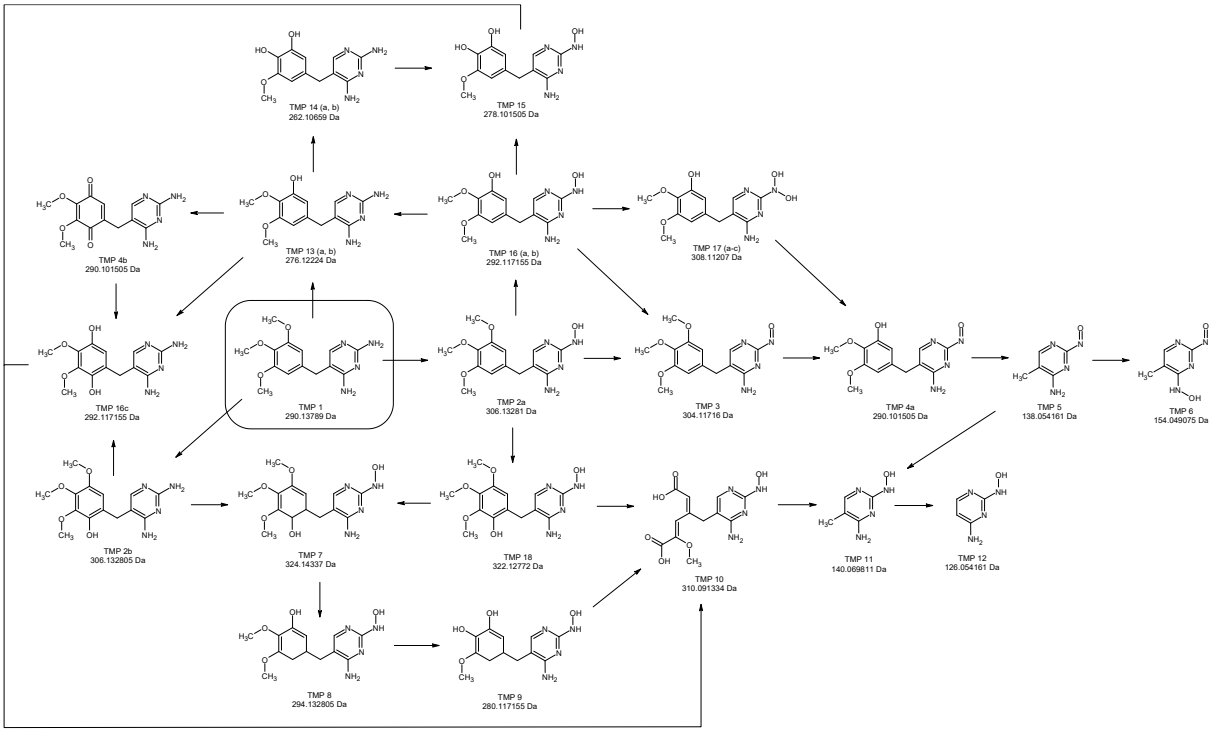


Figure 2.12. Proposed degradation pathway for TMP.

Another key process is the cleavage of the ether bond linking the methoxybenzyl and pyrimidine rings, resulting in lower molecular weight fragments, such as TMP 5 and TMP 6. Furthermore, deamination and subsequent oxidation of the amine groups present in the parent compound contribute to the formation of by-products containing hydroxyl or carbonyl functionalities, such as TMP 8 or TMP 12. The process indicates not only the disappearance of the parent molecules but also their progressive degradation and potential mineralisation, as evidenced by the formation of low-molecular-weight by-products such as TMP 11 and TMP 12, which reveal signs of ring opening and molecular rearrangements.

The photocatalytic degradation behavior of TMP closely resembles that of CIP, showing rapid decomposition under photocatalytic conditions (Figure 2.13). Notably, TMP does not undergo natural degradation under irradiation alone. Similar to CIP, the intermediates generated during the treatment are subsequently decomposed and eliminated over time (Figure 2.13b).

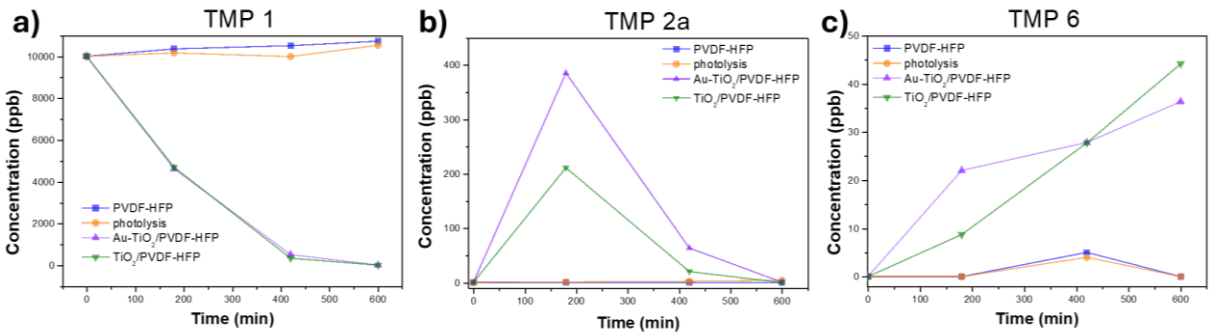


Figure 2.13. a) Degradation processes of TMP 1 over time and b) its degradation by-products over the time of the experiments in the samples subjected to photocatalysis.

The accumulation of TMP 6 at the end of the experiment suggests that this compound may be a terminal product within the degradation pathway (Figure 2.13c), although the formation of other endpoints cannot be excluded. The TMP 6 ($C_5H_6N_4O_2$) has been previously reported and attributed to 2,4-diaminopyrimidine-5-carboxylic acid (DAPC) detected on photocatalytic degradation of TMP, where it exhibits lower toxicity than the parent compound in fish and algae, however, it remained harmful to daphnia [90], reinforcing the need to experimentally evaluate the toxicity of the identified by-products.

The proposed degradation pathway of SDZ is illustrated in Figure 2.14. Although the photocatalytic degradation of SDZ by the synthesised membranes is evident, this antibiotic is the compound that did not achieve complete degradation after 600 min of treatment (Figure 2.15a). The presence of the sulphonamide group likely has a protective effect against certain oxygen radicals, thereby hindering complete degradation and indicating that longer irradiation times may be needed for efficient SDZ removal. Previous studies have also demonstrated that pH might play a crucial role in the photocatalytic degradation efficiency of sulfamides [91], indicating that certain contaminants may require specific optimisation of the reaction medium. As in the previous experiments, the photocatalytic degradation of SDZ also facilitates the removal of its degradation products, such as SDZ 2 (Figure 2.15b). This effect is particularly relevant for the elimination of degradation products generated through the natural degradation of SDZ, including SDZ 10 (Figure 2.15c), which would otherwise persist and accumulate in the absence of photocatalytic activity.

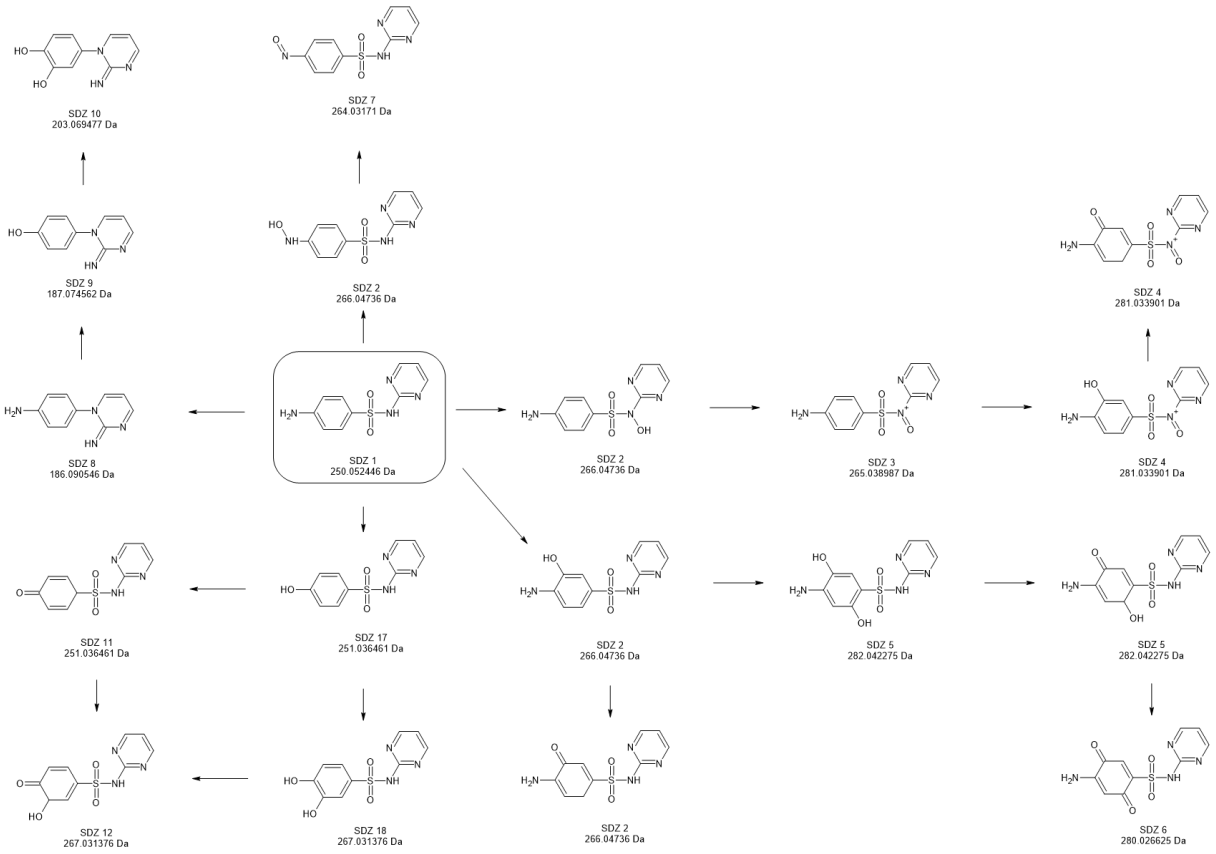


Figure 2.14. Proposed degradation pathway for SDZ.

LC-MS analysis reveals multiple oxidative pathways occurring simultaneously during SDZ degradation, leading to the formation of several characteristic intermediates (SDZ2, SDZ4, SDZ6, SDZ7, SDZ10, SDZ12). The initial step in this process is hydroxylation of the aromatic ring (SDZ1 → SDZ2), which increases the polarity of the compound and facilitates further oxidation. Subsequent reactions include oxidation of the amino group and the heterocyclic portion (SDZ1 → SDZ4, SDZ6, SDZ12, SDZ7), with the SDZ1 → SDZ7 transformation being consistent with the formation of N-oxide or nitroso derivatives. Another relevant pathway corresponds to desulfurization (SDZ1 → SDZ10), in which the sulfonyl group is removed simultaneously with the oxidation of the aromatic ring.

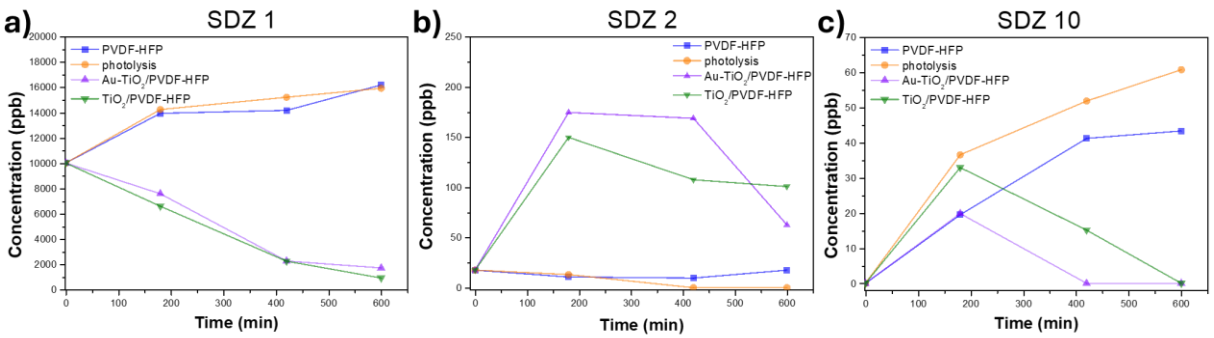


Figure 2.15. Concentrations of SDZ and its degradation by-products over the time of the experiments in the samples subjected to photocatalysis

These transformations result in the loss of SDZ biological activity and the generation of more polar intermediates. However, the formation of certain oxidized byproducts, particularly nitroso and quinone species, gives rise to concerns due to their potential reactivity and persistence. Notably, intermediates such as SDZ 2 ($C_{10}H_{10}N_4O_3S$) have been reported in other studies to be toxic to Daphnia and fish, and harmful to green algae, highlighting the importance of assessing the ecotoxicological impact of degradation products in addition to their removal from water [92].

2.3.6 Ecotoxicity Assessment

To evaluate the potential environmental impact of the developed composite membranes, ecotoxicity tests were performed using the bioluminescent bacterium Vibrio fischeri. Three types of samples were tested: 1) the composite membranes, 2) aqueous solutions of CIP, TMP and SDZ prepared at the same initial concentrations used in the photocatalytic experiments (5, 10 and 15 mg/L, respectively) and subsequently diluted in series to simulate the concentration decrease during degradation, and 3) degradation by-products collected from the photocatalytic experiments after 600 min of irradiation under UV or visible light. The inhibition of bacterial luminescence was monitored over a 240 min exposure period.

Figure 2.16a shows the luminescence inhibition results obtained following exposure to the composite membranes. The quantification of toxicity, expressed as luminescence inhibition (INH %) after 30 min of contact with the tested samples, is a reliable indicator of the presence of potentially toxic substances, according to ISO 11348, which standardizes the assessment of acute toxicity. This approach enables the direct evaluation of sample toxicity and the potential ecotoxicological effects of photocatalytic degradation

intermediates, thereby providing a comprehensive understanding of the environmental safety of the developed materials and the overall photocatalytic system.

Following a 30 min exposure period, no significant luminescence inhibition, indicative of ecotoxic activity, was observed in any of the tested materials. The inhibition values are 10.7% for pristine PVDF-HFP membrane, 12.8% for TiO_2/PVDF-HFP, and 13.3% for Au-TiO_2/PVDF-HFP. These values fall within the non-toxic range, confirming the material's stability and environmental compatibility. The results align with previous studies reporting that PVDF exhibits negligible toxicity towards marine organisms, such as *Artemia franciscana* and *Aurelia sp.*, where only minor behavioural changes are observed without any impact on survival or reproduction [93].

Extensive research into the ecotoxicity of TiO_2 has demonstrated that even under irradiated conditions, TiO_2 exhibits no toxic effects on *Daphnia similis* at concentrations of up to 100 mg/L, supporting its safe application in environmental systems [94]. Similarly, the incorporation of noble metals, such as silver and gold, into PVDF-based materials for aquatic remediation has been extensively studied, with no significant ecotoxic effects reported in aquatic microorganisms [95].

The ecotoxic effects of the selected antibiotics on *V. fischeri* were studied at different concentrations, along with the potential by-products formed during the photocatalytic process. The corresponding results are presented in Figures 2.16b and 2.16c, which show the percentage of luminescence inhibition as a function of exposure time to the contaminated solutions.

Across the tested concentration range, an increase in luminescence inhibition is observed with both longer exposure times and contaminant concentrations [96, 97].

After 30 min of exposure to CIP (Figure 2.16c), luminescence inhibition ranges from ≈10% at 0.25 mg/L to ≈48% at 5 mg/L. These values suggest that CIP exhibits concentration-dependent toxicity towards *V. fischeri*, with inhibitory effects increasing at higher concentrations. The observed inhibition levels are consistent with values reported in previous studies, where CIP concentrations between 0.01 mg/L and 0.1 mg/L, with equivalent exposure time, were in contact with *V. fischeri* and produced luminescence inhibition of 6% to 20% during the first hour of exposure, followed by a progressive increase over time [47, 96].

The observed effect may be attributed to the typical mode of action of fluoroquinolones, such as CIP, which inhibit bacterial DNA replication [98] by targeting DNA gyrase and topoisomerase IV. In *V. fischeri*, these compounds may also disrupt redox processes involved in bioluminescence [96], particularly through interactions with the amino group (NH_2) of reduced flavin mononucleotide ($FMNH_2$), which is

essential for hydrogen transfer during light emission [99, 100]. This interference likely explains the progressive inhibition of luminescence observed over time.

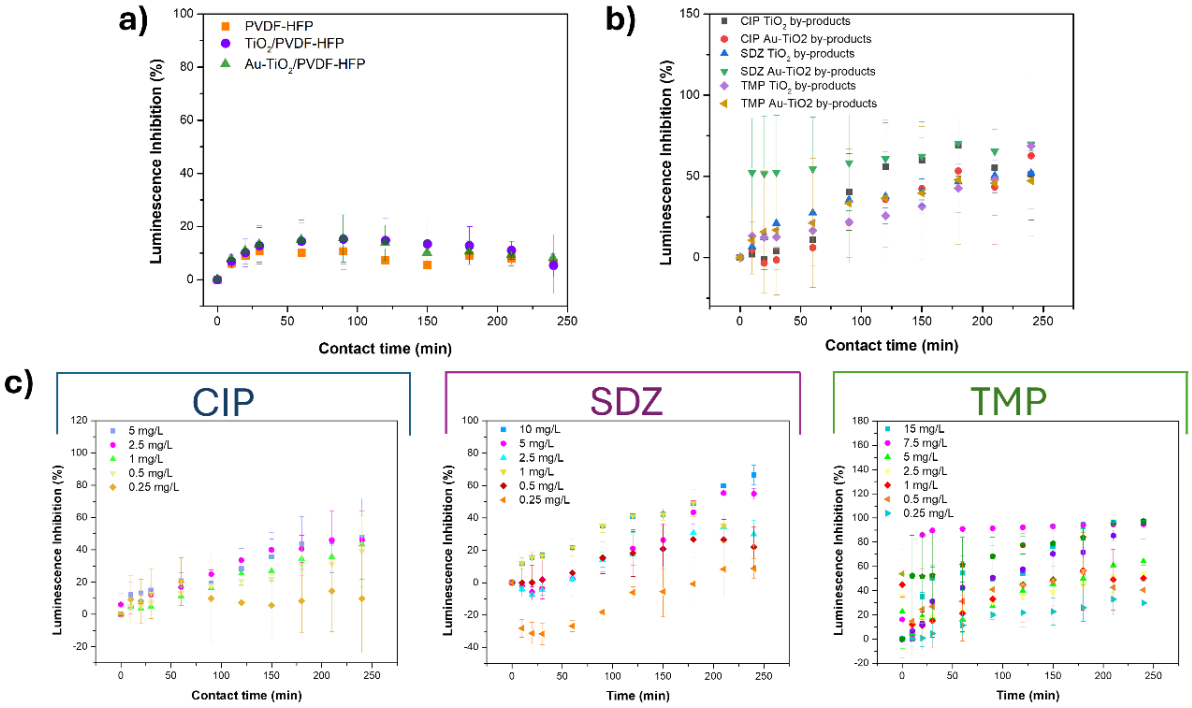


Figure 2.16. Luminescence inhibition (%) of *V. fischeri* after exposure to a) PVDF-HFP, TiO_2/PVDF-HFP and Au-TiO_2/PVDF-HFP membranes; b) photocatalytic degradation of by-products of CIP, SDZ and TMP generated after 600 min using TiO_2/PVDF-HFP and Au-TiO_2/PVDF-HFP composite membranes; c) aqueous solutions of antibiotics at different concentrations: CIP (5, 2.5, 1, 0.5 and 0.25 mg/L), TMP (10, 5, 2.5, 1, 0.5 and 0.25 mg/L), and SDZ (15, 7.5, 5, 2.5, 1, 0.5 and 0.25 mg/L). Measurements were conducted over a 240 min according to ISO 11348.

TMP exhibits a progressive toxic effect on *V. fischeri*, with luminescence inhibition reaching approximately 21% after 60 min and up to 66 % after 250 min of exposure at the highest tested concentration (10 mg/L). During the initial 120 min, inhibition remains low across all concentrations (0 to 20%), consistent with trends previously reported in literature [47, 101]. A closer examination of early exposure times (e.g., 30 min) reveals comparable sensitivity to TMP: in previous studies, exposure to 0.5 mg/L resulted in approximately 15% inhibition, while in the present study, 10 mg/L produced a similar effect (-16 %) at an equivalent contact time.

This gradual toxic response aligns with TMP's mode of action, which involves inhibition of the enzyme dihydrofolate reductase, thereby blocking the synthesis of tetrahydrofolic acid (THF) – an essential

precursor in DNA synthesis [102]. As this mechanism needs time to disrupt bacterial metabolism, *V. fischeri* typically exhibits a delayed but increasing luminescence inhibition over time [103, 104].

SDZ exhibits the most pronounced inhibitory effect on luminescence among the antibiotics tested. Following 60 min of exposure, inhibition levels reach approximately 54% at 15 mg/L and 90% at 7.5 mg/L. Despite the marked toxicity observed at higher concentrations, *V. fischeri* maintains a certain baseline luminescence at lower concentrations (0.25, 0.5, 2.5, and 5 mg/L), persisting after 250 min of exposure. These results contrast with those of previous studies, in which no effective concentrations (EC_{50}) were detected for SDZ at levels up to 200 mg/L, after 30 min of exposure [105]. This suggests that the toxic effects may develop progressively over time in this microorganism. The mode of action of SDZ involves structural mimicry of para-aminobenzoic acid (PABA), thereby inhibiting folic acid synthesis, a crucial pathway for bacterial growth and replication [105]. This distinctive mechanism likely accounts for the strong long-term inhibitory effect observed in *V. fischeri*, despite its initial tolerance. These findings highlight the importance of evaluating not only the acute toxicity of the parent compounds but also the potential effects of their transformation byproducts to fully evaluate the environmental risks associated with antibiotic contamination.

To evaluate the effects of photocatalytically generated by-products from all antibiotics, samples were collected after 600 min of irradiation in experiments using TiO_2/PVDF-HFP and Au–TiO_2/PVDF-HFP membranes.

Focusing first on the by-products generated during CIP degradation, acute toxicity is assessed after 30 minutes of exposure. The results show no detectable toxic effects, consistent with LC-MS analyses of the degradation mechanism. Furthermore, after 600 minutes of photocatalytic degradation, neither the parent compound nor any degradation products are detected, indicating complete mineralization, suggesting that, for CIP, the photocatalytic process leads to full degradation without generating ecotoxicologically relevant by-products.

The evaluation of TMP followed a similar approach, and the acute toxicity assays show no observable effects. The most abundant by-products (TMP 6) exhibit reduced toxicity in comparison to the parent compound, aligned with previous outcomes, wherein no deleterious effects are observed in other organisms, including algae and fish, although a slight sensitivity increase in microorganisms such as Daphnia may occur [90]. Together, these results indicate that TMP photocatalytic degradation produces by-products that are generally less toxic than the original antibiotic.

In contrast, SDZ exhibits markedly different behaviour. The effect is particularly evident for SDZ, whose by-products generated after only 30 min of photocatalysis already cause approximately 50% inhibition,

indicating acute toxicity. This observation aligns with the LC-MS analysis, which revealed the formation of highly oxidized intermediates, such as nitroso derivatives, N-oxides, and quinones (Figure 2.16) [106, 107]. These compounds have been demonstrated to interfere with microbial redox processes, thereby explaining the pronounced inhibition of bioluminescence observed in *V. fischeri* [108]. Furthermore, degradation profiles (see Figure 2.15) show a rapid formation of these intermediates during SDZ photocatalysis (particularly, SDZ 2), reinforcing the direct correlation between the identified degradation pathways and the observed ecotoxicological response.

Similar phenomena have been previously reported, where luminescence inhibition reaches 55% after 10 min of irradiation [89], suggesting that the observed toxicity arises not solely from the parent antibiotics or their primary transformation products, but also from secondary degradation compounds. These findings collectively suggest that the environmental toxicity observed may result from synergistic interactions between the antibiotics, their degradation products, and changes in environmental conditions induced during photocatalysis.

Overall, the ecotoxicity results, combined with the proposed degradation mechanism developed for all antibiotics, demonstrate that although photocatalytic membranes effectively degrade the parent antibiotics, the resulting by-products can exhibit higher toxicity than the original compounds. This creates the necessity of coupling degradation assessments with systematic identification of transformation products and ecotoxicological evaluations when developing advanced water treatment systems.

2.4 Conclusions

The present study reports the green synthesis of Ag–TiO_2 and Au–TiO_2 nanophotocatalysts, which exhibit enhanced visible-light absorption and improved charge separation, resulting in greater photocatalytic activity compared to pristine TiO_2. Among these, Au–TiO_2 demonstrated superior degradation of ciprofloxacin (CIP), sulfadiazine (SDZ), and trimethoprim (TMP), and was subsequently immobilised within a PVDF-HFP membrane to produce a reusable photocatalytic system with negligible nanoparticle leaching.

The resulting Au–TiO_2/PVDF-HFP membranes kept the physicochemical, mechanical, and structural integrity of the polymeric matrix while sustaining high photocatalytic activity under both UV and visible light irradiation. These membranes achieved efficient antibiotic degradation, high removal efficiencies, and stable performance across multiple reuse cycles, without loss of activity. Post-use physicochemical

characterisation confirmed morphological and structural stability, and increased surface hydrophilicity was found to enhance catalytic performance upon reuse.

Kinetic and mechanistic analyses reveal that antibiotic degradation proceeds via pseudo-first-order kinetics and involves oxidative hydroxylation, ring-opening, and deamination pathways, resulting in partial or complete mineralisation. Complete mineralisation was achieved for CIP, while TMP transformation products exhibited reduced toxicity compared to the parent compound. In contrast, SDZ produced transient oxidation products with higher acute toxicity, underlining the need to integrate degradation efficiency with ecotoxicological assessment. The ecotoxicity results provide essential evidence to guide sustainable-by-design decisions, ensuring that photocatalytic performance is evaluated alongside the environmental safety of transformation products.

In summary, the Au–TiO_2/PVDF-HFP nanocomposite membrane offers a practical approach for antibiotic removal from water matrices, integrating visible-light activation, operational reusability, material stability, and ecotoxicity validation. Future research should focus on process scale-up, optimisation of mineralisation efficiency, and long-term performance evaluation in complex water matrices to facilitate the implementation of photocatalytic membrane technologies in practical water treatment applications.

2.5 References

[1] L. Lin, H. Yang, X. Xu, Effects of water pollution on human health and disease heterogeneity: a review, Frontiers in environmental science, 10 (2022) 880246.

[2] A. Krishan, S. Yadav, A. Srivastava, Water Pollution's Global Threat to Public Health: A Mini-Review, International Journal of Scientific Research in Science, Engineering and Technology, (2023) 321-334.

[3] W. Xu, Y. Jin, G. Zeng, Introduction of heavy metals contamination in the water and soil: a review on source, toxicity and remediation methods, Green Chemistry Letters and Reviews, 17 (2024) 2404235.

[4] M. Syafrudin, R.A. Kristanti, A. Yuniarto, T. Hadibarata, J. Rhee, W.A. Al-Onazi, T.S. Algarni, A.H. Almarri, A.M. Al-Mohaimeed, Pesticides in drinking water—a review, International journal of environmental research and public health, 18 (2021) 468.

[5] A. Mandal, P. Senthil Kumar, C.S. Poorva, L. Srinivasa Raju, S.R. Balasubramani, G. Rangasamy, Research progress of persistent organic pollutants in water: classification, sources, potential risks, and treatment approaches, Water Practice & Technology, 19 (2024) 937-959.

[6] S.P.M. Menacherry, U.K. Aravind, C.T. Aravindakumar, Critical review on the role of mass spectrometry in the AOP based degradation of contaminants of emerging concern (CECs) in water, Journal of Environmental Chemical Engineering, 10 (2022) 108155.

[7] D. Yadav, S. Rangabhashiyam, P. Verma, P. Singh, P. Devi, P. Kumar, C.M. Hussain, G.K. Gaurav, K.S. Kumar, Environmental and health impacts of contaminants of emerging concerns: Recent treatment challenges and approaches, Chemosphere, 272 (2021) 129492.

[8] R.J. Nathanael, L.N. Adyanis, K. Oginawati, The last decade epidemiologic concern of drinking water contaminants of emerging concern (CECs) in Asian Countries: A scoping review, Heliyon, 10 (2024) e39236.

[9] J. Harrower, M. McNaughtan, C. Hunter, R. Hough, Z. Zhang, K. Helwig, Chemical Fate and Partitioning Behavior of Antibiotics in the Aquatic Environment—A Review, Environmental Toxicology and Chemistry, 40 (2021) 3275-3298.

[10] S. Mishra, A.K. Singh, L. Cheng, A. Hussain, A. Maiti, Occurrence of antibiotics in wastewater: Potential ecological risk and removal through anaerobic–aerobic systems, Environmental Research, 226 (2023) 115678.

[11] Y. Cai, T. Sun, G. Li, T. An, Traditional and Emerging Water Disinfection Technologies Challenging the Control of Antibiotic-Resistant Bacteria and Antibiotic Resistance Genes, ACS ES&T Engineering, 1 (2021) 1046-1064.

[12] E. Commission, COMMISSION IMPLEMENTING DECISION (EU) 2025/439 of 28 February 2025 establishing a watch list of substances for Union-wide monitoring in the field of water policy pursuant to Directive 2008/105/EC of the European Parliament and of the Council, Official Journal of the European Union, 2025, pp. 1-6.

[13] U. Szymańska, M. Wiergowski, I. Sołtyszewski, J. Kuzemko, G. Wiergowska, M.K. Woźniak, Presence of antibiotics in the aquatic environment in Europe and their analytical monitoring: Recent trends and perspectives, Microchemical Journal, 147 (2019) 729-740.

[14] L.H.M.L.M. Santos, M. Gros, S. Rodriguez-Mozaz, C. Delerue-Matos, A. Pena, D. Barceló, M.C.B.S.M. Montenegro, Contribution of hospital effluents to the load of pharmaceuticals in urban wastewaters: Identification of ecologically relevant pharmaceuticals, Science of The Total Environment, 461-462 (2013) 302-316.

[15] E. Bayan, L. Pustovaya, M. Volkova, Recent advances in TiO2-based materials for photocatalytic degradation of antibiotics in aqueous systems, Environmental Technology & Innovation, 24 (2021) 101822.

[16] B. Kasprzyk-Hordern, R.M. Dinsdale, A.J. Guwy, The removal of pharmaceuticals, personal care products, endocrine disruptors and illicit drugs during wastewater treatment and its impact on the quality of receiving waters, Water Research, 43 (2009) 363-380.

[17] L. Liu, W. Wu, J. Zhang, P. Lv, L. Xu, Y. Yan, Progress of research on the toxicology of antibiotic pollution in aquatic organisms, Acta Ecologica Sinica, 38 (2018) 36-41.

[18] F. Martin-Laurent, E. Topp, L. Billet, I. Batisson, C. Malandain, P. Besse-Hoggan, S. Morin, J. Artigas, C. Bonnineau, L. Kergoat, Environmental risk assessment of antibiotics in agroecosystems: ecotoxicological effects on aquatic microbial communities and dissemination of antimicrobial resistances and antibiotic biodegradation potential along the soil-water continuum, Environmental Science and Pollution Research, 26 (2019) 18930-18937.

[19] A.J. Bartlett, V. Balakrishnan, J. Toito, L. Brown, Toxicity of four sulfonamide antibiotics to the freshwater amphipod Hyalella azteca, Environmental toxicology and chemistry, 32 (2013) 866-875.

[20] J. Zhou, X. Yun, J. Wang, Q. Li, Y. Wang, A review on the ecotoxicological effect of sulphonamides on aquatic organisms, Toxicology Reports, 9 (2022) 534-540.

[21] J. Wang, R. Zhuan, Degradation of antibiotics by advanced oxidation processes: An overview, Science of The Total Environment, 701 (2020) 135023.

[22] L. Wang, J. Yu, Chapter 1 - Principles of photocatalysis, in: J. Yu, L. Zhang, L. Wang, B. Zhu (Eds.) Interface Science and Technology, Elsevier2023, pp. 1-52.

[23] S. Ahmadi, J.M. Quimbayo, V.B.K. Yaah, S.B. de Oliveira, S. Ojala, A critical review on combining adsorption and photocatalysis in composite materials for pharmaceutical removal: Pros and cons, scalability, TRL, and sustainability, Energy Nexus, 17 (2025) 100396.

[24] A.D. Scaccabarozzi, A. Basu, F. Aniés, J. Liu, O. Zapata-Arteaga, R. Warren, Y. Firdaus, M.I. Nugraha, Y. Lin, M. Campoy-Quiles, N. Koch, C. Müller, L. Tsetseris, M. Heeney, T.D. Anthopoulos, Doping Approaches for Organic Semiconductors, Chemical Reviews, 122 (2022) 4420-4492.

[25] A. Marikutsa, A. Novikova, M. Rumyantseva, N. Khmelevsky, A. Gaskov, Comparison of Au-functionalized semiconductor metal oxides in sensitivity to VOC, Sensors and Actuators B: Chemical, 326 (2021) 128980.

[26] F. Zheng, J.M. Queirós, P.M. Martins, R.F. de Luis, A. Fidalgo-Marijuan, J.L. Vilas-Vilela, S. Lanceros-Méndez, J. Reguera, Au-sensitised TiO2 and ZnO nanoparticles for broadband pharmaceuticals photocatalytic degradation in water remediation, Colloids and Surfaces A: Physicochemical and Engineering Aspects, 671 (2023) 131594.

[27] H. Salazar, P.M. Martins, B. Santos, M.M. Fernandes, A. Reizabal, V. Sebastián, G. Botelho, C.J. Tavares, J.L. Vilas-Vilela, S. Lanceros-Mendez, Photocatalytic and antimicrobial multifunctional nanocomposite membranes for emerging pollutants water treatment applications, Chemosphere, 250 (2020) 126299.

[28] K. Pham, H. Ali-Löytty, J. Saari, M. Zubair, M. Valden, K. Lahtonen, N. Kinnunen, M. Gunell, J.J. Saarinen, Functionalization of TiO2 inverse opal structure with atomic layer deposition grown Cu for photocatalytic and antibacterial applications, Optical Materials, 131 (2022) 112695.

[29] I.C. Gomes Espada, N. González-Ballesteros, C.J. Tavares, S. Lanceros-Méndez, P.M. Martins, Towards green visible range active photocatalytic Au/TiO2 nanocomposites through rutin-based synthesis and their application in the degradation of ciprofloxacin, RSC Sustainability, 2 (2024) 3090-3099.

[30] C. Hano, B.H. Abbasi, Plant-based green synthesis of nanoparticles: Production, characterization and applications, MDPI, 2021, pp. 31.

[31] P. Dhandapani, A.A. Prakash, M.S. AlSalhi, S. Maruthamuthu, S. Devanesan, A. Rajasekar, Ureolytic bacteria mediated synthesis of hairy ZnO nanostructure as photocatalyst for decolorization of dyes, Materials Chemistry and Physics, 243 (2020) 122619.

[32] H. Soliman, A. Elsayed, A. Dyaa, Antimicrobial activity of silver nanoparticles biosynthesised by Rhodotorula sp. strain ATL72, Egyptian Journal of Basic and Applied Sciences, 5 (2018) 228-233.

[33] J. Moavi, F. Buazar, M.H. Sayahi, Algal magnetic nickel oxide nanocatalyst in accelerated synthesis of pyridopyrimidine derivatives, Scientific reports, 11 (2021) 6296.

[34] S.F. Ahmed, M. Mofijur, N. Rafa, A.T. Chowdhury, S. Chowdhury, M. Nahrin, A.B.M.S. Islam, H.C. Ong, Green approaches in synthesising nanomaterials for environmental nanobioremediation: Technological advancements, applications, benefits and challenges, Environmental Research, 204 (2022) 111967.

[35] N. Karuvantevida, M. Razia, R. Bhuvaneshwar, G. Sathishkumar, S. Prabukumar, S. Sivaramakrishnan, Bioactive flavonoid used as a stabilizing agent of mono and bimetallic nanomaterials for multifunctional activities, Journal of Pure and Applied Microbiology, 16 (2022) 1652-1662.

[36] M.G. Peña-Juarez, L.O. Sanchez-Vargas, E.J. Gutierrez-Castañeda, R. Saldaña-Garcés, R. Lopez-Esparza, J.L. Cuellar-Camacho, J. Ruiz-Garcia, J.A. Gonzalez-Calderon, How green and simple can nontoxic antimicrobial nanoparticles be obtained? Deposition of AgNPs on the TiO2 surface in a neutral aqueous media by using the flavonoid quercetin, Applied Organometallic Chemistry, 37 (2023) e6963.

[37] N. González-Ballesteros, P.M. Martins, C.J. Tavares, S. Lanceros-Méndez, Quercetin-mediated green synthesis of Au/TiO2 nanocomposites for the photocatalytic degradation of antibiotic ciprofloxacin, Journal of Industrial and Engineering Chemistry, 143 (2025) 526-537.

[38] L. Aoudjit, J.M. Queirós, A.S. Castro, D. Zioui, N. González-Ballesteros, S. Lanceros-Mendez, P.M. Martins, Sunlight-Induced Photocatalytic Removal of Paracetamol Using Au-TiO2 Nanoparticles, Nanomaterials, 15 (2025) 358.

[39] J.M. Queirós, F. Zheng, R. Brito-Pereira, M.M. Fernandes, E.O. Carvalho, P.M. Martins, V. Lazić, J.M. Nedeljković, S. Lanceros-Mendez, Photocatalytic and antimicrobial polymer-based hybrid membranes with surface-modified TiO 2 nanoparticles with 5-aminosalicylic acid and silver nanoparticles, RSC Sustainability, (2025).

[40] A. Joseph, A. Vijayanandan, Review on support materials used for immobilization of nano-photocatalysts for water treatment applications, Inorganica Chimica Acta, 545 (2023) 121284.

[41] P.M. Martins, B. Santos, H. Salazar, S.A.C. Carabineiro, G. Botelho, C.J. Tavares, S. Lanceros-Mendez, Multifunctional hybrid membranes for photocatalytic and adsorptive removal of water contaminants of emerging concern, Chemosphere, 293 (2022) 133548.

[42] R. Brito-Pereira, J.M. Queirós, L. Celaya-Azcoaga, R.F. de Luiz, P. Martins, S. Lanceros-Mendez, Hexavalent chromium dual water remediation and sensing based on hybrid polymer/metal-organic framework composites, Journal of Environmental Chemical Engineering, 12 (2024) 113839.

[43] C.M. Costa, V.F. Cardoso, P. Martins, D.M. Correia, R. Gonçalves, P. Costa, V. Correia, C. Ribeiro, M.M. Fernandes, P.M. Martins, S. Lanceros-Méndez, Smart and Multifunctional Materials Based on Electroactive Poly(vinylidene fluoride): Recent Advances and Opportunities in Sensors, Actuators, Energy, Environmental, and Biomedical Applications, Chemical Reviews, 123 (2023) 11392-11487.

[44] J. Shi, J. Jiang, Q. Chen, L. Wang, K. Nian, T. Long, Production of higher toxic intermediates of organic pollutants during chemical oxidation processes: A review, Arabian Journal of Chemistry, 16 (2023) 104856.

[45] H. Saleem, S.J. Zaidi, Developments in the Application of Nanomaterials for Water Treatment and Their Impact on the Environment, Nanomaterials, 10 (2020) 1764.

[46] M. Ghanbarian, A.H. Mahvi, M. Ghanbarian, Data on bioassay of toxicity reduction of treated textile wastewater by using nanophotocatalytic process by Daphnia magna, Data in Brief, 21 (2018) 1321-1324.

[47] D. Nasuhoglu, P. Westlund, S. Isazadeh, S. Neamatallah, V. Yargeau, Development of a facile and high-throughput bioluminescence assay using Vibrio fischeri to determine the chronic toxicity of contaminated samples, Bulletin of environmental contamination and toxicology, 98 (2017) 196-203.

[48] P. Masner, B. Javůrková, L. Bláha, Rapid in situ toxicity testing with luminescent bacteria Photorhabdus luminescens and Vibrio fischeri adapted to a small portable luminometer, Environmental Science and Pollution Research, 24 (2017) 3748-3758.

[49] A. Silva, P. Martins, S. Teixeira, S. Carabineiro, K. Kuehn, G. Cuniberti, M. Alves, S. Lanceros-Mendez, L. Pereira, Ciprofloxacin wastewater treated by UVA photocatalysis: Contribution of irradiated TiO 2 and ZnO nanoparticles on the final toxicity as assessed by Vibrio fischeri, RSC advances, 6 (2016) 95494-95503.

[50] X. Qu, L.J. Kirschenbaum, E.T. Borish, Hydroxyterephthalate as a Fluorescent Probe for Hydroxyl Radicals: Application to Hair Melanin, Photochemistry and Photobiology, 71 (2000) 307-313.

[51] H. Yang, G. Li, T. An, Y. Gao, J. Fu, Photocatalytic degradation kinetics and mechanism of environmental pharmaceuticals in aqueous suspension of TiO2: A case of sulfa drugs, Catalysis Today, 153 (2010) 200-207.

[52] A. Zarandona, H. Salazar, M. Insausti, S. Lanceros-Méndez, Q. Zhang, Sonophotocatalytic removal of organic dyes in real water environments using reusable BiSI@PVDF-HFP nanocomposite membranes, Chemosphere, 357 (2024) 142069.

[53] H. Salazar, P.M. Martins, M.M. Fernandes, P. Costa, S. Ferdov, G. Botelho, S. Lanceros-Mendez, Reusable nanocomposite-filters for arsenite and arsenate dual real effluents remediation in an up-scaled membrane reactor, Journal of Hazardous Materials, 440 (2022) 129756.

[54] M. Maior, R. Carpa, R. Fetke, V. Muntean, Determination of the inhibitory effect of water samples on the light emission of Vibrio fischeri, FEBS JOURNAL, WILEY-BLACKWELL 111 RIVER ST, HOBOKEN 07030-5774, NJ USA, 2014, pp. 524-524.

[55] S. Parvez, C. Venkataraman, S. Mukherji, A review on advantages of implementing luminescence inhibition test (Vibrio fischeri) for acute toxicity prediction of chemicals, Environment International, 32 (2006) 265-268.

[56] J. López, A. Rey, E. Viñuelas-Zahinos, P.M. Álvarez, Preparation of a new green magnetic Fe3O4 @TiO2-P25 photocatalyst for solar advanced oxidation processes in water, Journal of Environmental Chemical Engineering, 11 (2023) 109999.

[57] G. Wang, L. Xu, J. Zhang, T. Yin, D. Han, Enhanced photocatalytic activity of TiO2 powders (P25) via calcination treatment, International Journal of Photoenergy, 2012 (2012) 265760.

[58] B.J. Cha, T.G. Woo, S.W. Han, S. Saqlain, H.O. Seo, H.K. Cho, J.Y. Kim, Y.D. Kim, Surface Modification of TiO2 for Obtaining High Resistance against Poisoning during Photocatalytic Decomposition of Toluene, Catalysts, 8 (2018) 500.

[59] Z. Rao, G. Lu, A. Mahmood, G. Shi, X. Xie, J. Sun, Deactivation and activation mechanism of TiO2 and rGO/Er3+-TiO2 during flowing gaseous VOCs photodegradation, Applied Catalysis B: Environmental, 284 (2021) 119813.

[60] P. Martins, S. Kappert, H. Nga Le, V. Sebastian, K. Kühn, M. Alves, L. Pereira, G. Cuniberti, M. Melle-Franco, S. Lanceros-Méndez, Enhanced Photocatalytic Activity of Au/TiO2 Nanoparticles against Ciprofloxacin, Catalysts, 2020.

[61] M.A. Mannaa, K.F. Qasim, F.T. Alshorifi, S.M. El-Bahy, R.S. Salama, Role of NiO nanoparticles in enhancing structure properties of TiO2 and its applications in photodegradation and hydrogen evolution, ACS omega, 6 (2021) 30386-30400.

[62] D. Kanakaraju, F.D. anak Kutiang, Y.C. Lim, P.S. Goh, Recent progress of Ag/TiO2 photocatalyst for wastewater treatment: Doping, co-doping, and green materials functionalization, Applied Materials Today, 27 (2022) 101500.

[63] F. Zheng, P.M. Martins, J.M. Queirós, C.J. Tavares, J.L. Vilas-Vilela, S. Lanceros-Méndez, J. Reguera, Size Effect in Hybrid TiO2:Au Nanostars for Photocatalytic Water Remediation Applications, International Journal of Molecular Sciences, 2022.

[64] F. Zheng, P.M. Martins, J.M. Queirós, C.J. Tavares, J.L. Vilas-Vilela, S. Lanceros-Méndez, J. Reguera, Hybrid TiO2:Au nanostars based polymeric membranes for photocatalytic degradation of ciprofloxacin in water samples, Chemosphere, 313 (2023) 137630.

[65] Y. Nosaka, A.Y. Nosaka, Generation and Detection of Reactive Oxygen Species in Photocatalysis, Chemical Reviews, 117 (2017) 11302-11336.

[66] M. Sayed, Z. Shi, F. Gholami, P. Fatehi, A.I.A. Soliman, Ag@TiO2 Nanocomposite as an Efficient Catalyst for Knoevenagel Condensation, ACS Omega, 7 (2022) 32393-32400.

[67] C. Ban, B. Li, J. Ma, Y. Feng, C. Lin, Y. Chen, Y. Wang, Y. Duan, K. Zhou, L. Gan, S. Wang, X. Zhou, Plasmonic Au–TiO2 interactions for augmented photocatalytic hydrogen evolution, Ceramics International, 50 (2024) 15444-15451.

[68] Y. Negrín-Montecelo, C. Brissaud, J.-Y. Piquemal, A.O. Govorov, M.A. Correa-Duarte, L.V. Besteiro, M. Comesaña-Hermo, Plasmonic photocatalysis in aqueous solution: assessing the contribution of thermal effects and evaluating the role of photogenerated ROS, Nanoscale, 14 (2022) 11612-11618.

[69] E.M. Rodríguez, G. Márquez, M. Tena, P.M. Álvarez, F.J. Beltrán, Determination of main species involved in the first steps of TiO2 photocatalytic degradation of organics with the use of scavengers: The case of ofloxacin, Applied Catalysis B: Environmental, 178 (2015) 44-53.

[70] Y.-H. Tseng, I.-G. Chang, Y. Tai, K.-W. Wu, Effect of surface plasmon resonance on the photocatalytic activity of Au/TiO2 under UV/visible illumination, Journal of Nanoscience and Nanotechnology, 12 (2012) 416-422.

[71] J. Liu, R.H. Hurt, Ion release kinetics and particle persistence in aqueous nano-silver colloids, Environ Sci Technol, 44 (2010) 2169-2175.

[72] W. Younas, F.U. Khan, M. Zaman, D. Lin, A. Zuberi, Y. Wang, Toxicity of synthesized silver nanoparticles in a widespread fish: A comparison between green and chemical, Science of The Total Environment, 845 (2022) 157366.

[73] S.K. Balasubramanian, L. Yang, L.-Y.L. Yung, C.-N. Ong, W.-Y. Ong, L.E. Yu, Characterization, purification, and stability of gold nanoparticles, Biomaterials, 31 (2010) 9023-9030.

[74] A. Valverde, R. de Fernandez-de Luis, H. Salazar, B.F. Gonçalves, S. King, L. Almásy, M. Kriechbaum, J.M. Laza, J.L. Vilas-Vilela, P.M. Martins, On The Multiscale Structure and Morphology of PVDF-HFP@ MOF Membranes in The Scope of Water Remediation Applications, Advanced Materials Interfaces, 10 (2023) 2300424.

[75] J.P. Serra, A. Fidalgo-Marijuan, P.M. Martins, J.M. Queirós, R. Gonçalves, A. Gutiérrez-Pardo, F. Aguesse, C.M. Costa, S. Lanceros-Mendez, Porous Composite Bifunctional Membranes for Lithium-Ion Battery Separator and Photocatalytic Degradation Applications: Toward Multifunctionality for Circular Economy, Advanced Energy and Sustainability Research, 2 (2021) 2100046.

[76] C. Ribeiro, C.M. Costa, D.M. Correia, J. Nunes-Pereira, J. Oliveira, P. Martins, R. Gonçalves, V.F. Cardoso, S. Lanceros-Méndez, Electroactive poly (vinylidene fluoride)-based structures for advanced applications, Nature protocols, 13 (2018) 681-704.

[77] H. Salazar, P.M. Martins, A. Valverde, R. Fernández de Luis, J.L. Vilas-Vilela, S. Ferdov, G. Botelho, S. Lanceros-Mendez, Reusable nanocomposite membranes for highly efficient arsenite and arsenate dual removal from water, Advanced Materials Interfaces, 9 (2022) 2101419.

[78] R.A. Nuaimi, R.L. Thankamony, J.-P.B. Boross de Levay, B. Yuan, Z. Lai, Uniformly porous PVDF-co-HFP membranes prepared by mixed solvent phase separation for direct contact membrane distillation, Journal of Membrane Science, 711 (2024) 123175.

[79] L. Aoudjit, H. Salazar, D. Zioui, A. Sebti, P.M. Martins, S. Lanceros-Mendez, Reusable Ag@TiO2-Based Photocatalytic Nanocomposite Membranes for Solar Degradation of Contaminants of Emerging Concern, Polymers, 13 (2021) 3718.

[80] M.F.J. Dijkstra, A. Michorius, H. Buwalda, H.J. Panneman, J.G.M. Winkelman, A.A.C.M. Beenackers, Comparison of the efficiency of immobilized and suspended systems in photocatalytic degradation, Catalysis Today, 66 (2001) 487-494.

[81] L. Liu, Z. Xue, T. Gao, Q. Zhao, Y. Sun, Y. Wu, Photocatalytic degradation performance of Ag-modified flexible TiO2 nanofiber film, Optical Materials, 160 (2025) 116720.

[82] N. Kaneva, A. Bojinova, K. Papazova, Enhanced Removal of Organic Dyes Using Co-Catalytic Ag-Modified ZnO and TiO2 Sol-Gel Photocatalysts, Catalysts, 13 (2023) 245.

[83] L. Ma, Y. Chen, J. Zheng, An efficient, stable and reusable polymer/TiO2 photocatalytic membrane for aqueous pollution treatment, Journal of Materials Science, 56 (2021) 11335-11351.

[84] F. Jandaghian, A. Ebrahimian Pirbazari, O. Tavakoli, N. Asasian-Kolur, S. Sharifian, Comparison of the performance of Ag-deposited ZnO and TiO2 nanoparticles in levofloxacin degradation under UV/visible radiation, Journal of Hazardous Materials Advances, 9 (2023) 100240.

[85] M. Esfandiaribayat, M. Binazadeh, S. Sabbaghi, M. Mohammadi, S. Ghaedi, H. Rajabi, Tetracycline removal from wastewater via g-C3N4 loaded RSM-CCD-optimised hybrid photocatalytic membrane reactor, Scientific reports, 14 (2024) 1163.

[86] S. Matsuzawa, C. Maneerat, Y. Hayata, T. Hirakawa, N. Negishi, T. Sano, Immobilization of TiO2 nanoparticles on polymeric substrates by using electrostatic interaction in the aqueous phase, Applied Catalysis B: Environmental, 83 (2008) 39-45.

[87] S. Singh, H. Mahalingam, P.K. Singh, Polymer-supported titanium dioxide photocatalysts for environmental remediation: A review, Applied Catalysis A: General, 462-463 (2013) 178-195.

[88] D. Russo, A. Siciliano, M. Guida, E. Galdiero, A. Amoresano, R. Andreozzi, N.M. Reis, G. Li Puma, R. Marotta, Photodegradation and ecotoxicology of acyclovir in water under UV254 and UV254/H2O2 processes, Water Research, 122 (2017) 591-602.

[89] P. Calza, C. Medana, F. Carbone, V. Giancotti, C. Baiocchi, Characterization of intermediate compounds formed upon photoinduced degradation of quinolones by high-performance liquid chromatography/high-resolution multiple-stage mass spectrometry, Rapid Communications in Mass Spectrometry: An International Journal Devoted to the Rapid Dissemination of Up-to-the-Minute Research in Mass Spectrometry, 22 (2008) 1533-1552.

[90] J. Yang, G. Lv, C. Zhang, Z. Wang, X. Sun, Indirect Photodegradation of Sulfamethoxazole and Trimethoprim by Hydroxyl Radicals in Aquatic Environment: Mechanisms, Transformation Products and Eco-Toxicity Evaluation, International Journal of Molecular Sciences, 21 (2020) 6276.

[91] Y. Ma, K. Zhang, C. Li, T. Zhang, N. Gao, Oxidation of Sulfonamides in Aqueous Solution by UV-TiO2-Fe (VI), BioMed Research International, 2015 (2015) 973942.

[92] D. Madej-Knysak, E. Adamek, W. Baran, Biodegradation of Photocatalytic Degradation Products of Sulfonamides: Kinetics and Identification of Intermediates, International Journal of Molecular Sciences, 25 (2024) 6688.

[93] M. Di Giannantonio, C. Gambardella, R. Miroglio, E. Costa, F. Sbrana, M. Smerieri, G. Carraro, R. Utzeri, M. Faimali, F. Garaventa, Ecotoxicity of polyvinylidene difluoride (PVDF) and polylactic acid (PLA) microplastics in marine zooplankton, Toxics, 10 (2022) 479.

[94] G.P. Marcone, Á.C. Oliveira, G. Almeida, G.A. Umbuzeiro, W.F. Jardim, Ecotoxicity of TiO2 to Daphnia similis under irradiation, Journal of hazardous materials, 211 (2012) 436-442.

[95] W.C. Chong, Y.T. Chung, Y.H. Teow, M.M. Zain, E. Mahmoudi, A.W. Mohammad, Environmental impact of nanomaterials in composite membranes: Life cycle assessment of algal membrane photoreactor using polyvinylidene fluoride – composite membrane, Journal of Cleaner Production, 202 (2018) 591-600.

[96] M. Li, D. Wei, Y. Du, Acute toxicity evaluation for quinolone antibiotics and their chlorination disinfection processes, Journal of Environmental Sciences, 26 (2014) 1837-1842.

[97] D.G.J. Larsson, C. de Pedro, N. Paxeus, Effluent from drug manufactures contains extremely high levels of pharmaceuticals, Journal of Hazardous Materials, 148 (2007) 751-755.

[98] K.J. Aldred, R.J. Kerns, N. Osheroff, Mechanism of Quinolone Action and Resistance, Biochemistry, 53 (2014) 1565-1574.

[99] W. Dongbin, Z. Aiqian, W. Zhongbo, H. Shuokui, W. Liansheng, A Case Study of Logistic QSAR Modeling Methods and Robustness Tests, Ecotoxicology and Environmental Safety, 52 (2002) 143-149.

[100] Y. Luo, Y.J. Liu, Bioluminophore and flavin mononucleotide fluorescence quenching of bacterial bioluminescence—a theoretical study, Chemistry–A European Journal, 22 (2016) 16243-16249.

[101] E. De Vasconcelos, C. Dalke, C. de Oliveira, Influence of select antibiotics on Vibrio fischeri and Desmodesmus subspicatus at μg L− 1 concentrations, Environmental Management, 60 (2017) 157-164.

[102] T. Backhaus, K. Froehner, R. Altenburger, L. Grimme, Toxicity testing with Vibrio fischeri: A comparison between the long term (24 h) and the short term (30 min) bioassay, Chemosphere, 35 (1997) 2925-2938.

[103] K. Froehner, W. Meyer, L. Grimme, Time-dependent toxicity in the long-term inhibition assay with Vibrio fischeri, Chemosphere, 46 (2002) 987-997.

[104] K. Froehner, T. Backhaus, L. Grimme, Bioassays with Vibrio fischeri for the assessment of delayed toxicity, Chemosphere, 40 (2000) 821-828.

[105] M.R. Pino-Otín, A. Valenzuela, C. Gan, G. Lorca, N. Ferrando, E. Langa, D. Ballestero, Ecotoxicity of five veterinary antibiotics on indicator organisms and water and soil communities, Ecotoxicology and Environmental Safety, 274 (2024) 116185.

[106] X. Zhang, J. Guo, Y. Huang, G. Lu, Toxicity evolution and control for the UV/H2O2 degradation of nitrogen-containing heterocyclic compounds: SDZ and PMM, Chemosphere, 338 (2023) 139541.

[107] C.M. Martínez-Escudero, I. Garrido, F. Contreras, P. Hellín, P. Flores, L.O. León-Morán, N. Arroyo-Manzanares, N. Campillo, M. Pastor, P. Viñas, J. Fenoll, Photodecomposition of antibiotics and their transformation products in wastewaters using ZnO and TiO2 with LED lamps, Journal of Photochemistry and Photobiology A: Chemistry, 454 (2024) 115732.

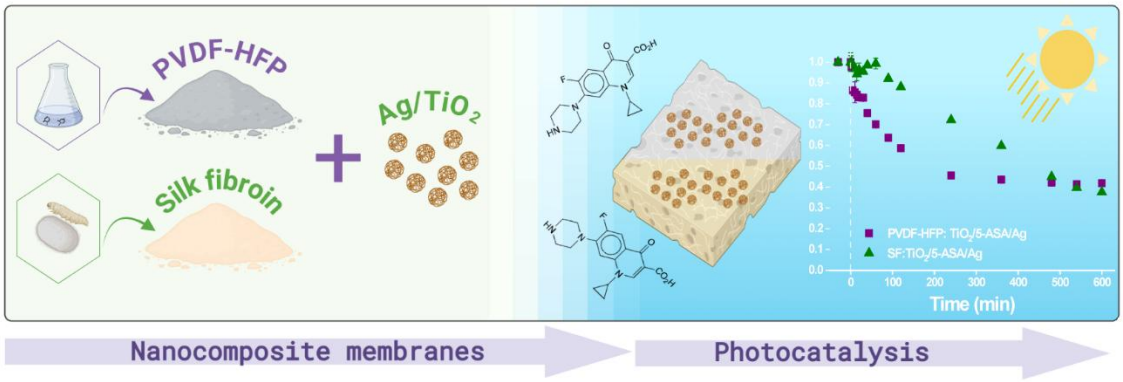
[108] E. Vetrova, N. Kudryasheva, V. Kratasyuk, Redox compounds influence on the NAD (P) H: FMN—oxidoreductase—luciferase bioluminescent system, Photochemical & Photobiological Sciences, 6 (2007) 35-40.

CHAPTER 3

NATURAL AND SYNTHETIC POLYMER-BASED COMPOSITE MEMBRANES FOR PHOTOCATALYTIC DEGRADATION OF ANTIBIOTICS AND ANTIMICROBIAL PROPERTIES

This chapter explores silk fibroin, a natural polymer matrix, as a sustainable alternative to PVDF-HFP. Incorporating Ag-functionalised TiO_2 nanoparticles into both synthetic and natural polymer matrices preserves photocatalytic performance and reusability while also conferring antimicrobial properties to the membranes. The transition of this multifunctionality from synthetic polymer-based systems to bio-based alternatives is a significant step towards a more sustainable approach within the circular materials paradigm .

This chapter is based on the following publication: **Joana M. Queirós**, Fangyuan Zheng, Ricardo Brito-Pereira, Margarida M. Fernandes, Estela O. Carvalho, Pedro M. Martin, Vesna Lazić, Jovan M. Nedeljković, Senentxu Lanceros-Mendez, Photocatalytic and antimicrobial synthetic and natural polymer-based hybrid membranes with surface-modified TiO_2 nanoparticles with 5-aminosalicylic acid and silver nanoparticles, RSC Sustainability, 2025, 3.10: 4568-4582.



3.1 Introduction

Water pollution is one of humankind's most critical challenges [1, 2], contributing to nearly 1.5 million deaths yearly due to the consumption of unsafe water [3]. In recognition of this, ensuring access to clean water and sanitation was established as the sixth goal of the United Nations SDGs [4-6].

Among water contaminants, contaminants of emerging concern CECs [7-9] have received growing attention due to their frequent detection in aquatic ecosystems at low concentrations (ng/L–µg/L) [10, 11]. Pharmaceuticals constitute one of the largest groups of CECs, gaining prevalence due to their wide use to treat various diseases and areas persistent in water bodies [12-14]. Antibiotics are especially concerning, as they have been detected in various types of water matrices worldwide, including groundwater and drinking water [15, 16].

Quinolones, such as ofloxacin, ciprofloxacin, and norfloxacin, are extensively used in the treatment of human and animal infections [17, 18]. A substantial portion of these drugs remains unmetabolised and is excreted through urine and faeces, entering wastewater systems [19, 20]. Ciprofloxacin (CIP) is a widely prescribed and valued for its broad efficacy and cost-effectiveness [21]. However, its incomplete removal in conventional wastewater treatment plants (WWTPs) contributes to its environmental dissemination. CIP exposure has been associated with health risks including altered intestinal microflora, increased susceptibility to infections, and potential carcinogenic effects [22-24]. Moreover, the release of antibiotics into the environment fosters the development of antimicrobial resistance in microorganisms, facilitating the emergence of antibiotic-resistant bacteria (ARB) [25-27]. This reduces the effectiveness of antibiotics in treating bacterial infections [28]. For instance, some studies have shown that CIP concentrations as low as 0.1 µg/mL in drinking water can induce resistance in *Staphylococcus aureus*, *Pseudomonas sp.*, and *Enterococcus sp.* [28, 29].

In this context, the development of materials capable of degrading persistent antibiotics and simultaneously presenting antimicrobial properties is urgently needed.

Photocatalytic nanomaterials have received considerable attention in water remediation for CEC degradation and application against ARB [11, 30-32]. An effective strategy for extending the photocatalytic activity of wide band gap oxides, such as TiO_2, into the visible range is to form an Interfacial Charge Transfer (ICT) complex with organic ligands [33, 34]. These hybrids can be formed by coordinating salicylate-type ligands such as 5-aminosalicylic acid (5-ASA), an anti-inflammatory drug known as mesalazine, to the surface Ti atom. Furthermore, introducing noble metals as Ag improves charge separation [35, 36] and provides strong antimicrobial activity [37].

The immobilisation of photocatalysts leads to a more cost-effective process by allowing reusability and preventing possible secondary pollution from nanoparticles (NPs) released into water bodies [38-41]. Polymers are widely used as nanoparticle support materials since they are inexpensive, flexible, thermal, chemical, and mechanically stable [42, 43]. Among them, synthetic polymers polyvinylidene fluoride (PVDF) and its copolymers, including polyvinylidene fluoride-co-hexafluoropropylene (PVDF-HFP) [44] have been extensively used as membrane materials for water remediation applications [45–47] due to their mechanical robustness, UV resistance, and compatibility with various processing technologies [46–49]. Nevertheless, PVDF-HFP is derived from non-renewable [50] fossil resources and is resistant to natural degradation [51], raising concerns about the potential release of toxic compounds and microplastics [51,52], which could have long-term environmental impacts [53–55]. Additionally, its processing is commonly associated with the use of toxic solvents (e.g., dimethyl formamide (DMF)) [50,52].

Though synthetic polymers are still the best option for high-performance applications. Regarding other applications, it is possible to focus on alternatives based in green chemistry and circular economy paradigms, developing sustainable materials [56–59] to address climate change [51,56]. In this context, natural polymers, such as cellulose [56], chitosan [60], and silk [61], arise as a potential solution, as they are biodegradable and are produced from renewable sources such as plants, animals, and microbes [51,62,63].

Among them, silk obtained from the *Bombyx mori* silkworm has attracted much attention [64–66]. Silk fibroin (SF), the main structural protein of silk [67,68], is composed of α-helices, β-sheet crystal structure and random coils assembled by repetitive amino acid sequences [67,69}. SF also presents biocompatibility, flexibility, and stability in most organic solvents and water, making it a good candidate for environmentally friendly materials development [67,68,70,71]. Moreover, SF, similarly to PVDF, can

be processed into different morphologies, such as film [72] 3D porous scaffolds and membranes [73], electrospinning [74], spin coating [72], salt-leaching [73], among others. Thus, SF-based materials have been used in biomedical, electronic, sensing, optical applications, and water remediation [75–79].

Combining the activity of green functionalised photocatalysts with visible spectral range activity and antimicrobial effects incorporated into a natural polymer matrix presents a novel alternative to conventional PVDF-based membranes. The resulting hybrid materials may offer performance comparable to fossil-based polymers while significantly reducing environmental impact. This approach aligns with sustainable development goals and represents a step forward in advanced water treatment technologies.

In this study, TiO_2 nanoparticles were functionalised with Ag nanoparticles using 5-aminosalicylic acid as a green methodology. Afterwards, the nanocomposite particles were incorporated into PVDF-HFP and SF polymer matrices. The resulting membranes were tested for their photocatalytic efficiency in degrading ciprofloxacin, their antibacterial properties against Gram-positive and Gram-negative bacteria, as well as their reusability in cycling experiments. This work aims to validate the green transition from synthetic to natural polymer in the development of multifunctional membranes for the sustainable treatment of contaminated water.

3.2 Materials and methods

3.2.1 Materials

Bombyx mori silkworm cocoons were supplied by APPACDM from Castelo Branco (Portugal). Sodium carbonate (Na_2CO_3), formic acid (FA, CH_2O_2), calcium chloride ($CaCl_2$) and sodium chloride (NaCl) were sourced from Sigma-Aldrich. Distilled water was prepared on-site in the laboratory. Poly(vinylidene fluoride-co-hexafluoropropylene) (PVDF-HFP, SOLEF®) was purchased from Solvay, while Fischer-Scientific supplied N,N-dimethylformamide (DMF, ≥99%). Ciprofloxacin ($C_{17}H_{18}FN_3O_3$) was purchased from Sigma-Aldrich. Silver nitrate ($AgNO_3$) was acquired from VWR, and 5-aminosalicylic acid from Alfa Aesar. All chemicals and solvents were used without further purification.

3.2.2 Synthesis and characterisation of nanoparticles

The surface functionalisation of TiO_2 nanoparticles (Degussa P-25, with a specific surface area (BET) of 35–65 m_2 g_{-1}) with 5-ASA was carried out according to the procedure described in [80]. In brief, 100 mg of TiO_2 nanoparticles were dispersed in 30 mL of deionised water containing 30.6 mg 5-ASA and stirred overnight. The change in the nanoparticles' colour evidences the successful formation of the ICT

complex. Afterwards, the modified TiO_2 nanoparticles were separated via centrifugation, thoroughly rinsed with water five times, and vacuum-dried at 40 °C in a GCA Corporation, USA, oven.

A nanocomposite of Ag NPs on the surface of TiO_2 nanoparticles functionalised with 5-ASA was synthesised by utilising the reducing properties of the free amino groups in 5-ASA molecules [81]. Specifically, 200 mg of surface-modified TiO_2 with 5-ASA was mixed with 20 mg of $AgNO_3$ in 50 mL of Ar-saturated water, and the mixture was refluxed at 60 °C for 6 hours under continuous stirring. The resulting nanocomposite was isolated by centrifugation, repeatedly washed with water, and dried under vacuum at 40 °C in a GCA Corporation oven. For simplicity, the surface-modified TiO_2 with 5-ASA and the nanocomposite consisting of Ag NPs supported on TiO_2 with 5-ASA will be referred to as TiO_2/5-ASA and TiO_2/5-ASA/Ag, respectively.

The TiO_2/5-ASA/Ag nanocomposite composition, including silver and titanium content, was quantified using inductively coupled plasma optical emission spectroscopy (ICP-OES Thermo Scientific iCAP 7400). Transmission electron microscopy (TEM) imaging was performed using a JEOL JEM-2100 LaB6 instrument operated at 200 kV, with images acquired using a Gatan Orius CCD camera set to 2× binning. X-ray diffraction (XRD) was carried out using a Rigaku SmartLab system with Cu Kα1,2 radiation, employing a continuous angular scanning rate at 2° min^{-1}. Reflectance spectra of TiO_2/5-ASA and TiO_2/5-ASA/Ag samples were measured using a Shimadzu UV-Visible UV-2600 spectrophotometer equipped with an integrated sphere ISR-2600 Plus.

3.2.3 Extraction of SF

The extraction of SF from *Bombyx mori* silkworm cocoons was performed using a soap degumming method [82]. The cocoons were cleaned, cut into 2 cm^2 pieces, and boiled in a 0.05 wt% Na_2CO_3 solution for 30 min, maintaining an SF-to-water solution ratio (w/v) of 1 : 40. The resultant fibres of SF underwent extensive rinsing with distilled water before being air-dried at room temperature for 24 hours. These fibres were dissolved in a 0.19 M FA/$CaCl_2$ solution in a 10 : 1 v/w ratio (FA : SF). Impurities were removed by centrifugation (Hettich EBA 21) at 6000 rpm for 10 min, and the supernatant SF/FA/$CaCl_2$ solution was filtered. The filtered solution was then cast onto a Petri dish and allowed to dry at room temperature for 24 hours for FA evaporation. The final transparent, plastic-like material was rinsed in a distilled water bath to eliminate residual $CaCl_2$ and air-dried at room temperature for 24 hours, resulting in a brittle, whitish solid form of SF.

3.2.4 Development of polymer-based porous membranes

The synthesised nanoparticles TiO_2/5-ASA and TiO_2/5-ASA/Ag were immobilised into a PVDF-HFP and silk-based membrane by temperature-induced phase separation (TIPS) combined with salt leaching techniques. This combination of methods allows greater control over the pore size range and promotes enhanced pore interconnectivity [83]. The preparation of the PVDF-HFP-based membranes followed the methodology described in Chapter 2. TiO_2/5-ASA and TiO_2/5-ASA/Ag nanoparticles were dispersed in DMF by ultrasonication prior to polymer addition, yielding nanocomposite membranes with a PVDF-HFP-to-nanoparticle mass ratio of 10 : 1 [11]. Pristine membranes were also prepared and identified as PVDF-HFP. The solution was mechanically agitated until the polymer was completely dissolved. At this stage, 9 g of NaCl, previously sieved (100 μm mesh), was added to the solution and stirred until a homogeneous and viscous solution was obtained. The nanoparticle/polymer/salt solution was poured into a Petri dish. The DMF was evaporated at room temperature for nearly one week until complete solvent evaporation. When the membranes were dried entirely, they were submerged under agitation to allow the NaCl to leach for 5 days, changing the water frequently. Electrical conductivity measurements were performed on the water solution to confirm constant values, indicating that NaCl had been completely removed from the polymer microstructure (Fig. 3.1).

To produce SF membranes, the TiO_2/5-ASA and TiO_2/5-ASA/Ag nanoparticles were dispersed in 10 mL of FA in an ultrasonication bath for 2 h to achieve good nanoparticle dispersion. Subsequently, 1 g of SF was added to obtain a 10 : 1 v/w FA : SF solution. The solution was mechanically agitated for 1 h to ensure complete dissolution. SF (pristine membranes) were also developed. At this point, 9 g of NaCl, sifted through a 100 μm mesh, was incorporated into the solution and agitated until a uniform and viscous solution was achieved. Then, the nanoparticles/polymer/salt solution was placed in a Petri dish and left to dry for 24 hours to evaporate the solvent fully. These membranes were designated SF, SF : TiO_2/5-ASA, and SF : TiO_2/5-ASA/Ag. Similar to the PVDF-HFP membranes, the SF-based membranes were submerged in water under agitation to allow the NaCl to leach for 5 days, changing the water frequently. The porous membranes were then obtained and dried in an airing chamber (Christ Beta 2–8 LDplus) for 24 h. The preparation procedure of the membranes is summarised in Fig. 3.1.

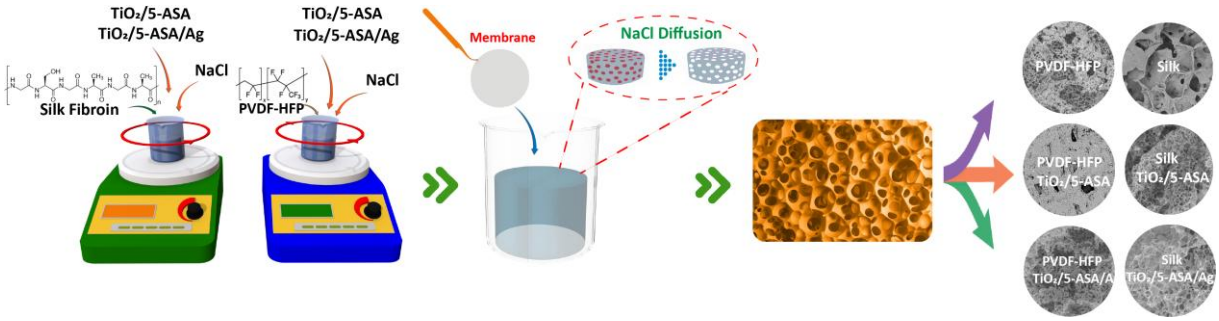


Figure 3.1. Schematic representation of the methodology to develop the PVDF-HFP- and SF-based pristine and nanocomposite membranes.

3.2.5 Polymer-based membranes' physical-chemical characterisation

The morphological analysis of the produced composites membranes was performed by SEM using a NanoSEM FEI Nova 200 (FEG-SEM), operating at an accelerating voltage of 10 kV. Prior to analysis, all samples were sputter-coated with a 20 nm thick gold layer using a Polaron SC502 apparatus.

Surface wettability was evaluated by static water contact angle measurements using an Ossila contact angle goniometer, following the procedure previously described in Chapter 2.

The physicochemical characterisation of the membranes was carried out following the methodologies described in Chapter 2 (Section 2.2.5), with minor adaptations where specified. FTIR measurements for PVDF-HFP-based and SF-based membranes were conducted under the same experimental conditions and data treatment procedures. For SF-based membranes, the amide I region was deconvolved using OriginPro 8.1 software (OriginLab, Northampton) to estimate the relative content of secondary structures. Linear baseline correction (Savitzky–Golay method, 15 points) was applied, and peak positions identified from the second derivative were used as initial parameters for iterative Gaussian curve fitting using the Levenberg–Marquardt algorithm (R^2 > 0.999). The relative contribution of each component was determined by normalising the integrated peak area to the total amide I area.

DSC analyses were carried out following the protocol described in Chapter 2. PVDF-HFP-based membranes were heated from 25 to 200 °C, while SF-based membranes were heated from 25 to 170 °C, cooled to 25 °C to remove absorbed water, and subsequently reheated up to 350 °C. All heating and cooling cycles were performed at a rate of 10 °C/min under a nitrogen atmosphere. The relative β-phase content and crystallinity of the PVDF-HFP-based membranes were calculated using Eq. 2.3 and Eq. 2.4, respectively [3,84–86].

3.2.6 Polymer-based membranes' functional performance

3.2.6.1 Polymer-based membranes' photocatalytic activity

The photocatalytic performance of the nanocomposites membranes was evaluated using ciprofloxacin (CIP) as a model contaminant under ultraviolet (UV) and simulated solar radiation (VIS). The experimental procedure largely followed the methodology described in Chapter 2 (Section 2.2.3.2 and 2.2.6) for immobilised membranes, including a 30 min dark period to reach adsorption-desorption equilibrium.

For these tests, 5 cm × 3 cm membrane sample were affixed to the inner wall of a beaker containing 50 mL of CIP solution (C_0 = 5 mg L^{-1}, pH = 2.9) and irradiated for 600 min. UV irradiation was provided by eight 8 W UV lamps (PHILIPS TL 8 W BLS, Poland, λ= 385 nm, irradiance 3.3 W/m^2, distance 13.5 cm), while visible irradiation was provided by a Xenon lamp (λ = 550 nm, irradiance 300 W/m^2, distance 21 cm).

The degradation of CIP was monitored by measuring the variation in its maximum absorption peak at 277 nm using an Infinite M Plex spectrophotometer (TECAN). Degradation efficiencies were calculated according to Eq. 3.1:

$$\eta\% = \frac{C_0 - C}{C_0} \times 100 \qquad \text{Eq. 3.1}$$

where C_0 and C represent the initial and current concentrations of the pollutant, respectively. The reaction kinetics were fitted to a pseudo-first-order model as described in Chapter 1 using Eq. 1.3.

3.2.6.2 Polymer-based membrane's antibacterial activity

Pre-inoculum preparation: The antimicrobial activity of the membranes was tested using Gram-positive *Staphylococcus epidermidis* (NCTC 11,047) and Gram-negative *Escherichia coli* k12 (NCTC 10538) strains obtained from The National Collection of Type Cultures (NCTC). The pre-inocula were prepared by suspending a single colony from stock cultures in nutrient broth (NB) and incubating overnight at 37 °C with shaking at 110 rpm.

Antibacterial activity: The bactericidal activity of the membranes was evaluated using a modified version of the ASTM-E2149-01 standard shake flask method. Bacterial cells from the pre-inoculum were harvested through two rounds of centrifugation (5000 rpm for 5 min) and resuspended in a 0.9 % NaCl (w/v) solution. The suspension's optical density (OD) was measured at 600 nm and adjusted to 0.1, corresponding to an inoculum of approximately 1×106 CFU/mL^{-1}. Simultaneously, membrane pieces

(1×1 cm^2) were sterilised under UV light before testing. The inoculum was combined with the samples and incubated at 37 °C with shaking at 200 rpm for 2 hours. The resulting suspensions were serially diluted in sterile 0.9 % NaCl (w/v), plated onto NB agar, and incubated at 37 °C for 24 hours to quantify surviving bacterial colonies. The reduction in bacterial counts was expressed as $\log_{10}$ reduction, providing quantitative data on the membrane's antibacterial efficacy compared to control conditions (no material).

Polymer-based membrane's induced ROS formation: A lamp that mimics the sunlight (FL T8 – 900 mm 30W Sylvania), which had previously been placed in the incubator, was used to apply the light stimuli to the samples, and further quantification of the reactive oxygen species (ROS). The samples were in contact with the bacterial inoculum for 2 h at 37 °C and 200 rpm at the incubator with the sun-mimicking light (SLM). The samples incubated without stimuli were used as controls. Then, the probe 2-7-dichlorodihydrofluorescein diacetate (DCFH2-DA) at a final concentration of 10 μM was added to the bacterial solution and incubated at 37 °C for 20 min. The DCFH2-DA was used as a substrate for quantitatively measuring the intracellular oxidant production. This non-fluorescent molecule is oxidised to the fluorescent 2-7-dichlorofluorescein (DCF) by the action of bacterial cellular oxidants. The DCFH fluorescence intensity was detected using a multimode reader at an excitation wavelength of 488 nm and an emission wavelength of 525 nm to further quantify the ROS level.

3.3 Results and discussion

3.3.1 Synthesis and characterisation of nanoparticles

The inorganic-organic hybrid (TiO_2/5-ASA/Ag) was synthesised to improve performance in eliminating bacteria and degradation of antibiotics by photo-driven reactions. The initial synthesis step in forming the ICT complex between TiO_2 and 5-ASA. This was achieved through a condensation reaction involving the surface hydroxyl groups of both inorganic and organic components [80,81]. The amino group from 5-ASA remains free, thus enabling its role in the subsequent step, whereby it reduces Ag+ ions and facilitates the attachment of the formed Ag NPs to the TiO_2/5-ASA. The TEM analysis of the TiO_2/5-ASA/Ag nanocomposites (Figure 3.2a and b) reveals the presence of small (<5 nm) spherical Ag NPs distributed randomly across the surface of the commercial TiO_2 nanoparticles. The XRD pattern of the TiO_2/5-ASA/Ag nanocomposite is presented in (Figure 3.2c). The indexed diffraction peaks at 37.9, 44.2, 64.2, and 77.3° correspond to the (111), (200), (220), and (311) crystal planes of face-centred-cubic silver, respectively (card no. 9013050). The remaining diffraction peaks at 25.3° and 48.0° (anatase) and 27.3° and 54.1° (rutile) originate from commercial Degussa P25 (000640863 and 000211276 are card

numbers of anatase and rutile phases, respectively). XRD did not detect the small amount of 5-ASA and Ag on the surface of TiO_2 due to low amounts and reduced nanoparticle size. Additionally, there are no changes in the diffractogram of TiO_2/5-ASA/Ag when compared to the pristine TiO_2, indicating that the functionalisation of TiO_2 with ASA and Ag did not modify the crystalline structure of the nanocatalysts.

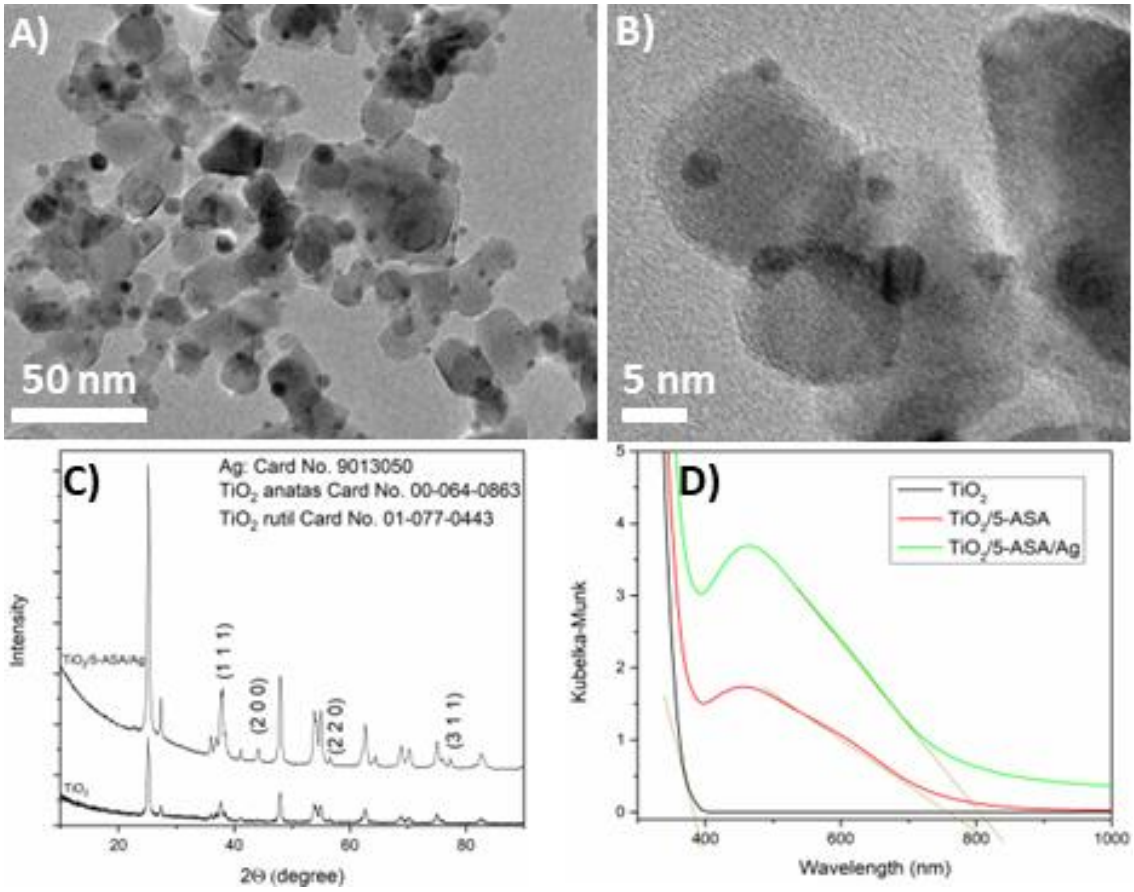


Figure 3.2. a) Low and b) high-magnification TEM images of TiO_2/5-ASA/Ag nanocomposites. c) XRD of TiO_2/5-ASA/Ag nanocomposites. d) Kubelka-Munk transformation of reflection spectra of commercial TiO_2 and synthesised TiO_2/5-ASA and TiO_2/5-ASA/Ag nanocomposites.

The composition of the TiO_2/5-ASA/Ag composite was estimated using the ICP-OES technique after digesting the hybrid with concentrated HNO_3 and H_2O_2. The experimental data indicated 58 and 2.6 wt% of Ti and Ag in the TiO_2/5-ASA/Ag composite, respectively. Assuming a stoichiometric ratio between Ti and O in TiO_2, the content of TiO_2 is around 96.5 wt%, while the remaining, about 1 wt%, is the content of the organic phase (5-ASA) (Table 3.1).

Table 3.1. ICP-OES measurement of Ti and Ag content.

Samples	Ti content, %	TiO_2 content, %	5-ASA	Ag content, %
TiO_2/5-ASA	59.4	98.9	1.1	-
TiO_2/5-ASA/Ag	58.0	96.5	0.9	2.6

Optical changes after each synthetic step were followed by diffuse reflection spectroscopy. The Kubelka–Munk transformations [87] of diffuse reflection data for TiO_2, TiO_2/5-ASA, and TiO_2/5-ASA/Ag nanoparticles are shown in (Figure 3.2d).

Unmodified TiO_2 has a steep absorption increase towards the UV spectral range starting from 400 nm. The TiO_2/5-ASA displays a significant redshift with an absorption onset close to 800 nm induced by the ICT complex formation. The calculated band gap, determined from the reflectance spectra, is 3.8 and 1.6 eV for TiO_2 and TiO_2/5-ASA, respectively. The presence of free electron-donating functional groups in the organic component of the ICT complex, in this case, amino groups, additionally shifts absorption towards the near-infrared spectral region compared to the ICT complex with an organic component without these types of functional groups [88]. The optical properties of the TiO_2/5-ASA/Ag hybrids are similar to the TiO_2-based ICT complex with 5-ASA, since there is an overlap between the absorption of TiO_2/5-ASA and the expected position of the surface plasmon resonance band of a nanometre in size Ag NPs [89].

3.3.2 Polymer-based membranes characterisation

After characterising the synthesised nanoparticles and confirming their structural and optical properties, they were added to porous polymeric matrices to obtain a nanocomposite membrane with photocatalytic and antimicrobial properties. The polymeric matrix exploited for the nanocomposite development was PVDF-HFP, a synthetic and highly stable polymer, and SF, a naturally derived polymer. SEM images of the membranes (Figure 2.3a) indicate the formation of well-distributed micrometric porous structures by TIPS due to the thermally induced phase separation process and the slow evaporation of the solvent [90], the addition of NaCl as a porogen promotes the formation of highly porous materials, regardless of the polymer used [41]. Adding TiO_2/5-ASA and TiO_2/5-ASA/Ag nanoparticles to the PVDF-HFP polymer matrix did not result in a significant alteration of the membrane microstructure, nor did it promote the formation of agglomerates compared to the pristine membrane (Figure 3.3a). Similarly, the

morphology of the SF matrix remained unchanged between the pure membrane and the addition of NPs, maintaining a highly porous microstructure with interconnected pores (Figure 3.3a).

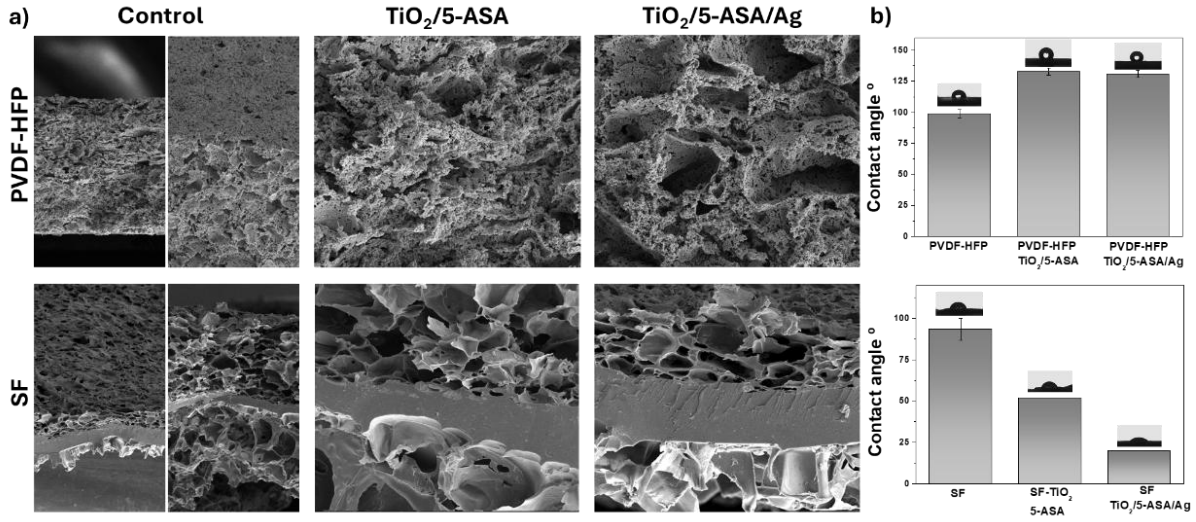


Figure 3.3. a) Cross-sectional and tilted SEM images of porous membranes composed of PVDF-HFP and SF with TiO_2/5-ASA and TiO_2/5-ASA/Ag fillers. SEM images of controls are at 250x magnification, while fillers are at 1000x magnification. b) Contact angle of the different membranes.

Contact angle measurements were performed to assess the membranes' wettability. The PVDF-HFP-based membranes revealed the typical hydrophobic behaviour, with the contact angle increasing from 95° for the pristine PVDF-HFP membrane to 130° when the nanoparticles are incorporated into the polymeric matrix (Figure 3.3b). These findings align with the results reported in the literature [7,83].

Conversely, in SF-based membranes, the samples are hydrophilic, and incorporating NPs enhances their hydrophilicity. The contact angle highly decreases from 90° for SF membranes to 50° in the case of SF : TiO_2/5-ASA and to 20° in the case of SF : TiO_2/5-ASA/Ag (Figure 3.3b), a fact that increased hydrophilicity with the incorporation of fillers, which has been previously reported [91].

FTIR and DSC techniques, respectively, were used to investigate the chemical and thermal properties of the produced membranes (Figure 3.4). FTIR analysis assessed the vibrational bands of the polymer matrices before and after the incorporation of nanoparticles, thereby providing insight into potential chemical interactions between the polymer and nanoparticles. The FTIR spectra of the PVDF-HFP-based membranes (Figure 3.4a) reveal the presence of characteristic bands associated with the β-phase of the polymer, specifically at 840 and 1400 cm^{-1}, and the α-phase at 766 cm^{-1} [42,92].

The calculated β-phase content for each PVDF-HFP-based membrane (Eq. 2.3) is illustrated in Figure 3.4e, demonstrating that the β-phase is the predominant phase across all membranes, irrespective of nanoparticle addition. This observation aligns with previous findings indicating that solvent evaporation at room temperature predominantly induces the crystallisation of PVDF-HFP in the electroactive β-phase [41,44,48,85]. However, a slight reduction in β-phase content is observed upon nanoparticle incorporation, which can be attributed to electrostatic interactions between the polymer and nanofillers during crystallisation, consistent with existing literature [7].

Figure 3.4b presents the FTIR spectra of SF-based membranes. The primary absorption bands for SF are observed at approximately 3300 cm^{-1} (NH stretching), 1620 cm^{-1} (C=O stretching), 1520 cm^{-1} (CN stretching and NH bending), and 1235 cm^{-1} (C–N stretching), which correspond to Amide A, Amide I, Amide II, and Amide III, respectively [93]. All these absorption bands can be observed in the spectra, indicating that the primary structure of the SF-based membranes is preserved even when nanoparticles are incorporated. The secondary structure of SF-based membranes was also investigated by analysing the Amide I region at 1700–1580 cm^{-1}. The Amide I band deconvolution allowed to determine the relative amount of β-sheet, random coils, α-helix and turns conformations in each sample (Figure 3.4f). The β-sheet conformation is the most prevalent, accounting for more than 60% of the total amide I peak area in all samples. Thus, according to the degree of crystallinity formula for SF compounds [94], the SF-based membranes exceed 60% crystallinity, with the pristine SF membrane exhibiting the highest values. On the other hand, in nanoparticle-containing samples, the random coil structure and α-helix increase compared to pristine ones, which suggests a slight preference for amorphous conformation. This implies that nanoparticles act as a steric impediment, restricting protein chains from totally packing and thus crystalline units from stabilising.

DSC measurements were also performed, which allowed to study the melting temperature and the degree of crystallinity of the membranes. Observing the DSC thermograms from PVDF-HFP-based membranes (Figure 3.4c), all the samples showed similar behaviour with a single endothermic peak around 141 °C corresponding to the melting temperature of the polymers [41,86]. Incorporating the nanoparticles did not significantly change the thermal stability of the crystalline phase, with a melting temperature for the composites similar to that of the pristine PVDF-HFP.

The calculated degree of crystallinity of the PVDF-HFP-based membranes is shown in Figure 3.4e. All the samples presented a degree of crystallinity higher than 30% [48]. However, the incorporation of nanoparticles led to a decrease in the crystallinity of the membranes [41], as the nanoparticles acted as the defect during the crystallisation process of the polymer [95]. The DSC thermograms of SF-based

membranes (Figure 3-4d) show that all membranes exhibit similar behaviour regardless of the addition of nanoparticles, indicating an endothermic peak around 290 °C [96], attributed to the thermal degradation of protein chains, essentially the decomposition of β-sheet crystalline units [97].

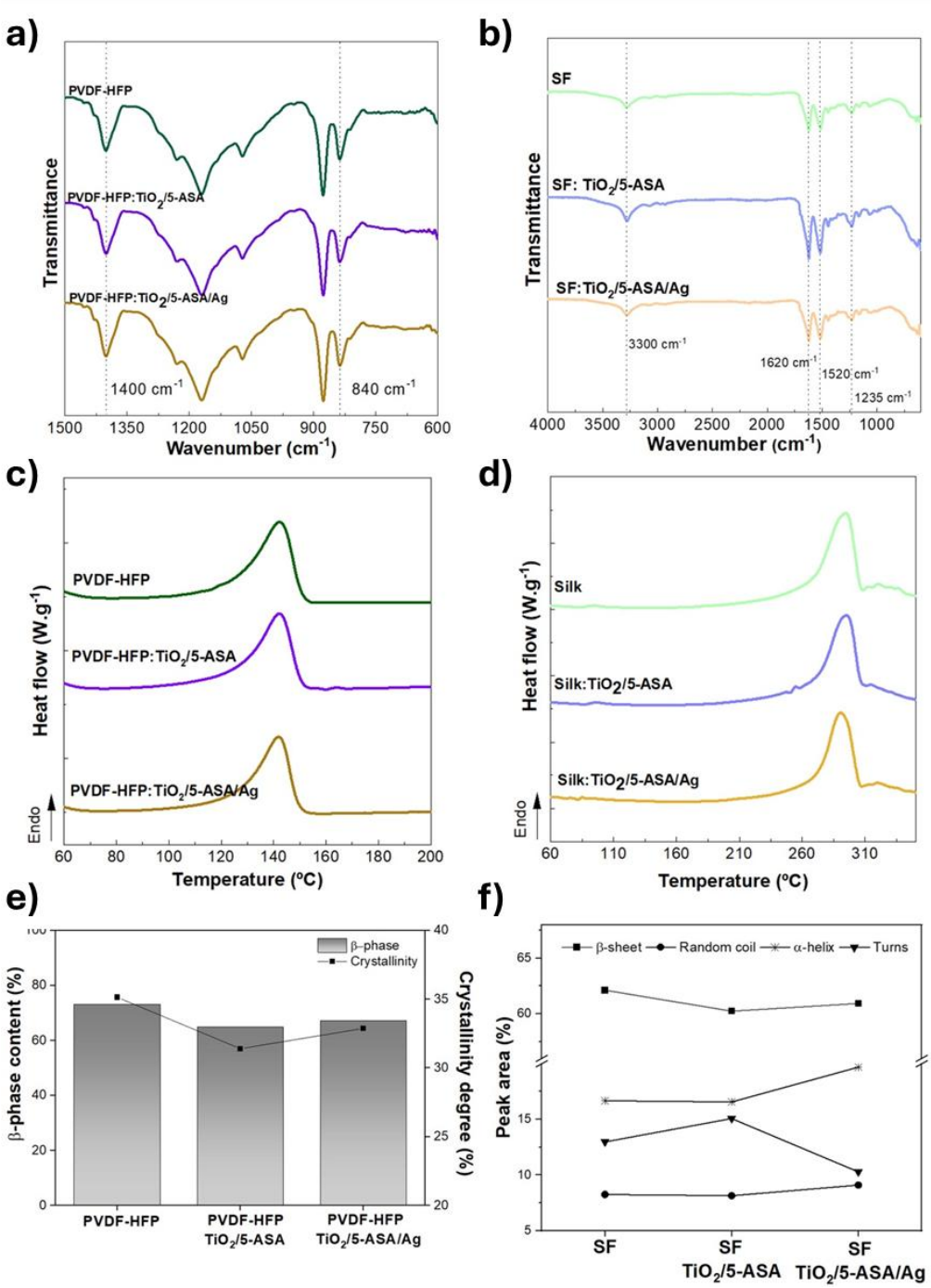


Figure 3.4. FTIR spectra of the a) PVDF-HFP-based and b) SF-based membranes; DSC thermograms of the c) PVDF-HFP-based and d) SF-based membranes; e) β-phase quantification and degree of crystallinity of PVDF-HFP-based membranes and f) secondary structures of SF-based membranes disclosed by deconvolution of the amide I bands.

3.3.3 Photocatalytic performance of nanocomposite membranes

The ability of the membranes to degrade CIP through the photocatalytic process was evaluated under UV and VIS irradiation over time, with samples being withdrawn at determined time intervals for UV-vis spectroscopy analysis and monitoring of the highest absorbance peak of CIP (277 nm) (Figure 3.5 and summarised in Table 3.2) [9]. Before performing the photocatalytic tests with the produced samples, the photostability of CIP was evaluated under UV irradiation for 600 minutes, demonstrating residual or slight degradation (7% – Table 2.1). Afterwards, the photocatalytic activity of the pure PVDF-HFP membranes and the PVDF-HFP/TiO_2 and PVDF-HFP/Ag/TiO_2 nanocomposites under UV irradiation was evaluated. It is essential to note that all samples were left in the dark for 30 minutes to reach the CIP adsorption/desorption equilibrium with the produced pure polymeric and nanocomposite membranes. The pure PVDF-HFP sample and the PVDF/TiO_2/5-ASA/Ag sample did not reveal any adsorption, and only the PVDF-HFP/TiO_2/5-ASA sample showed a slight adsorption of approximately 5%. These results confirm the low affinity of CIP towards the matrix and the photocatalytic nanoparticles in the absence of radiation. Then, UV irradiation was started, and there was no CIP degradation for the pure PVDF-HFP membrane. The PVDF-HFP/TiO_2/5-ASA and PVDF/TiO_2/5-ASA/Ag nanocomposite samples showed ≈38% and ≈63% of CIP photocatalytic degradation after 600 minutes of irradiation, respectively.

Similarly, the SF/TiO_2/5-ASA and SF/TiO_2/5-ASA/Ag membranes exhibit ≈38% and ≈50% photocatalytic activity efficiencies for the same experimental conditions. These results, obtained with PVDF-HFP and SF-based membranes, along with the calculated reaction rates summarised in Table 3.2, demonstrate the significant improvement in the pollutant's photocatalytic degradation efficiency when Ag is added to the nano photocatalyst, which is approximately 1.7 in PVDF-HFP membranes and 1.3 in the case of the SF.

Functionalising TiO_2/5-ASA with Ag improved the degradation efficiency of CIP under UV irradiation regardless of the polymeric matrix. Literature has already addressed this phenomenon, indicating that Ag nanoparticles in the mesoporous TiO_2 structure can induce a Schottky junction at the interface, thus introducing intermediate energy levels [98]. When excited, electrons from the conduction bands (CB) transfer to the Ag nanoparticles while the holes in the valence band (VB) are retained in the TiO_2, decreasing electron–hole recombination and prolonging the lifetime of the holes generated. As a result, the photocatalytic activity of the composite is enhanced [40,99]. Additionally, it has been shown that Ag in the nanocomposite extends the TiO_2 absorption range from UV to visible regions through surface plasmon resonance, coupled with a band gap reduction [100]. These findings are backed up by the

characterisation of the nanoparticles, which reveals reflectance in the visible range (~500 nm), and the calculation of the bandgap (Figure 3.2d).

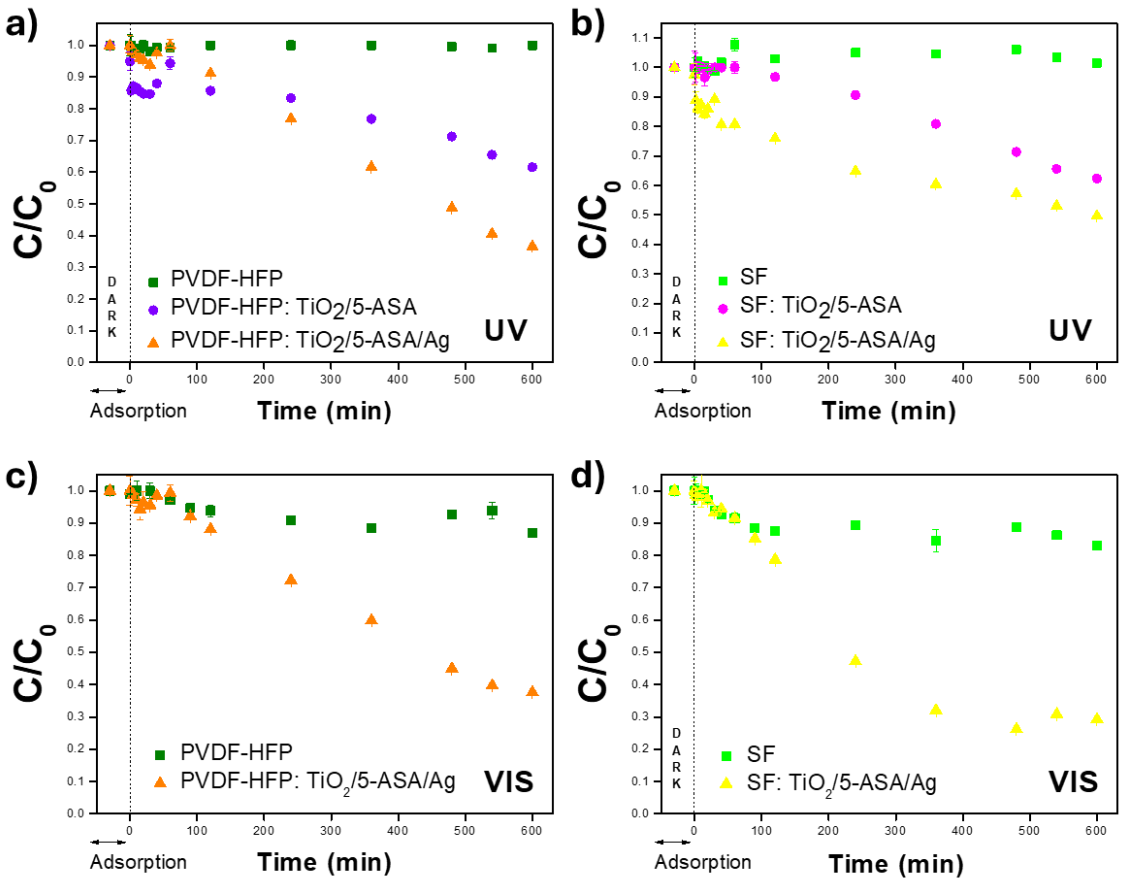


Figure 3.5. Photocatalytic degradation of CIP (C_0=5 mg/L) with a) PVDF-HFP and b) SF-based membranes over 600 min of UV irradiation; with c) PVDF-HFP and d) SF-based membranes over 600 min of VIS irradiation.

TiO_2/5-ASA/Ag nanoparticles were tested in suspension in a CIP solution under Xenon lamp irradiation to confirm this. These tests revealed degradation efficiencies of ~84% in 90 minutes of exposure (Fig. S1A and S1B), which corroborates the findings presented in previous literature [11,101]. After confirming the ability of the particles to absorb visible radiation, we have also assessed the photocatalytic activity of the TiO_2/5-ASA/Ag nanoparticles immobilised into PVDF-HFP and SF matrices under a Xenon lamp irradiation for 600 min (Figure 3.5c and d). Similarly to the UV assays, the first tests were performed with the pristine membranes under simulated sunlight irradiation (VIS), revealing a CIP removal of 13% for PVDF-HFP and about 17% for SF.

Table 3.2. CIP degradation efficiencies (%), apparent reaction rates (k_{app}) and adsorption (%) under UV and VIS radiation for the different pristine and nanocomposite membranes.

SAMPLE	UV			Simulated sunlight (VIS)		
	Degradation (%)	***K_{app} (min^{-1})***	***Adsorption (%)***	***Degradation (%)***	***K_{app} (min^{-1})***	***Adsorption (%)***
PVDF-HFP	7	6.0×10^{-6}	0	16	2.0×10^{-4}	1.0
PVDF-HFP:TiO_2/5-ASA	38.4	5.0×10^{-4}	5.0	-	--	
PVDF-HFP:TiO_2/5-ASA/Ag	63.4	2.0×10^{-3}	0	62.4	2.0×10^{-3}	0
SF	≈0	4.0×10^{-5}	0	16.9	3.0×10^{-4}	0
SF:TiO_2/5-ASA	37.6	7.0×10^{-4}	0	-	--	
SF:TiO_2/5-ASA/Ag	50.3	$\times 10^{-3}$	2.4	70.8	2.0×10^{-3}	0

Regarding the nanocomposite membranes, the PVDF-HFP : TiO_2/5-ASA/Ag membrane degradation efficiency overperformed by attaining 62% of ciprofloxacin degradation. SF : TiO_2/5-ASA/Ag membrane degradation efficiency accomplished values higher than 71%, representing an increase of 49% and 54% compared to the corresponding controls, PVDF-HFP and SF (Table 3.2). Considering that the photocatalytic nanoparticles used in both polymeric nanocomposite membranes are the same and that the porous microstructure resembles both polymer matrices, it is possible to understand that the obtained microstructure is superimposed over wettability. In detail, the photocatalytic results obtained with the PVDF-HFP-based matrices (hydrophobic Figure 3.3b) are similar to the ones obtained with the SF-based membranes (hydrophilic Figure 3.3b). Thus, the employed processing method, salt leaching combined with solvent casting, led to interconnected pores in both polymer matrices, which is essential for the percolation of the solution across the porous microstructure of the membrane, more easily exposing the photocatalytic nanoparticles to contact with CIP, leading to increasing degradation efficiency. This processing method allowed the creation of similar porous microstructures for the PVDF-HFP and SF matrices, which also aids in explaining the similarities of the obtained results. To wrap up, the use of natural polymer matrices is validated in comparison with a synthetic polymer, which results from the proper processing of the polymer and porous tuning.

The literature extensively reports the incorporation of fillers on polymeric substrates for photocatalytic applications [102,103]. Semiconductors such as TiO_2 have been mentioned to be incorporated into

substrates such as polyethylene terephthalate (PET) for degrading antibiotics like trimethoprim. The composite has exhibited a degradation efficiency of 90%, utilising a UV radiation intensity of 500 W m^{-2} and an initial concentration five times lower than that employed in this study [104]. Previous studies have also reported NPs functionalised with noble metals, such as Au/TiO_2. For instance, 10% of these particles were immobilised on PVDF-HFP membranes to degrade norfloxacin, an antibiotic from the same group as the one used in this paper, yielding similar degradation rates of 2×10^{-3} min^{-1} [39]. Natural polymers have also been used as substrates for immobilising photocatalysts. Yontar *et al.* [105] processed polyvinyl alcohol (PVA) films by TIPS with 25% photocatalytic plant extracts, with the result that 0.2 g of film was capable of removing 61.3% of methylene blue (10 mg L^{-1}). Chitosan was used as a matrix for copper (Cu) in degrading Congo red dye, demonstrating high removal efficiencies for three consecutive cycles [106].

The study presents an innovative approach to the green functionalisation of nanoparticles within a natural polymer. This exploits the synergy with SF's porous microstructure, providing a sustainable and efficient alternative to the typical photocatalytic materials. This sustainable method efficiently degrades emerging contaminants and explores solar radiation as a renewable energy source, with no similar research published to date.

3.3.4 Reusability of the SF : TiO_2/5-ASA/Ag membranes

Since the reuse of PVDF has already been studied [11,38] and on the other hand, SF represents a more sustainable approach, where its reuse is less studied; therefore, a study on the reuse of SF : TiO_2/5-ASA/Ag membranes for three cycles under UV and simulated solar irradiation was performed. The results are presented in Figure 3.6a and c (UV irradiation) and Figure 3.6b and d (simulated solar irradiation). The experiments were carried out to assess the reproducibility of the material and its reusability. The same experimental conditions were employed as those previously described in which the membranes were washed with ultrapure water and dried at room temperature between uses before returning to contact with a fresh CIP solution and radiation exposure.

The analysis of the results regarding the degradation efficiencies of the first and the third use shows that the particles and the polymer are efficiently attached, corroborated by the low efficiency losses, which are around 9% and 6% for UV and VIS degradation (Figure 3.6c and d) [107]. This agrees with what is reported in the literature, where, for instance, Momeni *et al.*, observed losses of 7% after cycles of methylene blue degradation [108]. Furthermore, in another study, Zhou *et al.* used Ag@AgCl on polyurethane/silk fibroin porous films to degrade a model organic pollutant (Rhodamine B). The composite material was subjected to consecutive cycles, resulting in slightly more significant efficiency

losses than those obtained in this work [109]. An inefficient immobilisation or a more superficial deposition of the particles is pointed out as one of the possible causes of the leaching of the particles for the loss of efficiency in CIP degradation after the first use [110].

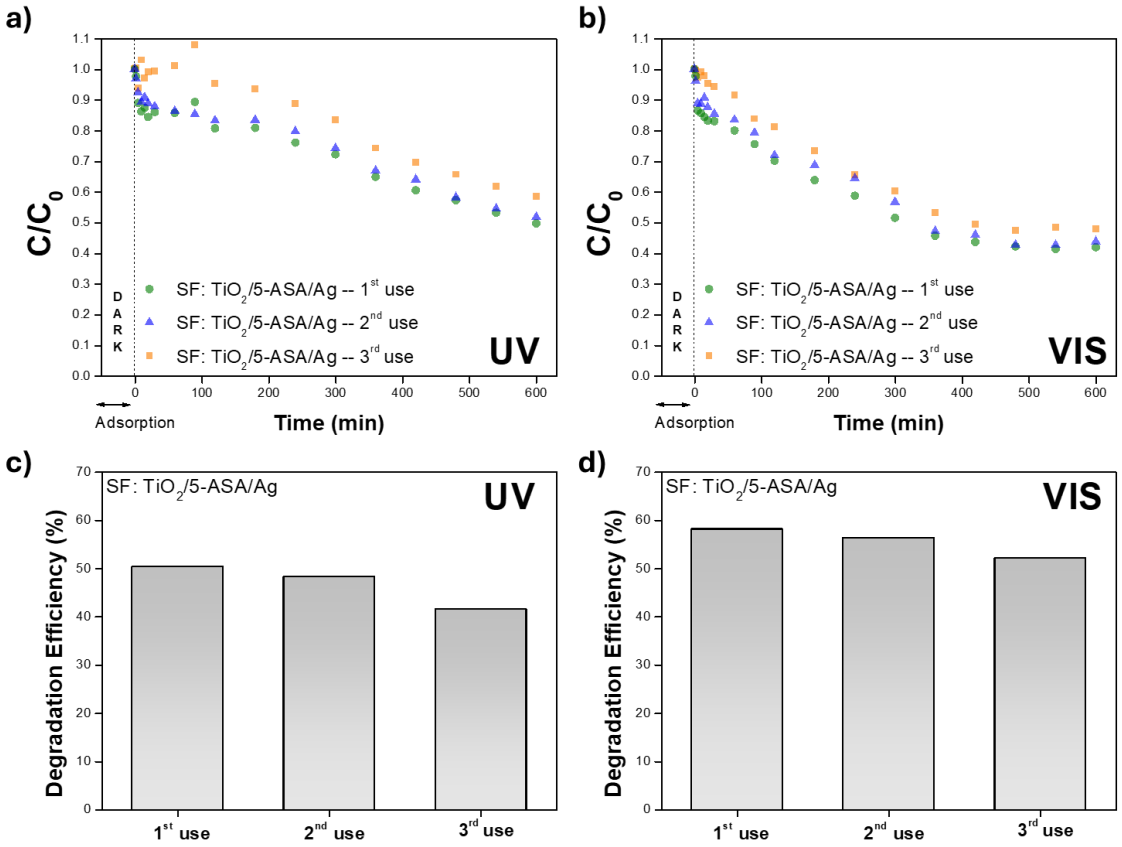


Figure 3.6. Photocatalytic degradation of CIP (C_0=5 mg/L) in three consecutive uses of SF: TiO_2/5-ASA/Ag membranes irradiated for 600 min with a) UV, b) VIS and their respective degradation efficiency (%) in c) and d).

The herein produced SF-based membrane has demonstrated suitability for immobilising photocatalysts, as evidenced by the high efficiencies and low reuse losses observed, indicating the stability of the produced membranes. If the microstructure of the membrane or the attachment of nanoparticles were compromised, the efficiency loss would have increased significantly between uses. Ultimately, this approach constitutes a green and biodegradable alternative to synthetic membranes in terms of performance and long-term stability.

3.3.5 Antimicrobial properties of nanocomposite membranes

The antimicrobial performance of the membranes was also evaluated towards *S. epidermidis* and *E. coli*, herein used as Gram-positive and Gram-negative bacteria models. While *E. coli* and *S. epidermidis* are bacteria commonly found in various environments, including on surfaces and in materials, *E. coli* is commonly found in contaminated water, posing significant risks to human health and the environment [111].

Overall, *E. coli* was found to be more susceptible to both silk and PVDF-based materials, showing higher bacterial $\log_{10}$ reductions when compared to S. epidermidis (Figure 3.7a and b). When the nanoparticles were present in the material, bacterial load was reduced for *E. coli* 1–2 $\log_{10}$ and *S. epidermidis* 0.5 $\log_{10}$, mainly when the particles were functionalised with silver (Figure 3.7a and b). Silver has long been recognised as a potent antimicrobial due to its ability to disrupt cell membranes, bind to proteins, interfere with DNA, and generate ROS oxygen species, which collectively inhibit bacterial growth [112]. Nevertheless, since the material was found to possess photocatalytic properties, mainly in the presence of silver, due to the shift in the plasmon resonance of the particles to the visible range, making them able to induce the formation of ROS through photocatalytic events, a quantification of ROS was performed.

Thus, besides the antimicrobial effect of silver, it is acceptable to assume that the formation of ROS can disrupt the bacterial cell's structure and function, ultimately killing the microorganisms. Thus, to prove this concept, the quantification of ROS on the most susceptible bacterium (*E. coli*), after applying a sun-mimicking light (VIS), was performed (Figure 3.7c and d). According to the results, this light, which includes UV wavelengths typically present in the sunlight (3–5%), induces the highest percentage of ROS. This finding demonstrates that developing photocatalytic materials engineered to produce ROS makes them valuable for antibacterial purposes. Nevertheless, it is essential to highlight that ROS formation is present even in typical bacterial cultures without light [113]. Some nanoparticles, particularly those made of TiO_2 and Ag, can undergo chemical reactions or even release ions, resulting in the generation of ROS.

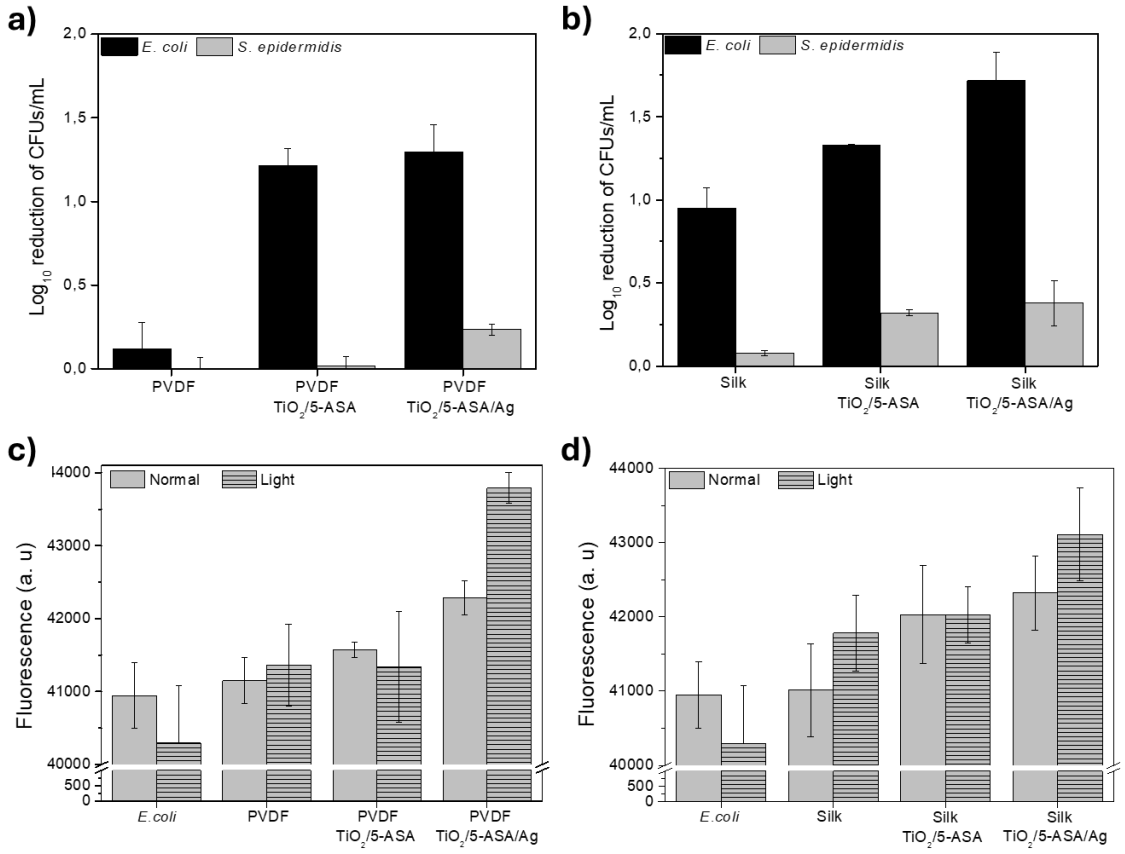


Figure 3.7. Antibacterial activity of a) PVDF-HFP-based membranes and b) SF-based membranes in terms of *E. coli* and *S. epidermidis* $\log_{10}$ reduction, and dichlorofluorescein fluorescence intensity in *E. coli* in contact with c) PVDF-HFP-based membranes and d) SF-based membranes, in "normal" conditions and after application of the sun-mimicking light.

As mentioned before, the effect of the tested material, regardless of the type of matrix used, was more pronounced with *E. coli*, which is one of the most problematic bacteria in the environment [114]. The differences in the cell wall's composition and the outer membrane of the bacteria used herein may be the reason why *E. coli* is more susceptible compared to *S. epidermidis*. *E. coli* is a Gram-negative bacterium with a thinner peptidoglycan layer in its cell wall compared to *S. epidermidis*, a Gram-positive bacterium with a thicker peptidoglycan layer. The thinner cell wall of *E. coli* may make it more susceptible to damage from physical and chemical agents present in materials [115]. Moreover, *E. coli* has an outer membrane that contains lipopolysaccharides (LPS), which can be more susceptible to disruption by certain materials or environmental conditions [116]. This outer membrane provides less protection than the thick peptidoglycan layer of Gram-positive bacteria like *S. epidermidis*.

3.4 Conclusions

This study successfully employed a green approach to produce TiO_2 nanoparticles functionalised with salicylic acid and smaller Ag nanoparticles (TiO_2/5-ASA and TiO_2/5-ASA/Ag), endowing the pristine TiO_2 material with the absorption of visible range radiation. This was experimentally confirmed by band gap reduction from 3.6 to 1.6 eV and photocatalytic degradation of CIP under simulated solar radiation (% deg) using TiO_2/5-ASA and TiO_2/5-ASA/Ag nanoparticles. Afterwards, these active nanoparticles were immobilised into two different polymer matrices: high-performing synthetic PVDF-HFP and natural Silk Fibroin – SF. The same solvent casting and salt leaching techniques were employed to obtain an interconnected, highly porous microstructure in both PVDF-HFP and SF membranes. The characterisation of the nanocomposite membranes indicated that incorporating the TiO_2/5-ASA and TiO_2/5-ASA/Ag nanoparticles into the polymer matrices did not significantly change the membrane's physical–chemical properties, confirming the robustness of both polymeric photocatalytic nanocomposites. The PVDF-HFP : TiO_2/5-ASA/Ag sample outperformed, degrading 63 and 62% of CIP under UV and simulated solar irradiation, respectively. The SF : TiO_2/5-ASA/Ag nanocomposites accomplished 50 and 71% degradation under the same conditions and retained their efficiency with a loss of less than 10% loss after three consecutive cycles. These results validate solvent casting and salt leaching techniques for synthetic and natural polymer matrices for photocatalytic applications. Furthermore, the distinct physicochemical characteristics of the membranes illustrate a variation in nanoparticle encapsulation, which may lead to disparate performances between PVDF-HFP and SF. When considered alongside their natural origins, SF membranes could be utilised in diverse aquatic environments with varying contaminants, potentially supplanting high-performance polymers. The validation of SF nanocomposite membranes' reusability is also paramount, as natural-based materials are commonly associated with low reusability/robustness. The materials evaluation also confirmed the antimicrobial properties of all the nanocomposites containing Ag, with a reduction in bacterial load by 1–2 $\log_{10}$, likely due to ROS formation.

In short, this work lays a solid foundation for the future of multifunctional materials based on natural polymers in water decontamination. Employing the robust processing technique can mitigate intrinsic material differences, favouring their efficient functional practicability.

3.5 References

[1] R.P. Schwarzenbach, T. Egli, T.B. Hofstetter, U. Von Gunten, B. Wehrli, Global water pollution and human health, Annual review of environment and resources, 35 (2010) 109-136.

[2] G.I. Tovar, A. Valverde, C. Mendes-Felipe, S. Wuttke, A. Fidalgo-Marijuan, E.S. Larrea, L. Lezama, F. Zheng, J. Reguera, S. Lanceros-Méndez, M.I. Arriortua, G. Copello, R.F. de Luis, Chitin/Metal-Organic Framework Composites as Wide-Range Adsorbent, ChemSusChem, 14 (2021) 2892-2901.

[3] W.H. Organization, Progress on household drinking water, sanitation and hygiene 2000-2017: special focus on inequalities, World Health Organization, 2019.

[4] U.N.E. Programme, Making Peace with Nature - A scientific blueprint to tackle the climate, biodiversity and pollution emergencies. Nairobi, 2021.

[5] T.B. Cetrulo, R.C. Marques, T.F. Malheiros, N.M. Cetrulo, Monitoring inequality in water access: Challenges for the 2030 Agenda for Sustainable Development, Science of the total environment, 727 (2020) 138746.

[6] A.K. Yadav, H.K. Yadav, A. Naz, M. Koul, A. Chowdhury, S. Shekhar, Arsenic removal technologies for middle- and low-income countries to achieve the SDG-3 and SDG-6 targets: A review, Environmental Advances, 9 (2022) 100262.

[7] L. Aoudjit, H. Salazar, D. Zioui, A. Sebti, P.M. Martins, S. Lanceros-Mendez, Reusable Ag@TiO2-Based Photocatalytic Nanocomposite Membranes for Solar Degradation of Contaminants of Emerging Concern, Polymers, 13 (2021) 3718.

[8] S. Dey, F. Bano, A. Malik, Pharmaceuticals and personal care product (PPCP) contamination—a global discharge inventory, Pharmaceuticals and personal care products: waste management and treatment technology, Elsevier2019, pp. 1-26.

[9] F. Zheng, J.M. Queirós, P.M. Martins, R.F. de Luis, A. Fidalgo-Marijuan, J.L. Vilas-Vilela, S. Lanceros-Méndez, J. Reguera, Au-sensitised TiO2 and ZnO nanoparticles for broadband pharmaceuticals photocatalytic degradation in water remediation, Colloids and Surfaces A: Physicochemical and Engineering Aspects, 671 (2023) 131594.

[10] A.R. Bracamontes-Ruelas, L.A. Ordaz-Díaz, A.M. Bailón-Salas, J.C. Ríos-Saucedo, Y. Reyes-Vidal, L. Reynoso-Cuevas, Emerging Pollutants in Wastewater, Advanced Oxidation Processes as an Alternative Treatment and Perspectives, Processes, 10 (2022) 1041.

[11] H. Salazar, P. Martins, B. Santos, M. Fernandes, A. Reizabal, V. Sebastián, G. Botelho, C.J. Tavares, J.L. Vilas-Vilela, S. Lanceros-Mendez, Photocatalytic and antimicrobial multifunctional nanocomposite membranes for emerging pollutants water treatment applications, Chemosphere, 250 (2020) 126299.

[12] D. Yadav, S. Rangabhashiyam, P. Verma, P. Singh, P. Devi, P. Kumar, C.M. Hussain, G.K. Gaurav, K.S. Kumar, Environmental and health impacts of contaminants of emerging concerns: Recent treatment challenges and approaches, Chemosphere, 272 (2021) 129492.

[13] I.C. Vasilachi, D.M. Asiminicesei, D.I. Fertu, M. Gavrilescu, Occurrence and fate of emerging pollutants in water environment and options for their removal, Water, 13 (2021) 181.

[14] N.J.D. Reyes, F.K.F. Geronimo, K.A.V. Yano, H.B. Guerra, L.-H. Kim, Pharmaceutical and personal care products in different matrices: Occurrence, pathways, and treatment processes, Water, 13 (2021) 1159.

[15] U. Szymańska, M. Wiergowski, I. Sołtyszewski, J. Kuzemko, G. Wiergowska, M.K. Woźniak, Presence of antibiotics in the aquatic environment in Europe and their analytical monitoring: Recent trends and perspectives, Microchemical Journal, 147 (2019) 729-740.

[16] J. Lach, L. Stępniak, A. Ociepa-Kubicka, Antibiotics in the environment as one of the barriers to sustainable development, Problemy Ekorozwoju, 13 (2018).

[17] L.S. Redgrave, S.B. Sutton, M.A. Webber, L.J.V. Piddock, Fluoroquinolone resistance: mechanisms, impact on bacteria, and role in evolutionary success, Trends in Microbiology, 22 (2014) 438-445.

[18] T.P. Van Boeckel, C. Brower, M. Gilbert, B.T. Grenfell, S.A. Levin, T.P. Robinson, A. Teillant, R. Laxminarayan, Global trends in antimicrobial use in food animals, Proceedings of the National Academy of Sciences, 112 (2015) 5649-5654.

[19] V. Homem, L. Santos, Degradation and removal methods of antibiotics from aqueous matrices–a review, Journal of environmental management, 92 (2011) 2304-2347.

[20] P. Grenni, V. Ancona, A.B. Caracciolo, Ecological effects of antibiotics on natural ecosystems: A review, Microchemical Journal, 136 (2018) 25-39.

[21] J.C. Nwabuife, C.A. Omolo, T. Govender, Nano delivery systems to the rescue of ciprofloxacin against resistant bacteria "E. coli; P. aeruginosa; Saureus; and MRSA" and their infections, Journal of Controlled Release, 349 (2022) 338-353.

[22] S.D. Richardson, S.Y. Kimura, Water analysis: emerging contaminants and current issues, Analytical Chemistry, 92 (2019) 473-505.

[23] M. Kumari, A. Kumar, Human health risk assessment of antibiotics in binary mixtures for finished drinking water, Chemosphere, 240 (2020) 124864.

[24] R. Daghrir, P. Drogui, Tetracycline antibiotics in the environment: a review, Environmental chemistry letters, 11 (2013) 209-227.

[25] M. Foroughi, M. Khiadani, S. Kakhki, V. Kholghi, K. Naderi, S. Yektay, Effect of ozonation-based disinfection methods on the removal of antibiotic resistant bacteria and resistance genes (ARB/ARGs) in water and wastewater treatment: a systematic review, Science of the Total Environment, (2021) 151404.

[26] T.-K. Kim, T. Kim, H. Park, I. Lee, A. Jo, K. Choi, K.-D. Zoh, Degradation of ciprofloxacin and inactivation of ciprofloxacin resistant E. faecium during UV-LED (275 nm)/chlorine process, Chemical Engineering Journal, 394 (2020) 124803.

[27] R. Anjali, S. Shanthakumar, Simultaneous degradation of amoxicillin, ciprofloxacin and acetaminophen in a mixture by ozonation: Kinetics and mechanisms pathway, Journal of Cleaner Production, 378 (2022) 134509.

[28] E. Sanganyado, W. Gwenzi, Antibiotic resistance in drinking water systems: Occurrence, removal, and human health risks, Science of The Total Environment, 669 (2019) 785-797.

[29] S. Kawecki, G. Kuleck, J.H. Dorsey, C. Leary, M. Lum, The prevalence of antibiotic-resistant bacteria (ARB) in waters of the Lower Ballona Creek Watershed, Los Angeles County, California, Environmental Monitoring and Assessment, 189 (2017) 261.

[30] P. Karaolia, I. Michael-Kordatou, E. Hapeshi, C. Drosou, Y. Bertakis, D. Christofilos, G.S. Armatas, L. Sygellou, T. Schwartz, N.P. Xekoukoulotakis, Removal of antibiotics, antibiotic-resistant bacteria and their associated genes by graphene-based TiO2 composite photocatalysts under solar radiation in urban wastewaters, Applied Catalysis B: Environmental, 224 (2018) 810-824.

[31] F. Biancullo, N.F. Moreira, A.R. Ribeiro, C.M. Manaia, J.L. Faria, O.C. Nunes, S.M. Castro-Silva, A.M. Silva, Heterogeneous photocatalysis using UVA-LEDs for the removal of antibiotics and antibiotic resistant bacteria from urban wastewater treatment plant effluents, Chemical Engineering Journal, 367 (2019) 304-313.

[32] N. Castro, J.M. Queirós, D.C. Alves, M.M.M. Fernandes, S. Lanceros-Méndez, P.M. Martins, A 3D-Printed Portable UV and Visible Photoreactor for Water Purification and Disinfection Experiments, Nanomaterials, 14 (2024) 525.

[33] I.A. Janković, Z.V. Šaponjić, M.I. Čomor, J.M. Nedeljković, Surface Modification of Colloidal TiO2 Nanoparticles with Bidentate Benzene Derivatives, The Journal of Physical Chemistry C, 113 (2009) 12645-12652.

[34] T.D. Savić, Z.V. Šaponjić, M.I. Čomor, J.M. Nedeljković, M.D. Dramićanin, M.G. Nikolić, D. Veljković, S.D. Zarić, I.A. Janković, Surface modification of anatase nanoparticles with fused ring salicylate-type

ligands (3-hydroxy-2-naphthoic acids): a combined DFT and experimental study of optical properties, Nanoscale, 5 (2013) 7601-7612.

[35] Y. Sun, J.B. Mwandeje, L.M. Wangatia, F. Zabihi, J. Nedeljković, S. Yang, Enhanced Photocatalytic Performance of Surface-Modified TiO2 Nanofibers with Rhodizonic Acid, Advanced Fiber Materials, 2 (2020) 118-122.

[36] Z. Barbieriková, D. Lončarević, J. Papan, I.D. Vukoje, M. Stoiljković, S. Phillip Ahrenkiel, J.M. Nedeljković, Photocatalytic hydrogen evolution over surface-modified titanate nanotubes by 5-aminosalicylic acid decorated with silver nanoparticles, Advanced Powder Technology, 31 (2020) 4683-4690.

[37] M. Shahriari-Khalaji, F. Zabihi, A. Bahi, D. Sredojević, J.M. Nedeljković, D.K. Macharia, M. Ciprian, S. Yang, F. Ko, Photon-driven bactericidal performance of surface-modified TiO2 nanofibers, Journal of Materials Chemistry C, 11 (2023) 5796-5805.

[38] J.M. Queirós, H. Salazar, A. Valverde, G. Botelho, R. Fernández de Luis, J. Teixeira, P.M. Martins, S. Lanceros-Mendez, Reusable composite membranes for highly efficient chromium removal from real water matrixes, Chemosphere, 307 (2022) 135922.

[39] P.M. Martins, B. Santos, H. Salazar, S.A.C. Carabineiro, G. Botelho, C.J. Tavares, S. Lanceros-Mendez, Multifunctional hybrid membranes for photocatalytic and adsorptive removal of water contaminants of emerging concern, Chemosphere, 293 (2022) 133548.

[40] P. Martins, S. Kappert, H. Nga Le, V. Sebastian, K. Kühn, M. Alves, L. Pereira, G. Cuniberti, M. Melle-Franco, S. Lanceros-Méndez, Enhanced photocatalytic activity of Au/TiO2 nanoparticles against ciprofloxacin, Catalysts, 10 (2020) 234.

[41] F. Zheng, P.M. Martins, J.M. Queirós, C.J. Tavares, J.L. Vilas-Vilela, S. Lanceros-Méndez, J. Reguera, Hybrid TiO2:Au nanostars based polymeric membranes for photocatalytic degradation of ciprofloxacin in water samples, Chemosphere, 313 (2023) 137630.

[42] P.M. Martins, J.M. Ribeiro, S. Teixeira, D.Y. Petrovykh, G. Cuniberti, L. Pereira, S. Lanceros-Méndez, Photocatalytic microporous membrane against the increasing problem of water emerging pollutants, Materials, 12 (2019) 1649.

[43] S. Singh, H. Mahalingam, P.K. Singh, Polymer-supported titanium dioxide photocatalysts for environmental remediation: A review, Applied Catalysis A: General, 462 (2013) 178-195.

[44] C.M. Costa, V.F. Cardoso, P. Martins, D.M. Correia, R. Gonçalves, P. Costa, V. Correia, C. Ribeiro, M.M. Fernandes, P.M. Martins, Smart and multifunctional materials based on electroactive poly (vinylidene fluoride): recent advances and opportunities in sensors, actuators, energy, environmental, and biomedical applications, Chemical reviews, 123 (2023) 11392-11487.

[45] H. Salazar, J. Nunes-Pereira, D. Correia, V. Cardoso, R. Gonçalves, P. Martins, S. Ferdov, M. Martins, G. Botelho, S. Lanceros-Méndez, Poly (vinylidene fluoride-hexafluoropropylene)/bayerite composite membranes for efficient arsenic removal from water, Materials Chemistry and Physics, 183 (2016) 430-438.

[46] H. Salazar, P.M. Martins, A. Valverde, R. Fernández de Luis, J.L. Vilas-Vilela, S. Ferdov, G. Botelho, S. Lanceros-Mendez, Reusable nanocomposite membranes for highly efficient arsenite and arsenate dual removal from water, Advanced Materials Interfaces, 9 (2022) 2101419.

[47] P.M. Martins, B. Santos, H. Salazar, S.A.C. Carabineiro, G. Botelho, C.J. Tavares, S. Lanceros-Mendez, Multifunctional hybrid membranes for photocatalytic and adsorptive removal of water contaminants of emerging concern, Chemosphere, 293 (2022) 133548.

[48] C. Ribeiro, C.M. Costa, D.M. Correia, J. Nunes-Pereira, J. Oliveira, P. Martins, R. Gonçalves, V.F. Cardoso, S. Lanceros-Mendez, Electroactive poly (vinylidene fluoride)-based structures for advanced applications, Nature protocols, 13 (2018) 681-704.

[49] F. Zheng, P.M. Martins, J.M. Queirós, C.J. Tavares, J.L. Vilas-Vilela, S. Lanceros-Méndez, J. Reguera, Size Effect in Hybrid TiO2:Au Nanostars for Photocatalytic Water Remediation Applications, International Journal of Molecular Sciences, 23 (2022) 13741.

[50] P. Yadav, N. Ismail, M. Essalhi, M. Tysklind, D. Athanassiadis, N. Tavajohi, Assessment of the environmental impact of polymeric membrane production, Journal of Membrane Science, 622 (2021) 118987.

[51] I. Jahan, L. Zhang, Natural polymer-based electrospun nanofibrous membranes for wastewater treatment: A review, Journal of Polymers and the Environment, (2021) 1-21.

[52] R. Lohmann, I.T. Cousins, J.C. DeWitt, J. Gluge, G. Goldenman, D. Herzke, A.B. Lindstrom, M.F. Miller, C.A. Ng, S. Patton, Are fluoropolymers really of low concern for human and environmental health and separate from other PFAS?, Environmental science & technology, 54 (2020) 12820-12828.

[53] H.S. Auta, C. Emenike, S. Fauziah, Distribution and importance of microplastics in the marine environment: a review of the sources, fate, effects, and potential solutions, Environment international, 102 (2017) 165-176.

[54] M.M. Borges-Ramírez, E.F. Mendoza-Franco, G. Escalona-Segura, J. Rendón-von Osten, Plastic density as a key factor in the presence of microplastic in the gastrointestinal tract of commercial fishes from Campeche Bay, Mexico, Environmental Pollution, 267 (2020) 115659.

[55] N.P. Ivleva, A.C. Wiesheu, R. Niessner, Microplastic in Aquatic Ecosystems, Angewandte Chemie International Edition, 56 (2017) 1720-1739.

[56] A.C. Silva, A.J. Silvestre, C. Vilela, C.S. Freire, Natural polymers-based materials: A contribution to a greener future, Molecules, 27 (2021) 94.

[57] D. Ayre, Technology advancing polymers and polymer composites towards sustainability: A review, Current Opinion in Green and Sustainable Chemistry, 13 (2018) 108-112.

[58] E. Matei, A.M. Predescu, M. Râpă, A.A. Ţurcanu, I. Mateş, N. Constantin, C. Predescu, Natural Polymers and Their Nanocomposites Used for Environmental Applications, Nanomaterials, 12 (2022) 1707.

[59] C.J.C. Yann Bouchery, Jan C. Fransoo, Tarkan Tan, Sustainable Supply Chains - A Research-Based Textbook on Operations and Strategy, 1 ed., Springer Cham.

[60] Q. Chen, Y. Qi, Y. Jiang, W. Quan, H. Luo, K. Wu, S. Li, Q. Ouyang, Progress in Research of Chitosan Chemical Modification Technologies and Their Applications, Marine Drugs, 20 (2022) 536.

[61] A. Apriyanto, J. Compart, J. Fettke, A review of starch, a unique biopolymer–Structure, metabolism and in planta modifications, Plant Science, (2022) 111223.

[62] P. Muthukumaran, P. Suresh Babu, S. Karthikeyan, M. Kamaraj, J. Aravind, Tailored natural polymers: a useful eco-friendly sustainable tool for the mitigation of emerging pollutants: a review, International Journal of Environmental Science and Technology, 18 (2021) 2491-2510.

[63] G. Alberti, C. Zanoni, V. Losi, L.R. Magnaghi, R. Biesuz, Current trends in polymer based sensors, Chemosensors, 9 (2021) 108.

[64] R. Brito-Pereira, A.S. Macedo, C. Ribeiro, V.F. Cardoso, S. Lanceros-Méndez, Natural based reusable materials for microfluidic substrates: The silk road towards sustainable portable analytical systems, Applied Materials Today, 28 (2022) 101507.

[65] A. Reizabal, C.M. Costa, L. Pérez-Álvarez, J. Vilas-Vilela, S. Lanceros-Méndez, Silk Fibroin as Sustainable Advanced Material: Material Properties and Characteristics, Processing, and Applications, Advanced Functional Materials, 33 (2023) 2210764.

[66] A. Reizabal, C. Costa, L. Pérez-Álvarez, J. Vilas-Vilela, S. Lanceros-Méndez, The new silk road: silk fibroin blends and composites for next generation functional and multifunctional materials design, Polymer Reviews, 63 (2023) 1014-1077.

[67] T.P. Nguyen, Q.V. Nguyen, V.-H. Nguyen, T.-H. Le, V.Q.N. Huynh, D.-V.N. Vo, Q.T. Trinh, S.Y. Kim, Q.V. Le, Silk fibroin-based biomaterials for biomedical applications: a review, Polymers, 11 (2019) 1933.

[68] C. Narita, Y. Okahisa, I. Wataoka, K. Yamada, Characterization of ground silk fibroin through comparison of nanofibroin and higher order structures, ACS omega, 5 (2020) 22786-22792.

[69] D.-L. Wen, D.-H. Sun, P. Huang, W. Huang, M. Su, Y. Wang, M.-D. Han, B. Kim, J. Brugger, H.-X. Zhang, Recent progress in silk fibroin-based flexible electronics, Microsystems & nanoengineering, 7 (2021) 1-25.

[70] D.T. Pham, N. Saelim, W. Tiyaboonchai, Crosslinked fibroin nanoparticles using EDC or PEI for drug delivery: physicochemical properties, crystallinity and structure, Journal of Materials Science, 53 (2018) 14087-14103.

[71] R.F. Pereira, R. Brito-Pereira, R. Gonçalves, M.P. Silva, C.M. Costa, M.M. Silva, V.n. de Zea Bermudez, S. Lanceros-Méndez, Silk fibroin separators: a step toward lithium-ion batteries with enhanced sustainability, ACS applied materials & interfaces, 10 (2018) 5385-5394.

[72] D. Terada, Y. Yokoyama, S. Hattori, H. Kobayashi, Y. Tamada, The outermost surface properties of silk fibroin films reflect ethanol-treatment conditions used in biomaterial preparation, Materials Science and Engineering: C, 58 (2016) 119-126.

[73] L.-P. Yan, J.M. Oliveira, A.L. Oliveira, S.G. Caridade, J.F. Mano, R.L. Reis, Macro/microporous silk fibroin scaffolds with potential for articular cartilage and meniscus tissue engineering applications, Acta biomaterialia, 8 (2012) 289-301.

[74] A. Alessandrino, B. Marelli, C. Arosio, S. Fare, M.C. Tanzi, G. Freddi, Electrospun silk fibroin mats for tissue engineering, Engineering in life sciences, 8 (2008) 219-225.

[75] W. Zhou, H. Huang, S. Du, Y. Huo, J. He, S. Cui, Removal of copper ions from aqueous solution by adsorption onto novel polyelectrolyte film-coated nanofibrous silk fibroin non-wovens, Applied Surface Science, 345 (2015) 169-174.

[76] H. Wang, L. Liang, X. Cheng, Y. Luo, S. Sun, Facile Fabrication of Porous ZnS and ZnO Films by Coaxial Electrospinning for Highly Efficient Photodegradation of Organic Dyes, Photochemistry and Photobiology, 94 (2018) 17-26.

[77] J. Zhou, Y. Zhang, Y. Yang, Z. Chen, G. Jia, L. Zhang, Silk fibroin-graphene oxide functionalized melamine sponge for efficient oil absorption and oil/water separation, Applied Surface Science, 497 (2019) 143762.

[78] I. Garrido, S. Aznar-Cervantes, M. Aliste, M.J. Yáñez-Gascón, N. Vela, J.L. Cenis, S. Navarro, J. Fenoll, Photocatalytic Performance of Electrospun Silk Fibroin/ZnO Mats to Remove Pesticide Residues from Water under Natural Sunlight, Catalysts, 10 (2020) 110.

[79] C.S. Ki, E.H. Gang, I.C. Um, Y.H. Park, Nanofibrous membrane of wool keratose/silk fibroin blend for heavy metal ion adsorption, Journal of Membrane Science, 302 (2007) 20-26.

[80] B. Milićević, V. Doradević, D. Lončarević, S.P. Ahrenkiel, M.D. Dramićanin, J.M. Nedeljković, Visible light absorption of surface modified TiO2 powders with bidentate benzene derivatives, Microporous and Mesoporous Materials, 217 C7 - 7187 (2015) 184-189.

[81] V. Lazić, I. Smičiklas, J. Marković, D. Lončarević, J. Dostanić, S.P. Ahrenkiel, J.M. Nedeljković, Antibacterial ability of supported silver nanoparticles by functionalized hydroxyapatite with 5-aminosalicylic acid, Vacuum, 148 (2018) 62-68.

[82] A. Reizabal, S. Gonçalves, R. Brito-Pereira, P. Costa, C.M. Costa, L. Pérez-Álvarez, J.L. Vilas-Vilela, S. Lanceros-Méndez, Optimized silk fibroin piezoresistive nanocomposites for pressure sensing applications based on natural polymers, Nanoscale Advances, 1 (2019) 2284-2292.

[83] H. Salazar, P.M. Martins, M.M. Fernandes, P. Costa, S. Ferdov, G. Botelho, S. Lanceros-Mendez, Reusable nanocomposite-filters for arsenite and arsenate dual real effluents remediation in an up-scaled membrane reactor, Journal of Hazardous Materials, 440 (2022) 129756.

[84] H. Yang, S. Yang, J. Kong, A. Dong, S. Yu, Obtaining information about protein secondary structures in aqueous solution using Fourier transform IR spectroscopy, Nature Protocols, 10 (2015) 382-396.

[85] P. Martins, A.C. Lopes, S. Lanceros-Mendez, Electroactive phases of poly(vinylidene fluoride): Determination, processing and applications, Progress in Polymer Science, 39 (2014) 683-706.

[86] R.E. Sousa, J. Nunes-Pereira, J.C.C. Ferreira, C.M. Costa, A.V. Machado, M.M. Silva, S. Lanceros-Mendez, Microstructural variations of poly(vinylidene fluoride co-hexafluoropropylene) and their influence on the thermal, dielectric and piezoelectric properties, Polymer Testing, 40 (2014) 245-255.

[87] S.S. Abdullahi, S. Güner, Y. Musa, B.I. Adamu, M.I. Abdulhamid, Sımple method for the determınatıon of band gap of a nanopowdered sample usıng Kubelka Munk theory, NAMP J, 35 (2016) 241-246.

[88] D.K. Božanić, G.A. Garcia, L. Nahon, D. Sredojević, V. Lazić, I. Vukoje, S.P. Ahrenkiel, V. Djoković, Ž. Šljivančanin, J.M. Nedeljković, Interfacial Charge Transfer Transitions in Colloidal TiO2 Nanoparticles Functionalized with Salicylic acid and 5-Aminosalicylic acid: A Comparative Photoelectron Spectroscopy and DFT Study, Journal of Physical Chemistry C, 123 (2019) 29057-29066.

[89] D. A.O, A. Olalekan, A. Olatunya, A.O. Dada, Langmuir, Freundlich, Temkin and Dubinin–Radushkevich Isotherms Studies of Equilibrium Sorption of Zn 2+ Unto Phosphoric Acid Modified Rice Husk, J. Appl. Chem., 3 (2012) 38-45.

[90] R. Brito-Pereira, D. Correia, C. Ribeiro, A. Francesko, I. Etxebarria, L. Pérez-Álvarez, J. Vilas, P. Martins, S. Lanceros-Mendez, Silk fibroin-magnetic hybrid composite electrospun fibers for tissue engineering applications, Composites Part B: Engineering, 141 (2018) 70-75.

[91] E.O. Carvalho, M. Rincón-Iglesias, R. Brito-Pereira, E. Lizundia, M.M. Fernandes, S. Lanceros-Mendez, Designing antimicrobial biomembranes via clustering amino-modified cellulose nanocrystals on silk fibroin β-sheets, International Journal of Biological Macromolecules, 242 (2023) 125049.

[92] P.M. Martins, R. Miranda, J. Marques, C.J. Tavares, G. Botelho, S. Lanceros-Mendez, Comparative efficiency of TiO2 nanoparticles in suspension vs. immobilization into P(VDF–TrFE) porous membranes, RSC Advances, 6 (2016) 12708-12716.

[93] A. Reizabal, N. Castro, N. Pereira, C.M. Costa, L. Pérez, J.L. Vilas-Vilela, S. Lanceros-Méndez, Silk Fibroin Nanocomposites with Indium Tin Oxide toward Sustainable Capacitive Touch Sensing Applications, ACS Applied Electronic Materials, 4 (2022) 1901-1909.

[94] Z. Shao, F. Vollrath, J. Sirichaisit, R.J. Young, Analysis of spider silk in native and supercontracted states using Raman spectroscopy, Polymer, 40 (1999) 2493-2500.

[95] P. Martins, C. Caparros, R. Gonçalves, P. Martins, M. Benelmekki, G. Botelho, S. Lanceros-Mendez, Role of nanoparticle surface charge on the nucleation of the electroactive β-poly (vinylidene fluoride) nanocomposites for sensor and actuator applications, The Journal of Physical Chemistry C, 116 (2012) 15790-15794.

[96] A. Reizabal, R. Brito-Pereira, M.M. Fernandes, N. Castro, V. Correia, C. Ribeiro, C.M. Costa, L. Perez, J.L. Vilas, S. Lanceros-Méndez, Silk fibroin magnetoactive nanocomposite films and membranes for dynamic bone tissue engineering strategies, Materialia, 12 (2020) 100709.

[97] M.K. Sah, K. Pramanik, Preparation, characterization and in vitro study of biocompatible fibroin hydrogel, African Journal of Biotechnology, 10 (2011) 7878-7892.

[98] Y. Kim, B. Park, Photo-persistent effect-induced energy band bending at the TiO2/Ag nanoparticle surface plasmonic interface, Materials Letters, 316 (2022) 132001.

[99] C.H. Nguyen, T.T.V. Tran, M.L. Tran, R.-S. Juang, Facile synthesis of reusable Ag/TiO2 composites for efficient removal of antibiotic oxytetracycline under UV and solar light irradiation, Journal of the Taiwan Institute of Chemical Engineers, 145 (2023) 104825.

[100] J.-S. Choi, S. Kim, Y. Choi, K.B. Kim, H.-J. Kim, T.J. Park, Y.M. Park, Ag-decorated CuO NW@TiO2 heterojunction thin film for improved visible light photocatalysis, Surfaces and Interfaces, 34 (2022) 102380.

[101] M.M. Momeni, M. Mirhosseini, N. Mohammadi, Efficient photo catalytic degradation of methyl orange over Ag–CuO nanostructures grown on copper foil under visible light irradiation, Journal of Materials Science: Materials in Electronics, 27 (2016) 6542-6551.

[102] L. Lin, H. Wang, W. Jiang, A.R. Mkaouar, P. Xu, Comparison study on photocatalytic oxidation of pharmaceuticals by TiO2-Fe and TiO2-reduced graphene oxide nanocomposites immobilized on optical fibers, Journal of Hazardous Materials, 333 (2017) 162 —168.

[103] S. Teixeira, B. Magalhães, P. M. Martins, K. Kühn, L. Soler, S. Lanceros-Méndez and G. Cuniberti, Reusable Photocatalytic Optical Fibers for Underground, Deep-Sea, and Turbid Water Remediation, Global Challenges, 2 (2018) 1700124.

[104] N. Malesic-Eleftheriadou, E.N. Evgenidou, G.Z. Kyzas, D.N. Bikiaris, D.A. Lambropoulou, Removal of antibiotics in aqueous media by using new synthesized bio-based poly(ethylene terephthalate)-TiO2 photocatalysts, Chemosphere, 234 (2019) 746-755.

[105] A.K. Yontar, S. Avcioğlu, S. Çevik, Nature-based nanocomposites for adsorption and visible light photocatalytic degradation of methylene blue dye, Journal of Cleaner Production, 380 (2022) 135070.

[106] N. Ali, Awais, T. Kamal, M. Ul-Islam, A. Khan, S.J. Shah, A. Zada, Chitosan-coated cotton cloth supported copper nanoparticles for toxic dye reduction, International Journal of Biological Macromolecules, 111 (2018) 832-838.

[107] S. Elbakry, M.E.A. Ali, M. Abouelfadl, N.A. Badway, K.M.M. Salam, Photocatalytic degradation of organic compounds by TFC membranes functionalized with Ag/rGO nanocomposites, Journal of Photochemistry and Photobiology A: Chemistry, 430 (2022) 113957.

[108] M.M. Momeni, Y. Ghayeb,S. Gheibee, Silver nanoparticles decorated titanium dioxide-tungsten trioxide nanotube films with enhanced visible light photo catalytic activity, Ceramics International, 43 (2017) 564 —570.

[109] H. Zhou, X. Wang, T. Wang, J. Zeng, Z. Yuan, J. Jian, Z. Zhou, L. Zeng, H. Yang, In situ decoration of Ag@AgCl nanoparticles on polyurethane/silk fibroin composite porous films for photocatalytic and antibacterial applications, European Polymer Journal, 118 (2019) 153-162.

[110] S. Teixeira, P. Martins, S. Lanceros-Méndez, K. Kühn, G. Cuniberti, Reusability of photocatalytic TiO2 and ZnO nanoparticles immobilized in poly (vinylidene difluoride)-co-trifluoroethylene, Applied surface science, 384 (2016) 497-504.

[111] T. Navab-Daneshmand, M.N. Friedrich, M. Gächter, M.C. Montealegre, L.S. Mlambo, T. Nhiwatiwa, H.-J. Mosler, T.R. Julian, Escherichia coli contamination across multiple environmental compartments (soil, hands, drinking water, and handwashing water) in urban Harare: correlations and risk factors, The American journal of tropical medicine and hygiene, 98 (2018) 803.

[112] W. Sim, R.T. Barnard, M.A.T. Blaskovich, Z.M. Ziora, Antimicrobial Silver in Medicinal and Consumer Applications: A Patent Review of the Past Decade (2007–2017), Antibiotics, 7 (2018) 93.

[113] C.N. Paiva, M.T. Bozza, Are reactive oxygen species always detrimental to pathogens?, Antioxidants & redox signaling, 20 (2014) 1000-1037.

[1143] M.M. Fernandes, E.O. Carvalho, D.M. Correia, J.M. Esperança, J. Padrão, K. Ivanova, J. Hoyo, T. Tzanov, S. Lanceros-Mendez, Ionic liquids as biocompatible antibacterial agents: a case study on structure-related bioactivity on Escherichia coli, ACS applied bio materials, 5 (2022) 5181-5189.

[115] T.D. Tavares, J.C. Antunes, J. Padrão, A.I. Ribeiro, A. Zille, M.T.P. Amorim, F. Ferreira, H.P. Felgueiras, Activity of specialized biomolecules against gram-positive and gram-negative bacteria, Antibiotics, 9 (2020) 314.

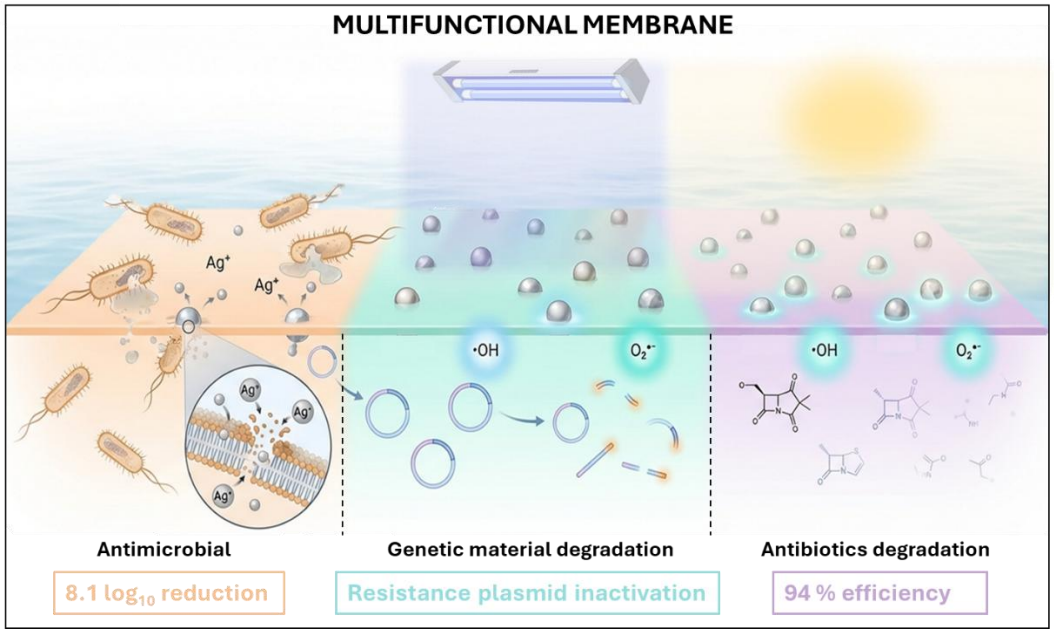
[116] T.A. Seregina, I.Y. Petrushanko, R.S. Shakulov, P.I. Zaripov, A.A. Makarov, V.A. Mitkevich, A.S. Mironov, The inactivation of LPS biosynthesis genes in E. coli cells leads to oxidative stress, Cells, 11 (2022) 2667.

CHAPTER 4

MULTIFUNCTIONAL PVDF-HFP MEMBRANES FOR SIMULTANEOUS REMOVAL OF ANTIBIOTICS, ARB, AND ARGS

This chapter builds on the previous chapter's foundation by exploring the development of multifunctional PVDF-HFP membranes designed to address both chemical and biological contaminants simultaneously. By optimizing the amount of silver (Ag) and the concentration of fillers in the polymer matrix, the membranes' multifunctionality can be ensured while remaining stable, reusable, and effective for challenging water treatment applications. This stage marks the shift from basic photocatalytic systems to more advanced, robust multifunctional membranes.

This chapter is based on the following publication: **Joana M. Queirós**, Ana Rita Bragança, Noelia González-Ballesteros, H. Salazar, Sónia A.C. Carabineiro, Carlos Tavares, Raúl Machado, Alberto Dias, S. Lanceros-Mendez, P.M. Martins, Unlocking multifunctional water decontamination: Antibiotics, Antibiotic-Resistant Bacteria and Antibiotic-Resistance Genes (*Under submission*)



4.1 Introduction

The widespread use of antibiotics in human, veterinary, and agricultural activities has significantly contributed to their dissemination into aquatic environments [1]. A significant percentage of these compounds is not fully absorbed or metabolised by living organisms. It is instead excreted through faeces and urine, with estimates indicating that approximately 80-90% of the administered doses are released into the environment [2-6]. For instance, sulfamethoxazole (SMX) and cefalexin have been found in herbivorous carp in aquaculture environments [7-9], and several veterinary antibiotics and their main metabolites have been detected in fish and mussels from different aquatic environments, posing a risk to public health [10].

The environmental persistence of these compounds is intensified by the continuous rise in global antibiotic consumption, which increased by 16.3% between 2016 and 2023, particularly in middle-income countries [11, 12]. Projections suggest a further increase by 2030, the number could rise by approximately 52.3% [13]. Combined with the limited effectiveness of wastewater treatment plants (WWTP), this trend has led to widespread antibiotic contamination across various water matrices, including drinking water sources [14].

The continuous presence of these persistent contaminants imposes selective pressure on microbial communities, promoting a favourable environment for the proliferation of antibiotic-resistant bacteria (ARB) and the dissemination of antibiotic-resistance genes (ARGs) [15], also considered contaminants of emerging concern [16]. Bacteria such as *Escherichia coli*, *Pseudomonas aeruginosa*, *Klebsiella*

pneumoniae, and *Enterococcus faecalis* have been highlighted in the literature as the most prevalent bacterial species commonly found in WWTPs, spreading ARGs, which contain antibiotic resistance information, commonly *sul1*, *tetM*, *ampC*, and *ermB* genes, equally frequent in urban and drinking water treatment plants [17-19]. Additionally, the presence of this genetic material can facilitate the transfer of genes between microbial populations via HGT, including pathogenic and non-pathogenic bacterial strains, thereby accelerating the evolution of multidrug-resistant organisms [1], such as Methicillin-resistant *S. aureus* (MRSA) [20] and extended-spectrum beta-lactamase (ESBL) producing *E. coli* [21].

Recognising the urgency of this issue, the World Health Organisation (WHO) has identified ARBs and ARGs as one of the most significant threats to global public health in the 21st century [22]. However, conventional water treatment technologies have been largely ineffective at removing these emerging contaminants, underlining the need for advanced, integrated treatment strategies that address both chemical and biological contaminants [23].

In this context, advanced oxidation processes (AOPs) have attracted increasing attention as alternatives due to their ability to degrade persistent, non-biodegradable organic pollutants [24]. Among the different AOPs, photocatalysis has emerged as a promising technology due to its high efficiency, low energy demand, and environmental sustainability. The process relies on the activation of a semiconductor material (e.g., titanium dioxide) by light irradiation in the ultraviolet (UV) or visible spectrum, which promotes the generation of reactive oxygen species (ROS) capable of oxidising and mineralising a wide variety of organic pollutants [25, 26]. Beyond degrading chemical compounds, several studies demonstrate that photocatalysis can also inactivate resistant bacteria and degrade genetic material associated with antibiotic resistance [18, 27]. For example, some studies have investigated photocatalysis with TiO_2 and ZnO [28] or even carbon-based materials [29, 30], where a reduction in both ARB and ARG associated with resistance was observed, effectively limiting the spread of antibiotic resistance. The efficiency of these photocatalytic processes is dependent upon the properties of the photocatalyst employed, influencing both chemical degradation and microbial inactivation.

Among the most widely used semiconductors is TiO_2 [31], which has been extensively studied due to its chemical stability, high photocatalytic activity, and low cost [32]. However, its application is limited by the need for high-energy UV radiation for activation, which reduces its efficiency under natural sunlight (only 3-5% of the sun's radiation is UV) [33]. To overcome this limitation, TiO_2 can be functionalised with noble metals, such as gold (Au) [34], platinum (Pt) [35], silver (Ag) [36], or copper (Cu) [37], enabling the absorption of visible light by improving the separation of photoinduced charges and reducing the recombination of electron-hole pairs [38]. The use of silver not only extends the catalysts absorption range

to the visible radiation range but also endows the inactivation of bacteria (antimicrobial) [25, 36]. Furthermore, there has been growing attention to the adoption of green synthesis methodologies for the functionalisation of nanoparticles (NPs), to minimise the use of toxic reagents and thereby reduce environmental impact [39, 40]. To fully leverage these advantages, it is essential to consider the implementation and management of these photocatalysts within scalable environments.

One challenge in the practical implementation of photocatalytic NPs is the recovery process following treatment. When used in suspension, these NPs require an additional separation step, increasing the overall system's complexity and cost. The immobilisation of NPs on a support has been proposed as a practical solution, enabling reuse and minimising their release into the aquatic environment [41]. To attain this, the ideal support should provide structural stability while ensuring a porous morphology that allows water percolation and maximises the contact between pollutants and photocatalysts' active sites [42, 43]. At the same time, the material must be compatible with NPs incorporation to promote a homogeneous dispersion and ensure balanced efficiency [44]. Polymeric substrates have emerged as a viable solution to address these requirements while conferring additional advantages, such as low cost and a wide range of processing options, making them attractive candidates as support matrices for photocatalysts [45]

Within this class of materials, polyvinylidene fluoride (PVDF) and its copolymers have been the focus of extensive research as matrices for the immobilisation of NPs, owing to their high thermal and chemical resistance, mechanical stability, and durability under adverse environmental conditions [46, 47]. PVDF-HFP, widely studied for aquatic remediation, can be processed through multiple manufacturing routes, including phase inversion [48], electrospinning [25], and additive manufacturing [49].

Preventing fouling of these materials by microorganisms found in aquatic environments is an important consideration, as it significantly limits operational stability [50]. To extend the lifecycle of these materials, incorporating Ag NPs not only enhances photocatalytic activity but also provides short- and long-term antimicrobial properties, thereby preventing biofilm formation on the membrane surface [51, 52].

In this context, the present study proposes the development of a multifunctional material based on a polyvinylidene fluoride-co-trifluoroethylene (PVDF-HFP) polymeric matrix incorporating TiO_2 NPs functionalised with Ag through a green synthesis methodology. The composite membranes were evaluated for their photocatalytic performance in degrading model antibiotics, their antimicrobial activity by inhibiting bacterial proliferation and long-term surface colonisation, and their capacity to degrade ARG. This strategy aims to contribute to the development of sustainable, efficient technologies for the remediation of aquatic environments contaminated by multiple contaminants.

4.2 Materials and methods

4.2.1 Reagents

Quercetin hydrate (≥95%) and silver nitrate (≥99.99%) were purchased from Sigma-Aldrich. Titanium dioxide nanoparticles (P25 TiO_2) were supplied by Evonik (Evonik Corporation, USA). Quercetin hydrate 95% and silver nitrate were purchased from Sigma Aldrich. Sodium hydroxide (NaOH, 98.0–100.5%) and glacial acetic acid (CH_3COOH, 99.7%) were purchased from Panreac. PVDF-HFP was purchased from Solvay, and N,N-dimethylformamide (DMF) from Merck. Ciprofloxacin (formula) and Trimethoprim were purchased by Thermo Fisher Scientific (Kandel) GmbH. All chemicals were used as received without additional purification, and Milli-Q water was employed in all experimental procedures.

4.2.2 Synthesis of AgNPs with Quercetin

Control experiments were first conducted to verify the ability of quercetin to reduce silver ions and promote the formation of AgNPs in the absence of TiO_2. For this purpose, a 0.05% (w/v) stock solution of quercetin was prepared in a basic medium and diluted to 5 mL with ultrapure water under continuous stirring at room temperature (RT), yielding final quercetin concentration of 20 μg/mL. A 0.05% (w/v) $AgNO_3$ solution was then added in appropriate volumes to reach final silver concentrations of 25 and 50 μg/mL. The reactions were carried out at RT and monitored by UV-Vis spectroscopy, while the resulting nanoparticles were further examined by TEM. These preliminary assays confirmed that quercetin alone could mediate AgNP synthesis, supporting its subsequent use in combination with TiO_2.

4.2.3 Synthesis of Ag-TiO_2

Ag-TiO_2 nanocomposites were synthesised as illustrated in Figure 4.1. Typically, 200 mg of TiO_2 were dispersed in 40 mL of ultrapure water and sonicated (ULTRASONS-HD, JP Selecta, Spain) for 30 min at RT. Subsequently, different volumes of a 0.05% (w/v) $AgNO_3$ solution were added to obtain nominal silver loadings of 0.2, 0.5, and 1.0 wt.%. The suspensions were stirred for 15 min to ensure homogeneous ion distribution before the addition of quercetin (final concentration 20 μg/mL). The mixtures were left to react at RT until a colour change from pale yellow to brown confirmed nanoparticle formation. The products were washed twice to remove excess quercetin by centrifugation (Sigma 4-16KS, Sigma, Germany) at 14,000 rpm for 30 min, followed by redispersion in ultrapure water under sonication. Finally, the samples were dried overnight at 80 °C in an oven (Digitronic, JP Selecta, Spain) and denoted as X% Ag-TiO_2, where X corresponds to the nominal silver loading.

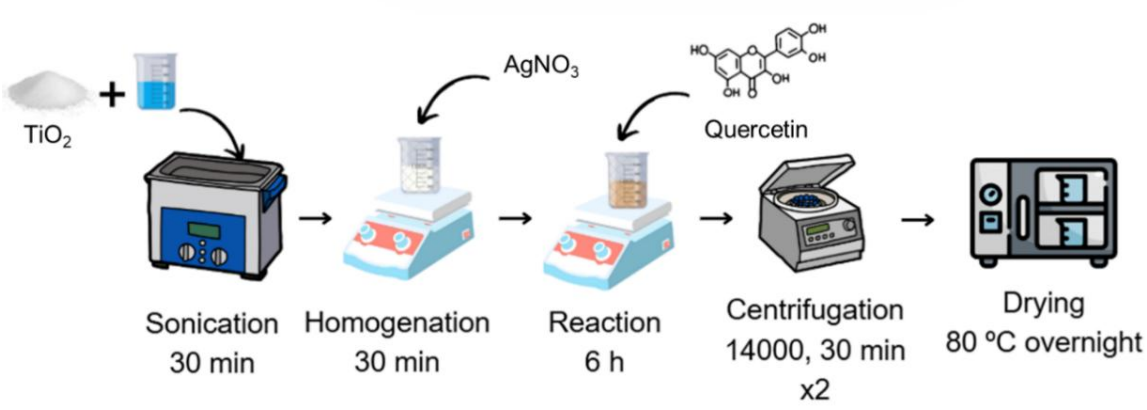


Figure 4.1. Protocol of the synthesis of Ag-TiO_2.

4.2.4 Nanoparticles characterisation

The morphology of the Ag-TiO_2 nanoparticles was performed using TEM following the methodologies described in Chapter 2 (Section 2.2.3). Additionally, high-resolution transmission electron microscopy (HRTEM) and scanning transmission electron microscopy (STEM) analyses were performed on a JEOL JEM2010F TEM at 200 kV, allowing a detailed evaluation of the crystalline structure and morphology of the particles. The composition and distribution of silver were determined by elemental mapping, and the composition was obtained via energy-dispersive X-ray (EDS) (Oxford Inca Energy 200) and processed with Digital Micrograph and INCA Energy software.

The crystallinity of the nanoparticles was analysed by XRD and the chemical composition by FTIR, as described above (Section 2.2.3). For optical characterisation, reflectance was recorded by DRS and converted to absorbance by the Kubelka–Munk function (Eq. 2.1 and 2.2). The hydrodynamic diameter and zeta potential (ζ) were determined by DLS under the same conditions presented in Chapter 2.

4.2.5 Nanoparticles Photocatalytic Performance

The photocatalytic performance of the synthesised Ag-TiO_2 samples was investigated for the degradation of the two model antibiotics – CIP at 5 mg/L and TMP at 10 mg/L– under visible light irradiation, following the methodology described in Chapter 2 (Section 2.2.3.2) [39, 40]. Control experiments were conducted in the absence of the catalyst to evaluate the contribution of photolysis.

The experimental tests were conducted in suspension, maintaining conditions similar to those previously described.

Antibiotic concentrations in the supernatant were monitored by recording UV–Vis spectra in the 230–350 nm range with quantification performed at the characteristic absorption wavelengths of CIP (λ= 277 nm) and TMP (λ= 230 nm). The kinetic analysis was performed using the pseudo-first-order model, according to the Langmuir-Hinshelwood approach (Eq. 2.1 and Eq. 2.2).

4.2.6 Nanocomposite Membrane Production

The Ag-TiO_2/PVDF-HFP and TiO_2/PVDF-HFP nanocomposite membranes were prepared according to the immobilisation and membrane formation procedure described in Chapter 2 (Section 2.2.4), based on guidelines previously reported in the literature. [54].

In this study, the concentration of immobilised nanoparticles was set to 20 wt.% to improve antibacterial performance, since previous studies showed that 10 wt.% provided limited bacterial reduction while preserving membrane structural stability [25, 36].

The nanocomposite membranes were obtained by TIPS, with the polymer solution spread to a controlled thickness of 750 μm, while the remaining experimental conditions were maintained as described above.

4.2.7 Composite Membrane Characterisation

The morphological, structural, thermal, and surface characterisation of the nanocomposite membranes was performed according to the methodologies described in Chapter 2 (Section 2.2.5).

The morphology of the membranes was assessed by SEM, while the porous structure was characterised by MIP. The chemical composition and vibrational structure of PVDF-HFP, TiO_2/PVDF-HFP, and Ag-TiO_2/PVDF-HFP were analysed by FTIR spectroscopy, and the relative fraction of the β-phase of the polymer was determined from the spectra obtained, according to Eq. 2.3.

The thermal properties of the pristine PVDF-HFP and the nanocomposite membranes were evaluated by DSC, and the degree of crystallinity (X_c) was calculated based on Eq. 2.4, using the values of melting enthalpies of α and β phases reported in the literature.

The surface wettability was assessed from CAs measurements, following the procedure described above, with the mean value and corresponding standard deviation calculated from independent measurements.

4.2.8 Evaluation of the Antibacterial Activity

To evaluate the antibacterial activity of the produced composites, *Escherichia coli* ATCC 8739 (*E. coli*) and *Staphylococcus aureus* ATCC 6538 (*S. aureus*) were used as representatives of Gram-negative and Gram-positive bacteria, respectively. These strains were selected to assess the antibacterial activity of the samples, as they are among the most common pathogens in the aquatic environment.

Shake-flask method: For each strain, a single colony from the corresponding stock culture was incubated overnight at 37 °C and 200 rpm in NB. The bacterial activity was assessed using a modified version of the standard shake-flask method (ASTM-E2149–01), a method that enabled quantitative evaluation by determining the reduction in the number of bacterial colonies. The results are expressed as colony-forming units per millilitre of buffer solution (CFU mL^{-1}). Both previously inoculated bacterial cultures were centrifuged at 5000 rpm for 5 min and washed twice with a 0.9% w/v NaCl solution. The OD was measured at 600 nm and adjusted to an optimal OD of 0.1 ± 0.01 using the saline solution. This resulted in a working inoculum of approximately 7.3×10^7 CFU/mL for *E. coli* and 6.1×10^9 CFU/mL for *S. aureus*.

The composite membranes (area = 1.75 cm^2), sterilised by UVC light, were then placed in contact in a 24-well tissue culture plate with 500 µL of a bacterial suspension at 37 °C and 200 rpm for 2h. The obtained suspensions were subjected to a series of dilutions with 0.9% w/v NaCl buffer solution. The suspensions were placed on an agar plate and incubated at 37 °C for 24h to quantify the surviving bacterial population. A schematic representation of the experimental procedure is shown in Figure 4.2.

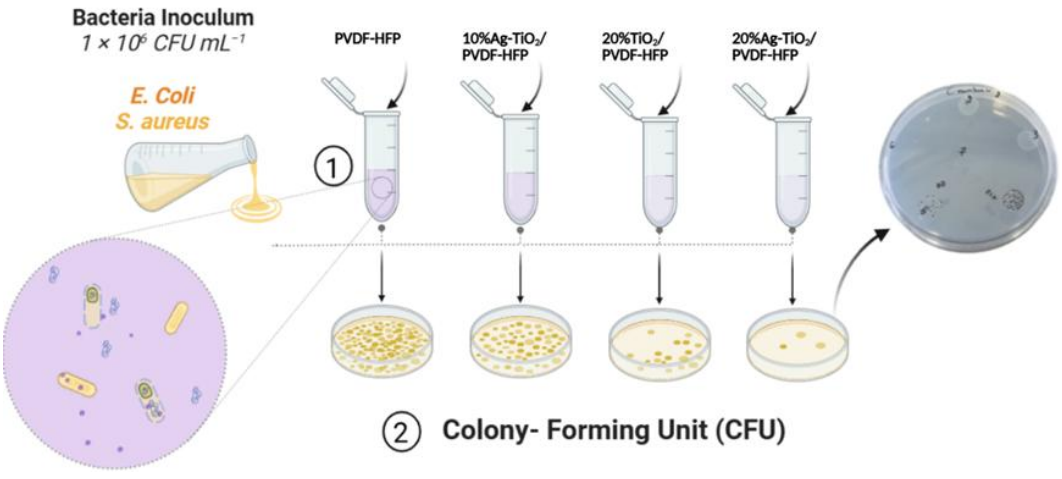


Figure 4.2. Schematic illustration of antimicrobial activity assessment. Sterilised PVDF-HFP-based membranes (pristine and nanocomposites) were 1) placed in contact with *E. coli and* S. aureus

suspensions under controlled conditions, followed by serial dilution, plating, and 2) quantification of viable bacteria by CFU counting.

Antibacterial activity is reported as a percentage of bacterial logarithmic reduction, determined by the ratio of surviving bacteria after contact with the material to the initial bacterial count, according to the following Eq. 4.1:

$$Bacterial\ reduction\ (\%) = \frac{(A-B)}{B} \times 100 \qquad \text{Eq. 4.1}$$

where *A* and *B* are the average number of bacteria before and after contact with the material, respectively, the results were further expressed as $\log_{10}$ reduction by calculating the $\log_{10}$ of bacterial reduction.

Crystal violet assay for biofilm formation: Each strain was incubated in tryptic soy broth (TSB) overnight at 37 °C and 200 rpm. The OD of both bacterial cultures was adjusted to 0.05 (≈ 5×10^6 CFU/mL) with tryptic soy broth (TBS), and 500 µL of a bacterial suspension was placed in contact with composite membranes (area =1.75 cm^2) in a 24-well tissue culture plate for 24 hours at 37 °C under static conditions to allow bacteria to form biofilms.

Following the 24h period, non-adherent bacterial cells were removed through a series of three washes with distilled water. After the biofilm washing process, the 24-well plate was placed in an oven at 60 °C for 1h to promote biofilm adhesion to the material surface. A 0.1 w/v% crystal violet solution was added and left in contact with the samples for approximately 10 minutes. The excess was then removed by rinsing the samples with distilled water and drying them at 60 °C. To dissolve the retained crystal violet, a 30% (v/v) acetic acid solution was added, and the plate was left at room temperature for 15 minutes. Subsequently, 200 µL of the solution from each well was transferred to a 96-well microplate, and the absorbance was measured at 595 nm. The quantity of crystal violet retained is directly proportional to the total biomass present on the material.

4.2.9 Photocatalytic Degradation of ARG

Preparation and transformation of Competent Escherichia coli Cells with plasmid DNA: Competent *Escherichia coli* XL1-Blue cells were prepared using the rubidium chloride protocol described by Hanahan (1983) [55]. Chemically competent E. coli cells were transformed with an empty pET-25b(+) vector,

containing an ampicillin resistance gene (AmpR). The transformation was performed using an adapted protocol from Hanahan (1983) [55]. Briefly, 1 µL of plasmid DNA (100 ng) was added to 100 µL of competent cells and incubated on ice for 30 minutes. Cells were subjected to a 1-minute heat shock at 42 °C, followed by 10 minutes on ice. Subsequently, pre-warmed Luria Broth (LB) medium was added to a final volume of 1 mL. The suspension was incubated at 37 °C for 1 hour with shaking at 200 rpm. A volume of 100 µL of the culture was plated on LB agar supplemented with 100 µg/mL ampicillin and incubated overnight at 37 °C. The grown-transformed colonies were inoculated into fresh solid medium.

Plasmid DNA Extraction: Transformed *E. coli* cells were inoculated into liquid LB medium supplemented with 100 µg/mL of ampicillin, and the plasmid DNA was extracted using the NZYMiniprep Kit (NZYTech), according to the manufacturer's instructions. DNA was eluted in nuclease-free bidistilled water and quantified using a NanoDrop spectrophotometer (Thermo Scientific).

Photocatalytic experiments: Plasmid DNA was exposed to UVA radiation to characterise the degradation profile induced by radiation, aiming to evaluate its specific and isolated effects on DNA integrity. The degradation caused by UVA was conducted within a photoreactor that was equipped with twelve PHILIPS TL 8 W UVA lamps (λ=365 nm) at 28 cm from the solution. This resulted in an irradiance of 6.8 W/m^2. The experimental procedures were conducted in an orbital shaker operating at 100 rpm.

To evaluate the degradation capacity of membrane-based assays, 1 mL of plasmid DNA at 25 ng/µL was added to sterile 12-well microplates containing the 20%Ag-TiO_2/PVDF-HFP and 20%TiO_2/PVDF-HFP nanocomposite membranes. The PVDF-HFP membrane was used as a negative control. All the membranes were exposed to 1.5, 3, 6, and 10 hours of UVA radiation.

For all the aforementioned assays, DNA integrity was assessed by electrophoresis on a 1% (w/v) agarose gel in 1x Tris-acetate-EDTA (TAE) buffer at 90 V for 35 minutes. DNA quantification was performed using a NanoDrop spectrophotometer (Thermo Scientific). All photocatalytic experiments were conducted in triplicate for each condition and repeated independently three times (n = 3).

Transformation of E. coli with Treated Plasmid DNA: Following photocatalytic assays, competent *E. coli* XL1-Blue cells were transformed with 5 µL of the treated plasmid DNA, exposed to 6 and 10 hours, for each tested membrane condition (PVDF-HFP, TiO_2/PVDF-HFP and Ag-TiO_2/PVDF-HFP), following the same transformation protocol described above. Plasmid DNA exposed to 6 and 10 hours of UV_A radiation, and untreated DNA was used as a negative control, corresponding to 100% transformation efficiency. The assays were performed in triplicate. CFUs were quantified using ImageJ software (National Institutes of Health, USA).

Data analysis: All experiments were performed in triplicate, and the results are presented as mean ± standard deviation (SD). Statistical analyses were performed using GraphPad Prism 8.0 software. For antimicrobial assays, differences among treatments were evaluated using a one-way ANOVA followed by Tukey's multiple-comparison test to identify significant differences among the tested systems. For plasmid DNA degradation assays, a two-way ANOVA followed by Tukey's post hoc test was applied to evaluate the influence of system type and irradiation time on degradation efficiency. In all analyses, differences were considered statistically significant for $p < 0.05$.

4.2.10 Photocatalytic Degradation of Antibiotic

Following preliminary suspension tests under visible radiation, the NPs exhibiting the most promising composition regarding antibiotic degradation were immobilised on PVDF-HFP membranes. The composite membranes (surface area = 15 cm^2) were placed with tape in a 100 ml beaker wall to ensure uniform irradiation exposure across the samples.

Afterwards, the composite membranes were exposed to UV and visible light. UV-induced degradation was conducted within the same photoreactor described in Section 4.2.9 (Photocatalytic experiments). The same irradiation conditions described in Section 4.2.5 were used to degrade the sample under visible light. The membrane degradation tests were extended to 600 min. Membrane stability and reusability were evaluated over three consecutive degradation cycles, with intermediate washes using ultrapure water.

Antibiotic degradation was monitored according to the methodology outlined in Section 2.2.3.2, and the resulting kinetic data were fitted to a pseudo-first-order model.

4.3 Results and Discussion

4.3.1 Synthesis of AgNPs using the flavonoid Quercetin

Quercetin, a naturally occurring flavonoid, has been identified as a promising agent for the synthesis of metal nanoparticles [56]. Different studies have reported the synthesis of silver nanoparticles using quercetin as a reducing and stabilising agent, obtaining different size distributions of AgNPs based on the conditions of the synthesis, such as solvents, pH or temperature [57-59]. Before the production of AgNPs, it was assessed whether small particles could be synthesised under mild reaction conditions, such as in an aqueous environment at room temperature. Figure 4.3 shows that small particles were obtained, with a mean size of 11.6 nm.

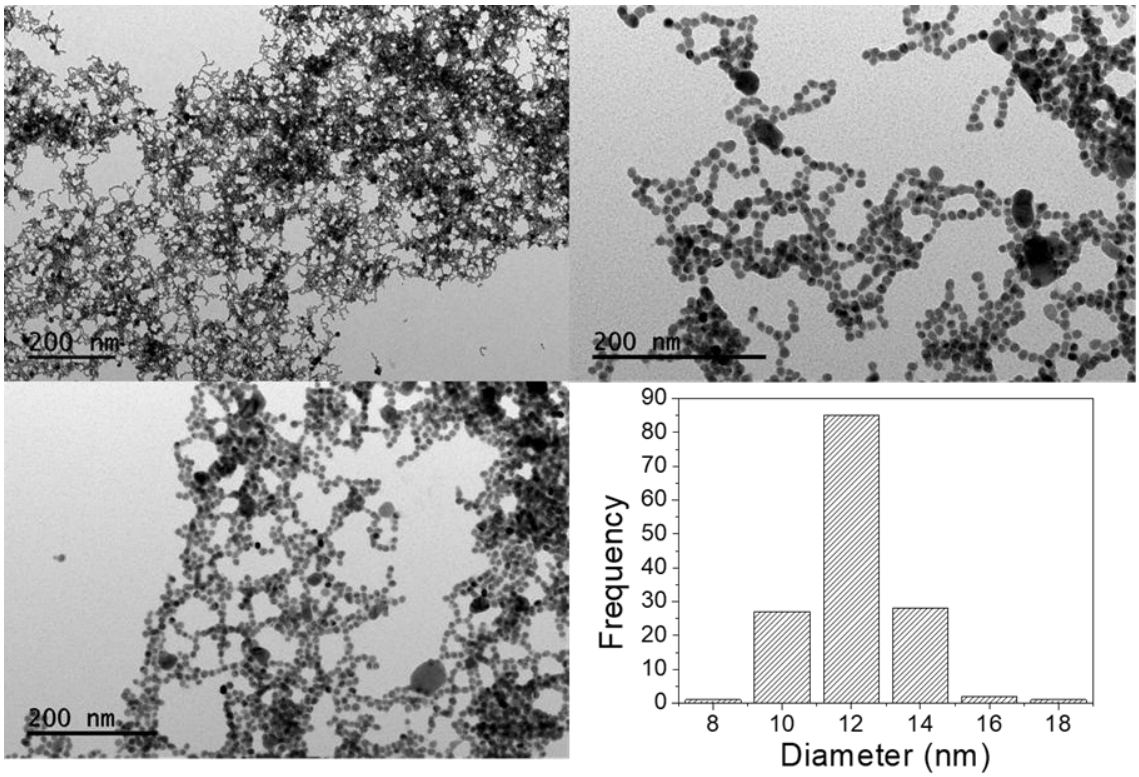


Figure 4.3. TEM images of AgNPs synthesised using the flavonoid quercetin and their size distribution histogram.

The structure of quercetin, multiple hydroxyl groups on its aromatic rings, s strong redox activity. These hydroxyl moieties can donate electrons, thereby reducing silver ions (Ag^{+}) to metallic silver (Ag^{0}) and enabling the nucleation and growth of AgNPs. During this process, hydroxyl groups may undergo oxidation to form semiquinone or quinone-like structures, which stabilise through resonance. Although hydroxyls at the 3′,4′-dihydroxy configuration in the B ring and the 3-hydroxy-4-keto group in the C ring are often proposed as the most reactive sites, the precise contribution of each group remains unclear [58, 60-62]. This uncertainty suggests that multiple hydroxyl positions may cooperate in the overall reduction mechanism. Figure 4.4 presents a proposed mechanism for the reaction synthesis using quercetin.

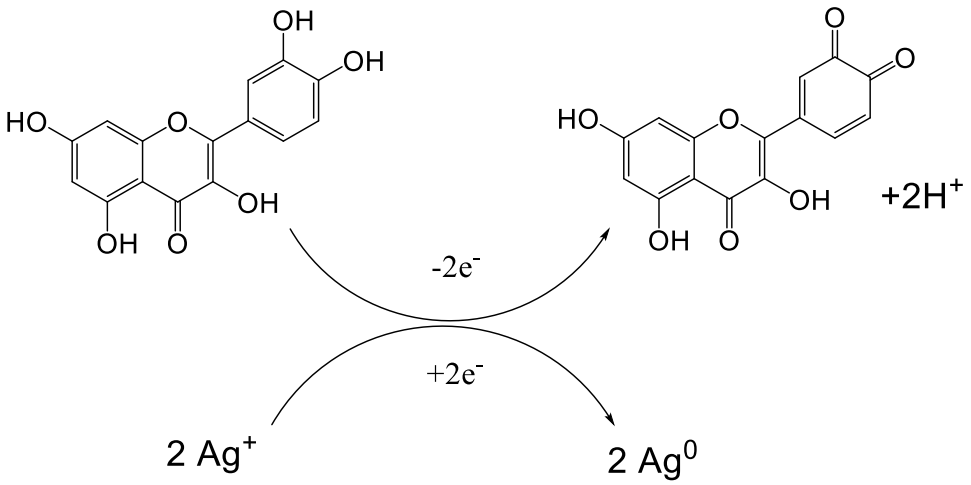


Figure 4.4. Proposed mechanism of the reaction for the synthesis of AgNPs using quercetin.

4.3.2 Synthesis and characterisation of Ag-TiO_2

Ag-TiO_2 nanocomposites were prepared by incorporating several amounts of Ag into an aqueous TiO_2 suspension (0.2, 0.5 and 1.0 wt.%). Upon the addition of quercetin at room temperature, the dispersion underwent a visible colour change from pale yellow to brown. After purification and drying, powders with different brownish tones were obtained, as illustrated in Figure 4.5.

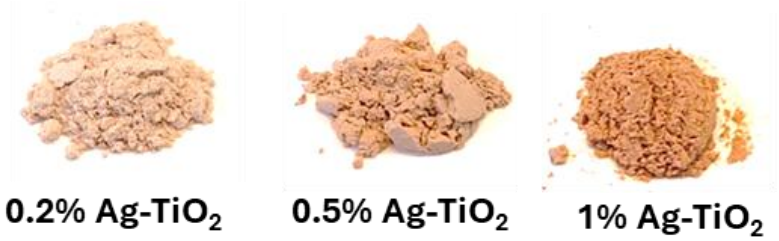


Figure 4.5. Synthesised Ag-TiO_2 nanocomposite.

Figure 4.6 shows the TEM images of pristine TiO_2 and Ag-TiO_2 nanocomposites with different silver loadings. In conventional TEM, the contrast does not allow a clear distinction between Ag nanoparticles and the TiO_2 support, especially at low Ag concentrations, both particles have very similar sizes. Consequently, the micrographs of samples appear quite comparable, and no evident trend regarding the presence or distribution of silver can be established. This limitation is related to the reduced Ag content and its high dispersion within the oxide matrix, which hinders visualisation in TEM mode. For this reason, all detailed microstructural and compositional analyses are provided in the Supporting Information. Specifically, STEM imaging with compositional contrast was applied (Figure S4a), in which the higher

atomic number of Ag yields brighter features than Ti. The presence of silver was further confirmed by EDX analysis (Figure S4b) and elemental mapping (Figures S4c-e), which clearly evidences the Ag (red) alongside Ti (blue) and O (green).

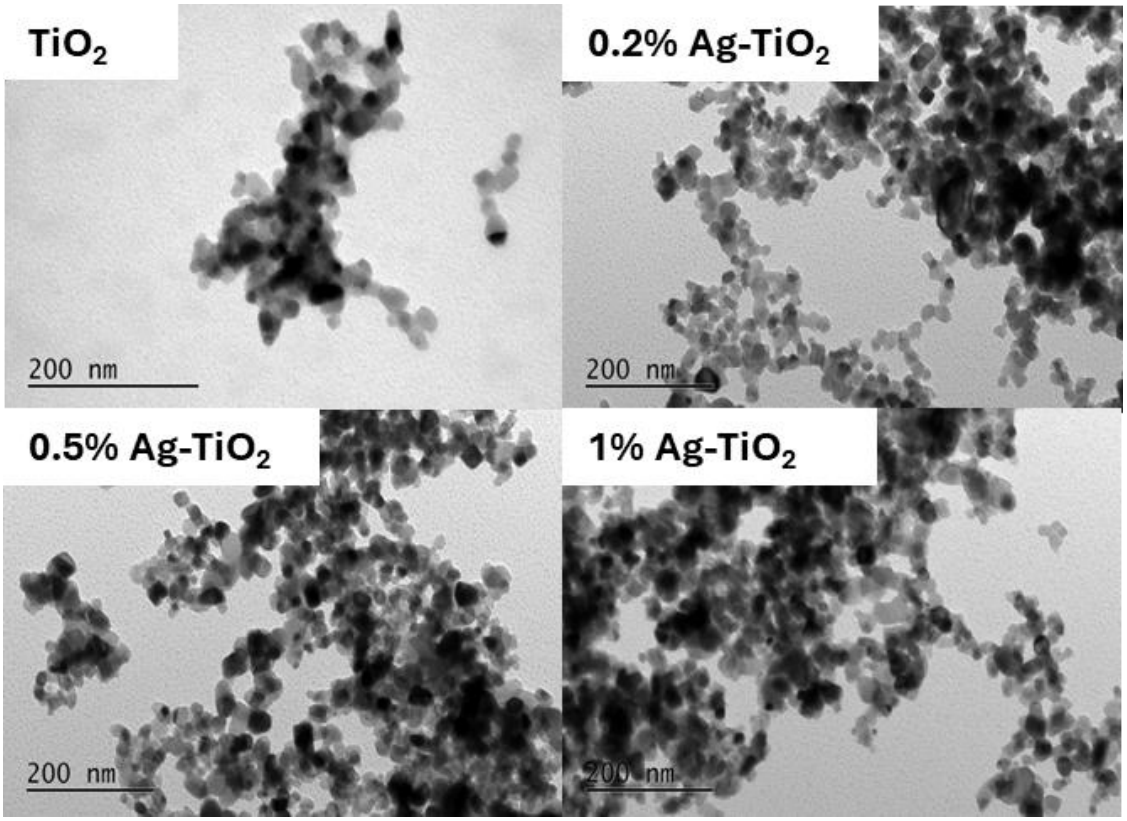


Figure 4.6. Representative TEM images of TiO_2 and Ag-TiO_2 samples prepared with varying Ag concentrations.

The crystallinity of Ag-TiO_2 nanocomposites with 0.2, 0.5 and 1 wt.% Ag was evaluated by XRD and compared to that of pristine TiO_2 (Figure 4.7a). The diffraction patterns indicate that the synthesis procedure does not alter the oxide's crystalline structure. All samples exhibit the characteristic reflections of anatase (25.3, 36.9, 37.9, 48.0, 54.0, 55.1, 62.8 and 69.0°) and rutile (27.4, 36.1 and 41.3°) phases of TiO_2. No additional peaks attributable to metallic silver were detected at any of the studied loadings. This absence can be ascribed to the relatively low Ag content in the composites, which makes its signal negligible compared to the strong diffraction from TiO_2. In addition, the most intense diffraction peak of silver, reported at 38.3° (JCPDS file 04-0783, dotted lines in Figure 4.7a, coincides with one of the main anatase reflections, and therefore may be masked by the TiO_2 signal.

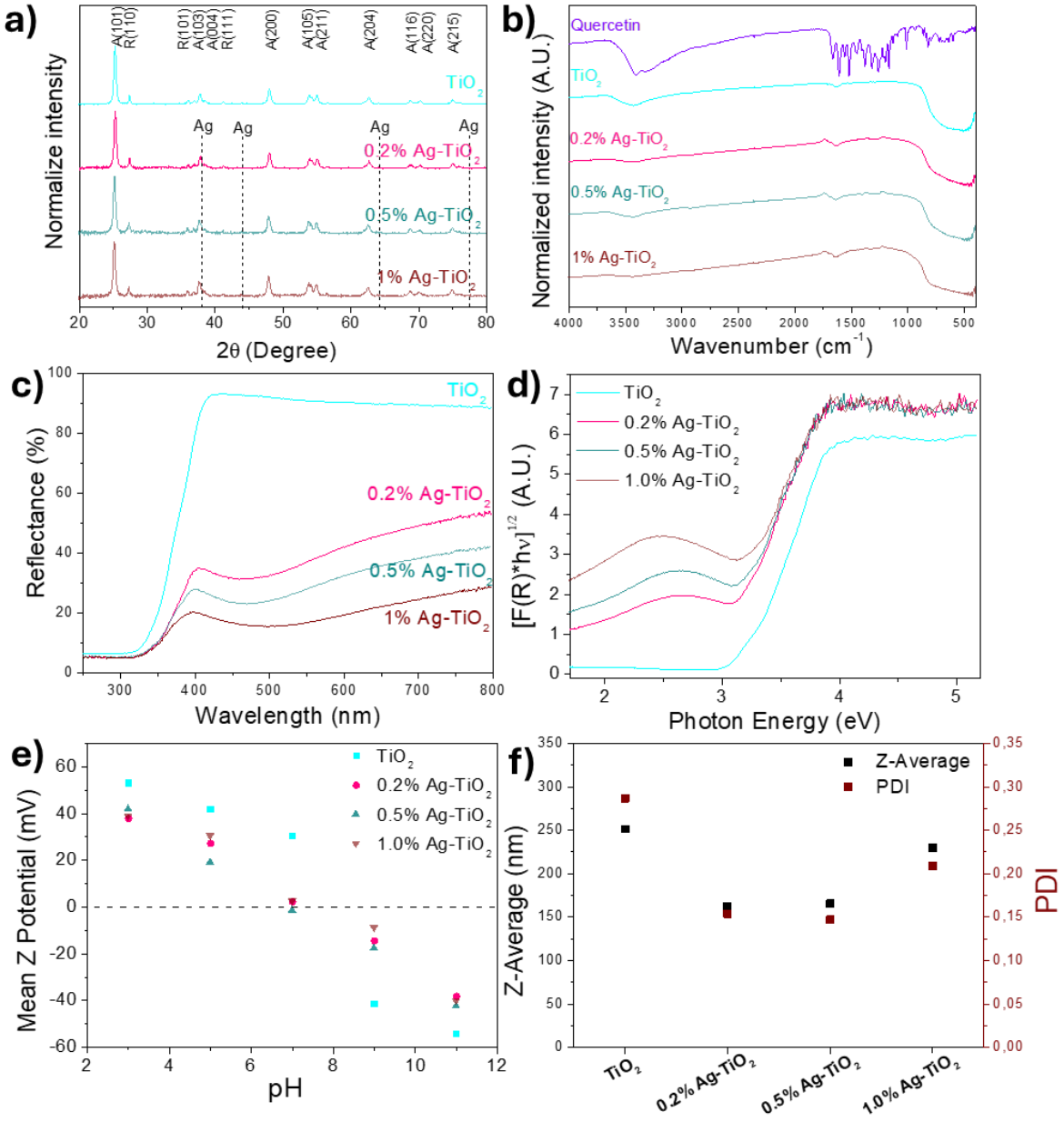


Figure 4.7. a) XRD patterns of pristine TiO_2 and Ag-TiO_2 nanocomposites with different Ag loadings; b) FTIR spectra of Ag-TiO_2 compared with the spectra of TiO_2 and quercetin; c) UV-Vis reflectance spectra and of Ag-TiO_2 compare with pristine TiO_2; d) Kubelka–Munk plots of Ag-TiO_2 compare with pristine TiO_2 employed to estimate the band-gap energy; e) ζ-potential values of TiO_2 and Ag-TiO_2 samples as a function of pH and f) hydrodynamic size (ζ-average) and polydispersity index (PDI) of pristine TiO_2 and Ag-TiO_2 nanocomposites.

FTIR spectra of the composites (Figure 4.7b) revealed only the characteristic vibrations of TiO_2: a broad absorption around 3400 cm^{-1} corresponding to O-H stretching, a signal near 1600 cm^{-1} associated with O-H bending, and a wide band below 1000 cm^{-1} attributed to Ti-O-Ti vibrations [63, 64]. The introduction

of silver into the TiO_2 did not produce noticeable spectral variations, likely due to the relatively low Ag content [65]. Moreover, no signals attributable to quercetin were detected, confirming efficient purification of the materials. This is particularly relevant, as residual organic species can negatively affect photocatalytic activity [66].

DRS was employed to investigate the optical response of pristine TiO_2 and Ag-TiO_2 nanocomposites (Figure 4.7c). Pure TiO_2 exhibited high reflectance (≈90%) in the visible range (400-800 nm), while in the UV region (<350 nm), the reflectance dropped to approximately 10%. In contrast, the Ag-TiO_2 materials showed a pronounced reduction in reflectance across the visible region, reaching about 50% at the lowest silver loading and 28% at the highest. This behaviour is attributed to the LSPR of Ag nanoparticles, which generates a characteristic absorption band in the 400-500 nm region that intensifies with increasing silver content. These findings are consistent with previous reports, confirming that silver incorporation extends the absorption profile of TiO_2 relative to the pristine, unmodified material.

The bandgap energies of the synthesised samples were estimated using the Kubelka–Munk approach (Eq. 2.1) and Tauc plots (Eq. 2.2), as illustrated in Figure 4.7d. The corresponding values are summarised in Table 4.1. For pristine TiO_2, a bandgap of 3.05 eV was obtained, in line with previously reported values for TiO_2 P25 nanoparticles (2.96-3.10 eV) [53, 67]. Upon Ag incorporation, an evident band-gap narrowing was observed, with all hybrid samples exhibiting energies below 2.90 eV. The most significant shift occurred for the composite containing 1 wt.% Ag, which displayed a band gap of 2.78 eV.

These values are in line with previous studies, which reported band-gap energies for Ag-TiO_2 nanocomposites ranging from 3.30 to 2.66 eV, depending on the silver content and synthesis strategy [68-70]. This agreement supports the reliability of our results and confirms the effect of Ag incorporation on bandgap narrowing in TiO_2.

The colloidal stability of the Ag-TiO_2 nanocomposites was evaluated through ζ-potential measurements of aqueous dispersions in the pH range 3-11 and compared to pristine TiO_2 (Figure 4.7e). All samples exhibited high stability ($|Z| > 30$ mV) at acidic (pH < 6) and alkaline (pH > 9) conditions, carrying positive charges in acidic media and negative charges at basic pH. The isoelectric point was found between pH 7 and 8, similar to pristine TiO_2, although the incorporation of Ag slightly shifted the Z-potential values. This behaviour suggests that Ag addition does not drastically alter the surface charge characteristics of TiO_2. The hydrodynamic size and PDI are presented in Figure 4.7f. Pristine TiO_2 show an average size of ≈250 nm with a PDI of 0.29, while the incorporation of Ag leads to smaller sizes between ≈162, with lower PDI values (0.15). These results indicate that Ag-TiO_2 nanocomposites display reduced aggregation and narrower size distributions compared with pure TiO_2, likely due to the stabilising

effect of silver species on the surface, which increases electrostatic repulsion and prevents agglomeration. This improved colloidal stability and reduced aggregation of Ag-TiO_2 are expected to enhance photocatalytic performance in aqueous media, as better dispersion and greater surface area availability can favour light absorption and interaction with target molecules.

Table 4.1. Band gap energy estimated for the synthesised Ag-TiO_2 nanocomposites compared with TiO_2 nanoparticles.

Sample	Eg (eV)
TiO_2	3.05±0.02
0.2% Ag-TiO_2	2.90±0.06
0.5% Ag-TiO_2	2.86±0.07
1% Ag-TiO_2	2.78±0.06

4.3.3 Screening of photocatalytic nanoparticles

Preliminary tests were conducted to identify the most efficient and balanced photocatalyst composition for the degradation of CIP (5 mg/L) and TMP (10 mg/L) under simulated solar radiation, to develop a viable, economical, and sustainable process. To select the most suitable photocatalyst for subsequent immobilisation, a screening procedure was performed using pristine TiO_2 and Ag-functionalised TiO_2 NPs. Different silver loadings (0.2%, 0.5%, and 1.0 wt%) were tested to evaluate the impact of Ag incorporation on photocatalytic performance and to define the optimal composition. This step was crucial for balancing the increase in visible-light-driven photocatalysis, avoiding the harmful effects of excessive metal content, and shielding the semiconductor.

The photocatalytic performance was evaluated in suspension, with 1 g/L of the photocatalyst in contact with the antibiotic solutions, by monitoring the decrease in concentration over time. The results of the degradation kinetics are presented in Figure 4.8, and the degradation efficiencies and k reaction values are summarised in Table 4.2. The results indicate that adsorption played an insignificant role in the overall removal of both antibiotics, confirming that photocatalysis was the dominant mechanism.

Table 4.2. Degradation efficiencies (%DE), adsorption capacity (%Ads) and degradation kinetics (*k*) of TiO_2 and Ag-TiO_2 nanocomposites on CIP and TMP degradation under simulated sunlight radiation.

		Simulated sunlight radiation					
		CIP			***TMP***		
Sample	**Ag wt.%**	*% Ads*	*%DE (90 min)*	*k (min^{-1})*	*% Ads*	*%DE (90 min)*	*k (min^{-1})*
TiO_2	0	-	65.98	0.016	-	59.66	0.009
	0.2	0.98	72.86	0.018	-	66.84	0.013
Ag-TiO_2	0.5	6.99	67.59	0.015	-	58.58	0.010
	1.0	1.66	72.75	0.016	-	64.30	0.008

Regarding adsorption capacity, CIP removal in the dark showed a marginal increase (up to ≈7%) for Ag-TiO_2 samples compared with pure TiO_2 (0%), suggesting that Ag nanoparticles may enhance local adsorption affinity or modify the catalyst's surface charge. However, this phenomenon does not occur to TMP adsorption, as neither pure TiO_2 nor Ag-TiO_2 possesses the capacity to adsorb the antibiotic.

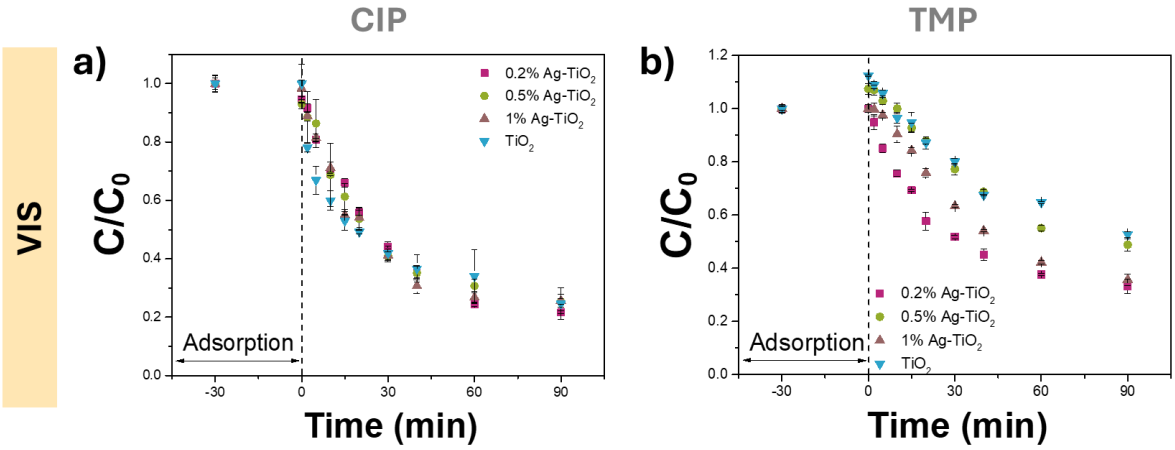


Figure 4.8. Photocatalytic degradation of a) CIP and b) TMP using TiO_2 and Ag-TiO_2 samples with different Ag loadings under simulated sunlight irradiation (VIS).

In the degradation of CIP, pristine TiO_2 achieves a degradation efficiency of 66% (k = 0.016 min^{-1}), whereas the incorporation of 0.2% of Ag increased the efficiency to ≈73% (k = 0.018 min^{-1}). The higher contents of silver (0.5% and 1.0%) did not enhance the performance, and in the case of 0.5% Ag, resulted in a reduction in the degradation rate (k = 0.015 min^{-1}), suggesting that excessive concentrations may act as recombination centres or block active sites on the surface of the nanoparticles, and partially hinder light harvesting by shielding the semiconductor from effective irradiation [71]. A similar pattern was

observed for TMP, although with lower degradation rates, reflecting differences in molecular structure and affinity. The results demonstrate that pristine TiO_2 achieved 59.66% (k = 0.009 min^{-1}), and 0.2% Ag-TiO_2 exhibited the highest performance (66.84%, k = 0.013 min^{-1}).

The enhanced performance of Ag-TiO_2 under visible-light irradiation is supported by the materials' optical properties. As shown by the bandgap values (see Table 4.1), where the minor decrease from 3.05 eV (TiO_2) to 2.90 eV (0.2%Ag-TiO_2) improves visible-light absorption and facilitates charge separation, which is consistent with the higher degradation efficiency observed for both CIP and TMP. This behaviour is typically attributed to the localised surface plasmon resonance (LSPR) of metallic Ag nanoparticles, which extends the absorption of TiO_2 into the visible region and promotes interfacial charge transfer [72-74]. Upon illumination, plasmon-excited electrons in Ag can be injected into the TiO_2 conduction band. Also, holes remain on the metal surface, thereby suppressing electron–hole recombination and favouring the formation of reactive oxygen species responsible for antibiotic degradation.

Importantly, increasing the Ag content does not result in a linear increase in photocatalytic activity. Higher noble-metal loadings can promote nanoparticle aggregation, partially shield the TiO_2 surface from incident light, and form recombination centres, ultimately reducing efficiency [75]. These cues align with literature reports showing that lower noble-metal content often outperforms higher levels because it offers an improved balance between plasmonic enhancement and charge recombination [39]. For example, an Ag/TiO_2 photocatalyst containing ≈0.5% Ag achieved approximately 84% ciprofloxacin removal after 300 minutes of visible-light irradiation [76], a performance comparable to that obtained in the present study within only 90 minutes, despite using less than half the Ag content.

Establishing a direct comparison with previously published Ag-TiO_2 studies is, however, challenging, given the strong dependence of photocatalytic performance on different experimental configurations. Parameters such as catalyst loading, initial antibiotic concentration, solution pH, and irradiance can markedly influence degradation outcomes. In a recent study, a 5 wt.% Ag/TiO_2-P25 photocatalyst produced via chemical reduction, achieving 89–90% CIP degradation within 60 minutes under a solar simulator using two 60 W white lamps [77, 78]. Abd El-Lateef *et al.* synthesised Ag/TiO_2 using mushroom biomass as a natural capping agent and reported 82.5% degradation after 300 minutes [76]. More advanced photochemical routes have also been shown to be highly active, achieving degradation values above 90% after 240 minutes [79]. By contrast, Castro *et al.* observed only 31% degradation under visible LED irradiation (65–110 mW cm^{-2}), highlighting the limited activity of TiO_2 under predominantly visible light and the key role of irradiation conditions [80].

Overall, the photocatalytic efficiencies achieved in the present study are comparable to or higher than those reported in previous works, demonstrating the effectiveness of the synthesised Ag-TiO_2 catalysts under optimised preparation and irradiation conditions.

Following these preliminary suspension tests, the most promising composition was identified and served as the basis for the polymeric-based membranes. Selecting 0.2% Ag-TiO_2 delivers the best photocatalytic performance while reducing the amount of silver required, making the process more economical and sustainable, and ensuring an optimal balance between efficiency, cost, and environmental impact.

4.3.4 Nanocomposite Membrane Characterisation

A series of systematic characterisations was performed to analyse the morphology and validate the stability of composite membranes incorporating the photocatalyst NPs.

The SEM images are presented in Figure 4.9a, representing the pristine PVDF-HFP, 20%TiO_2/PVDF-HFP membranes, and 20%Ag-TiO_2/PVDF-HFP. The images show a typical gradual solvent evaporation morphology, characteristic of PVDF-HFP processed by TIPS, leading to the uniform development of a microporous structure [81]. The incorporation of 20% NPs results in minimal impact on the membrane's internal structure, promoting a more spherulitic polymer crystallisation. Furthermore, smaller pores persist within larger ones, thus forming a well-interconnected internal structure [82].

The average pore diameter, measured by mercury porosimetry (Figure 4.9e), shows a reduction in pore size from 6.6 μm for the PVDF-HFP membrane to 1.9 μm and 2.7 μm for the 20%TiO_2/PVDF-HFP and 20% Ag-TiO_2/PVDF-HFP membranes, respectively. The same tendency is observed in total porosity, which decreases from 81% to 70% and 72% [83]. This total porosity could be related to the reduction in pore size, which may also be beneficial, promoting water percolation trough the porous matrix of the membrane, increasing the internal surface area and contact and retention of pollutants in the membrane interstices, thereby improving the removal process. In any case, the pore size and morphology are consistent with the findings reported in the literature concerning PVDF-HFP processed by TIPS. In this context, highly porous membranes with uniform pore distributions and pore sizes ranging from 1 to 8 μm have been reported [84].

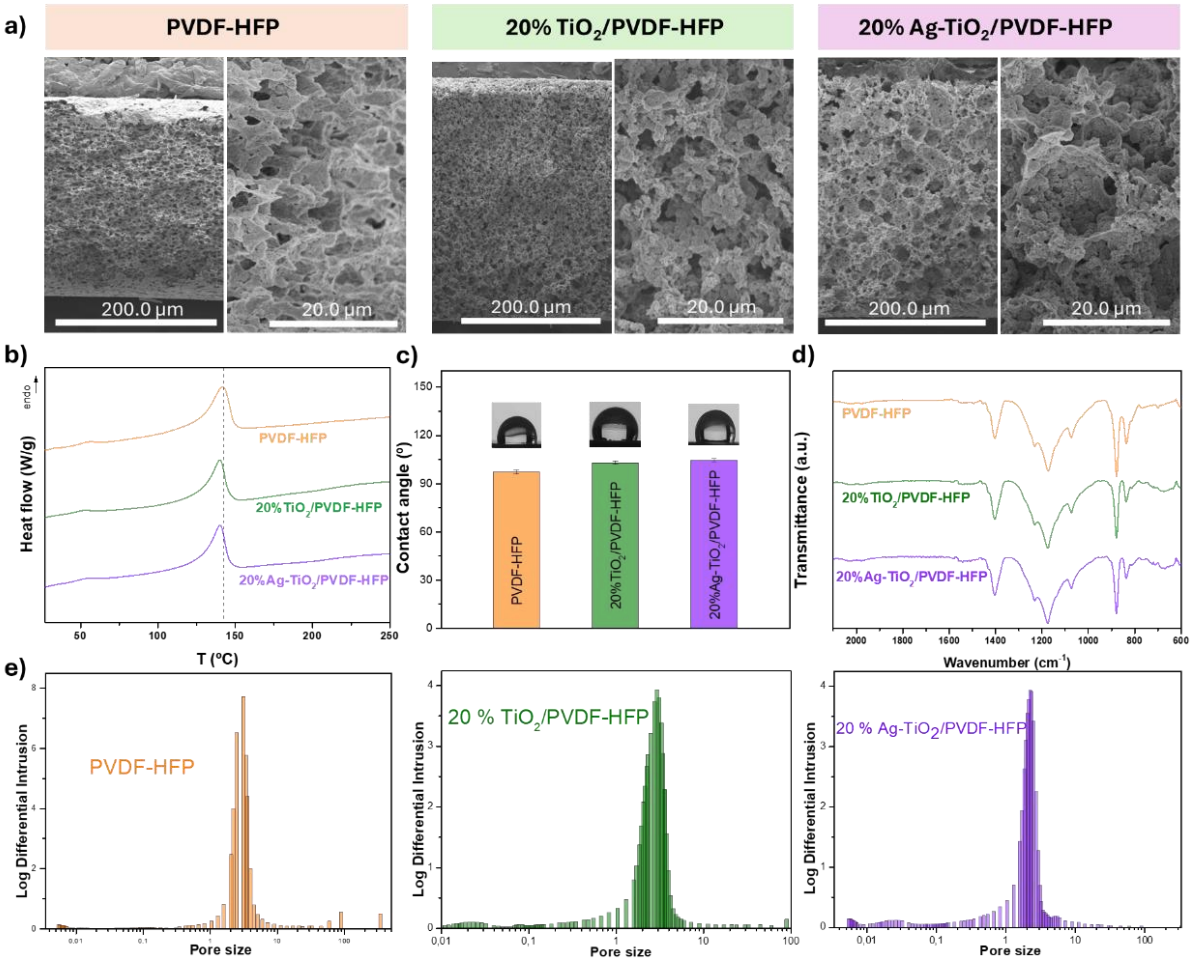


Figure 4.9. a) SEM images of PVDF-HFP-based membranes: pristine PVDF-HFP, 20%TiO_2/PVDF-HFP, and 20%Ag-TiO_2/PVDF-HFP. Cross-sectional views (250×, 2000×) revealing membrane porosity, pore interconnectivity, and internal membrane structure. b) DSC thermograms of PVDF-HFP-based membranes (pristine PVDF-HFP, 20%TiO_2/PVDF-HFP, and 20%Ag-TiO_2/PVDF-HFP, c) contact angle, d) FTIR spectra and e) pore size distribution.

The thermal and chemical stability of the membranes was evaluated to detect any differences resulting from the introduction of 20% NPs. As illustrated in Figure 4.9b, the DSC thermograms show an endothermic melting peak of PVDF-HFP at 142°, with a melting enthalpy corresponding to a degree of crystallinity of 30.6%, in agreement with findings reported in the literature [85]. The incorporation of 20%TiO_2 and 20%Ag-TiO_2 into the PVDF-HFP polymer matrix results in a slight reduction of the peak to 140°, without compromising the arrangement of the polymer chain. This decrease also translates into a reduction of the degree of crystallinity to values around 28%–29%, suggesting that this addition of 20% NPs acts as crystallisation defects, without causing substantial modification to the melting process of the

membrane [86, 87]. Similar behaviour has been reported for PVDF-TiO_2 membranes, where the incorporation of 20% TiO_2 led to a slight decrease in melting temperature (from 167 °C to 165 °C) and crystallinity, attributed to restricted polymer chain mobility and partial disruption of crystalline domains [88].

Contact angle (Figure 4.9c) was assessed to evaluate the wettability of the PVDF-HFP membranes with and without NPs incorporated. The measurements revealed values exceeding 90°, confirming the material's hydrophobic nature [89]. In the case of the pristine PVDF-HFP membrane, the contact angle was approximately 97°, while the incorporation of 20% TiO_2 slightly increased it to 103°, and to approximately 104° with 20% Ag-TiO_2. The slight increase in hydrophobicity (approximately 5-6°) may be related to changes in membrane topography and surface roughness [90].

The FTIR spectra of pristine PVDF-HFP membranes and PVDF-HFP membranes with 20% immobilised NPs are presented in Figure 4.9d. The characteristic bands of PVDF-HFP demonstrate absorptions at 769 cm^{-1}, which are associated with the α phase, and a band at 834 cm^{-1}, which is associated with the β phase [47]. The incorporation of 20% TiO_2 resulted in a consistent absorption trend for the bands, although with variations in relative intensities, indicating an enhancement in the contribution of the β phase. This effect became more pronounced in the membrane containing 20% Ag-TiO_2, where the band at 840 cm^{-1} was significantly intensified. The results indicate that the presence of nanoparticles promotes a reorganisation of the polymer chains, favouring the polar conformation (β phase), in agreement with the literature on similar systems [91]. Furthermore, the region between 500–600 cm^{-1} exhibited subtle changes attributed to Ti–O–Ti vibrations, thereby confirming the incorporation of nanoparticles into the matrix [92]. The interactions between the $–CF_2$ groups of PVDF-HFP and the modified surface of the NPs may justify this behaviour, suggesting their good incorporation into the composite.

4.3.5 Evaluation of the Antibacterial Activity

The antibacterial activity of the composite membranes was evaluated using two complementary approaches: a short-term contact test (2 hours) and a biofilm formation test (24 hours). These tests were selected to simulate different exposure scenarios relevant to aqueous environments. These scenarios comprise the immediate inhibition of bacterial proliferation, which is paramount in preventing the development of ARB, and the reduction of long-term surface colonisation, ensuring the material's efficiency and prolonging its lifetime.

Previous studies have reported that polymeric membranes with 10% of Ag-TiO_2 incorporation, containing approximately 2.6% Ag NPs on the TiO_2 surface, exhibit low log_{10} reduction values, limiting their antibacterial efficacy [36]. Based on these results, the incorporation percentage was increased from 10% to 20% to enhance antimicrobial activity. Simultaneously, the silver loading on the nanoparticles was reduced, resulting in an optimized Ag content that enhances photocatalytic efficiency while maintaining the sustainability of the process.

The antibacterial activity obtained for the membranes was quantified in terms of log reduction over a 2-hour contact period with *E. coli* and *S. aureus* bacteria (Figure 4.10a). The 20%Ag-TiO_2/PVDF-HFP composite membrane exhibited significantly higher activity compared to the other membranes (≈8.1), while the PVDF-HFP pristine membrane exhibited a negative log_{10} reduction. This negative value suggests bacterial proliferation, possibly enhancing bacterial protection due to the high surface and internal porosity, as confirmed by SEM, which showed a value similar to that of the 10%Ag-TiO_2/PVDF-HFP. The 20%TiO_2/PVDF-HFP membrane exhibited low reduction behaviour, reinforcing the importance of silver incorporation for improved performance.

In the case of *S. aureus*, all membranes with 20% NPs had a reduction of approximately 0.5 log, whereas the incorporation of 10% Ag-TiO_2 resulted in the lowest antimicrobial activity. These results indicate that the increase in the concentration of Ag-TiO_2 is crucial for a more effective activity against *E. coli*, although the inhibitory effect is less pronounced against *S. aureus*. This difference can be attributed to the structural characteristics of the cell walls. Gram-positive bacteria possess a thicker peptidoglycan layer, which endows them with greater rigidity and resistance. In contrast, Gram-negative bacteria have a thin and an outer lipopolysaccharide membrane, which are more susceptible to the penetration of Ag^+ ions [93]. The electrostatic interaction between Ag^+ ions and negatively charged bacterial membranes has been demonstrated to promote the formation of cavities, increase permeability, and disrupt vital processes, ultimately leading to cell death [94, 95]. A similar trend has been reported by Vatanpour *et al.*, who found that polyamide membranes incorporating Ag_3PO_4 NPs displayed better antibacterial activity against *E. coli* than against *S. aureus*, confirming that gram-negative bacteria are generally more susceptible to Ag-based nanocomposites [96]. In line with these findings, the 20%Ag-TiO_2/PVDF-HFP membrane exhibited a considerable log_{10} reduction, which, in comparison to the 10%Ag-TiO_2/PVDF-HFP membrane developed in another study, attained the desired outcome of enhancing antibacterial activity from 2 log_{10} to 8 log_{10} from 0.25 log_{10} to 0.5 log_{10}, amplifying activity by 4 and 2-fold, respectively [36].

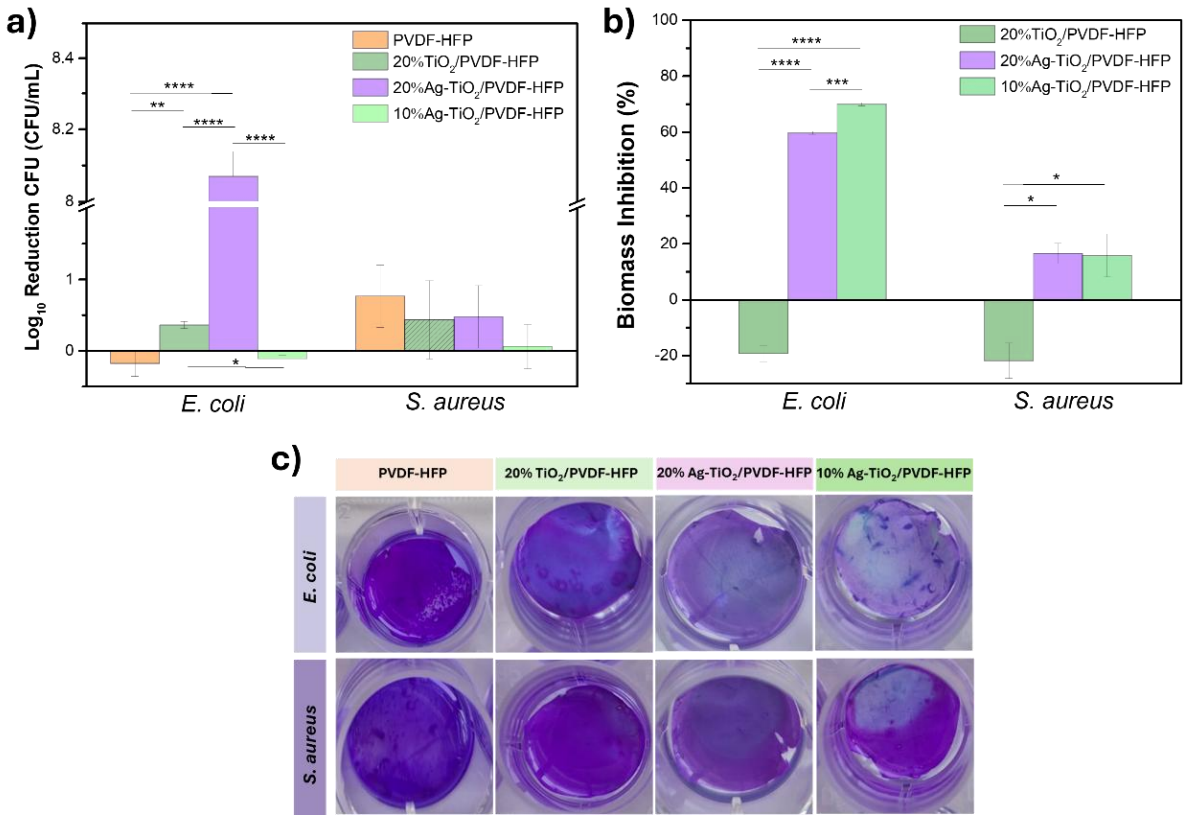


Figure 4.10. a) Antibacterial activity after 2h in suspension by direct contact with PVDF-HFP membrane (control), and PVDF-HFP loaded with 10% of Ag-TiO_2, 20% of TiO_2, and 20% of Ag-TiO_2 NPs against *E. coli* and *S. aureus*; b) biomass inhibition growth after 24h in contact with the same composite membranes. ns: non-significant; $p < 0.05$ (*), $p < 0.01$ (**), $p < 0.001$ (***), $p < 0.0001$ (****) when compared with each other, and c) representative membranes stained with crystal violet, illustrating the biofilm formation for each sample and visually supporting the quantitative results of biomass inhibition.

The crystal violet assay was employed to evaluate the membranes' capacity to prevent biofilm formation following 24 hours of contact. Compared with viability methods, this method quantifies extracellular polymeric substances (EPS), proteins, and other matrix components, providing a more comprehensive assessment of bacterial adhesion and colonisation [97]. Preventing biofilm growth is particularly relevant for this application, where dense biofilm can shield the photocatalytic material from light, thereby compromising degradation efficiency.

The results demonstrated that membranes containing Ag-TiO_2 were the only ones effective in inhibiting biofilm formation in both bacterial strains (Figure 4.10b-c). By contrast, the 20%TiO_2/PVDF-HFP membrane has no effect. These results are consistent with those of the short-contact test, in which *E. coli* biofilms were found to be more susceptible to inhibition than *S. aureus* biofilms. The 10% and 20% Ag-

TiO_2 PVDF-HFP-based membranes achieved biomass reductions of 60% and 70%, respectively, for *E. coli*, and 17% and 16%, respectively, for *S. aureus*. Comparable values were reported by Samree *et al.*, who observed that PVDF membranes coated with TiO_2 and Ag NPs reduced *E. coli* biofilms by approximately 65% compared to the pristine PVDF membrane [98]. A further study demonstrated that incorporating Ag NPs into PVDF ultrafiltration membranes effectively suppressed bacterial adhesion and biofilm formation in *E. coli* and *S. aureus* strains, reinforcing the role of silver as a key antibiofouling agent [99].

Although antibacterial assays were performed using non-resistant reference strains, selected to evaluate the antibacterial potential of the composite membranes, the study also addresses ARB. This was accomplished by evaluating the capacity for photocatalytic degradation of plasmid DNA carrying ARG. That way, while bacterial growth inhibition provides a general indication of antibacterial effect, the degradation of genetic information associated with resistance provides a more specific and relevant insight into the role of the produced composite membrane in mitigating the spread of ARB into aquatic environments.

4.3.6 Photocatalytic Degradation of ARG

After evaluating the antimicrobial activity exhibited by the composite membranes, it is paramount to understand whether microbial inactivation is followed by the degradation of the associated genetic material, since the elimination of viable bacterial cells does not guarantee mitigation of the environmental risk, as ARGs can persist in the environment and be transferred to other bacteria [100].

To assess the composite's capacity to degrade the plasmid containing antibiotic resistance information, the membranes were tested by placing them in contact with a 1 mL plasmid DNA suspension at 25 ng/µL with an empty pET-25b(+) vector, containing an ampicillin resistance gene (*AmpR*), for a total time of 10 hours.

Figure 4.11a shows the time-dependent degradation of ARGs (1h30, 3h, 6h, and 10h) for different systems under UVA irradiation, which includes the two controls (photolysis and PVDF-HFP membrane) and the photocatalytic membranes containing 20%TiO_2/PVDF-HFP and 20%Ag-TiO_2/PVDF-HFP.

In the initial phases of exposure (up to 3 hours), all systems exhibited reduced degradation (less than 7%), suggesting that UVA irradiation or contact with the PVDF-HFP does not significantly affect the plasmid DNA integrity. However, after 6 hours, a significant increase in degradation was observed when the plasmid DNA was in contact with the nanocomposite membranes. The 20%TiO_2/PVDF-HFP membranes exhibited a degradation reaching 27 %, while the 20%Ag-TiO_2/PVDF-HFP membrane demonstrated a

degradation of 36 % over the same period. Following a 10-hour radiation exposure, the degradation was intensified, reaching 52% for the 20%TiO_2 composite and 73% for the 20%Ag-TiO_2 composite. In contrast, the controls exhibited minimal degradation, with values of 3% and 22% for photolysis and the PVDF-HFP membrane, respectively, after 10 hours.

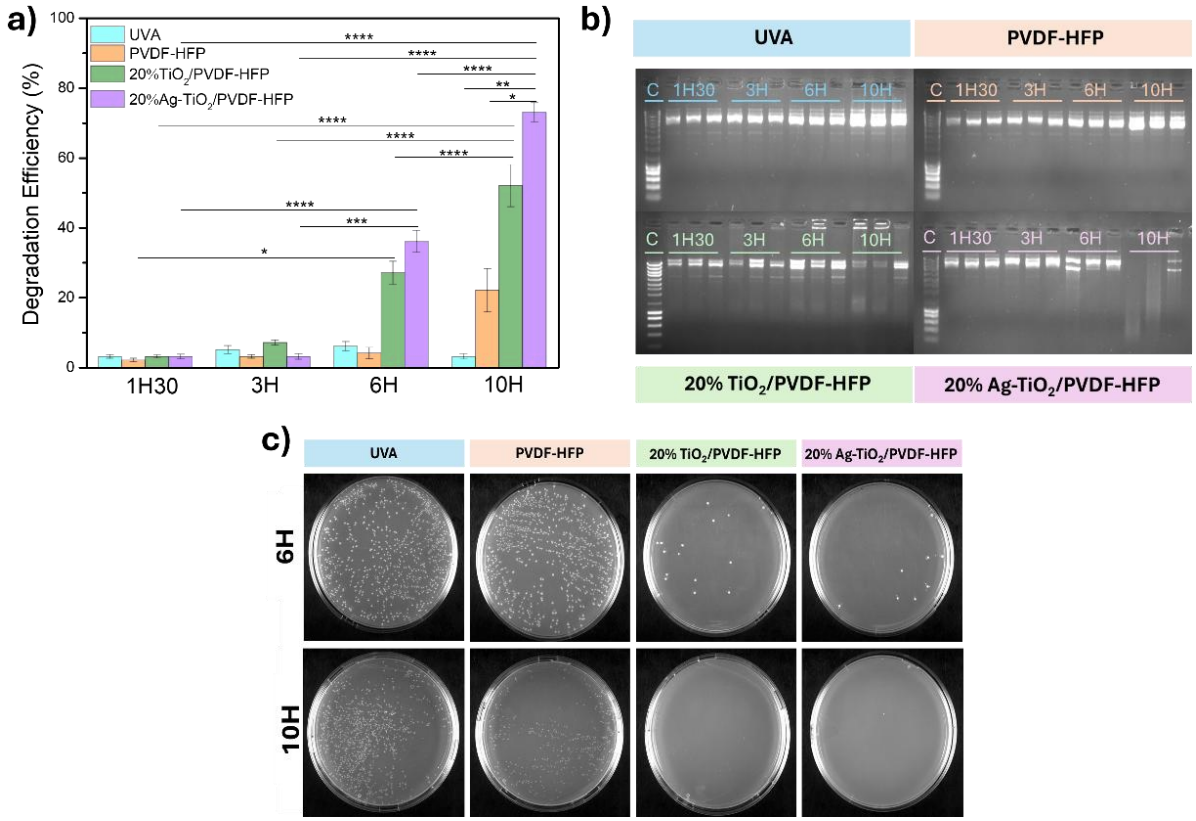


Figure 4.11. Evaluation of plasmid DNA degradation and loss of functionality under UVA irradiation: a) The percentage of plasmid degradation over time (1.5 h, 3 h, 6 h and 10 h) for the different systems: UVA (photolysis), PVDF-HFP, 20% TiO_2/PVDF-HFP and 20% Ag–TiO_2/PVDF-HFP, $p < 0.05$ (*), $p < 0.01$ (**), $p < 0.001$ (***), $p < 0.0001$ (****) when compared with each other; b) Agarose gel electrophoresis of plasmid DNA samples collected at each irradiation time point; c) LB agar plates containing ampicillin (a selective antibiotic) were used to evaluate plasmid functionality after 6 and 10 hours of irradiation.

Figure 4.11b corroborated these results by agarose gel electrophoresis analysis, in which the samples containing the nanoparticles reveal a progressive loss of plasmid integrity. This loss is characterised by the separation of plasmid fragments, more pronounced after 6 hours of contact, and, after 10 hours, a smear becomes evident, indicating plasmid degradation. Regarding the control samples, UVA and PVDF-

HFP membranes, after 10 hours, only a slight separation of bands is observed compared to the initial state. This indicates a low susceptibility to ARG degradation in the absence of the photocatalyst. Since the energy of individual UVA photons is insufficient to directly break covalent bonds or induce DNA strand scission, as observed in previous studies [101], UVA-induced oxidative damage generally relies on the presence of photosensitive materials capable of generating reactive oxygen species. In this context, TiO_2 and Ag-TiO_2 nanoparticles function as effective photocatalysts. Accordingly, the limited change observed in the control samples suggests that UVA irradiation alone or the membrane material (PVDF-HFP) cause no DNA degradation, resulting instead in possible minor structural alterations such as helix distortion, base oxidation, or occasional single-strand breaks, after a long period of exposure [102].

Despite the photocatalytic degradation of ARG has been extensively documented in suspension systems, studies utilising photocatalysts immobilised remain limited. The paucity of comparative literature, in combination with differences in experimental conditions, hinders direct quantitative comparisons and highlights the relevance of the present study based on TiO_2 and Ag-TiO_2 composite membranes.

It is reported evidence of immobilised semiconductors that have demonstrated reductions in ARGs concentration. For instance, in a simplified aqueous system, TiO_2 films under UV irradiation and in the presence of H_2O_2 allowed reduction of more the 4-5 log units of ARGs [103].

In contrast, suspension systems have been shown to report higher efficiencies. Hierarchical TiO_2 nanotubes were developed under UV irradiation, achieving removals of ≈70–82% in residual sludge, with inhibition of horizontal gene transfer [104]. In a similar line, Felis *et al.*, demonstrated that simulated solar photocatalysis with TiO_2 in suspension (0.5 g L^{-1}, 3 h) in treated wastewater resulted in ARG removals of ≈83–89%, including selective degradation of mobile markers such as *intI1* (>93%) [105].

However, it is important to note that these systems benefit from large catalytic contact areas, while immobilisation in polymeric membranes implies diffusion limitations that condition the degradation kinetics. The results presented here demonstrate that TiO_2 and Ag-TiO_2 photocatalytic membranes promote significant degradation of plasmid DNA under UVA irradiation, reinforcing their potential as sustainable systems for mitigating the spread of antimicrobial resistance in environmental applications.

Following the photocatalytic degradation tests on the ARGs, a further assessment was conducted to determine whether the residual genetic material retained the ability to confer resistance to other bacteria. Samples collected after 6 and 10 hours of UVA irradiation were used to transform a non-resistant strain of *E. coli* for this purpose. This test verified whether plasmid DNA degraded by the different systems (UVA, PVDF-HFP, TiO_2/PVDF-HFP, and Ag–TiO_2/PVDF-HFP) retained antibiotic resistance in a selective medium.

Figure 4.11c shows LB-agar plates containing ampicillin as the selective antibiotic, where only cells transformed with intact plasmids grew. The results indicate that plasmid DNA exposed to UVA radiation alone for 6 and 10 hours retained a transformation efficiency of approximately 78% and 72%, respectively. DNA exposed to the PVDF-HFP membrane showed similar efficiencies of about 75% and 63%, respectively. In contrast, DNA samples irradiated in the presence of TiO_2 and Ag-TiO_2 nanocomposite materials exhibited transformation efficiencies below 1% after 6 hours of exposure, and no colonies were observed after 10 hours for either material.

The statistical analysis of the tests revealed highly significant differences between treatment times, especially in conditions containing photocatalysts. A comparison between 6 and 10 hours of irradiation in 20% TiO_2/PVDF-HFP and 20% Ag-TiO_2/PVDF-HFP samples demonstrated a significant reduction in DNA functional integrity, indicating that 10 hours of irradiation is critical to ensure complete degradation of genetic material. This is in line with the microbiological results in selective medium (Figure 4.11c), where residual colonies were still observed after 6 hours, and no further growth occurred after 10 hours, confirming the total loss of transformation capacity of the remaining DNA.

It is noteworthy that, despite the degradation quantified by analytical methods not reaching total degradation (≈73%) with the 20% Ag-TiO_2/PVDF-HFP membranes, the DNA remaining after exposure to photocatalysts completely loses its biological functionality, lacking the structural integrity to confer antibiotic resistance. This is a critical result for ARG containment, demonstrating the excellent photocatalytic efficiency of the nanocomposites in degrading ARG.

4.3.7 Photocatalytic Performance

To evaluate the performance of these composite membranes, photocatalytic tests were performed under UV and visible radiation, using the same experimental conditions as in the NPs in suspension tests, with the exposure time increased to 600 minutes.

The tests included controls such as photolysis, pure PVDF-HFP membrane, and the PVDF-HFP membrane containing pure TiO_2. The membranes were maintained in the dark for 30 minutes before exposure to achieve adsorption/desorption equilibrium. The contribution of direct photolysis exhibited minimal degradation, with values of only 4.3 % and 16.0 % for CIP under UV and VIS, respectively, and no degradation for TMP under both conditions (Tables 4.3–4.4).

Table 4.3. Adsorption capacity, photocatalytic degradation efficiencies, and kinetics degradation of CIP (5 mg/L), and TMP (10 mg/L) under UV, comparing the performance of photolysis, PVDF-HFP, 20%TiO_2/PVDF-HFP, and 20%Ag-TiO_2/PVDF-HFP membranes over 600 min.

	Ultraviolet radiation (UV)					
	CIP			***TMP***		
Sample	*% Ads*	*%DE (600 min)*	*k (min^{-1})*	*% Ads*	*%DE (600 min)*	*k (min^{-1})*
Photolysis	-	4.3	-		0	-
PVDF-HFP	1.3	16.0	-	2.7	0	-
20%TiO_2/PVDF-HFP	1.3	93.4	0.006	6.2	58.7	0.002
20%Ag-TiO_2/PVDF-HFP	1.3	95.6	0.005	5.5	60.0	0.002

These results confirm the low susceptibility of these antibiotics to photodegradation, particularly TMP, whose more stable structure is often described as resistant to the direct effect of radiation [106]. Similarly, the pristine PVDF-HFP membrane showed no significant adsorption capacity. Although slight variations in removal values were observed (16 % for CIP under UV, and 14 % for CIP and TMP under VIS), these are within the expected range for adsorption processes. Both photolysis and the pristine membrane served as controls and did not contribute significantly to antibiotic removal.

Table 4.4. Adsorption capacity, photocatalytic degradation efficiencies, and kinetics degradation of CIP (5 mg/L), and TMP (10 mg/L) under VIS (simulated sunlight radiation), comparing the performance of photolysis, PVDF-HFP, 20%TiO_2/PVDF-HFP, and 20%Ag-TiO_2/PVDF-HFP membranes over 600 min.

	Simulated sunlight radiation (VIS)					
	CIP			***TMP***		
Sample	*% Ads*	*%DE (600 min)*	*k (min^{-1})*	*% Ads*	*%DE (600 min)*	*k (min^{-1})*
Photolysis	-	16	-		0	-
PVDF-HFP	-	13.9	-	-	14.1	-
20%TiO_2/PVDF-HFP	2.4	34.2	0.0006	-	66.7	0.002
20%Ag-TiO_2/PVDF-HFP	1.3	93.8	0.005	-	67.3	0.002

When exposed to UV radiation (see Figure 4.12a and 4.12b), PVDF-HFP membranes containing TiO_2 and Ag–TiO_2 exhibited significantly higher photocatalytic activity than the control groups.

In the case of CIP, the 20%TiO_2/PVDF-HFP membrane achieved a degradation efficiency of 93.4 % (k = 0.006 min^{-1}). In comparison, the incorporation of Ag-TiO_2 resulted in a slightly higher degradation of 95.6 % (k = 0.005 min^{-1}), check Table 4.3 for efficiencies and kinetics. These slight differences suggest that silver incorporation enhances charge separation and increases ROS production, thereby promoting moderately more efficient degradation [107].

For TMP, lower degradation values were observed, with 58.7 % (k = 0.002 min^{-1}) for 20%TiO_2/PVDF-HFP and 60.0 % (k = 0.002 min^{-1}) for 20%Ag-TiO_2/PVDF-HFP. The more stable chemical structure explains this lower efficiency and less reactive structure of TMP, reflected in the lower k values, while the higher degradation rate observed for CIP results from its greater photosensitivity and reactivity under UV/TiO_2/Ag-TiO_2, strongly influenced by its ionisation state and the presence of functional groups susceptible to ROS attack [108]. Nevertheless, the slight improvement trend with Ag–TiO_2 remains, suggesting that Ag favours electron transfer and reduces electron–hole recombination, as observed in CIP degradation efficiencies.

Under visible radiation, a distinct difference in behaviour between the two antibiotics can be observed, as illustrated in Figures 4.12c and 4.12d.

For CIP, the difference between the membranes containing TiO_2 and Ag–TiO_2 is found to be significant. While 20%TiO_2/PVDF-HFP demonstrated a degradation of 34.2 % (k = 0.006 min^{-1}), 20%Ag-TiO_2/PVDF-HFP exhibited a degradation of 93.8 % (k = 0.005 min^{-1}). This suggests that the incorporation of silver has a significant impact on the activation of the material under visible light.

On the other hand, for TMP, the difference between both systems was minimal — 66.7 % for TiO_2 and 67.3 % for Ag–TiO_2, with kinetics of k = 0.002 min^{-1} in both cases. This behaviour suggests that the photocatalytic response of TMP is not significantly influenced by the presence of silver, possibly because its structure limits interaction with the generated oxidising species.

The low activity observed for pure TiO_2 under visible radiation is expected, since its band gap (≈3.05 eV) limits absorption to wavelengths below 390 nm. Thus, only the ultraviolet fraction of the visible spectrum (3-5%) can promote electronic excitation of the semiconductor, making it inefficient in the visible region [109]. The incorporation of Ag nanoparticles, however, introduces a significant modification to this scenario via LSPR. This enables the absorption of visible light and the transfer of excited electrons to the conduction band of TiO_2 [110]. Furthermore, Ag can act as an electron trap, thereby minimising electron-hole recombination and promoting ROS formation [75].

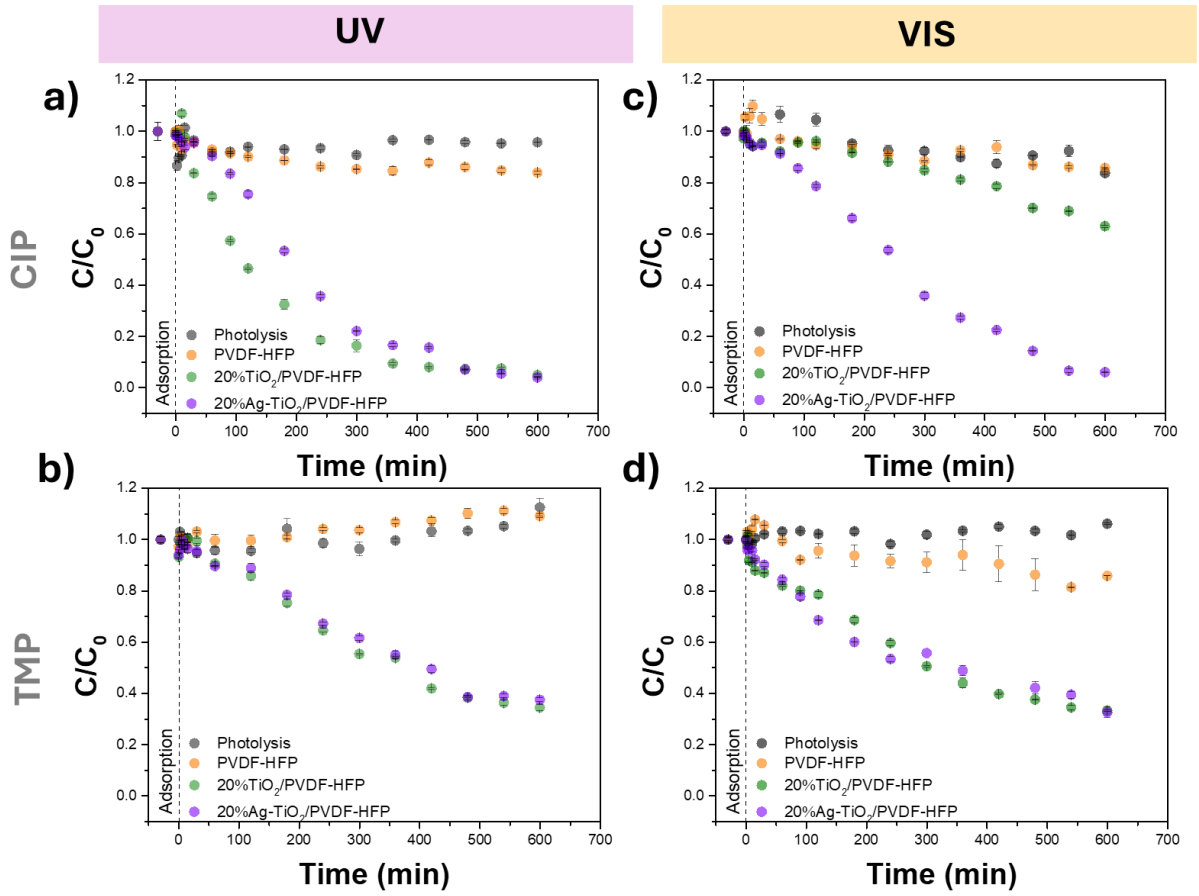


Figure 4.12. Photocatalytic degradation of a) CIP (5 mg/L) and b) TMP (10 mg/L) under UV irradiation, and c) CIP and d) TMP under visible (VIS) irradiation, for 600 min. Experiments were performed using pristine PVDF-HFP, 20%TiO_2/PVDF-HFP and 20% Ag-TiO_2/PVDF-HFP membranes. Photolysis was included as a control in all tests.

This effect is particularly pronounced in the degradation of CIP, which may be related to the antibiotic's higher UV–Vis light absorption coefficient and more favourable interaction with the generated oxidising species [111]. In contrast, silver's lower impact on TMP degradation may be due to its lower photosensitivity and molecular structures that are less susceptible to direct oxidation [112].

A study was reported for PVDF/TiO_2 nanofiber containing different concentrations of TiO_2 (1%, 3%, 5%, 10%, and 20%), where the 20% TiO_2 composite achieved approximately 80% degradation of Rhodamine B (RhB) in 6 hours under visible light. It took approximately 49 days to be completely degraded [113]. However, as demonstrated in the present study, activity under visible radiation remains limited when only TiO_2 is used. A similar phenomenon was observed in the study of the tourmaline-TiO_2 composite, which indicated that a 20% composition was most effective. The study demonstrated that complete degradation

of tetrabromobisphenol A (TBBPA) occurred within 60 minutes of UV light irradiation [114]. PVDF-HFP membranes prepared by solvent casting with Ag–TiO_2 immobilised, demonstrate significant performance under visible light. In the cited study, the authors reported 80.7 % degradation of norfloxacin (NOR), a fluoroquinolone antibiotic, after 300 minutes of exposure to visible radiation, markedly higher than the 10 % achieved with pure TiO_2 [25]. This highlights the effectiveness of silver functionalisation in enhancing the visible-light response of TiO_2. Compared with the membranes developed in the present study, similarly high degradation efficiencies are observed for both CIP and TMP, confirming that silver incorporation is a key factor in promoting visible-light activity.

Overall, these results demonstrate that the incorporation of Ag is an effective strategy for expanding the photocatalytic activity of TiO_2 to the visible range. Still, the final effect is dependent upon the chemical structure of the target pollutant, which is aligned with earlier studies that reported efficiency gains associated with modified semiconductors, improving charge separation.

- Reutilisation of the nanocomposite membrane

The validation of membrane stability and viability is crucial for assessing their reusability in continuous water treatment applications. Performance was analysed over three consecutive degradation cycles under the same experimental conditions, with ultrapure water washing between cycles, for the 20%Ag-TiO_2/PVDF-HFP membrane (Figure 4.13), totalling 1800 min. Degradation efficiencies are shown in Table 4.5.

Table 4.5. Reuse of 20%Ag-TiO_2/PVDF-HFP membranes under UV and visible radiation during the degradation of CIP and TMP. Each test was performed in three consecutive cycles (1800 min).

		UV	VIS
CIP	1st 20%Ag-TiO_2/PVDF-HFP	95.9 %	93.8 %
	2nd 20%Ag-TiO_2/PVDF-HFP	100 %	93.1 %
	3rd 20%Ag-TiO_2/PVDF-HFP	100 %	100 %
TMP	1st 20%Ag-TiO_2/PVDF-HFP	60.1 %	67.3 %
	2nd 20%Ag-TiO_2/PVDF-HFP	76.5 %	68.9 %
	3rd 20%Ag-TiO_2/PVDF-HFP	71. 4%	64.0 %

For CIP, a high level of photocatalytic stability, with an initial efficiency of ≈96 % under UV and ≈94 % under VIS radiation, reaching 100% degradation in both types of radiation after the third cycle. This enhancement over successive cycles was previously reported in earlier studies, which used PVDF as the polymer matrix to immobilise nanoparticles for photocatalysis, also processed by solvent casting. The

continuous exposure of the material to radiation increased the hydrophobicity of the membranes after three cycles of use, and this increase may enhance water percolation and the diffusion of contaminants to the catalytic sites, thereby further improving degradation efficiency. Simultaneously, continuous contact with water may promote the removal of compounds within the membrane, such as solvent or nanoparticle agglomerates, making pores more open and nanoparticles more dispersed, exposing previously blocked active sites, and facilitating more efficient interactions between contaminants and nanoparticles/ROS. Previous studies have corroborated this trend on the immobilisation of nanoparticles on PVDF substrates, where efficiency enhancements have been observed after cycles.

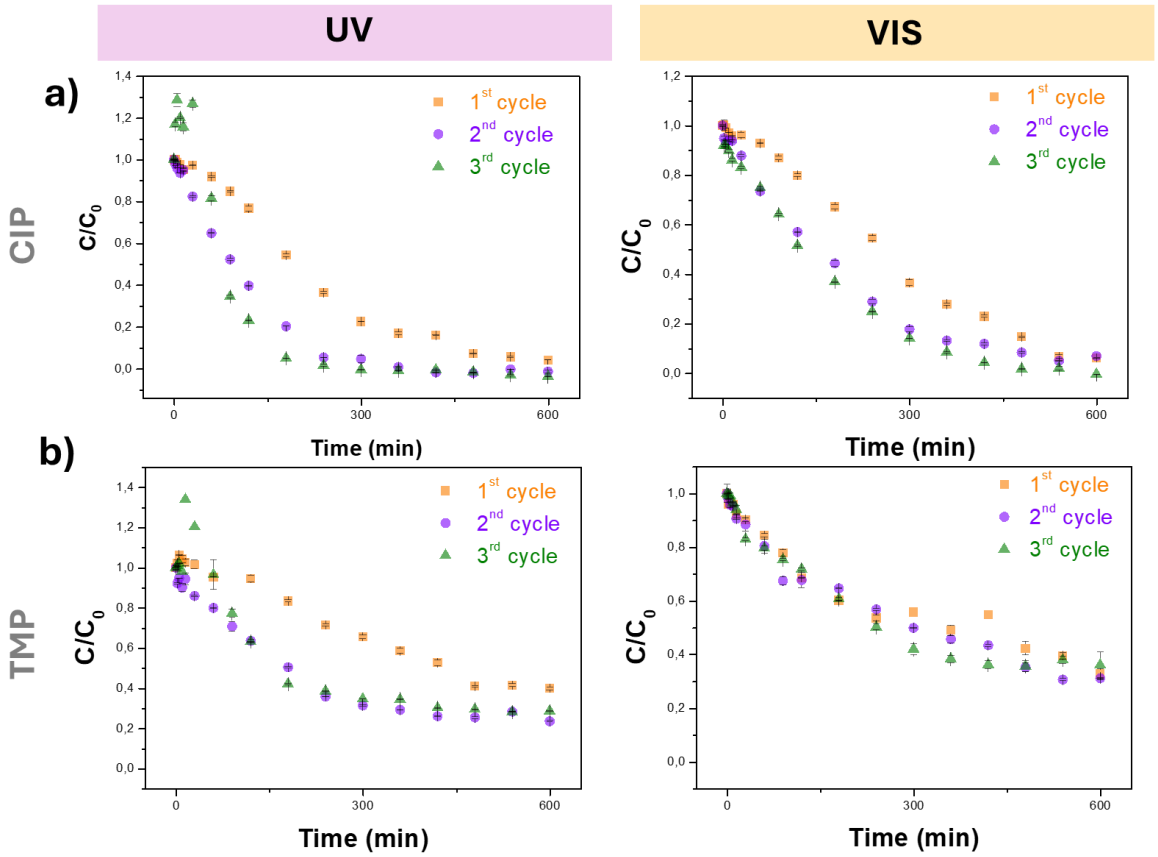


Figure 4.13. Reusability of 20%Ag–TiO_2/PVDF-HFP membranes under UV radiation and visible irradiation for the degradation of a) CIP, and b) TMP. Each test was performed over three consecutive cycles (1800 min).

Conversely, the behaviour exhibited by TMP was distinct. As shown in Figure 4.13b regarding UV experiments, the degradation efficiency increased from ≈60% in the first cycle to ≈77% in the second cycle, then decreased slightly to ≈71% in the third cycle. However, this still represents an improvement

over the initial cycle. In the presence of visible radiation, the efficiencies demonstrated greater stability, ranging from ≈67 % to ≈64 %, indicating effective immobilisation. However, no substantial enhancements were observed after repeated cycles.

Despite the differences, which may be associated with the chemical structure and intrinsic stability of each antibiotic, in both cases, however, the maintenance of high efficiencies over three consecutive cycles confirms the structural robustness of the membrane, indicating that the nanoparticles remain firmly immobilised in the polymer matrix, without significant loss of activity. Preserving and enhancing photocatalytic activity reinforces the material's potential for continuous water-treatment applications, making the process more economical and sustainable.

All in all, the results obtained in this work indicate the successful development of a multifunctional membrane for targeting diverse classes of persistent contaminants. The material demonstrated its efficacy as a photocatalyst for the degradation of various antibiotics under both UV and visible radiation. Moreover, it demonstrated significant antimicrobial activity and potential to degrade genetic material, thus addressing multiple scenarios, including chemical and biological sources of contamination. Although efficiency varies depending on the compound, the membranes positive response to all the studied targets is indicative of its versatility and practical applicability in real wastewater treatment with complex matrices.

As summarised in Table 4.6, a consistent improvement across all evaluated functionalities is observed upon the incorporation of silver, highlighting its role in enhancing photocatalytic efficiency, antimicrobial performance, and genetic material degradation.

It is also essential to highlight the material´s durability, evidenced by its stability in reusability tests and by slight improvements in efficiency after three consecutive cycles, in parallel with the proven inhibition of biofilm formation. This reduces operating costs and mitigates performance losses over time, making the process more sustainable and economically viable.

The collective evidence suggests the potential for a comprehensive solution for multifunctional aquatic remediation, capable of simultaneously targeting antibiotics, resistant microorganisms, and associated genetic determinants.

Table 4.6. Summary of the multifunctional performance of the developed composite membranes, comparing photocatalytic degradation efficiencies under UV and visible radiation for both antibiotics, antimicrobial reduction and biomass inhibition against two different strains, and ARG degradation for PVDF-HFP membranes containing 20%TiO_2 and 20%Ag-TiO_2.

Material Composite	Antibiotics (UV/Vis) (%)		Log_{10} reduction/biomass inhibition (%)		Plasmid DNA (%)
	CIP	*TMP*	*E. coli*	*S. Aureus*	
PVDF-HFP	16/14	0/14	-/-	0.8/-	22
20%TiO2/PVDF-HFP	93/34	59/67	0.9/-	0.4/0	52
20%Ag-TiO2/PVDF-HFP	96/94	60/67	8.1/70	0.5/16	73

4.4 Conclusions

In this work, a multifunctional photocatalytic membrane composite was successfully developed, based on the immobilisation of silver-functionalised TiO_2 nanoparticles, synthesised through an ecological and sustainable approach, in a PVDF polymer matrix. This strategy ensures the environmental compatibility of the material not only during its application but also throughout its life cycle.

Characterisation confirmed the incorporation of silver into the nanoparticles, inducing a shift in absorption to the visible range and a reduction in the bandgap (3.05 eV for pristine TiO_2 to 2.78 eV for 1%Ag-TiO_2). Concurrently, the characterisation of the membranes demonstrated that the incorporation of nanoparticles did not compromise the microporous morphology or the chemical and thermal stability of the composite material.

From a functional perspective, the membranes exhibited consistent multifunctional performance, demonstrating effective photocatalytic degradation of various antibiotics under UV and visible radiation, significant antimicrobial activity, and inhibition of biofilm formation by up to approximately 70%. Additionally, has been demonstrated ability to promote the degradation of genetic material associated with antimicrobial resistance, achieving up to 73% degradation of plasmid DNA with the 20%Ag-TiO_2/PVDF-HFP composite, along with the loss of bacterial viability in selective media after photocatalytic treatment.

The incorporation of silver has been proven to enhance the response to visible light and the multifunctional performance of the system, while the immobilisation of nanoparticles in the polymer matrix has been shown to ensure structural stability, facilitate reuse, and maintain activity over consecutive cycles. By combining green synthesis, robust immobilisation strategies, and simultaneous

action on chemical, biological, and genetic contaminants, this study advances the development of photocatalytic membranes as integrated, sustainable, and promising solutions for wastewater treatment in real and complex matrices.

4.5 References

[1] Z. Zhang, Q. Zhang, T. Wang, N. Xu, T. Lu, W. Hong, J. Penuelas, M. Gillings, M. Wang, W. Gao, Assessment of global health risk of antibiotic resistance genes, Nature communications, 13 (2022) 1553.

[2] O. Baaloudj, I. Assadi, N. Nasrallah, A. El Jery, L. Khezami, A.A. Assadi, Simultaneous removal of antibiotics and inactivation of antibiotic-resistant bacteria by photocatalysis: A review, Journal of Water Process Engineering, 42 (2021) 102089.

[3] H. Müller, E. Sib, M. Gajdiss, U. Klanke, F. Lenz-Plet, V. Barabasch, C. Albert, A. Schallenberg, C. Timm, N. Zacharias, R.M. Schmithausen, S. Engelhart, M. Exner, M. Parcina, C. Schreiber, G. Bierbaum, Dissemination of multi-resistant Gram-negative bacteria into German wastewater and surface waters, FEMS Microbiology Ecology, 94 (2018).

[4] C. Mallick, A. Sreedevi, T.K. Mukherjee, D. Pal, R. Das, S. Mondal, M. Gautam, Accessibility, detection, bioaccumulation, concentration and toxicity studies of antibiotics in fish, Aquatic Toxicology, 287 (2025) 107525.

[5] A.P. da Costa Araujo, C. Mesak, M.F. Montalvao, I.N. Freitas, T.Q. Chagas, G. Malafaia, Anti-cancer drugs in aquatic environment can cause cancer: insight about mutagenicity in tadpoles, Science of the Total Environment, 650 (2019) 2284-2293.

[6] K. Kümmerer, A. Al-Ahmad, V. Mersch-Sundermann, Biodegradability of some antibiotics, elimination of the genotoxicity and affection of wastewater bacteria in a simple test, Chemosphere, 40 (2000) 701-710.

[7] R.B. González-González, P. Sharma, S.P. Singh, J.H.P. Américo-Pinheiro, R. Parra-Saldívar, M. Bilal, H.M.N. Iqbal, Persistence, environmental hazards, and mitigation of pharmaceutically active residual contaminants from water matrices, Science of The Total Environment, 821 (2022) 153329.

[8] C. Reyes, J. Fernández, J. Freer, M.A. Mondaca, C. Zaror, S. Malato, H.D. Mansilla, Degradation and inactivation of tetracycline by TiO2 photocatalysis, Journal of Photochemistry and Photobiology A: Chemistry, 184 (2006) 141-146.

[9] H. Chen, S. Liu, X.-R. Xu, Z.-H. Diao, K.-F. Sun, Q.-W. Hao, S.-S. Liu, G.-G. Ying, Tissue distribution, bioaccumulation characteristics and health risk of antibiotics in cultured fish from a typical aquaculture area, Journal of Hazardous Materials, 343 (2018) 140-148.

[10] R. Fernandez-Torres, M.A.B. Lopez, M.O. Consentino, M.C. Mochon, J.L. Perez-Bernal, Application of enzymatic probe sonication extraction for the determination of selected veterinary antibiotics and their main metabolites in fish and mussel samples, Analytica Chimica Acta, 675 (2010) 156-164.

[11] E.Y. Klein, I. Impalli, S. Poleon, P. Denoel, M. Cipriano, T.P. Van Boeckel, S. Pecetta, D.E. Bloom, A. Nandi, Global trends in antibiotic consumption during 2016–2023 and future projections through 2030, Proceedings of the National Academy of Sciences, 121 (2024) e2411919121.

[12] H. Fatima, A. Bhattacharya, S. Gupta, S.K. Khare, Combating antibiotic pollution and its impacts on the environment through sustainable remediation options: Current developments and challenges, International Biodeterioration & Biodegradation, 205 (2025) 106166.

[13] T.P. Van Boeckel, C. Brower, M. Gilbert, B.T. Grenfell, S.A. Levin, T.P. Robinson, A. Teillant, R. Laxminarayan, Global trends in antimicrobial use in food animals, Proceedings of the National Academy of Sciences, 112 (2015) 5649-5654.

[14] U. Szymańska, M. Wiergowski, I. Sołtyszewski, J. Kuzemko, G. Wiergowska, M.K. Woźniak, Presence of antibiotics in the aquatic environment in Europe and their analytical monitoring: Recent trends and perspectives, Microchemical Journal, 147 (2019) 729-740.

[15] M. Foroughi, M. Khiadani, S. Kakhki, V. Kholghi, K. Naderi, S. Yektay, Effect of ozonation-based disinfection methods on the removal of antibiotic resistant bacteria and resistance genes (ARB/ARGs) in water and wastewater treatment: a systematic review, Science of The Total Environment, 811 (2022) 151404.

[16] A. Vassallo, S. Kett, D. Purchase, M. Marvasi, Antibiotic-Resistant Genes and Bacteria as Evolving Contaminants of Emerging Concerns (e-CEC): Is It Time to Include Evolution in Risk Assessment?, Antibiotics, 10 (2021) 1066.

[17] C. Muoghalu, H.C. Kaboggoza, S. Semiyaga, S. Lebu, C. Liu, C. Niwagaba, F. Nansubuga, M. Manga, Antibiotic resistant bacteria (ARB) and genes (ARGs) in urban wastewater treatment plants: influencing factors, mechanisms, and removal efficiency, Environmental Pollution, 383 (2025) 126851.

[18] P. Karaolia, I. Michael-Kordatou, E. Hapeshi, C. Drosou, Y. Bertakis, D. Christofilos, G.S. Armatas, L. Sygellou, T. Schwartz, N.P. Xekoukoulotakis, D. Fatta-Kassinos, Removal of antibiotics, antibiotic-resistant bacteria and their associated genes by graphene-based TiO2 composite photocatalysts under solar radiation in urban wastewaters, Applied Catalysis B: Environmental, 224 (2018) 810-824.

[19] Y. Hu, T. Zhang, L. Jiang, Y. Luo, S. Yao, D. Zhang, K. Lin, C. Cui, Occurrence and reduction of antibiotic resistance genes in conventional and advanced drinking water treatment processes, Science of The Total Environment, 669 (2019) 777-784.

[20] D. van Duin, D.L. Paterson, Multidrug resistant bacteria in the community: an update, Infectious disease clinics of North America, 34 (2020) 709.

[21] A. Beshiru, N.A. Isokpehi, I.H. Igbinosa, O. Akinnibosun, A.G. Ogofure, E.O. Igbinosa, Extended-spectrum beta-lactamase (ESBL)-and non-ESBL producing Escherichia coli surveillance in surface water sources in Edo State, Nigeria: a public health concern, Scientific Reports, 14 (2024) 21658.

[22] N. Alygizakis, K. Ng, Ľ. Čirka, T. Berendonk, F. Cerqueira, E. Cytryn, G. Deviller, G. Fortunato, I.C. Iakovides, I. Kampouris, I. Michael-Kordatou, F.Y. Lai, L. Lundy, C.M. Manaia, R.B.M. Marano, G.K. Paulus, B. Piña, E. Radu, L. Rizzo, K. Ślipko, N. Kreuzinger, N.S. Thomaidis, V. Ugolini, I. Vaz-Moreira, J. Slobodnik, D. Fatta-Kassinos, Making waves: The NORMAN antibiotic resistant bacteria and resistance genes database (NORMAN ARB&ARG)–An invitation for collaboration to tackle antibiotic resistance, Water Research, 257 (2024) 121689.

[23] K. Stefaniak, M. Harnisz, M. Męcik, E. Korzeniewska, ARB inactivation, ARGs and antibiotics degradation in hospital wastewater, Journal of Hazardous Materials, 495 (2025) 138833.

[24] J. Wang, R. Zhuan, L. Chu, The occurrence, distribution and degradation of antibiotics by ionizing radiation: An overview, Science of The Total Environment, 646 (2019) 1385-1397.

[25] H. Salazar, P.M. Martins, B. Santos, M.M. Fernandes, A. Reizabal, V. Sebastián, G. Botelho, C.J. Tavares, J.L. Vilas-Vilela, S. Lanceros-Mendez, Photocatalytic and antimicrobial multifunctional nanocomposite membranes for emerging pollutants water treatment applications, Chemosphere, 250 (2020) 126299.

[26] M.M. Khan, Chapter 1 - Principles and mechanisms of photocatalysis, in: M. Sakar, R.G. Balakrishna, T.-O. Do (Eds.) Photocatalytic Systems by Design, Elsevier2021, pp. 1-22.

[27] M. Umar, F. Roddick, L. Fan, Moving from the traditional paradigm of pathogen inactivation to controlling antibiotic resistance in water - Role of ultraviolet irradiation, Science of The Total Environment, 662 (2019) 923-939.

[28] M. Hwangbo, E.C. Claycomb, Y. Liu, T.E.G. Alivio, S. Banerjee, K.-H. Chu, Effectiveness of zinc oxide-assisted photocatalysis for concerned constituents in reclaimed wastewater: 1,4-Dioxane, trihalomethanes, antibiotics, antibiotic resistant bacteria (ARB), and antibiotic resistance genes (ARGs), Science of The Total Environment, 649 (2019) 1189-1197.

[29] X. Yu, Z. Wang, Y. Lou, J. Zhang, C. Pan, Y. Zhu, J. Xu, Highly efficient elimination performance of graphene/supramolecular porphyrin-based photocatalysis-self-Fenton system towards sulfonamide antibiotics, resistant bacteria and resistance genes, Chemical Engineering Journal, 484 (2024) 149552.

[30] J. Xu, P. Liang, X. Shen, F. Wang, Y. Lou, J. Zhang, C. Pan, Y. Zhu, Z. Wang, High-efficiency removal of organic pollutants, antibiotic resistant bacteria and resistance genes by a photocatalysis-self-Fenton system based on S, K co-doped g-C3N4 nanosheets, Separation and Purification Technology, 339 (2024) 126734.

[31] B.S.G. Rubim, L.C. Almeida, R.R. Peña Garcia, E.C. Silva-Filho, E.C. Muniz, M.B. Furtini, J.A. Osajima, The effect of cassava gum on TiO2 synthesis for heterogeneous photocatalysis of a pollutant in aqueous solution, Journal of Molecular Liquids, 437 (2025) 128268.

[32] C. Thambiliyagodage, Efficient photocatalysis of carbon coupled TiO2 to degrade pollutants in wastewater – A review, Environmental Nanotechnology, Monitoring & Management, 18 (2022) 100737.

[33] F. Zheng, P.M. Martins, J.M. Queirós, C.J. Tavares, J.L. Vilas-Vilela, S. Lanceros-Méndez, J. Reguera, Size Effect in Hybrid TiO2:Au Nanostars for Photocatalytic Water Remediation Applications, International Journal of Molecular Sciences, 23 (2022) 13741.

[34] L. Aoudjit, J.M. Queirós, A. Castro, D. Zioui, N. González-Ballesteros, S. Lanceros-Mendez, P.M. Martins, Sunlight-Induced Photocatalytic Removal of Paracetamol Using Au-TiO2 Nanoparticles, Nanomaterials, 15 (2025) 358.

[35] P. Zhang, X. Du, L. Zhao, K. Chai, Y. Yu, X. Su, Q. Su, Y. Han, H. Gao, Localized surface plasmon resonance Pt QDs-modified TiO2 as an electron pump for antibiotic photodegradation, Vacuum, 241 (2025) 114600.

[36] J.M. Queirós, F. Zheng, R. Brito-Pereira, M.M. Fernandes, E.O. Carvalho, P.M. Martins, V. Lazić, J.M. Nedeljković, S. Lanceros-Mendez, Photocatalytic and antimicrobial polymer-based hybrid membranes with surface-modified TiO 2 nanoparticles with 5-aminosalicylic acid and silver nanoparticles, RSC Sustainability, (2025).

[37] H. Esfandian, S. Mirzaei, A.S. Chari, R.A. Ghadi, I.H. Moqadam, Photocatalytic degradation of chlorpyrifos pesticide in aqueous solution using Cu-doped TiO2/GO photocatalysis vicinity of UV and visible light, Materials Science and Engineering: B, 305 (2024) 117385.

[38] R. Rashid, I. Shafiq, M.R.H.S. Gilani, M. Maaz, P. Akhter, M. Hussain, K.-E. Jeong, E.E. Kwon, S. Bae, Y.-K. Park, Advancements in TiO2-based photocatalysis for environmental remediation: Strategies for enhancing visible-light-driven activity, Chemosphere, 349 (2024) 140703.

[39] N. González-Ballesteros, P.M. Martins, C.J. Tavares, S. Lanceros-Méndez, Quercetin-mediated green synthesis of Au/TiO2 nanocomposites for the photocatalytic degradation of antibiotic ciprofloxacin, Journal of Industrial and Engineering Chemistry, 143 (2025) 526-537.

[40] I.C.G. Espada, N. González-Ballesteros, C.J. Tavares, S. Lanceros-Méndez, P.M. Martins, Towards green visible range active photocatalytic Au/TiO 2 nanocomposites through rutin-based synthesis and their application in the degradation of ciprofloxacin, RSC Sustainability, 2 (2024) 3090-3099.

[41] S. Suriyaraj, M.M. Pillai, A. Bhattacharyya, R. Selvakumar, Scavenging of nitrate ions from water using hybrid Al 2 O 3/bio-TiO 2 nanocomposite impregnated thermoplastic polyurethane nanofibrous membrane, RSC Advances, 5 (2015) 68420-68429.

[42] J.H. Pan, H. Dou, Z. Xiong, C. Xu, J. Ma, X. Zhao, Porous photocatalysts for advanced water purifications, Journal of Materials Chemistry, 20 (2010) 4512-4528.

[43] P.M. Martins, J.M. Ribeiro, S. Teixeira, D.Y. Petrovykh, G. Cuniberti, L. Pereira, S. Lanceros-Méndez, Photocatalytic microporous membrane against the increasing problem of water emerging pollutants, Materials, 12 (2019) 1649.

[44] R. Hong, Q. Chen, Dispersion of inorganic nanoparticles in polymer matrices: challenges and solutions, Organic-Inorganic Hybrid Nanomaterials, Springer2014, pp. 1-38.

[45] B. Hazarika, M. Ahmaruzzaman, M.S. Santosh, D. Barceló, S. Rtimi, Advances in polymer-based nanocomposite membranes for water remediation: Preparation methods, critical issues and mechanisms, Journal of Environmental Chemical Engineering, 11 (2023) 111401.

[46] L.A. Mendoza, S.-H. Liou, I.V. Maggay, G.V. Dizon, Y. Chang, L.L. Tayo, C. Hu, A. Venault, Achieving complete remediation of tetracycline contaminated water using a PVDF/δ-MnO2 photocatalytic membrane reactor, Journal of Membrane Science, 728 (2025) 124097.

[47] C.M. Costa, V.F. Cardoso, P. Martins, D.M. Correia, R. Gonçalves, P. Costa, V. Correia, C. Ribeiro, M.M. Fernandes, P.M. Martins, S. Lanceros-Méndez, Smart and Multifunctional Materials Based on Electroactive Poly(vinylidene fluoride): Recent Advances and Opportunities in Sensors, Actuators, Energy, Environmental, and Biomedical Applications, Chemical Reviews, 123 (2023) 11392-11487.

[48] R. Brito-Pereira, J.M. Queirós, L. Celaya-Azcoaga, R.F. de Luiz, P. Martins, S. Lanceros-Mendez, Hexavalent chromium dual water remediation and sensing based on hybrid polymer/metal-organic framework composites, Journal of Environmental Chemical Engineering, 12 (2024) 113839.

[49] D.C. Alves, P.M. Martins, R. Pinto, P. Costa, B. Bazán, R.F. de Luis, D.M. Correia, S. Lanceros-Méndez, 3D-printed multilayer membranes for photocatalytic degradation of ciprofloxacin, Applied Materials Today, 44 (2025) 102728.

[50] S. Liang, K. Fu, X. Li, Z. Wang, Unveiling the spatiotemporal dynamics of membrane fouling: A focused review on dynamic fouling characterization techniques and future perspectives, Advances in Colloid and Interface Science, 328 (2024) 103179.

[51] C. Gao, W. Tan, B. Liang, Y. Guo, Y. Xing, S. Ji, Ultrahigh antifouling ultrafiltration membrane based on Ag NPs photoreduction modified PVP/BiOCl nanoflower for efficient membrane fouling removal, Environmental Research, 270 (2025) 120842.

[52] C. Li, H. Wan, X. Qiu, S. Zhai, P. Sun, Y. Zhao, Multi-dimensional fouling process analysis and anti-fouling strategies for catalytic membranes in long-term water treatment, Water Research, 286 (2025) 124156.

[53] P. Martins, S. Kappert, H. Nga Le, V. Sebastian, K. Kühn, M. Alves, L. Pereira, G. Cuniberti, M. Melle-Franco, S. Lanceros-Méndez, Enhanced Photocatalytic Activity of Au/TiO2 Nanoparticles against Ciprofloxacin, Catalysts, 10 (2020) 234.

[54] C. Ribeiro, C.M. Costa, D.M. Correia, J. Nunes-Pereira, J. Oliveira, P. Martins, R. Gonçalves, V.F. Cardoso, S. Lanceros-Méndez, Electroactive poly (vinylidene fluoride)-based structures for advanced applications, Nature protocols, 13 (2018) 681-704.

[55] D. Hanahan, Studies on transformation of Escherichia coli with plasmids, Journal of Molecular Biology, 166 (1983) 557-580.

[56] S. Sysak, B. Czarczynska-Goslinska, P. Szyk, T. Koczorowski, D.T. Mlynarczyk, W. Szczolko, R. Lesyk, T. Goslinski, Metal Nanoparticle-Flavonoid Connections: Synthesis, Physicochemical and Biological Properties, as Well as Potential Applications in Medicine, Nanomaterials, 13 (2023) 1531.

[57] D.M. Aziz, A.A.M. Amin, S.A. Hassan, H. Özmen, G.K. Incili, Y. Say, One-pot synthesis of quercetin-functionalized silver and copper nanoparticles for enhanced optical, antimicrobial, and computational properties, Scientific Reports, 15 (2025) 26391.

[58] A. Chahardoli, P. Hajmomeni, M. Ghowsi, F. Qalekhani, Y. Shokoohinia, A. Fattahi, Optimization of quercetin-assisted silver nanoparticles synthesis and evaluation of their hemocompatibility, antioxidant, anti-inflammatory, and antibacterial effects, Global Challenges, 5 (2021) 2100075.

[59] D. Sharma, A. Chaudhary, Synthesis of Quercetin Functionalized Silver Nanoparticles and Their Application for the Colorimetric Detection of L-Cysteine in Biologically Complex Fluids, ChemistrySelect, 7 (2022) e202104147.

[60] S. Jain, M.S. Mehata, Medicinal Plant Leaf Extract and Pure Flavonoid Mediated Green Synthesis of Silver Nanoparticles and their Enhanced Antibacterial Property, Scientific Reports, 7 (2017) 15867.

[61] S. Al-Zahrani, S. Astudillo-Calderón, B. Pintos, E. Pérez-Urria, J.A. Manzanera, L. Martín, A. Gomez-Garay, Role of Synthetic Plant Extracts on the Production of Silver-Derived Nanoparticles, Plants, 10 (2021) 1671.

[62] S. B. Aziz, G. Hussein, M.A. Brza, S. J. Mohammed, R. T. Abdulwahid, S. Raza Saeed, A. Hassanzadeh, Fabrication of Interconnected Plasmonic Spherical Silver Nanoparticles with Enhanced Localized Surface Plasmon Resonance (LSPR) Peaks Using Quince Leaf Extract Solution, Nanomaterials, 9 (2019) 1557.

[63] V. Uthiravel, K. Narayanamurthi, V. Raja, S. Anandhabasker, K. Kuppusamy, Green synthesis and characterization of TiO2 and Ag-doped TiO2 nanoparticles for photocatalytic and antimicrobial applications, Inorganic Chemistry Communications, 170 (2024) 113327.

[64] M.B. Poudel, A.A. Kim, Silver nanoparticles decorated TiO2 nanoflakes for antibacterial properties, Inorganic Chemistry Communications, 152 (2023) 110675.

[65] S. Ünal, M. Orhan, M. Canbaz, Sustainable antibacterial performance in cementitious systems using Ag-modified TiO2 compounds, Frontiers of Structural and Civil Engineering, 19 (2025) 1061-1074.

[66] D. Awfa, M. Ateia, M. Fujii, C. Yoshimura, Photocatalytic degradation of organic micropollutants: Inhibition mechanisms by different fractions of natural organic matter, Water Research, 174 (2020) 115643.

[67] M.A. Mannaa, K.F. Qasim, F.T. Alshorifi, S.M. El-Bahy, R.S. Salama, Role of NiO Nanoparticles in Enhancing Structure Properties of TiO2 and Its Applications in Photodegradation and Hydrogen Evolution, ACS Omega, 6 (2021) 30386-30400.

[68] N.U.H. Altaf, M.Y. Naz, S. Shukrullah, A. Ghaffar, M. Irfan, D. Walczak, A. Głowacz, M.H. Mahnashi, S. Rahman, G. Królczyk, A.O. Alqarni, U.M. Niazi, Concurrent Synthesis and Immobilization of Ag Nanoparticles over TiO2 via Plasma Reduction for Photocatalytic Treatment of Methyl Blue in Water, Materials, 14 (2021) 6082.

[69] T. Pasang, K. Namratha, T. Parvin, C. Ranganathaiah, K. Byrappa, Tuning of band gap in TiO2 and ZnO nanoparticles by selective doping for photocatalytic applications, Materials Research Innovations, 19 (2015) 73-80.

[70] F. Khadar A, A.K. Mani, Anticancer and Photocatalytic Activity of Ag-doped TiO2 Nanoparticles Synthesized Using Carica papaya Leaf Extract, Journal of Cluster Science, 35 (2024) 2117-2131.

[71] N. Lu, Y. Wang, S. Ning, W. Zhao, M. Qian, Y. Ma, J. Wang, L. Fan, J. Guan, X. Yuan, Design of plasmonic Ag-TiO2/H3PW12O40 composite film with enhanced sunlight photocatalytic activity towards o-chlorophenol degradation, Scientific Reports, 7 (2017) 17298.

[72] M.L. de Souza, D.P. Dos Santos, P. Corio, Localized surface plasmon resonance enhanced photocatalysis: an experimental and theoretical mechanistic investigation, RSC advances, 8 (2018) 28753-28762.

[73] R. Gang, Y. Xia, L. Xu, L. Zhang, S. Ju, Z. Wang, S. Koppala, Size controlled Ag decorated TiO2 plasmonic photocatalysts for tetracycline degradation under visible light, Surfaces and Interfaces, 31 (2022) 102018.

[74] X. Lv, S. Cui, J. Chen, L. Wang, Y. Liu, J. Li, G. Du, X. Liu, J. Chen, R. Ledesma-Amaro, L. Liu, Cascaded de novo biosynthesis of lacto-proteins from CO2 by engineered Pichia pastoris††Electronic supplementary information (ESI) available. See DOI: https://doi.org/10.1039/d3gc00867c, Green Chemistry, 25 (2023) 5460-5469.

[75] H. Chakhtouna, H. Benzeid, N. Zari, A.e.k. Qaiss, R. Bouhfid, Recent progress on Ag/TiO2 photocatalysts: photocatalytic and bactericidal behaviors, Environmental Science and Pollution Research, 28 (2021) 44638-44666.

[76] H.M. Abd El-Lateef, C.-Q. Zeng, M.M. Khalaf, I.M.A. Mohamed, Green Synthesis of Silver-Incorporated Rutile TiO2 for Enhanced Photocatalytic Degradation of Ciprofloxacin and Carmine G Dye Pollutants, Catalysts, 14 (2024) 904.

[77] A. Machín, L. Soto-Vázquez, C. Colón-Cruz, C.A. Valentín-Cruz, G.J. Claudio-Serrano, K. Fontánez, E. Resto, F.I. Petrescu, C. Morant, F. Márquez, Photocatalytic Activity of Silver-Based Biomimetics Composites, Biomimetics, 6 (2021) 4.

[78] A. Machín, K. Fontánez, D. García, P. Sampayo, C. Colón-Cruz, G.J. Claudio-Serrano, L. Soto-Vázquez, E. Resto, F.I. Petrescu, C. Morant, F. Márquez, Hydrogen Production and Degradation of Ciprofloxacin by Ag@TiO2-MoS2 Photocatalysts, Catalysts, 12 (2022) 267.

[79] J. Wang, L. Svoboda, Z. Němečková, M. Sgarzi, J. Henych, N. Licciardello, G. Cuniberti, Enhanced visible-light photodegradation of fluoroquinolone-based antibiotics and E. coli growth inhibition using Ag–TiO 2 nanoparticles, RSC advances, 11 (2021) 13980-13991.

[80] N. Castro, J.M. Queirós, D.C. Alves, M.M.M. Fernandes, S. Lanceros-Méndez, P.M. Martins, A 3D-Printed Portable UV and Visible Photoreactor for Water Purification and Disinfection Experiments, Nanomaterials, 14 (2024) 525.

[81] C. Hou, Z. Pang, S. Xie, Z. Yang, N.H. Wong, J. Sunarso, Y. Peng, Dual PVP roles for preparing PVDF hollow fiber membranes with bicontinuous structures via the complex thermally induced phase separation (c-TIPS), Separation and Purification Technology, 332 (2024) 125766.

[82] A. Valverde, R. de Fernandez-de Luis, H. Salazar, B.F. Gonçalves, S. King, L. Almásy, M. Kriechbaum, J.M. Laza, J.L. Vilas-Vilela, P.M. Martins, On The Multiscale Structure and Morphology of PVDF-HFP@ MOF Membranes in The Scope of Water Remediation Applications, Advanced Materials Interfaces, 10 (2023) 2300424.

[83] L. Yan, Y.S. Li, C.B. Xiang, S. Xianda, Effect of nano-sized Al2O3-particle addition on PVDF ultrafiltration membrane performance, Journal of Membrane Science, 276 (2006) 162-167.

[84] C. Ferreira, V. Cardoso, A. Lopes, G. Botelho, S. Lanceros-Méndez, Tailoring microstructure and physical properties of poly (vinylidene fluoride–hexafluoropropylene) porous films, Journal of Materials Science, 50 (2015) 5047-5058.

[85] J. Teixeira, V.F. Cardoso, G. Botelho, A.M. Morão, J. Nunes-Pereira, S. Lanceros-Mendez, Effect of Polymer Dissolution Temperature and Conditioning Time on the Morphological and Physicochemical Characteristics of Poly(Vinylidene Fluoride) Membranes Prepared by Non-Solvent Induced Phase Separation, Polymers, 13 (2021) 4062.

[86] J.T. Jung, J.F. Kim, H.H. Wang, E. di Nicolo, E. Drioli, Y.M. Lee, Understanding the non-solvent induced phase separation (NIPS) effect during the fabrication of microporous PVDF membranes via thermally induced phase separation (TIPS), Journal of Membrane Science, 514 (2016) 250-263.

[87] U. Gradišar Centa, M. Mihelčič, V. Bobnar, M. Remškar, L. Slemenik Perše, The Effect of PVP on Thermal, Mechanical, and Dielectric Properties in PVDF-HFP/PVP Thin Film, Coatings, 12 (2022) 1241.

[88] D.-T. Tran, J.-P. Méricq, J. Mendret, S. Brosillon, C. Faur, Influence of Preparation Temperature on the Properties and Performance of Composite PVDF-TiO2 Membranes, Membranes, 11 (2021) 876.

[89] I. Tournis, D. Tsiourvas, Z. Sideratou, L.G. Boutsika, A. Papavasiliou, N.K. Boukos, A.A. Sapalidis, Superhydrophobic nanoparticle-coated PVDF–HFP membranes with enhanced flux, anti-fouling and anti-wetting performance for direct contact membrane distillation-based desalination, Environmental Science: Water Research & Technology, 8 (2022) 2373-2380.

[90] M.J. Toh, P.C. Oh, T.L. Chew, A.L. Ahmad, Antiwettability enhancement of PVDF-HFP membrane via superhydrophobic modification by SiO 2 nanoparticles, Comptes Rendus. Chimie, 22 (2019) 369-372.

[91] N. Chakhchaoui, R. Farhan, A. Eddiai, M. Meddad, O. Cherkaoui, M.h. Mazroui, Y. Boughaleb, L. Van Langenhove, Improvement of the electroactive β-phase nucleation and piezoelectric properties of PVDF-HFP thin films influenced by TiO2 nanoparticles, Materials Today: Proceedings, 39 (2021) 1148-1152.

[92] S. Abbad, K. Guergouri, S. Gazaout, S. Djebabra, A. Zertal, R. Barille, M. Zaabat, Effect of silver doping on the photocatalytic activity of TiO2 nanopowders synthesized by the sol-gel route, Journal of Environmental Chemical Engineering, 8 (2020) 103718.

[93] J. Moreira, B.D.D. Cruz, J.M. Queirós, N. Peřinka, M.M. Fernandes, P.M. Martins, D.M. Correia, S. Lanceros-Méndez, Ionic liquid based cellulose acetate composites: an approach for controlling infection caused by microorganisms, International Journal of Biological Macromolecules, 321 (2025) 146424.

[94] X. Fan, L.H. Yahia, E. Sacher, Antimicrobial Properties of the Ag, Cu Nanoparticle System, Biology, 10 (2021) 137.

[95] J.S. Kim, E. Kuk, K.N. Yu, J.-H. Kim, S.J. Park, H.J. Lee, S.H. Kim, Y.K. Park, Y.H. Park, C.-Y. Hwang, Y.-K. Kim, Y.-S. Lee, D.H. Jeong, M.-H. Cho, Antimicrobial effects of silver nanoparticles, Nanomedicine: Nanotechnology, Biology and Medicine, 3 (2007) 95-101.

[96] V. Vatanpour, M. Al-Shaeli, A.H. Behroozi, Enhancing the antifouling properties and permeability of polyamide TFC RO membranes via Ag3PO4 nanoparticle incorporation, Desalination, 615 (2025) 119272.

[97] S. Saini, S. Tewari, J. Dwivedi, V. Sharma, Biofilm-mediated wastewater treatment: a comprehensive review, Materials Advances, 4 (2023) 1415-1443.

[98] K. Samree, P.U. Srithai, P. Kotchaplai, P. Thuptimdang, P. Painmanakul, M. Hunsom, S. Sairiam, Enhancing the Antibacterial Properties of PVDF Membrane by Hydrophilic Surface Modification Using Titanium Dioxide and Silver Nanoparticles, Membranes (Basel), 10 (2020).

[99] N. Alnairat, M. Abu Dalo, R. Abu-Zurayk, S. Abu Mallouh, F. Odeh, A. Al Bawab, Green Synthesis of Silver Nanoparticles as an Effective Antibiofouling Material for Polyvinylidene Fluoride (PVDF) Ultrafiltration Membrane, Polymers (Basel), 13 (2021).

[100] W. Calero-Cáceres, M. Muniesa, Persistence of naturally occurring antibiotic resistance genes in the bacteria and bacteriophage fractions of wastewater, Water Research, 95 (2016) 11-18.

[101] X. Yang, Y. Wang, Photocatalytic effect on plasmid DNA damage under different UV irradiation time, Building and Environment, 43 (2008) 253-257.

[102] A.G. Sánchez, A. Gabrielli, D.J. Keszenman, Impact of ecological UV radiation on the photochemistry of nuclear DNA, Biophysical Reviews, 17 (2025) 537-545.

[103] C. Guo, K. Wang, S. Hou, L. Wan, J. Lv, Y. Zhang, X. Qu, S. Chen, J. Xu, H2O2 and/or TiO2 photocatalysis under UV irradiation for the removal of antibiotic resistant bacteria and their antibiotic resistance genes, Journal of Hazardous Materials, 323 (2017) 710-718.

[104] H. Yu, X. Zhang, J. Zhao, T. Sun, Y. Zhu, Mechanism of TiO2 nanotube UV-photocatalytic degradation of antibiotic resistance genes in the wastewater sludge and blocking of the transfer, Frontiers in Environmental Science, 13 (2025) 1590101.

[105] E. Felis, M. Buta-Hubeny, W. Zieliński, J. Hubeny, M. Harnisz, S. Bajkacz, E. Korzeniewska, Solar-light driven photodegradation of antimicrobials, their transformation by-products and antibiotic resistance determinants in treated wastewater, Science of The Total Environment, 836 (2022) 155447.

[106] H.Y. Kim, T.-H. Kim, S. Yu, Photolytic degradation of sulfamethoxazole and trimethoprim using UV-A, UV-C and vacuum-UV (VUV), Journal of Environmental Science and Health, Part A, 50 (2015) 292-300.

[107] K. Huang, C. Li, Y. Zheng, L. Wang, W. Wang, X. Meng, Recent advances on silver-based photocatalysis: Photocorrosion inhibition, visible-light responsivity enhancement, and charges separation acceleration, Separation and Purification Technology, 283 (2022) 120194.

[108] D. Bertagna Silva, G. Buttiglieri, B. Babić, D. Ašperger, S. Babić, Performance of TiO2/UV-LED-Based Processes for Degradation of Pharmaceuticals: Effect of Matrix Composition and Process Variables, Nanomaterials, 12 (2022) 295.

[109] M.D. Hernández-Alonso, F. Fresno, S. Suárez, J.M. Coronado, Development of alternative photocatalysts to TiO 2: challenges and opportunities, Energy & Environmental Science, 2 (2009) 1231-1257.

[110] M. Murase, Y. Matsuoka, S. Sugano, T. Katayama, A. Furube, Enhancement of visible light response of TiO2 photocatalyst by 3D-deposited Ag nanowires and its charge separation mechanism, The Journal of Chemical Physics, 161 (2024).

[111] C. Tian, W. Huang, Z. Wei, C. Liang, Y. Dong, J. Shi, X. Zhang, G. Nong, S. Wang, J. Xu, Photocatalytic degradation of different antibiotics using TiO 2–carbon composites: a case study of tetracycline and ciprofloxacin, New Journal of Chemistry, 47 (2023) 19646-19656.

[112] X. Luo, Z. Zheng, J. Greaves, W.J. Cooper, W. Song, Trimethoprim: Kinetic and mechanistic considerations in photochemical environmental fate and AOP treatment, Water Research, 46 (2012) 1327-1336.

[113] L. Lou, J. Wang, Y.J. Lee, S.S. Ramkumar, Visible light photocatalytic functional TiO2/PVDF nanofibers for dye pollutant degradation, Particle & Particle Systems Characterization, 36 (2019) 1900091.

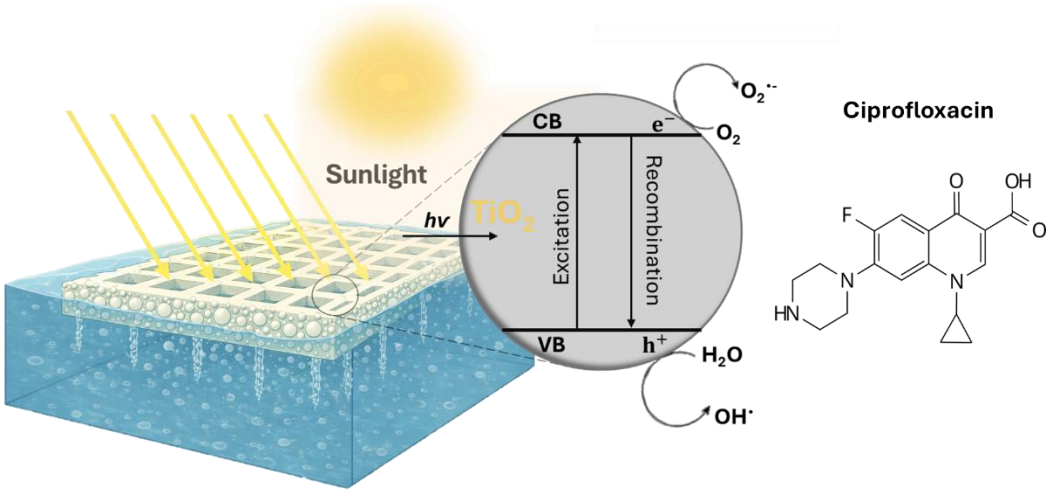
[114] N. Li, J. Zhang, C. Wang, H. Sun, Enhanced photocatalytic degradation of tetrabromobisphenol A by tourmaline–TiO2 composite catalyst, Journal of Materials Science, 52 (2017) 6937-6949.

CHAPTER 5

SCALABLE FLOATING PHOTOCATALYTIC MEMBRANES: 3D-PRINTED PVDF-HFP/TiO_2 GRIDS FOR WATER REMEDIATION

This final chapter addresses the transition from laboratory-scale membranes to scalable, application-oriented photocatalytic systems. By combining 3D printing with the salt-leaching method, floating PVDF-HFP/TiO_2 grids are developed as easily deployable and removable systems suitable for operation across different aquatic matrices. These systems are recoverable and powered by sunlight for aquatic remediation. The chapter demonstrates the potential of this floating open-grid architecture, which allows light to penetrate the water column while limiting direct interaction with the aquatic environment, thereby supporting its practical implementation under realistic water treatment conditions. Importantly, the system is shown to be effective in the photocatalytic degradation of ciprofloxacin, confirming its applicability for the removal of antibiotic contaminants from water bodies.

This chapter is based on the following publication: Dinis C.Alves, **Joana M. Queirós**, Fangyuan Zheng, Carmen R. Tubio, S.Lanceros-Méndez, P.M.Martins, Floating 3D-Printed Grids: New Approach for Photocatalytic Degradation of Contaminants under Real Sunlight Radiation (*Submitted*)



5.1 Introduction

Water contamination is an increasingly concerning environmental issue in the 21st century, threatening water matrices, which are a crucial resource for humans and all living beings. Although water contamination can arise from natural and anthropogenic sources, the rapid rates of industrialisation and population growth have significantly increased contamination, primarily through the discharge of untreated wastewater [1]. Every year, an estimated 500 million tonnes of harmful substances are released into water bodies by industrial facilities, leaving over 1 billion people without access to safe drinking water [2]. Among the most concerning contaminants are those known as contaminants of emerging concern (CECs). These recently identified synthetic or naturally occurring chemicals are found in the environment, typically at ng/L to µg/L [1], and are persistent contaminants that may have deleterious effects on humans and ecosystems [3]. These contaminants are not typically monitored or regulated and encompass a wide range of products, including cosmetics [2], pesticides [3], microplastics [4], industrial chemicals [5], household products, and pharmaceuticals [6].

In the European Union (EU), the prescription pharmaceutical market is projected to grow in revenue, with projections indicating 245 billion euros in 2025, a 3.6% increase compared with the previous year [7]. Among many causes for antibiotic prescriptions are urinary tract infections, and the antibiotics frequently used to treat them, such as ciprofloxacin (CIP) [3]. Those antibiotics are also among the most often detected in aquatic environments [8], from freshwater bodies [9], underground water [10], rivers [11], oceans [12] and even glaciers [13]. These molecules have been engineered to be stable and withstand harsh environments, making them resilient and difficult to degrade [14]. Following excretion, non-metabolised antibiotic residues reach aquatic environments, where they accumulate due to the inefficiency of conventional physical, chemical, and biological treatments in wastewater treatment plants

(WWTPs), leading to their discharge into natural water bodies [15, 16]. Their persistent presence in aquatic environments has been shown to have significant environmental impacts, including inhibiting chlorophyll metabolism in primary producers such as cyanobacteria and green algae by affecting photosynthesis and protein synthesis [17]. In animals such as rainbow trout, antibiotics may induce chromosome breakage and DNA damage [18]. In humans, the continuous presence of these contaminants exerts selective pressure on microbial communities, leading to problems affecting the human intestinal microbiome, favouring the emergence of antibiotic-resistant bacteria (ARB) [19].

To mitigate the presence of CECs, such as CIP, in the environment, various innovative techniques have been explored, including advanced oxidation processes (AOPs) such as ozonation [20], Fenton oxidation [21], sonolysis [22], and photocatalysis [23]. Among them, photocatalysis is notable because it requires only UV or visible radiation to activate a photocatalyst. It relies on the generation of highly reactive oxygen species (ROS), such as O_2^- and OH·, which degrade contaminants through oxidation [24]. This method is versatile, cost-effective, and highly energetically efficient, particularly when utilising solar radiation [25]. In recent decades, a vast range of semiconductors have been used as catalysts, including tin oxide (SnO_2) [26], iron oxide (Fe_2O_3) [27], zinc oxide (ZnO) [28], and titanium dioxide (TiO_2) [29]. The latter is the most studied one, and it is characterised by its affordability, chemical and physical stability, and high efficiency under UV radiation, attributed to its high band gap of 3.0-3.2 eV [30]. Most research in photocatalysis for water remediation employs suspended photocatalyst particles in a solution containing contaminants. This approach facilitates light penetration and optimises the efficiency of degradation.

On the other hand, it is associated with expensive and time-consuming recovery processes [31]. It poses a risk to aquatic life, as the putative release of photocatalyst into water can lead to undesirable secondary contamination [25]. To address the operational and environmental challenges associated with suspended photocatalysts, researchers have prioritised immobilisation and structural optimisation in the development of practical water remediation materials [32].

Thus, photocatalysts have been immobilised within different polymeric matrices, such as chitosan and cellulose from natural sources [26], and polyethersulfone (PES) [27] and PVDF [28] from synthetic sources, to create composite materials. These immobilised materials are typically prepared using conventional methods, such as solvent casting [29] for membranes, doctor blade casting [30] for thin films, electrospinning [33] for fibre membranes, or spray drying [34] for spheres. However, these techniques impose shape limitations, restricting the materials' morphology and structure.

To address these constraints, alternative production methods have been investigated, including additive manufacturing techniques such as fused deposition modelling (FDM) [35], selective laser

sintering (SLS) [36], stereolithography (SLA) [37], and direct ink writing (DIW) [38]. DIW is an extrusion-based additive manufacturing technique that extrudes a viscous ink layer by layer through a nozzle, solidifying or crystallising after deposition to form a stable structure [39] [40]. This method offers high versatility, as it allows the use of different materials, such as ceramics (e.g., hydroxyapatite or calcium phosphate [41]), metals (e.g., stainless steel [38] or silver [42]) or polymers (e.g., polyvinyl alcohol [43] or polyvinylidene fluoride [39]), enabling the production of a wide range of functional materials. Polyvinylidene fluoride (PVDF) and its copolymers are among the most widely used polymers for water remediation membranes, valued for their excellent durability, chemical resistance, processability, and ultraviolet (UV) resistance, making them highly compatible with photocatalytic applications [44, 45].

Recently, floating photocatalytic materials have attracted attention as a promising solution for water remediation, offering benefits such as straightforward recovery, enhanced light exposure, and versatility across various aquatic environments [46, 47]. Floating grids are easier to deploy and retrieve, require less energy to operate, and remain at the water's surface, where they can capture more light and support applications in natural (e.g., lakes, WWTP ponds, and surface waters) or artificial water bodies that exploit sunlight or UV radiation [48]. This not only enhances photocatalytic performance but also reduces disturbance to aquatic ecosystems—an important consideration for long-term environmental applications [45, 49, 50].

Despite the use of floating materials in other areas of remediation, such as adsorption [51] and oil-water separation [50], advances in photocatalytic water remediation technologies remain limited to small-scale studies that rely on energy-intensive processes and non-sustainable materials [45]. This work introduces an innovative approach that combines three-dimensional printing with the fabrication of floating polyvinylidene fluoride-co-hexafluoropropylene (PVDF-HFP) grids, using acetone as a greener solvent, for photocatalytic applications under sunlight irradiation. The strategy achieves an optimal balance among sustainability, practicability, and performance, enhancing efficiency and facilitating the translation of laboratory developments into practical applications in real contaminated scenarios.

5.2 Materials and Methods

5.2.1 Reagents

Titanium dioxide (P25 TiO_2, 21 nm particle size and 35-65 m^2/g surface area) was supplied by Evonik (Quimidroga, Spain). Sodium chloride (NaCl, purity > 99.5%) was purchased from Sigma-Aldrich. The polymer used to develop the grid was poly (vinylidene fluoride-co-hexafluoropropylene) (PVDF-HFP), Mw:

600,000 g/mol; 12 wt.% HFP, Solef 21216/1001), purchased from Solvay (Solvay Quimica S.L., Spain). Acetone (purity ≈ 99.8%) was purchased from Fisher Chemicals (Reinach, Switzerland). Ciprofloxacin ($C_{17}H_{18}FN_3O_3$, purity ≥98%) was purchased from Fluka. All materials were used as purchased.

5.2.2 Floating grid production and optimisation

The first step was the ink preparation, with 1 h of ultrasonic dispersion of 90 mg, 150 mg and 300 mg of TiO_2 in 20 mL of acetone, achieving concentrations of 3% weight/weight (w/w) TiO_2, 5% w/w TiO_2 and 10% w/w TiO_2 relative to the polymer mass, respectively. After dispersion, 3 g of polymer was added to the previous solution and stirred for 2 h under magnetic stirring. After dissolution, 1 g of NaCl was added per millilitre of solvent; in this case, 20 g of NaCl were added and mechanically dispersed.

The printing process was initiated by generating a G-code file with Cura v4.1.0, using printing parameters (Ø=1.8 mm, 50 mm/s) obtained from an optimisation procedure to manufacture the specific geometry. Three G-codes were created for three different grids with infill densities of 8%, 10% and 12% (Figure 5.1).

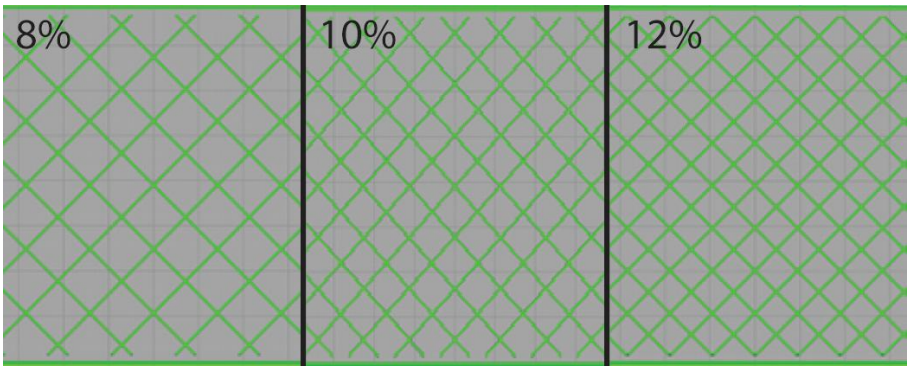


Figure 5.1. Geometry of the grids in the slicer for grids with different infills. From left to right, infill densities of 8%, 10%, and 12%.

The next step was printing the grid using a Tenlog TL-D3 Pro printer adapted for direct ink writing. The process begins by filling a syringe with 10 mL of the previously prepared formulation, then selecting the desired G-code and printing on a glass substrate (Figure 5.2a). Finally, the grid is placed at room temperature to allow solvent evaporation (Figure 2b). Subsequently, the grid is placed in a beaker containing water and agitated for 24 h to carry out the salt-leaching process (Figures 5.2c and 5.2d). It is recommended to change the water and measure conductivity after 24 h to confirm that all the salt has been leached.

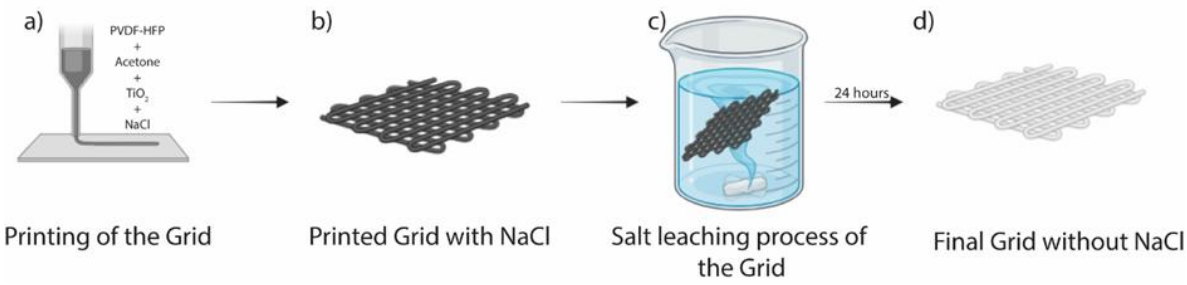


Figure 5.2. Scheme representing the printing process of floating grids of PVDF-HFP and PVDF-HFP/TiO_2 and the salt leaching processes.

5.2.3 Floating grid characterisation

The morphological, physicochemical, thermal, mechanical and surface characterisation of the pristine and nanocomposite PVDF-HFP printed grids was conducted following the methodologies previously described in Chapters 2 and 3, with specific adaptations.

Morphological analysis was examined using SEM using the same equipment and operating conditions described in Chapter 3. Prior to imaging, all samples were sputter-coated with a thin gold/palladium layer (≈15 nm) to ensure surface conductivity. SEM images acquired at magnifications of 20,000× and 50,000× were further analysed using ImageJ software (v1.54) to determine the average pore size.

Surface wettability was evaluated by static water contact angle measurements using an Ossila Contact Angle Goniometer, following the experimental procedure described in Chapter 2. In brief, three ultrapure water droplets (7 μL) were deposited on each grid surface, and contact angles were measured immediately after deposition.

The crystalline phases of the polymer in the grids were determined from FTIR spectroscopy under the same experimental conditions and data treatment procedures reported in Chapter 2. Thermal analysis of the samples was performed using DSC following also the protocol established in Chapter 2.

The mechanical properties of a small portion of the grid were evaluated under tensile mode using a Shimadzu Universal AG-IS 500N at a deformation rate of 1 mm/min until failure. Rectangular samples with dimensions of (13 mm x 70 mm x 1 mm) were used. Stress-strain curves were calculated based on the geometrical characteristics of each sample.

5.2.4 Photocatalytic Degradation Assays

- *UV irradiation set-up*

The photocatalytic efficiency of the PVDF-HFP/TiO_2 nanocomposites was tested by photocatalytic degradation of CIP under UV radiation in a tailor-made photoreactor (Figure 5.3). All grids were evaluated with CIP aqueous solution (5 mg/L). 300 mL of the solution was added to a rectangular tank with dimensions 28x8x6 cm containing the grid, which was agitated on an orbital shaker for 30 min in the dark. The tank was then placed inside a photoreactor. Under UV radiation, the beaker was vertically irradiated by eight lamps and laterally by four additional lamps (8 W, Philips), with a maximum intensity peak at 365 nm. The distance between the UV lamps and the water surface was 26 cm, and all experiments were conducted at room temperature under an incident light intensity of 0.7 mW/cm^2 for 540 min. The photocatalytic degradation efficiencies were analysed by monitoring the maximum absorption peak of CIP (276 nm) over time (0, 2, 5, 10, 15, 30, 60, 90, 120, 180, 240, 300, 540 min) using an Infinite M-Nano+ UV/Vis spectrophotometer. The degradation fitted the Langmuir-Hinshelwood mode, expressed by Eq. 1.3.

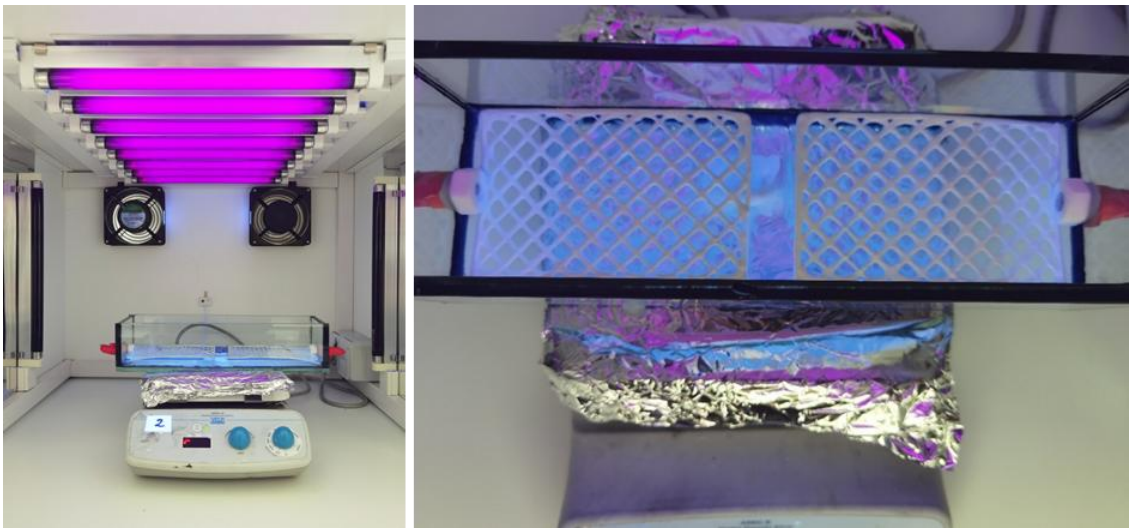


Figure 5.3. Set up of the UV photocatalytic tests.

- *Sunlight irradiation set-up*

The photocatalytic activity of PVDF-HFP/TiO_2 nanocomposites was also tested under natural sunlight. The same experimental conditions as those used in the UV tests were maintained, with 300 mL of a 5 mg/L CIP aqueous solution in the tank containing the floating grid (Figure 4a and b). The system was stirred mechanically in the dark (covered) for 30 min to achieve adsorption–desorption equilibrium before

exposure to sunlight. The system was subsequently exposed to direct sunlight (Figure 4c) on the University of Minho campus (Braga, Portugal), at coordinates 41˚33'44''N 8˚23'46''W (see Figure 4d), on day 23 of April 2025 for a total irradiation time of 360 min. Samples were drawn at scheduled intervals (0, 5, 10, 15, 30, 60, 120, 180, 240, 300, 360 min). The UV radiation at each sampling interval was measured using a UV radiometer (PCE-UV34) to monitor changes in natural solar radiation during the experiment; the measurements are shown in the supplementary information (Figure S2). A schematic representation of the setup is shown in Figure 4.

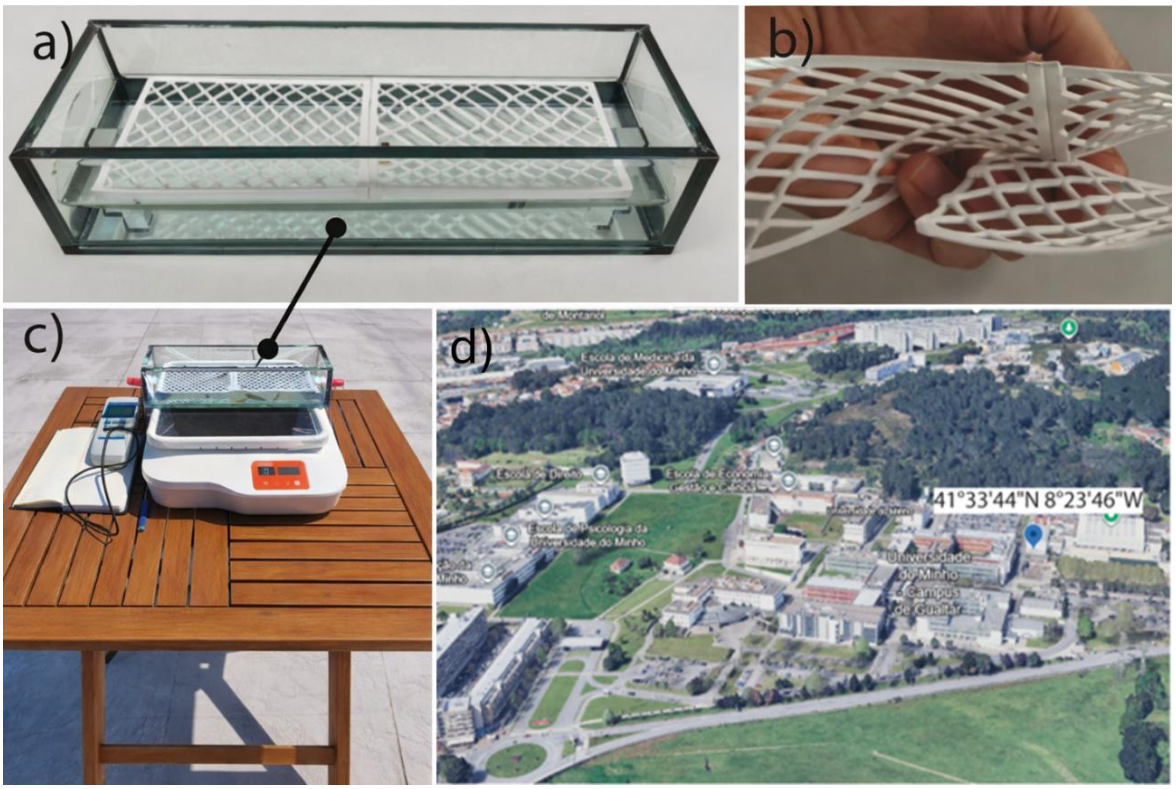


Figure 5.4. a) Tank containing 300 mL of a 5 mg/L CIP aqueous solution containing the floating grid; b) PVDF-HFP/TiO_2 shown folded, illustrating flexibility; c) Setup of the sunlight irradiation assay, orbital shaker, and tank with the TiO_2 floating grid inside; d) Map and coordinates of the spot where the assay was performed.

5.3 Results and Discussion

5.3.1 Floating grids characterisation

The printed grid samples are represented in Figure 5.5. They show dimensions of 130 mm x 85 mm x 1mm, as defined in the slicer software, and exhibit remarkable shape fidelity with no evident noosing.

Concerning the microstructure, SEM micrographs revealed that all the grids feature polygonal pores, as shown in Figure 5.6. Independently of the TiO_2 concentration, the grid's surface structure is very similar. Differences can be identified, on the other hand, when comparing the top and bottom surfaces of the grids.

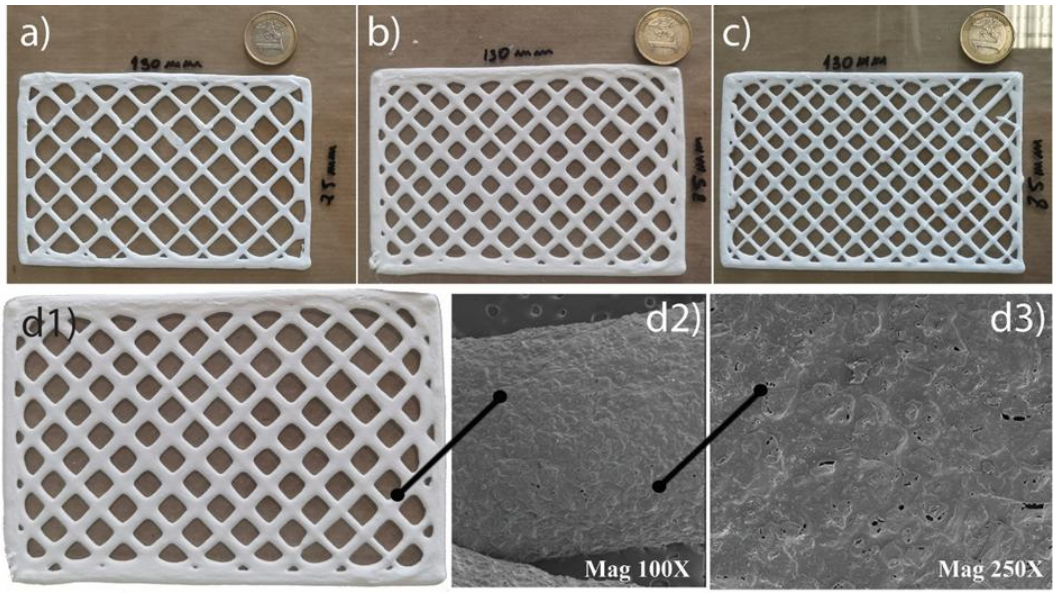


Figure 5.5. Final printed grids with different infill densities: a) 8%, b) 10%, c) 12%. d1) 10% grid and respective SEM ampliations with 100x magnification (d2) and 250x magnification (d3).

The top surface (the one in contact with the air in the printing process) exhibits lower porosity, attributed to the faster evaporation at the ink/air interface than at the ink/glass interface (bottom surface, facing the glass printing bed). The higher the evaporation rate, the more efficiently the polymer chain fills the free spaces left by acetone during evaporation, thereby reducing the pore volume in the final grid. This phenomenon has been observed in other studies and is not exclusive to PVDF-based grids. Ishikiriyama *et al.* studied the formation of microspheres via the TIPS technique from isotactic polypropylene solutions and observed that faster solvent evaporation at the air/solution interface results in a more compact surface. At the same time, less-exposed regions maintain higher porosity [52]. In another study, the application of a temperature-free production technique (Evaporation-Induced Phase Separation – EIPS) was demonstrated to induce the formation of a dense skin layer due to the local increase in polymer concentration at the air/solution interface, whilst the interior remains more solvent-rich, thereby promoting greater porosity through phase separation. These findings, consistent across

polymers and processing techniques, indicate that evaporation dynamics play a crucial role in determining the final morphology, consistent with the SEM results obtained in the present study [53].

Cross-sectional images, shown in Figure 5.6, confirm the presence of an interconnected porous structure, and the grids exhibit a uniform thickness of approximately 1 mm. The pore size varies from 94 µm to 197 µm. Regarding the addition of TiO_2, no significant changes are observed. It is essential to note that pore interconnectivity facilitates radiation penetration and contaminant solution percolation throughout the grid's polymeric porous structure, thereby potentially enhancing photocatalytic process efficiency.

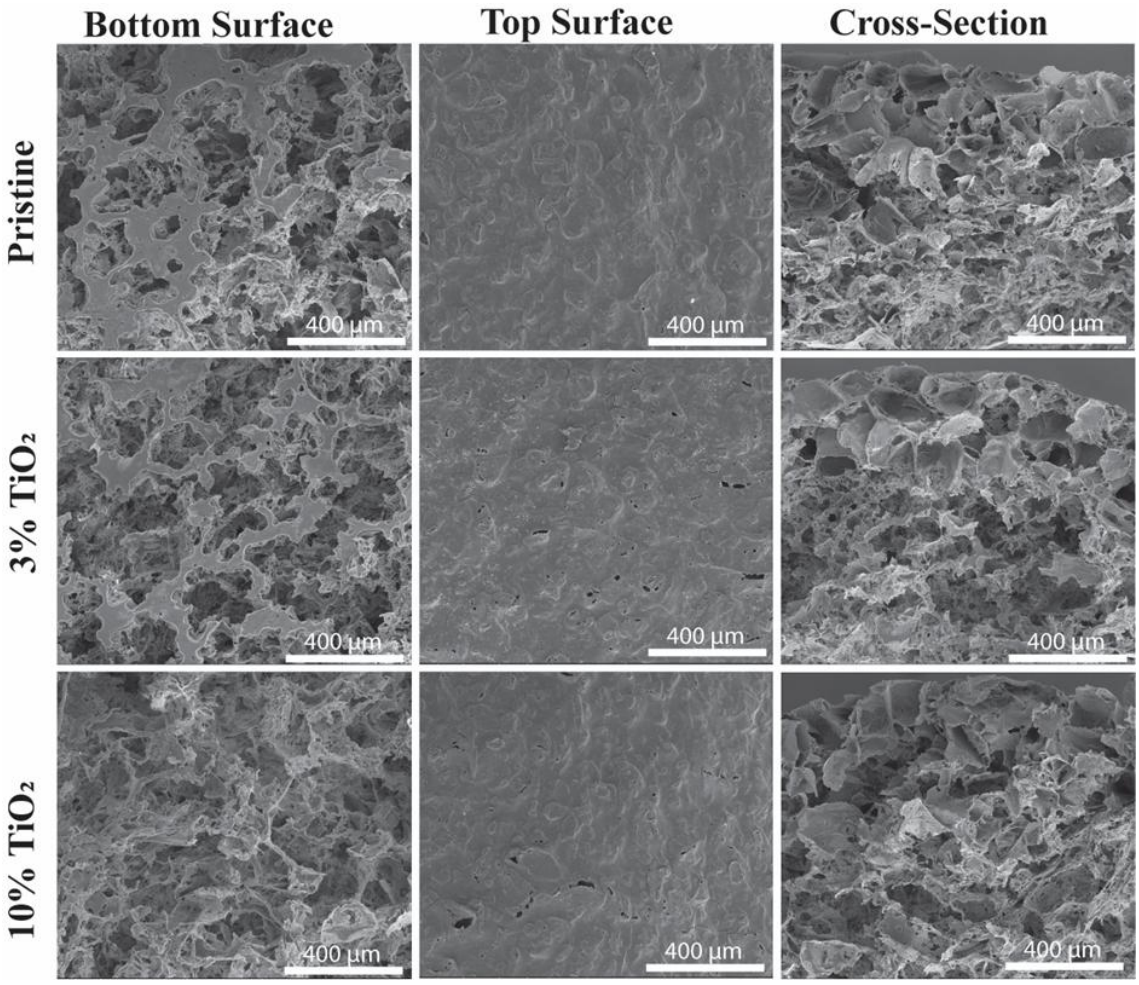


Figure 5.6. SEM images of the produced samples: Pristine bottom surface, top surface and cross-section; 3% TiO_2 bottom surface, top surface and cross-section; 10% TiO_2 bottom surface, top surface and cross-section.

The wettability of the grids was studied by measuring the contact angle of a water droplet, as represented in Figure 5.7a. Contact angle measurements showed an asymmetric wettability in all samples: the top surface of the grids exhibited hydrophobic behaviour (θ> 90°), while the bottom surface remained hydrophilic (θ< 90°), in contrast with the hydrophobic nature of PVDF-HFP-based materials [54]. The incorporation of TiO_2 (3, 5, 10%) further influenced this trend, leading to a gradual decrease in contact angles on both surfaces as nanoparticle loading increased. However, the top surface remained consistently more hydrophilic than the bottom surface. This behaviour is explained by the introduction of NaCl, which led to the formation of a homogeneous, interconnected, highly porous structure, both on the surface and internally, as corroborated by SEM (Figure 5.6, cross-section), thereby increasing the wettability of the printed structure. In fact, it has been reported that the wettability of PVDF samples increases with increasing porosity, with contact angles ranging from 60° to 70° [55].

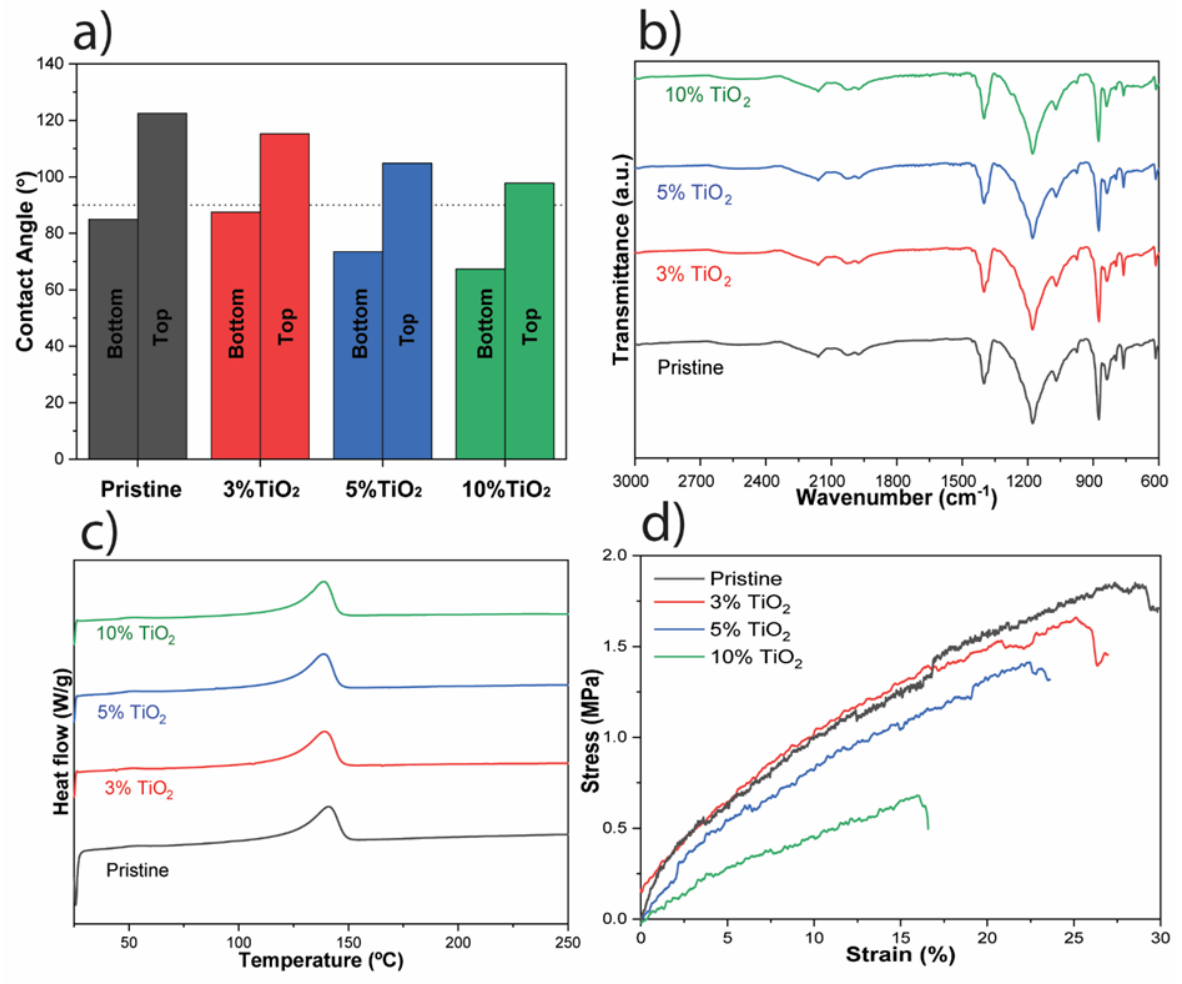


Figure 5.7. For the different grid samples: a) Contact angle measurements on both surfaces; b) FTIR spectra; c) DSC thermograms; d) Stress-strain graphs.

The influence of the incorporation of TiO_2 nanoparticles on the PVDF-HFP chemical characteristics of PVDF-HFP was evaluated by FTIR-ATR measurements (Figure 5.7b). Pristine P(VDF-HFP) sample shows the characteristic vibration modes of this polymer, including the ones at 840 cm^{-1} and 879 cm^{-1}, which are related to C–C–C asymmetrical stretching vibrations and C-F stretching vibration modes, respectively. The presence of an absorption band at 840 cm^{-1} and the absence of other characteristic absorption bands indicative of different crystalline phases indicate that the polymer crystallises into the electroactive β phase [56]. The absorption bands at 1069, 1179 and 1403 cm^{-1} correspond to the wagging of the CH_2 bonds, antisymmetric CF_2 stretching vibrations, and CF_3 deformations and to a symmetric stretch of the C-F bonds and the CH_2 wagging vibration bonds, respectively, indicating the polar β-phase chain conformation of the polymer [57-59]. Most importantly, the addition of TiO_2 does not significantly alter the grid's chemical characteristics.

DSC was used to study the thermal characteristics, as shown in Figure 5.7c. In all samples, an endothermic peak appears around 140 °C, indicating the melting of the polymeric matrix. A slight shift of these peaks to the left is observed upon the addition of nanoparticles to the polymer. The TiO_2 nanoparticles hinder the crystallisation of PVDF-HFP, leading to flawed crystalline structures, especially at the polymer-nanoparticle interfaces [29].

The mechanical stress-strain characteristic curves of the pristine grid (grey line) and TiO_2-loaded grid (red, blue, and green lines) are shown in Figure 5.7d. It is important to note that this assay is only valid to assume values to the grid itself, not the material, due to its different and characteristic morphology; this assay was also performed on the other grids with different morphologies like 8%, 10% and 12% infill (inf), showing that the lower the infill the most the elongation, as less infill means bigger gaps between the lines, that tend to elongate more when strained. The pristine 10inf grid showed a maximum strain of around 27%; in contrast, the TiO_2-loaded grids exhibited lower values: 25%, 22%, and 15% for 3%, 5%, and 10% TiO_2 loadings, respectively. Although porous, the grids exhibit greater elongation resistance than porous structures produced by other techniques [60]. This occurs due to the grid's specific morphology. The introduction of nanoparticles reduced the maximum stress from 1.84 MPa to 0.68 MPa when comparing the pristine grid with the 10% TiO_2-loaded grid. The latter still exhibits better properties than the DIW-printed grids reported in other works, although with different morphologies [39].

5.3.2 Photocatalytic Tests

5.3.2.1 Photocatalytic degradation of ciprofloxacin under UV radiation and grid reusability

The photocatalytic efficiency of the produced grids was assessed in a batch system using 300 mL of CIP solution (5 mg/L), with degradation monitored under UV radiation for 540 min, as shown in Figure 5.8a and b. Table 5.1 presents the calculated degradation efficiency and kinetic rate obtained using Eq. 1.3 for each grid. Photolysis of the CIP and the photocatalytic activity of the pristine grid, 10Inf, were also performed as control experiments. Minimal degradation of CIP was observed in the absence of the grid or nanoparticles compared to the TiO_2-immobilised grids after 540 min of UV exposure, indicating that neither UV irradiation alone nor the PVDF-HFP pristine grid without TiO_2 can achieve significant CIP degradation.

Afterwards, the CIP degradation results of the TiO_2-immobilised grids with different configurations were compared to determine the optimal balance between the material usage and photocatalytic efficiency (Figure 5.8a). The grids 8Inf/10% TiO_2, 10Inf/10% TiO_2, and 12Inf/10% TiO_2 were fabricated using the same ink formulation containing 10% w/w TiO_2 relative to the PVDF-HFP polymer. However, the 8Inf/10%TiO_2 grid used the least ink, producing a more open grid structure with greater spacing between printed lines, whilst the 12Inf/10%TiO_2 grid used the most, producing a denser grid structure with higher material coverage (See section 5.3.1, Figure 5.5). The degradation efficiencies for the 8Inf/10% TiO_2, 10Inf/10% TiO_2, and 12Inf/10% TiO_2 grids were 28%, 45%, and 73%, respectively, while the corresponding kinetic rates were 0.0005 min^{-1}, 0.0014 min^{-1}, and 0.0035 min^{-1}. An increase in CIP degradation efficiency and kinetic rate was observed with higher material usage during grid fabrication, attributed to greater material coverage and the amount of TiO_2 in the grid configuration, which increased the availability of active sites and thereby favoured photocatalytic performance.

Furthermore, the degradation efficiency increased from 28% for the 8Inf/10% TiO_2 grid to 45% for the 10Inf/10% configuration, indicating a clear improvement with increasing material coverage. A further increase to 12Inf/10% TiO_2 resulted in the highest degradation efficiency (73%), confirming that higher infill densities can enhance photocatalytic performance. However, the transition from 10Inf to 12Inf required a substantially larger amount of material to achieve a proportional increase in degradation efficiency. When considering performance gains relative to material usage and process efficiency, the 10Inf/10% TiO_2 configuration represents a more balanced and resource-efficient design.

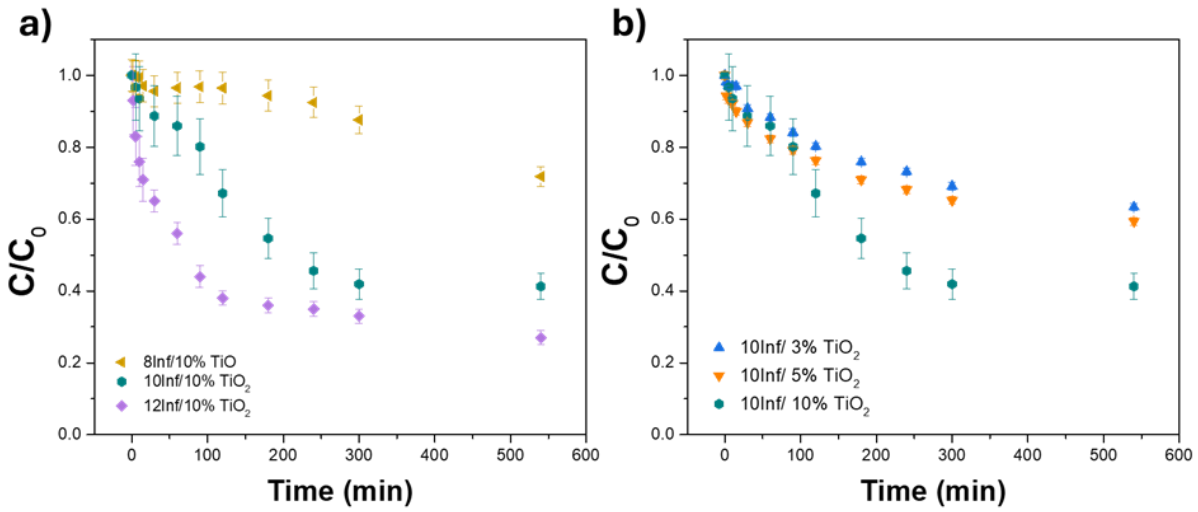


Figure 5.8. Photocatalytic degradation of CIP (5 mg/L) in ultrapure water using TiO_2-immobilised grids under 540 min of UV radiation: a) different grid configuration (8, 10, and 12Inf) with the same TiO_2 loading (10%); b) 10Inf grid configuration with different TiO_2 loading (3,5, and 10%).

It the following, we will focus on the 10Inf/10% TiO_2 grid as it provides a balance compromise between photocatalytic performance, material consumption, and process sustainability, while maintaining a robust and scalable fabrication strategy.

The next step was to determine the optimal TiO_2 loading in the ink formulation, as photocatalytic efficiency depends strongly on the amount of immobilised photocatalysts [25, 62]. The grids 10Inf/3% TiO_2, 10Inf/5% TiO_2, and 10Inf/10% TiO_2, with the same configuration (10Inf), were produced using an ink formulation containing 3%, 5%, and 10% w/w TiO_2 relative to the PVDF-HFP polymer, and the degradation efficiencies and kinetic rates are presented in Figure 5.8b and Table 5.1. The CIP degradation efficiency increased from 37% to 45% with a corresponding increase from 3 to 10 wt.% of nanoparticle loading, while the kinetic rate increased from 0.0011 min^{-1} to 0.0014 min^{-1}. This increase in degradation efficiency and reaction rate with increasing TiO_2 nanoparticle load in the grid was due to the greater available photocatalytic surface area, which enhanced photocatalytic degradation [29, 62].

Table 5.1. CIP (5 mg/L) degradation efficiency kinetic rate in ultrapure water under 540 min of UV radiation for pristine grid and TiO_2-immobilised grids with different configurations.

Sample	Degradation efficiency (%)	Kinetic rate (min^{-1})
Photolysis	14%	0.0002
Pristine grid	12%	0.0002
8inf/10%TiO_2	28%	0.0005
10inf/3%TiO_2	37%	0.0011
10inf/5%TiO_2	41%	0.0013
10inf/10%TiO_2	45%	0.0014
12inf/10%TiO_2	73%	0.0035

A comparative study of previous works employing 3D printing technology for photocatalytic applications in water remediation is presented in Table 5.2. Most existing works have used 3D printing processes and polymers, different from those used in the current work, to develop 3D-printed polymeric grids with mesh or grid-like configurations. Additionally, although a direct comparison cannot be made due to variations in experimental conditions and setups among the different works, this comparative analysis allows us to contextualise our findings within the existing literature. In general, the degradation efficiencies achieved in the present work are comparable to those reported in the literature. For instance, McQueen *et al.* immobilised TiO_2 in a polylactic acid (PLA) disc with a mesh configuration via 3D printing, which degraded 54% of polycyclic aromatic hydrocarbons (PAHs) after 6 h [63]. Similarly, Ortega-Columbrans *et al.* used 3D printing to fabricate a PLA plate with a mesh structure for TiO_2 immobilisation, achieving 60% degradation of methyl orange (MO) after 24 h [64]. Another study incorporated TiO_2 into 3D-printed low-density polyethylene (LDPE) mesh to reach 30% degradation efficiency of ofloxacin (OFX) after 2 h [65]. However, all these works were conducted under significantly lower initial contaminant concentrations or less persistent contaminants.

They also used more materials to fabricate the 3D support for photocatalyst immobilisation, or employed a higher-energy, higher-intensity light source than in the present work, which enhanced photocatalytic performance but also increased operational costs.

On the other hand, the present work examines the optimal balance between material use and photocatalytic efficiency, utilising a greener solvent for sample production, which aligns with the principles of the circular economy. The floating character of the 3D-printed grid allows it to remain at the air-water interface, thereby increasing light exposure and enhancing photocatalytic efficiency.

Moreover, this work evaluated the photocatalytic activity of the produced polymeric grid in a scale-up photoreactor, confirming its potential applicability for large-scale implementation in persistent antibiotic degradation.

Table 5.2. Comparison of the photocatalytic efficiency of 3D-printed grids with grid/mesh configuration.

Materials	Contaminant	[Contaminant] (mg/L)	Radiation	Degradation efficiency (%)	Time (h)	Reference
PLA/15%TiO_2	Polycyclic aromatic hydrocarbons (PAHs)	0.01	UV (2.5 W/m^2)	54	6	[63]
LDPE/1%TiO_2	Ofloxacin (OFX)	1	UV (300–380 nm)	30	2	[65]
PLA/15%TiO_2	Methyl orange (MO)	3	Simulated sunlight lamp (150 W)	60	24	[64]
PVDF-HFP/10%TiO_2	Ciprofloxacin (CIP)	5	UV (6 W/m^2)	45	9	This work

Although the immobilisation of photocatalysts can facilitate reuse and minimise their release into the environment, immobilised systems exhibit lower photocatalytic efficiency that non-immobilised counterparts due to the loss of active sites and poor nanoparticle attachment [62, 66]. Therefore, assessing the efficiency loss of the printed polymeric photocatalytic grids after reutilisation cycles is crucial to prove the reusability of the designed grids for cost-effective contaminant degradation.

The 10Inf/10% TiO_2 grid was thus assessed for reusability to confirm its stability after repeated photocatalytic applications. The same experimental conditions for the photocatalytic assays of grids under UV radiation were employed in three consecutive uses. The grid was washed with ultrapure water, dried at room temperature, and then contacted with a fresh 5 mg/L CIP solution in the photoreactor between each use cycle. Figure 5.9 illustrates the results of three reutilisation cycles, while the degradation efficiencies and kinetic rates are summarised in Table 5.3. Efficiencies of 45%, 52%, and 59% were observed in the first, second, and third use cycles, respectively. The degradation kinetic rates were 0.0014 min^{-1}, 0.0017 min^{-1}, and 0.0031 min^{-1}. This increase in efficiency and reaction rate during reutilisation is attributed to enhanced contact between the contaminant and the photocatalyst [62, 67].

A comparative evaluation of prior works on the reusability of photocatalysts immobilised onto 3D-printed polymeric supports for contaminant degradation was carried out. These remains a lack of studies

evaluating the reusability of 3D-printed photocatalytic grids with specific grid configurations. Thus, this comparison was made with reusable 3D-printed photocatalytic supports available in the literature, regardless of their geometry or structural configuration. Given differences in experimental conditions and materials across studies, the comparison focuses solely on the loss in degradation efficiency after the reusability assay, as this metric is less sensitive to these parameters and provides a more consistent basis for contextualising our results. In general, previously reported works demonstrated a greater loss of photocatalytic efficiency than in the present work for the degradation of less persistent contaminants.

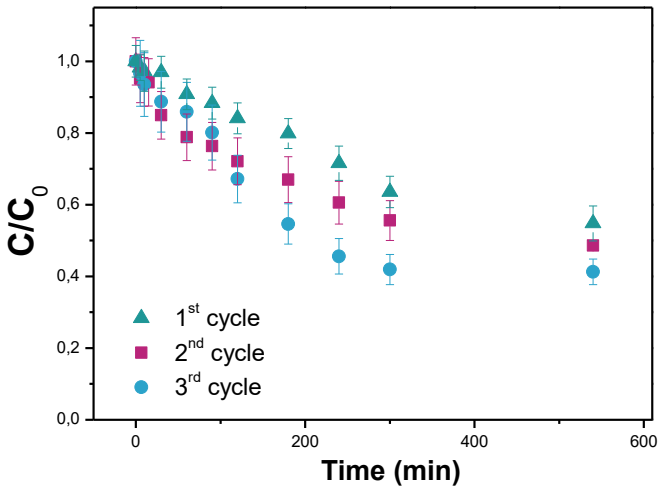


Figure 5.9. Photocatalytic degradation of CIP (5 mg/L) in three consecutive uses in ultrapure water with 10inf/10%TiO_2 grid under 540 min of UV radiation.

Table 5.3. CIP (5 mg/L) degradation efficiency and kinetic rate in three consecutive uses with 10Inf/10%TiO_2 in ultrapure water under 540 min of UV radiation.

Use cycle	Degradation efficiency (%)	kinetic rate (min^{-1})
1st	45	0.0014
2nd	52	0.0017
3rd	59	0.0031

Furthermore, most of these works were carried out in a small-scale reactor. For example, Grandcolas *et al.* tested the reusability of a 3D-printed polyamide/TiO_2 composite, which exhibited a 3% loss in

efficiency after five uses for methylene blue (MB) degradation [68]. Similarly, Do *et al.* explored the reusability of 3D-printed styrene-acrylate (DC668)/TiO_2 thin film for rose bengal (RB) degradation, observing a 5% efficiency loss after three uses [69]. In our previous work [39], a 3D-printed PVDF-HFP grid containing TiO_2 (PVDF-HFP/TiO_2) was used to degrade the same antibiotic as in this work, ciprofloxacin, resulting in a 14% efficiency loss after three uses. As previously mentioned, most reported works targeted less persistent contaminants and were conducted in small-scale reactors. In contrast, the present work evaluated the reusability of a 3D-printed photocatalytic grid for the degradation of a persistent antibiotic in a scale-up reactor, demonstrating its robustness, reusability, and potential for long-term application, paving the way for a sustainable and cost-effective water treatment process.

5.3.2.2 Photocatalytic degradation under natural sunlight

After evaluating the photocatalytic performance of the grids under artificial UV radiation, their efficiency was further assessed under natural sunlight to explore photocatalytic behaviour in a more realistic environment, without reliance on an artificial light source.

For this purpose, the 10Inf/10% TiO_2 grid was tested for the photocatalytic degradation of CIP (5 mg/L) under natural solar radiation for 360 min, as presented in Figure 5.10. The obtained degradation efficiency and kinetic rate are presented in Table 5.4. In parallel, control experiments, photolysis of the CIP and the photocatalytic activity of the pristine grid (10Inf), were also conducted (Figure 5.10). As expected, there was minimal CIP degradation in the absence of the grid or nanoparticles after 360 min of sunlight exposure, confirming that solar irradiation alone or the pristine polymeric grid contributed little to CIP photodegradation.

In contrast, 10Inf/10% TiO_2 grid exhibited a high photocatalytic performance, achieving a complete CIP degradation within only 120 min of sunlight exposure, with a corresponding kinetic rate of 0.0203 min^{-1}. However, under artificial UV radiation, the same grid achieved only 45% degradation efficiency after 540 min (Figure 5.8), corresponding to a kinetic rate of 0.0014 min^{-1}. This outstanding photocatalytic activity under sunlight is noteworthy, as TiO_2 is activated only by UV radiation (<387 nm), which accounts for ≈4% of the radiation provided by the sun [70-72].

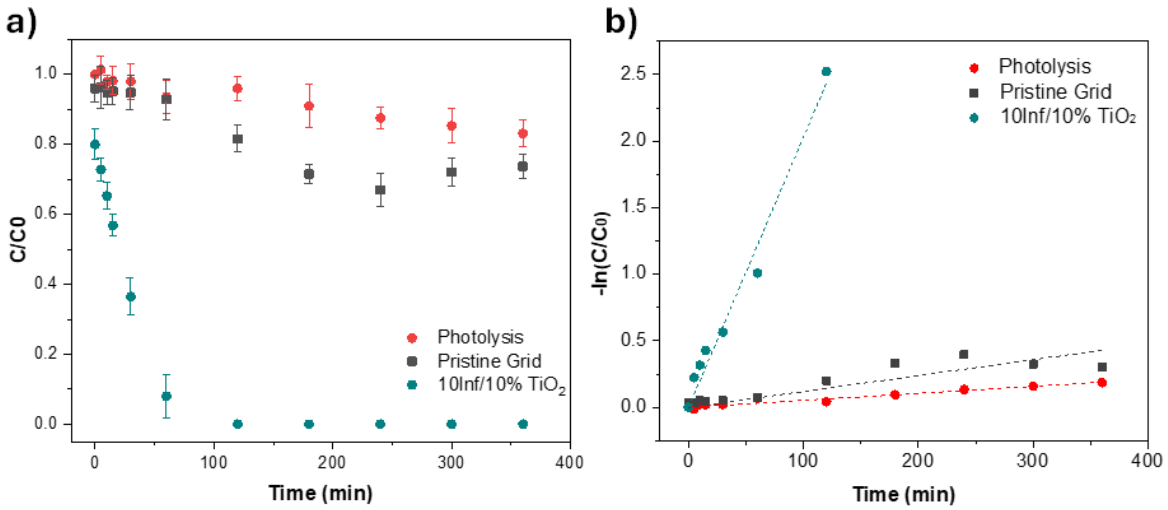


Figure 5.10. Photocatalytic degradation of CIP (5 mg/L) with pristine grid, 10Inf, and TiO_2-immobilised grid,10Inf/10%TiO_2 under 360 min of natural sunlight radiation: a) degradation efficiency; b) corresponding kinetic rate.

Table 5.4. CIP (5 mg/L) degradation efficiency and kinetic rate with 10Inf/10%TiO_2 in ultrapure water under 360 min of natural sunlight radiation.

Photocatalytic System	Degradation efficiency (%)	Kinetic rate (min^{-1})
Photolysis	17	0.0005
Pristine Grid	26	0.0012
10Inf/10% TiO_2	100	0.0203

On the other hand, a notable difference in CIP degradation was observed between the efficiency obtained under UV lamp irradiation and that achieved with natural sunlight as the energy source. This difference may be explained by variations in the intensity and spectral distribution of the irradiation source [73, 74]. The UV lamp provided an intensity of 6 W/m^2, whereas the UV from natural solar radiation reached nearly 30 W/m^2 during the photocatalytic experiment (Supplementary Information). Given that higher intensity provides more energy for TiO_2 activation, generating a larger amount of reactive oxygen species (ROS), the degradation efficiency of CIP was higher under solar radiation than artificial UV radiation [73]. Furthermore, the UV lamp has an emission peak at 365 nm. In contrast, natural sunlight spans the entire UV spectrum and some of the visible spectrum, with energy above the bandgap energy

(3.10 eV) of the photocatalyst TiO_2 [70], providing enough energy to activate TiO_2 and accelerate CIP degradation [75].

Moreover, the obtained results are first compared with those of previously studied immobilised floating photocatalytic materials (Table 5.5). There is only a minimal body of literature that has explored floating materials in photocatalysis for environmental applications, particularly those focused on immobilised systems fabricated using 3D printing technology. Furthermore, it is challenging to make a direct comparison because the experimental conditions and materials used differ across studies. However, this type of comparative analysis allows us to contextualise the performance of the developed floating photocatalytic system within the published works. In general, the present work achieved a degradation efficiency comparable to those reported in the existing literature. For instance, Bertram *et al.* immobilised TiO_2 onto floating poly(dimethylsiloxane) (PDMS) beads, degrading approximately 90% of methylene blue (MB) under UV-visible radiation after 3 h [76]. Similarly, Martin de Vidales *et al.* also explored the fabrication of floating materials by incorporating TiO_2 into low-density polyethylene (LDPE) mesh, which reached 30% degradation of ofloxacin (OFX) under UV radiation after 2 h [65]. Another study incorporated TiO_2 and graphdiyne (GDY) into polydimethylsiloxane (PDMS) to develop a self-floating photocatalytic system, achieving 61.2% MB degradation in the field under natural sunlight [77]. However, these works were conducted under higher light intensities, typically UV, with less persistent contaminants, at lower initial contaminant concentrations, or in small-scale reactors. In contrast, our study immobilised TiO_2 on a floating grid using 3D printing technology, achieving an optimal balance between material use and photocatalytic efficiency and enabling complete degradation of the persistent contaminant ciprofloxacin after 2 h under natural solar radiation. The fabricated floating grid was further tested in a scale-up photoreactor, confirming its potential applicability for large-scale photocatalytic applications.

Table 5.5. Comparison of photocatalytic efficiency for immobilised floating photocatalytic system based on TiO_2.

Materials	Contaminant	[Contaminant] (mg/L)	Radiation	Degradation efficiency (%)	Time (h)	Reference
TiO_2/PDMS	Methylene blue (MB)	10	UV–visible light (40 mW/m^2	90	3	[76]
TiO_2/LDPE	Ofloxacin (OFX)	1	UV (300–380 nm)	30	2	[65]

TiO_2/GDY/PDMS	Methylene blue (MB)	5	Natural sunlight (≈75 mW/cm²)	61.2	8	[77]
TiO_2/PVDF-HFP	Ciprofloxacin (CIP)	5	Natural sunlight (≈ 30 mW/cm²)	100	2	This work

Subsequently, the results are compared with studies on CIP photocatalytic degradation using nanoparticles in suspension under natural sunlight, as shown in Table 5.6. Again, it should be emphasised that direct comparisons of degradation efficiency are difficult due to variations in experimental conditions and setups, such as CIP concentration, photocatalytic system, and irradiation conditions. In this case, the comparison focuses on suspended vs. immobilised systems, which obviously differ significantly. However, this comparative exercise is relevant because it clearly demonstrates the remarkable efficiency of the floating grids, which can be compared with suspended nanoparticle setups. In general, each reported work showed high CIP degradation under natural solar radiation. Bhuin *et al.* used ZnO to degrade CIP under natural sunlight, achieving a 90% degradation efficiency after 2 h [78]. However, this efficiency is lower than that achieved in our work, despite the use of a lower initial CIP concentration. Other works have studied CIP degradation at higher initial concentrations than those used in the present work. For instance, Yilmaz *et al.* achieved a 94% degradation of 50 mg/L of CIP using a Fe_2O_4/ZnO/GO nanocomposite after 2 h [79]. Similarly, Bazzanella *et al.* reported a 95% degradation of 10 mg/L CIP using TiO_2 after 3 h [80]. In another study, Gayathri *et al.* developed potassium-doped g-C_3N_4 (K-g-C_3N_4) nanoparticles, achieving 99% degradation of CIP at an initial concentration of 30 mg/L after 3 h [81]. Although these studies demonstrated remarkable CIP degradation under natural solar radiation, they employed suspended photocatalysts, suggesting a high density of active sites for photocatalytic degradation [62]. In addition, this suspended photocatalytic system has several drawbacks, including difficulties in photocatalyst recovery and reuse [39] and potential secondary contamination [25]. On the contrary, the present work demonstrates significant photocatalytic degradation of CIP under natural sunlight, despite employing an immobilised photocatalytic system with fewer active sites than the suspended system [25]. Furthermore, our study offers a cost-effective, practical approach based on an immobilised floating system developed via 3D printing, demonstrating its potential for sustainable, customisable, large-scale photocatalytic water-treatment applications under realistic environmental conditions.

Table 5.6. Comparison of photocatalytic efficiency for CIP degradation under natural solar radiation.

Materials	Photocatalytic system	[CIP] (mg/L)	Degradation efficiency (%)	Time (h)	Reference
ZnO	Suspension	2.8	90	2	[78]
Fe_3O_4/ZnO/GO	Suspension	50	94	2	[79]
TiO_2	Suspension	10	95	3	[80]
K-g-C_3N_4	Suspension	30	99	3	[81]
TiO_2/PVDF-HFP	Immobilisation	5	100	2	This work

5.4 Conclusions

In this work, an innovative DIW 3D printing approach was developed to produce floating PVDF-HFP grids incorporating TiO_2, using acetone as a more sustainable solvent. The process was comprehensively optimised by tuning the infill parameters (8%, 10% and 12%), balancing the material used against photocatalytic efficiency, and evaluating different TiO_2 loadings (3, 5, and 10 wt. %) to maximise photocatalytic performance.

The resulting grids demonstrated chemical, thermal, and mechanical stability, as well as a uniform, interconnected porous structure that is favourable to the percolation of the contaminated solution. The 1 mm grid line thickness ensured light penetration to the photocatalyst, whereas TiO_2 incorporation progressively reduced the hydrophobicity of PVDF-HFP, thereby increasing water penetration and, consequently, enhancing contact between the contaminant and the photocatalyst.

The best performance was achieved for 12Inf/10% TiO_2 grid achieving a degradation efficiency of 73%. The 10Inf/10% TiO_2 grid, with a suitable balance between material use and functional performance, achieved 45% CIP degradation under UV radiation, with a 14% improvement after three reuse cycles. Under natural sunlight, the performance was even more remarkable, with complete degradation occurring within 120 min, and a kinetic rate (0.0203 min^{-1}) comparable to that of suspension systems, yet without the drawbacks of particle recovery, dispersion, or ecological impact.

Together, these results demonstrate that DIW-fabricated PVDF-HFP grids constitute a customisable, scalable, and sustainable platform for sunlight-driven remediation of emerging contaminants. Their inherent floatability enables effective operation on any water matrix, maximising irradiation exposure. At the same time, the 'open' geometry of the grid ensures continued light penetration into deeper water masses, thereby minimising the ecological impact on aquatic organisms. In this way, the herein developed

grids offer a unique trade-off between water remediation and low ecosystem impact. Moreover, the high photocatalytic efficiency obtained, together with a straightforward recovery and consistent reuse of the grids, corroborates their potential as a practical photocatalytic technology for real-world implementation.

This proposed approach represents a significant step toward energy-efficient, scalable, and environmentally responsible water treatment technologies, paving the way for the next generation of floating immobilised photocatalytic systems.

5.5 References

[1] A.C. da Silva, L.V. Alves de Oliveira, L. Amaral Alexandre, M. Rocha Ribas, J. Lemos Dal Pizzol, G. Rocha, J. Kasuko Palmeiro, M. Perin, R. Hoff, S. Verruck, Suspect screening and quantitative analysis of 165 contaminants of emerging concern in water, sediments, and biota using LC-MS/MS: Ecotoxicological and human health risk assessment, Science of The Total Environment, 963 (2025) 178434.

[2] B. Das, S. Sarkar, S. Paul, A. Zafar, D. Biswas, J.R. Panda, T. Chakraborty, Mitigation Strategies of Emerging Pollutants from Cosmetic Industry Effluent: A Review, European Journal of Theoretical and Applied Sciences, 2 (2024) 886-899.

[3] J. Peluso, A.M. Chehda, M.S. Olivelli, F.M. Ivanic, C.S. Pérez Coll, F. Gonzalez, L. Valenzuela, D. Rojas, D. Cristos, M. Butler, R.J. Candal, C.M. Aronzon, Metals, pesticides, and emerging contaminants on water bodies from agricultural areas and the effects on a native amphibian, Environmental Research, 226 (2023) 115692.

[4] M.N. Issac, B. Kandasubramanian, Effect of microplastics in water and aquatic systems, Environmental Science and Pollution Research, 28 (2021) 19544-19562.

[5] X. Li, X. Shen, W. Jiang, Y. Xi, S. Li, Comprehensive review of emerging contaminants: Detection technologies, environmental impact, and management strategies, Ecotoxicology and Environmental Safety, 278 (2024) 116420.

[6] A.S. Ripanda, M.J. Rwiza, E.C. Nyanza, K.N. Njau, S.A.H. Vuai, R.L. Machunda, A Review on Contaminants of Emerging Concern in the Environment: A Focus on Active Chemicals in Sub-Saharan Africa, Applied Sciences, 2022.

[7] Statista.com, Prescription Drugs - Europe, 2025.

[8] B.M. Al-howri, S. Ismail, M. Khajavian, comprehensive review of ciprofloxacin pollution in water: sources, environmental impacts, remediation techniques, and research challenges, Environmental Monitoring and Assessment, 197 (2025) 1095.

[9] N. Martins, R. Pereira, N. Abrantes, J. Pereira, F. Gonçalves, C.R. Marques, Ecotoxicological effects of ciprofloxacin on freshwater species: data integration and derivation of toxicity thresholds for risk assessment, Ecotoxicology, 21 (2012) 1167-1176.

[10] R. Wei, F. Ge, M. Chen, R. Wang, Occurrence of Ciprofloxacin, Enrofloxacin, and Florfenicol in Animal Wastewater and Water Resources, Journal of Environmental Quality, 41 (2012) 1481-1486.

[11] M. Sarafraz, S. Ali, M. Sadani, Z. Heidarinejad, A. Bay, Y. Fakhri, A. Mousavi Khaneghah, A global systematic, review-meta analysis and ecological risk assessment of ciprofloxacin in river water, International Journal of Environmental Analytical Chemistry, 102 (2022) 5106-5121.

[12] F. Hernández, N. Calısto-Ulloa, C. Gómez-Fuentes, M. Gómez, J. Ferrer, G. González-Rocha, H. Bello-Toledo, A.M. Botero-Coy, C. Boıx, M. Ibáñez, M. Montory, Occurrence of antibiotics and bacterial

resistance in wastewater and sea water from the Antarctic, Journal of Hazardous Materials, 363 (2019) 447-456.

[13] D. Mosca Angelucci, F. Piergiacomo, E. Donati, L. Pagani, E. Minuti, L. Brusetti, M.C. Tomei, Combined effects of ciprofloxacin and microplastics on alpine spring water microbiota: evidence from glacier-fed microcosm experiments, Frontiers in Microbiology, Volume 16 - 2025 (2025).

[14] U. Hubicka, J. Krzek, M. Walczak, Stability of ciprofloxacin and norfloxacin in the presence and absence of metal ions in acidic solution, Pharmaceutical Development and Technology, 15 (2010) 532-544.

[15] M.A. Al-Omar, Ciprofloxacin: Drug Metabolism and Pharmacokinetic Profile, in: H.G. Brittain (Ed.) Profiles of Drug Substances, Excipients and Related Methodology, Academic Press2005, pp. 209-214.

[16] R.J.A. Felisardo, E. Brillas, L.F. Romanholo Ferreira, E.B. Cavalcanti, S. Garcia-Segura, Degradation of the antibiotic ciprofloxacin in urine by electrochemical oxidation with a DSA anode, Chemosphere, 344 (2023) 140407.

[17] J. Hu, J. Chen, W. Wang, L. Zhu, Mechanism of growth inhibition mediated by disorder of chlorophyll metabolism in rice (Oryza sativa) under the stress of three polycyclic aromatic hydrocarbons, Chemosphere, 329 (2023) 138554.

[18] B. Fu, E. Li, Y. Yan, S. Jiang, Y. Wu, Y. Ma, Ecological criteria for antibiotics in aquatic environments based on species sensitivity distribution, Ecotoxicology and Environmental Safety, 287 (2024) 117261.

[19] Y. Wang, X. Dong, J. Zang, X. Zhao, F. Jiang, L. Jiang, C. Xiong, N. Wang, C. Fu, Antibiotic residues of drinking-water and its human exposure risk assessment in rural Eastern China, Water Research, 236 (2023) 119940.

[20] S. Lim, J.L. Shi, U. von Gunten, D.L. McCurry, Ozonation of organic compounds in water and wastewater: A critical review, Water Research, 213 (2022) 118053.

[21] M.-h. Zhang, H. Dong, L. Zhao, D.-x. Wang, D. Meng, A review on Fenton process for organic wastewater treatment based on optimization perspective, Science of The Total Environment, 670 (2019) 110-121.

[22] Y. Choi, D. Lee, S. Hong, S. Khan, B. Darya, J.-Y. Lee, J. Chung, S.-H. Cho, Investigation of the Synergistic Effect of Sonolysis and Photocatalysis of Titanium Dioxide for Organic Dye Degradation, Catalysts, 2020.

[23] H. Wang, Y. Wang, D.D. Dionysiou, Advanced Oxidation Processes for Removal of Emerging Contaminants in Water, Water, 2023.

[24] W.S. Koe, J.W. Lee, W.C. Chong, Y.L. Pang, L.C. Sim, An overview of photocatalytic degradation: photocatalysts, mechanisms, and development of photocatalytic membrane, Environmental Science and Pollution Research, 27 (2020) 2522-2565.

[25] P.M. Martins, R. Miranda, J. Marques, C.J. Tavares, G. Botelho, S. Lanceros-Mendez, Comparative efficiency of TiO2 nanoparticles in suspension vs. immobilization into P(VDF–TrFE) porous membranes, RSC Advances, 6 (2016) 12708-12716.

[26] C. Sun, J. Yang, M. Xu, Y. Cui, W. Ren, J. Zhang, H. Zhao, B. Liang, Recent intensification strategies of SnO2-based photocatalysts: A review, Chemical Engineering Journal, 427 (2022) 131564.

[27] C.N.C. Hitam, A.A. Jalil, A review on exploration of Fe2O3 photocatalyst towards degradation of dyes and organic contaminants, Journal of Environmental Management, 258 (2020) 110050.

[28] S. Abou Zeid, Y. Leprince-Wang, Advancements in ZnO-Based Photocatalysts for Water Treatment: A Comprehensive Review, Crystals, 2024.

[29] P.M. Martins, B. Santos, H. Salazar, S.A.C. Carabineiro, G. Botelho, C.J. Tavares, S. Lanceros-Mendez, Multifunctional hybrid membranes for photocatalytic and adsorptive removal of water contaminants of emerging concern, Chemosphere, 293 (2022) 133548.

[30] S.-Y. Lee, S.-J. Park, TiO2 photocatalyst for water treatment applications, Journal of Industrial and Engineering Chemistry, 19 (2013) 1761-1769.

[31] P.M. Martins, V. Gomez, A.C. Lopes, C.J. Tavares, G. Botelho, S. Irusta, S. Lanceros-Mendez, Improving Photocatalytic Performance and Recyclability by Development of Er-Doped and Er/Pr-Codoped TiO2/Poly(vinylidene difluoride–Trifluoroethylene Composite Membranes, The Journal of Physical Chemistry C, 118 (2014) 27944-27953.

[32] K. Fouad, M. Bassyouni, M.G. Alalm, M.Y. Saleh, Recent developments in recalcitrant organic pollutants degradation using immobilized photocatalysts, Applied Physics A, 127 (2021) 612.

[33] P.M. Martins, S. Ribeiro, C. Ribeiro, V. Sencadas, A.C. Gomes, F.M. Gama, S. Lanceros-Méndez, Effect of poling state and morphology of piezoelectric poly(vinylidene fluoride) membranes for skeletal muscle tissue engineering, RSC Advances, 3 (2013) 17938-17944.

[34] P.J. Bruinsma, A.Y. Kim, J. Liu, S. Baskaran, Mesoporous Silica Synthesized by Solvent Evaporation: Spun Fibers and Spray-Dried Hollow Spheres, Chemistry of Materials, 9 (1997) 2507-2512.

[35] R. Xing, R. Huang, W. Qi, R. Su, Z. He, Three-dimensionally printed bioinspired superhydrophobic PLA membrane for oil-water separation, AIChE Journal, 64 (2018) 3700-3708.

[36] P. Sun, L. Zhang, S. Tao, Preparation of hybrid chitosan membranes by selective laser sintering for adsorption and catalysis, Materials & Design, 173 (2019) 107780.

[37] L. Zárybnická, Z. Meloun, J. Šafka, V. Truxová, K. Dvořák, J. Machotová, 3D printed heterogeneous cation exchange membrane processed using stereolithography, Journal of Applied Polymer Science, 140 (2023) e54341.

[38] S.W.Z. Fong, J.Y. Tey, W.H. Yeo, S.F. Tee, Direct ink writing of 17–4PH stainless steel using green binder: Rheological sensitivity and performance assessment, Journal of Manufacturing Processes, 132 (2024) 519-531.

[39] D.C. Alves, P.M. Martins, R. Pinto, P. Costa, B. Bazán, R.F. de Luis, D.M. Correia, S. Lanceros-Méndez, 3D-printed multilayer membranes for photocatalytic degradation of ciprofloxacin, Applied Materials Today, 44 (2025) 102728.

[40] M.A.S.R. Saadi, A. Maguire, N.T. Pottackal, M.S.H. Thakur, M.M. Ikram, A.J. Hart, P.M. Ajayan, M.M. Rahman, Direct Ink Writing: A 3D Printing Technology for Diverse Materials, Advanced Materials, 34 (2022) 2108855.

[41] R. Trombetta, J.A. Inzana, E.M. Schwarz, S.L. Kates, H.A. Awad, 3D Printing of Calcium Phosphate Ceramics for Bone Tissue Engineering and Drug Delivery, Annals of Biomedical Engineering, 45 (2017) 23-44.

[42] A.A. Alsharif, J.M. Aviles, F.M. Zechel, N.A. Alsharif, N. El-Atab, Multi-material direct-ink-writing of silver-based flexible and highly deformable dry electrocardiogram biopatches, VIEW, 5 (2024) 20240008.

[43] P. Jiang, C. Yan, Y. Guo, X. Zhang, M. Cai, X. Jia, X. Wang, F. Zhou, Direct ink writing with high-strength and swelling-resistant biocompatible physically crosslinked hydrogels, Biomaterials Science, 7 (2019) 1805-1814.

[44] C. Ribeiro, C.M. Costa, D.M. Correia, J. Nunes-Pereira, J. Oliveira, P. Martins, R. Gonçalves, V.F. Cardoso, S. Lanceros-Méndez, Electroactive poly(vinylidene fluoride)-based structures for advanced applications, Nature Protocols, 13 (2018) 681-704.

[45] F.U. Ahmed, S. Sharma, D.D. Purkayastha, Buoyancy-Assisted Fabrication of Liquid Diode: Janus Nanofibrous Membrane for Efficient Wastewater Treatment, ACS Applied Materials & Interfaces, 16 (2024) 42641-42659.

[46] A.M. Nasir, J. Jaafar, F. Aziz, N. Yusof, W.N.W. Salleh, A.F. Ismail, M. Aziz, A review on floating nanocomposite photocatalyst: Fabrication and applications for wastewater treatment, Journal of Water Process Engineering, 36 (2020) 101300.

[47] Z. Xing, J. Zhang, J. Cui, J. Yin, T. Zhao, J. Kuang, Z. Xiu, N. Wan, W. Zhou, Recent advances in floating TiO2-based photocatalysts for environmental application, Applied Catalysis B: Environmental, 225 (2018) 452-467.

[48] K. Wang, G. Li, X. Bie, J. Yu, X. Guo, H. Jia, P. Liu, W. Kang, Z. Han, Y. Liu, Floatable Janus nanofiber membrane driven by photothermal bubbles: A novel platform for efficient photocatalytic water purification, Journal of Cleaner Production, 523 (2025) 146368.

[49] F.L. Rashid, M.A. Al-Obaidi, A.K. Hussein, N. Akkurt, B. Ali, O. Younis, Floating solar stills and floating solar-driven membranes: Recent advances and overview of designs, performance and modern combinations, Solar Energy, 247 (2022) 355-372.

[50] P. Christou, Buoyancy-Enhanced Membrane Filtration for Oilfield Produced Water Recycle and Reuse, SPE Annual Technical Conference and Exhibition, 2024, pp. D031S044R003.

[51] A.-M. Solonaru, M. Honciuc, A. Honciuc, Adsorption performance of water-floating composites for heavy metal removal in marine and freshwater systems, Journal of Environmental Chemical Engineering, 13 (2025) 119312.

[52] P. Zhu, Z. Cai, J. Shi, C. Zhu, M. Wang, C. Wang, H. Zhang, Liquid–Liquid Phase Separation, Crystallization, and Solvent Evaporation in Relation to Microsphere Formation from Isotactic Polypropylene Solution, The Journal of Physical Chemistry B, (2025).

[53] H. Manzanarez, J.P. Mericq, P. Guenoun, D. Bouyer, Modeling the interplay between solvent evaporation and phase separation dynamics during membrane, Journal of Membrane Science, 620 (2021) 118941.

[54] V.F. Cardoso, D.M. Correia, C. Ribeiro, M.M. Fernandes, S. Lanceros-Méndez, Fluorinated Polymers as Smart Materials for Advanced Biomedical Applications, Polymers, 10 (2018).

[55] M. Gryta, M.J.J.o.M.S. Barancewicz, Influence of morphology of PVDF capillary membranes on the performance of direct contact membrane distillation, 358 (2010) 158-167.

[56] X. Cai, T. Lei, D. Sun, L. Lin, A critical analysis of the α, β and γ phases in poly(vinylidene fluoride) using FTIR, RSC Advances, 7 (2017) 15382-15389.

[57] G.G. Kumar, K.S. Nahm, R.N. Elizabeth, Electro chemical properties of porous PVdF-HFP membranes prepared with different nonsolvents, Journal of Membrane Science, 325 (2008) 117-124.

[58] L.N. Sim, S.R. Majid, A.K. Arof, FTIR studies of PEMA/PVdF-HFP blend polymer electrolyte system incorporated with LiCF3SO3 salt, Vibrational Spectroscopy, 58 (2012) 57-66.

[59] H. Bai, X. Wang, Y. Zhou, L. Zhang, Preparation and characterization of poly(vinylidene fluoride) composite membranes blended with nano-crystalline cellulose, Progress in Natural Science: Materials International, 22 (2012) 250-257.

[60] D. Zioui, P.M. Martins, L. Aoudjit, H. Salazar, S. Lanceros-Méndez, Wastewater Treatment of Real Effluents by Microfiltration Using Poly(vinylidene fluoride–hexafluoropropylene) Membranes, Polymers, 2023.

[61] T. Rodrigues-Marinho, C.R. Tubio, S. Lanceros-Mendez, P.F.R. Costa, Tailoring the Electrical Response of Polyvinylidene Fluoride Nanocomposites with Electrically Conductive and Dielectric Fillers, Advanced Engineering Materials, 26 (2024) 2301596.

[62] F. Zheng, P.M. Martins, J.M. Queirós, C.J. Tavares, J.L. Vilas-Vilela, S. Lanceros-Méndez, J. Reguera, Hybrid TiO2:Au nanostars based polymeric membranes for photocatalytic degradation of ciprofloxacin in water samples, Chemosphere, 313 (2023) 137630.

[63] A.D. McQueen, M.L. Ballentine, L.R. May, C.H. Laber, A. Das, M.J. Bortner, A.J. Kennedy, Photocatalytic Degradation of Polycyclic Aromatic Hydrocarbons in Water by 3D Printed TiO2 Composites, ACS ES&T Water, 2 (2022) 137-147.

[64] P. Ortega-Columbrans, A. Ferrandez-Montero, J. Yus, A.J. Sanchez-Herencia, B. Ferrari, Processing of membranes and 3D scaffolds based on n-TiO2 colloidally dispersed on a thermoplastic matrix for photocatalytic pollutant removal, Catalysis Today, 426 (2024) 114371.

[65] M.J. Martín de Vidales, A. Nieto-Márquez, D. Morcuende, E. Atanes, F. Blaya, E. Soriano, F. Fernández-Martínez, 3D printed floating photocatalysts for wastewater treatment, Catalysis Today, 328 (2019) 157-163.

[66] S. Teixeira, P.M. Martins, S. Lanceros-Méndez, K. Kühn, G. Cuniberti, Reusability of photocatalytic TiO2 and ZnO nanoparticles immobilized in poly(vinylidene difluoride)-co-trifluoroethylene, Applied Surface Science, 384 (2016) 497-504.

[67] P.M. Martins, J.M. Ribeiro, S. Teixeira, D.Y. Petrovykh, G. Cuniberti, L. Pereira, S. Lanceros-Méndez, Photocatalytic Microporous Membrane against the Increasing Problem of Water Emerging Pollutants, Materials, 2019.

[68] M. Grandcolas, A. Lind, 3D-printed polyamide structures coated with TiO2 nanoparticles, towards a 360-degree rotating photocatalytic reactor, Materials Letters, 307 (2022) 131044.

[69] H.H. Do, T.K.C. Tran, T.D.T. Ung, N.T. Dao, D.D. Nguyen, T.H. Trinh, T.D. Hoang, T.L. Le, T.T.H. Tran, Controllable fabrication of photocatalytic TiO2 brookite thin film by 3D-printing approach for dyes decomposition, Journal of Water Process Engineering, 43 (2021) 102319.

[70] F. Zheng, P.M. Martins, J.M. Queirós, C.J. Tavares, J.L. Vilas-Vilela, S. Lanceros-Méndez, J. Reguera, Size Effect in Hybrid TiO2:Au Nanostars for Photocatalytic Water Remediation Applications, International Journal of Molecular Sciences, 2022.

[71] F. Zheng, J.M. Queirós, P.M. Martins, R.F. de Luis, A. Fidalgo-Marijuan, J.L. Vilas-Vilela, S. Lanceros-Méndez, J. Reguera, Au-sensitised TiO2 and ZnO nanoparticles for broadband pharmaceuticals photocatalytic degradation in water remediation, Colloids and Surfaces A: Physicochemical and Engineering Aspects, 671 (2023) 131594.

[72] P. Martins, S. Kappert, H. Nga Le, V. Sebastian, K. Kühn, M. Alves, L. Pereira, G. Cuniberti, M. Melle-Franco, S. Lanceros-Méndez, Enhanced Photocatalytic Activity of Au/TiO2 Nanoparticles against Ciprofloxacin, Catalysts, 2020.

[73] L. Aoudjit, P.M. Martins, F. Madjene, D.Y. Petrovykh, S. Lanceros-Mendez, Photocatalytic reusable membranes for the effective degradation of tartrazine with a solar photoreactor, Journal of Hazardous Materials, 344 (2018) 408-416.

[74] Y.Y. Gurkan, E. Kasapbasi, Z. Cinar, Enhanced solar photocatalytic activity of TiO2 by selenium(IV) ion-doping: Characterization and DFT modeling of the surface, Chemical Engineering Journal, 214 (2013) 34-44.

[75] L. Aoudjit, J.M. Queirós, A.S. Castro, D. Zioui, N. González-Ballesteros, S. Lanceros-Mendez, P.M. Martins, Sunlight-Induced Photocatalytic Removal of Paracetamol Using Au-TiO2 Nanoparticles, Nanomaterials, 2025.

[76] J.R. Bertram, M.J. Nee, A Buoyant, Microstructured Polymer Substrate for Photocatalytic Degradation Applications, Catalysts, 2018.

[77] J.Y. Son, Y. Jo, H. Lee, Y.J. Jang, H. Kim, Water hyacinth-inspired self-floating photocatalytic system for efficient and sustainable water purification, npj Clean Water, 8 (2025) 51.

[78] A. Bhuin, S. Udayakumar, J. Gopalarethinam, D. Mukherjee, K. Girigoswami, C. Ponraj, S. Sarkar, Photocatalytic degradation of antibiotics and antimicrobial and anticancer activities of two-dimensional ZnO nanosheets, Scientific Reports, 14 (2024) 10406.

[79] M. Yilmaz, H. Moein, A.D. Khatibi, N. Ahmadi, N. Mengelizadeh, D. Balarak, Degradation of Ciprofloxacin Using Magnetic Zinc Oxide Loaded Graphene Oxide for Enhanced Photocatalytic Performance Under Visible and Solar and UV Light Irradiation, ChemistrySelect, 10 (2025) e05864.

[80] N. Bazzanella, O.P. Bajpai, M. Fendrich, G. Guella, A. Miotello, M. Orlandi, Ciprofloxacin degradation with a defective TiO2-x nanomaterial under sunlight, MRS Communications, 13 (2023) 1252-1259.

[81] D. Gayathri, P. Haripriya, S. Pazhedath, N. Pandurangan, B.N. Reddy, D.V.R. Kumar, Doping versus crystallinity: improving the photocatalytic properties of g-C3N4 toward the degradation of ciprofloxacin under direct sunlight, Research on Chemical Intermediates, 51 (2025) 3543-3567.

CHAPTER 6

Conclusions and Future Work

This chapter presents the main conclusions of the work and provides ideas for future developments.

6.1 Conclusions

The persistent presence of antibiotics in aquatic environments represents a major environmental and public health challenge, due to their ecotoxicological impact and their role in the dissemination of antimicrobial resistance. Within this context, the main purpose of this thesis was the development of sustainable and multifunctional photocatalytic materials capable of simultaneously removing antibiotics, antibiotic-resistance bacteria (ARB) and antibiotic-resistant genes (ARGs), while overcoming key limitations of conventional photocatalysis, including catalyst recovery, limited solar activation, and the potential environmental impact of the materials employed.

As a starting point of this work, a systematic screening of (titanium dioxide) TiO_2 nanoparticles functionalised through a green approach was conducted, using quercetin as a reducing agent for the deposition of noble metals (gold - Au and silver - Ag). This strategy enabled not only the extension of TiO_2 light absorption into the visible region—reflected by decreases in diffuse reflectance of approximately 50% in the 500–600 nm range for Au–TiO_2 and 30% between 400 and 500 nm for Ag–TiO_2—but also the selection of nanocomposites exhibiting the most favourable balance between photocatalytic efficiency and durability for the degradation of antibiotics with distinct molecular complexity, namely ciprofloxacin (CIP), trimethoprim (TMP) and sulfadiazine (SDZ), with Au–TiO_2 emerging as the most promising material. Its immobilisation within polyvinylidene fluoride-co-trifluoroethylene (PVDF-HFP) membranes via the thermally induced phase separation (TIPS) technique resulted in a robust porous platform with high chemical, thermal, and mechanical stability, capable of achieving complete degradation of CIP and partial degradation of SDZ and TMP, in line with the structural complexity of each molecule. Importantly, the system maintained stable performance over three consecutive reuse cycles, exhibiting a homogeneous nanoparticle distribution and negligible leaching, as confirmed by scanning electron microscopy-energy dispersive X-ray spectroscopy analysis.

Beyond photocatalytic efficiency, this thesis placed particular emphasis on the environmental impact of the developed systems. The identification of degradation by-products and their assessment of ecotoxicity using luminescent marine bacteria revealed that, in cases of incomplete mineralisation - such as that observed for SDZ - by-products with higher toxicity than the parent compound may form, highlighting the need to integrate ecotoxicological assessment with efficiency studies. In contrast, all produced membranes, including PVDF-HFP, TiO_2/PVDF-HFP, and Au–TiO_2/PVDF-HFP, exhibited no toxic effects, supporting the environmental safety of PVDF-based nanocomposite membranes for potential applications in real aquatic environments.

To enhance sustainability and introduce additional functionalities, a green functionalisation of TiO_2 with Ag and 5-aminosalicylic acid (5-ASA) was explored, enabling bandgap reduction and the incorporation of antimicrobial properties. In parallel, and as part of a broader strategy towards more sustainable material platforms, the transition from synthetic to natural polymeric matrices was investigated by incorporating these nanocomposites into both PVDF-HFP and silk fibroin (SF) membranes. Processed via TIPS in combination with salt leaching, these systems exhibited well-distributed micro-scale porosity and controlled morphology, enabling simultaneous photocatalytic and antimicrobial performance. Despite the limitations often associated with natural polymer-based composites, the SF membranes proved to be a viable, more sustainable alternative, demonstrating good structural stability and reusability, with efficiency losses below 10% across three consecutive cycles. Furthermore, Ag-containing nanocomposites achieved bacterial reductions of 1–2 $\log_{10}$, mitigating the risk of bacterial proliferation in treated aquatic systems.

Maintaining a green, multifunctional materials strategy, quercetin was again used as a sustainable reducing agent for the functionalisation of TiO_2 with silver, allowing the optimisation of Ag loading to simultaneously maximise photocatalytic efficiency under UV–visible irradiation and antimicrobial activity. The functionalised nanoparticles were subsequently immobilised onto PVDF-HFP substrates to develop membranes capable of simultaneously targeting three classes of contaminants: antibiotics, ARB, and ARGs. To this end, the filler content immobilised within the polymeric matrix was increased to enhance antimicrobial activity without compromising material stability. From a functional perspective, the membranes fully achieved the proposed objectives, promoting the efficient degradation of CIP and TMP under both ultraviolet (UV) and simulated solar irradiation. In parallel, a significant improvement in antimicrobial performance was observed, with bacterial load reductions of approximately 8 $\log_{10}$ for *E. coli* and biofilm-inhibition on the material surface of up to ≈70%, a critical factor for the durability and operational lifetime of photocatalytic membranes.

In addition, the composites demonstrated the ability to degrade genetic material associated with antibiotic resistance, achieving efficiencies of up to 73% for the system containing 20%Ag–TiO_2/PVDF-HFP, in agreement with the loss of bacterial viability observed in selective media following photocatalytic treatment. Together, these results confirm the capability of the developed materials to simultaneously act on chemical and biological contaminants while maintaining a structurally stable platform across multiple reuse cycles. These materials' versatility enables direct and indirect intervention against the main vectors associated with the global spread of antibiotic resistance, as they are effective at eliminating the contaminants driving this resistance.

The transition towards a scale closer to real-world application was achieved through additive manufacturing by direct ink writing combined with salt leaching, enabling precise control over material geometry and porosity, without raw material waste and with high adaptability to different application scenarios, using acetone as a non-toxic solvent. Within this framework, a floating PVDF-HFP grid containing 10% TiO_2 was developed and optimised, exhibiting an interconnected porous structure and high chemical, thermal, and mechanical stability. This system achieved CIP removals of approximately 45% under UV irradiation, with improved performance after three consecutive reuse cycles. When exposed to natural solar radiation, complete degradation of the contaminant was achieved within 120 min, with a kinetic rate constant of 0.0203 min^{-1}, comparable to that of suspension-based systems, yet without the drawbacks associated with particle recovery or ecological impact.

More than a membrane developed in a laboratory context, this grid proposes a system designed for real-world application: simple, lightweight, floating, and easily removable, capable of operating directly at the surface of different aquatic matrices without disturbing ecosystems. Its open geometry and natural buoyancy allow efficient use of solar radiation, combining high photocatalytic performance with a reduced environmental impact. This simplicity makes it particularly relevant for developing regions, where water contamination is critical and conventional treatment solutions are insufficient or inaccessible.

Overall, this thesis goes beyond the development of a conventional photocatalytic material and presents a multifunctional platform capable of effectively degrading antibiotics, ARB, and ARGs. The combination of the photocatalyst mechanism with a tailored polymeric microstructure as a reusable platform was designed to operate efficiently under solar irradiation and with reduced environmental impact, giving the system high performance and robustness.

This work acts as an open door to a tuneable system capable not only of addressing the emerging contaminants studied but also of inspiring future solutions for other classes of pollutants, contributing to more resilient, effective, and accessible aquatic remediation in real-world contexts.

6.2 Future work

Although the objectives defined for this thesis were successfully achieved, namely the development of sustainable, multifunctional, and reusable photocatalytic platforms for the simultaneous removal of antibiotics, ARB, and ARGs, the results obtained open new research opportunities. In particular, the transition towards conditions closer to real-world application, together with an integrated assessment of

environmental safety, material durability, and functional optimisation, emerges as a natural next step to consolidate the potential of these platforms in realistic aquatic remediation scenarios.

-Scalability and real conditions: Evaluation of photocatalytic membranes and grids in natural waters and WWTP effluents, assessing the simultaneous removal of antibiotics, ARB and ARGs, and other contaminants of emerging concern in complex matrices.

-Environmental assessment and safety: Monitoring of nanoparticles leaching and evaluation of the ecotoxicity of degradation by-products using local bacterial banks or simulated microbiomes, including chronic toxicity assays to reflect long-term or continuous exposure scenarios.

-Materials and complementary approaches: Integration of adsorbent materials (e.g., metal organic frameworks) or additional functional phases into photocatalytic membranes, aiming to capture contaminants or degradation by-products that are not fully mineralised.